

Water-soluble inorganic trace gases and related aerosol compounds in the tropical boundary layer

An analysis based on real-time measurements at a pasture site in the
Amazon Basin

Promotor:

prof. dr. F. X. Meixner

associate professor at the department of Physics, University of Zimbabwe (Harare)
Max Planck Institute for Chemistry, Biogeochemistry department (Mainz, Germany)

prof. dr. J. Slanina

hoogleraar in de ontwikkeling meetmethodologie in atmosferisch onderzoek
Wageningen Universiteit (Nederland)

Co-promotor:

prof. dr. M. O. Andreae

professor of oceanography
visiting Professor at the Caltech Institute of Technology (Pasadena, California, U.S.A.)
Max Planck Institute for Chemistry, Director Biogeochemistry department (Mainz, Germany)

Promotiecommissie:

dr. G. Spindler

Institute for Tropospheric Research (Leipzig, Germany)

prof. dr. P. Kabat

Wageningen Universiteit (Nederland)

prof. dr. A.A.M. Holtslag

Wageningen Universiteit (Nederland)

dr. L. Ganzeveld

Max Planck Institute for Chemistry, Air chemistry department (Mainz, Germany)

Het onderzoek is uitgevoerd bij de onderzoekschool WIMEK (Wageningen Instituut voor Milieu- en Klimaatonderzoek).

Water-soluble inorganic trace gases and related aerosol compounds in the tropical boundary layer

An analysis based on real-time measurements at a pasture site in the
Amazon Basin

Ivonne Trebs

Proefschrift
ter verkrijging van de graad van doctor
op gezag van de rector magnificus
van Wageningen Universiteit,
prof. dr. ir. L. Speelman
in het openbaar te verdedigen
op maandag 30 Mei 2005
om 16:00 uur in de Aula.

Water-soluble inorganic trace gases and related aerosol compounds in the tropical boundary layer: An analysis based on real-time measurements at a pasture site in the Amazon Basin / Ivonne Trebs

Proefschrift Wageningen Universiteit, Faculteit Meteorologie en Luchtkwaliteit

Samenvatting in het Nederlands

ISBN 90-8504-173-2

Trefw.: anorganische sporengassen en verwante aerosolen, Amazone gebied

The sun and moon must shine for us day and night; the sky must give us rain, clouds, shade, and dew; the earth must give us all kinds of growing things and animals; the waters must give us fish and countless necessities; the air must supply birds as well as our breath; fire must warm us and give us countless benefits. And who can enumerate everything? It cannot be otherwise or better expressed than in these short words: "Great are the works of the Lord."

Martin Luther

PREFACE

The initial and also quite preliminary motivation for doing my PhD at the Max Planck Institute for Chemistry (MPIC) was a proposed trip to Africa. That happened, when I was sitting with my supervisor and boss, Franz X. Meixner, in Manacapuru (Brazil, Amazon Basin) looking at the measurement results from the LBA-CLAIRE 2001 campaign. Franz was very enthusiastic about the data, such that he asked me if I would be willing to do my PhD in his group. Since I was not very much in favor of that idea, he tried to convince me by inviting me to go on a research trip to Africa. He knows how much I like to travel, so he managed to catch me with that idea. I have not been to Africa yet, but I have finished my dissertation.

Franz offered me several different topics to work on, and I wound up for some reason, choosing the most difficult and challenging one. Additionally, because of the instrument I used for my PhD work in the Amazon Basin, I had the good fortune to have Jacob Slanina be my PhD advisor. However, once I started, it took me quite some time to really internalize what I was doing and moreover, why I was doing it. The reason was that during my education as an engineer I heard only very little about atmospheric sciences. Once I had figured out what it was all about I really had a lot of fun doing this work, although it was quite tough, stressful and tiring sometimes.

Many people have supported me during the last three years. However, the one who supported me the most was of course my supervisor and boss, Franz X. Meixner. I would like to thank him from the bottom of my heart for all the things that he has done for me and for always being available to discuss my scientific problems. I thank him not only for his scientific support and all the very fruitful and endless discussions we had about my PhD work, but also for all the pleasure he gave me as a human. His faith and his belief in me were the only things which kept me going sometimes when I was really struggling.

I am also grateful to Günter Helas, whose advice was incredibly valuable to me, in particular regarding chemistry issues. Although he has never been my direct supervisor, he was always there for me and answered my questions with a lot of patience. I am indebted to Meinrat O. Andreae, who steadily supported my studies and advised me in scientific, but also in logistic issues. I would like to thank him and all the staff from the MPIC for providing excellent research possibilities. I am very grateful to my PhD advisor, Jacob Slanina who supported my PhD plans and prepared the way for me being accepted as a PhD student by the Wageningen University. I am also very thankful to Jörn von Jouanne for his valuable comments and corrections of chapter 3. The successful operation of the instrument in the

Amazon Basin was due to René Otjes and Piet Jongejan from the Energy Research Center of the Netherlands who taught and prepared me intensively for that challenging task. I would like to thank them for their patience in answering the thousands of questions I had and for never giving up on me.

My PhD studies would not have been possible without the financial support from the European Commission (contract SMOCC N° EVK2-CT-2001-00110 SMOCC) and by the Max Planck Society. Additionally, the Brazilian financial agencies that have supported the projects FAPESP (RACCI) and CNPq (MilênioLBA) are acknowledged. I am thankful to Paulo Artaxo and Jörn von Jouanne for the organization of the field experiment and their initiative and support in setting up the sampling location. Also, I wish to thank Marcos A. L. Moura and Rosiberto S. da Silva, Jr. for performing the meteorological measurements. I gratefully acknowledge Alcides Camargo, Olga L. Mayol-Bracero, Pascal Guyon and Jörn von Jouanne for their help during the field measurements. Also, I would like to thank Swen Metzger for performing the model runs that are discussed in chapter 2 and Spyros Pandis for providing the ISORROPIA and GEFMN model, John H. Seinfeld for providing the SCAPE2 model, and Satoschi Takahama for assistance with the GEFMN model. I am also thankful to Terry Dillon and Tracey W. Andreae for correcting the English of chapters 2 and 3, respectively. I thank Daniel Nyanganyura for being the best office mate I have ever had and for his ability to help me relax and cheer me up. I am grateful to Ralph Dlugi, Laurens Ganzeveld, Swen Metzger, Lydia Lehmann, Michael Kortner and Udo Rummel for teaching me about aerosols, modeling, soils, and micrometeorology etc. and for being always willing to answer my questions and to discuss scientific issues. Also, I thank my colleagues and friends András Hoffer and Göran Frank who always had an open ear for my complaints and who have been nice party-mates from time to time.

Finally, I would like to thank my friends Sandy Kuhnitzsch and Madeleine Bellstedt for always being there for me and for understanding when my PhD took priority over my social life. I am indebted to Olga L. Mayol-Bracero, who has kept our friendship over distance and time. I would like to thank her for always being there when I needed support and for believing in me and my ability to finish this PhD thesis. Additionally, I am grateful to the EnChristo community in Mainz for feeding my spirit in the last year of my PhD work. Most of all, I want to thank my parents Jochen and Ellen Trebs for their patience and trust in me; although I know that it was not always easy for them (as for others) to really understand what I was doing, all that I have achieved in the last years would not have been possible without them.

CONTENTS

Summary	1
Samenvatting.....	2
1 Introduction.....	3
1.1 Motivation and Background.....	3
1.2 Problem definition	7
1.3 Research objectives.....	9
1.4. Thesis outline.....	9
2 Real-time measurements of ammonia, acidic trace gases and water-soluble inorganic aerosol species at a rural site in the Amazon Basin	11
2.1 Introduction.....	13
2.2 Available measurement methods.....	15
2.3 Experimental.....	17
2.3.1 Site description	17
2.3.2 Inlet system.....	17
2.3.3 Sampling and analysis	21
2.4 Results and Discussion.....	23
2.4.1 Estimation of measurement uncertainty	23
2.4.2 Limit of detection (LOD).....	25
2.4.3. Seasonal variation of mixing ratios	27
2.4.4 Diel variations of trace gases.....	29
2.4.5. Diel variations of aerosol species	32
2.4.6. Diel characteristics of total ammonium, nitrate and chloride	34
2.5 Conclusions	36
3 The $\text{NH}_4^+\text{-NO}_3^-\text{-Cl}^-\text{-SO}_4^{2-}\text{-H}_2\text{O}$ aerosol system and its gas phase precursors at a pasture site in the Amazon Basin: How relevant are mineral cations and soluble organic acids?	39
3.1 Introduction.....	41
3.2 Site description and methods.....	43
3.2.1 Measurement site.....	43
3.2.2 WAD/SJAC sampling and analysis.....	43
3.2.3 Supporting measurements.....	44
3.2.4 Thermodynamic equilibrium models (EQMs).....	45
3.3 Results.....	47
3.3.1 Gas and aerosol phase mixing ratios.....	47
3.3.2 Meteorological conditions.....	50
3.3.3 Diel variations of species measured with the WAD/SJAC system	51
3.3.4 Gas/aerosol relationships	54
3.4 Discussion	57
3.4.1 Charge balance of ionic aerosol species.....	57
3.4.2 The thermodynamic equilibrium assumption at FNS	60
3.4.3 Equilibrium model (EQM) simulations.....	62
3.4.4 Overall EQM performance	68
3.5 Summary and conclusion.....	70

4 Dry and wet deposition of atmospheric inorganic nitrogen compounds in a tropical environment (Rondônia, Brazil)	73
4.1 Introduction	74
4.2 Experimental	76
4.2.1 Field site	76
4.2.2 Sampling and analysis	77
4.3 Theory: Estimation of dry and wet N deposition	80
4.3.1 Trace gas fluxes	80
4.3.2 Aerosol fluxes	84
4.3.3 Determination of characteristic time scales	85
4.3.4 Wet N deposition	87
4.4 Results and Discussion	88
4.4.1 Meteorological conditions	88
4.4.2 Concentrations	89
4.4.3 Characteristic time scales	92
4.4.4 The inferential approach: Discussion of input parameters	94
4.4.5 Resistances, NH_3 canopy compensation point, transfer- and deposition velocities	97
4.4.6 Surface-atmosphere exchange fluxes	103
4.4.7 Seasonal cycles of dry and wet N deposition	107
4.4.8 Annual budget of surface-atmosphere exchange	110
4.5 Summary and conclusion	112
5 Main findings, Conclusions and Outlook	115
5.1 Main findings and Conclusions	115
5.2 Outlook	121
Bibliography	123
Curriculum Vitæ	144

SUMMARY

This dissertation investigates the behavior of water-soluble inorganic trace gases and related aerosol species in the tropical boundary layer. Mixing ratios of ammonia (NH_3), nitric acid (HNO_3), nitrous acid (HONO), hydrochloric acid (HCl), sulfur dioxide (SO_2) and the corresponding water-soluble aerosol species, ammonium (NH_4^+), nitrate (NO_3^-), nitrite (NO_2^-), chloride (Cl^-) and sulfate (SO_4^{2-}) were measured at a pasture site in the Amazon Basin (Rondônia, Brazil). Sampling was performed from 12 Sep. to 14 Nov. 2002, covering the late dry (biomass burning) season, the transition period and the onset of the wet season (clean conditions) (LBA-SMOCC*). Measurements were made continuously using a wet-annular denuder (WAD) in combination with a Steam-Jet Aerosol Collector (SJAC) followed by on-line analysis. Real-time data were combined with measurements of the aerosol compounds sodium (Na^+), potassium (K^+), calcium (Ca^{2+}), magnesium (Mg^{2+}) and low-molecular weight polar organic acids determined using integrated filter samples. Additionally, on-line measured mixing ratios of nitric oxide (NO), nitrogen dioxide (NO_2) and ozone (O_3) as well as (micro)-meteorological quantities are considered. Gaseous NH_3 was present in mixing ratios an order of magnitude higher than those of HNO_3 , HONO , HCl and SO_2 . Thermodynamic equilibrium models are used to explore the impact of mineral cations (particularly pyrogenic K^+) and LMW polar organic acids on the $\text{NH}_4^+\text{-NO}_3^-\text{-Cl}^-\text{-SO}_4^{2-}\text{-H}_2\text{O}$ aerosol system. Mineral cations present in Amazonian fine mode aerosols significantly balanced aerosol NO_3^- and SO_4^{2-} during daytime and $(\text{NH}_4)_2\text{SO}_4$ appeared to be only a minor aerosol component. Thermodynamic equilibrium permitted the formation of aqueous NH_4NO_3 and NH_4Cl only during nighttime at $RH > 90\%$. During daytime, excess NH_3 neutralized LMW polar organic acids, forming aerosol NH_4^+ . Local dry and wet deposition rates of inorganic N are presented. Dry N deposition was inferred using the “big leaf multiple resistance approach” and a canopy compensation point model. Dry N deposition is dominated by NH_3 and NO_2 , which featured highest mixing ratios as a consequence of biomass burning activities during the dry season. The pasture site was likely to have a strong potential for daytime NH_3 (re-)emission, owing to high canopy compensation points, which are related to high surface temperatures and to direct NH_3 emissions from cattle excreta. Total (dry + wet) N deposition was estimated to be $7.3 - 9.8 \text{ kgN ha}^{-1} \text{ yr}^{-1}$, which exceeds predictions for the Amazon region by global chemistry and transport models by at least factor of two.

* LBA-SMOCC: Large Scale Biosphere Atmosphere Experiment in Amazonia - Smoke Aerosols, Clouds, Rainfall and Climate: Aerosols from Biomass Burning Perturb Global and Regional Climate)

SAMENVATTING

Dit proefschrift concentreert zich op het gedrag van in water oplosbare anorganische sporengassen en verwante aerosolen in de tropische grenslaag. Op een weide-meetstation in het Amazone gebied (Rondônia, Brazilië) werden mengverhoudingen van ammoniak (NH_3), salpeterzuur (HNO_3), salpeterigzuur (HONO), zoutzuur (HCl), zwaveldioxyde (SO_2) en de bijbehorende in water oplosbare aerosolbestanddelen, ammonium (NH_4^+), nitraat (NO_3^-), nitriet (NO_2^-), chloride (Cl^-) en sulfaat (SO_4^{2-}) gemeten. De bemonstering vond plaats tussen 12 september en 14 november 2002, tijdens het late droge (biomass burning) seizoen, de overgangsperiode en het begin van het natte seizoen (LBA-SMOCC). De metingen werden uitgevoerd met behulp van een wet-annular denuder (WAD) in combinatie met een Steam-Jet Aerosol Collector (SJAC), gevolgd door on-line analyse. De gegevens werden gecombineerd met metingen van de aerosolbestanddelen natrium (Na^+), kalium (K^+), calcium (Ca^{2+}), magnesium (Mg^{2+}) en polaire organische zuren met een laag moleculair gewicht, die met behulp van geïntegreerde filtermonsters werden bepaald. Bovendien werden on-line gemeten mengverhoudingen van stikstofmonoxide (NO), stikstofdioxide (NO_2) en ozon (O_3), evenals (micro)-meteorologische parameters gebruikt voor de analyse van de gegevens. De mengverhouding van gasvormig NH_3 was een grootteorde hoger dan die van HNO_3 , HONO , HCl en SO_2 . Thermodynamische evenwichts modellen werden gebruikt om het effect van minerale kationen (in het bijzonder pyrogeen K^+) en polaire organische zuren met een laag moleculair gewicht op het $\text{NH}_4^+\text{-NO}_3^-\text{-Cl}^-\text{-SO}_4^{2-}\text{-H}_2\text{O}$ aerosol systeem te onderzoeken. Gedurende de dag balanceren minerale kationen in de fijne aerosolfractie de aerosol NO_3^- and SO_4^{2-} grotendeels. Tevens bleek $(\text{NH}_4)_2\text{SO}_4$ een onbelangrijk aerosol bestanddeel. Thermodynamisch evenwicht liet de vorming van wateroplosbaar NH_4NO_3 en NH_4Cl alleen toe gedurende de nacht bij $\text{RH} > 90\%$. Gedurende de dag neutraliseerde overtollig NH_3 polaire organische zuren met een laag moleculair gewicht en vormde aerosol NH_4^+ . Lokale droge en natte depositie snelheden van anorganisch N worden gepresenteerd. Droge depositie van N werd bepaald met behulp van de “big leaf multiple resistance approach” en een “canopy compensation point model”. Droge depositie van N werd overheerst door NH_3 en NO_2 , die de hoogste mengverhoudingen lieten zien gedurende het droge seizoen ten gevolge van het verbranden van biomassa. Het weide-meetstation is waarschijnlijk belangrijk voor NH_3 (re-)emissie, als gevolg van hoge „canopy compensation points“, die samenhangen met de hoge oppervlaktetemperaturen en met directe NH_3 emissies van dierlijke fecaliën. De totale (droge + natte) depositie van N wordt geschat op $7.3 - 9.8 \text{ kgN ha}^{-1} \text{ jaar}^{-1}$, wat de voorspellingen voor het Amazone gebied van globale chemie- en transportmodellen met minstens een factor twee overschrijdt.

1.1 Motivation and Background

“A Conexão Hambúrguer Alimenta a Destruição da Amazônia” – “Hamburger Connection Fuels Amazon Destruction” is the title of a recently published report by the Center for International Forestry Research (CIFOR, Indonesia). One of the statements is: “Cattle expansion in the Amazon in the last twelve years has been phenomenal. During this period, the number of cattle more than doubled, from 26 million in 1990 to 57 million in 2002” ... “Although there is no consolidated data available on the ranking of exports for 2003, some experts claim that Brazil now ranks as the world's largest beef exporter”.

Destruction of the Amazon rain forest. The Amazon Basin covers an area of approximately 7 million square kilometers (about 5 % of the earth's land surface) and supports the largest contiguous forest communities in the world. The Amazon rain forest is a major source of heat and water vapor for the global atmosphere and constitutes an important reservoir of atmospheric carbon dioxide (CO_2) [Gash *et al.*, 2004]. Over the past 30 years Brazilian governmental settlement strategies have lead to successive destruction of this tropical ecosystem. To date, about 15 % of the original Amazon rain forest has been deforested, mainly by slash-and-burn activities. Usually, deforested areas are converted to crop land, but their eventual fate is the establishment of pastures that are used for cattle ranching. In 2002 and 2003, the rate of deforestation in Brazilian Amazonia climbed to nearly 24,000 km^2 per year – equivalent to 11 football fields a minute [Laurance *et al.*, 2004].

Biomass burning. About 80 % of the global biomass burning takes place in the tropics [Hao and Liu, 1994] and thereof about 30 % in South America alone. Biomass burning activities in the Amazon Basin are most concentrated during the dry season (June through September). The combustion of vegetation leads to enormous emissions of particulate matter (aerosols) and traces gases to the atmosphere. These emissions are not only distributed on regional scales, but they may be transported over long distances, mainly by rapid convective transport to higher altitudes due to strong convection associated with the International Tropical Convergence Zone (ITCZ) and the Hadley Circulation [e.g., Andreae *et al.*, 2001; Pickering *et al.*, 1996]. Thus, deforestation and land-use changes in the Amazon Basin are not only relevant from a local and regional standpoint, but are expected to have considerable effects on the global atmosphere.

Trace gases. Trace gas emissions from biomass burning consists to a large extent of CO_2 , but also products of incomplete combustion, such as carbon monoxide

(CO), hydrogen (H₂), hydrocarbons, aldehydes, ketones, alcohols and organic acids, that are relevant for atmospheric chemistry and climate, are emitted [*Crutzen and Andreae*, 1990]. Moreover, inorganic reactive gases, such as sulfur dioxide (SO₂), hydrochloric acid (HCl), ammonia (NH₃) and nitrogen oxides (NO_x) (nitric oxide (NO) + nitrogen dioxide (NO₂)) are released as a result of incomplete combustion. Whereas SO₂ emissions from biomass burning are considered to contribute only marginally to the global SO₂ budget (3 – 5 %) [e.g., *Crutzen and Andreae*, 1990; *Smith et al.*, 2003], the emission of HCl and reactive N (NO_x and NH₃) has been estimated to account for 10 to 15 % of the global emissions [*Keene et al.*, 1999; *Holland et al.*, 1999 and references therein]. SO₂, HCl, NH₃ and NO_x have gained particular scientific interest in the last decades, because they (i.) influence the oxidation capacity of the atmosphere, (ii.) are precursors for the formation of water-soluble aerosol species that affect the earth’s radiative balance *directly* and *indirectly* and (iii.) they are responsible for pollution problems, such as acid deposition and eutrophication of ecosystems.

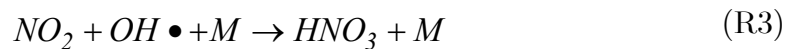
Atmospheric (photo-)chemistry. NO is a key-catalyst in the formation of tropospheric ozone (O₃) and constitutes a major factor controlling the formation of hydroxyl (OH) radicals. NO, O₃ and NO₂ are in photo-stationary equilibrium in the troposphere during daytime [*Jacob*, 1999]:



It has been suggested that NO₂ can be partly removed from the atmosphere by heterogeneous reaction with surface water, a process which is considered to be a source of nitrous acid (HONO) [e.g., *Harrison et al.*, 1996]:

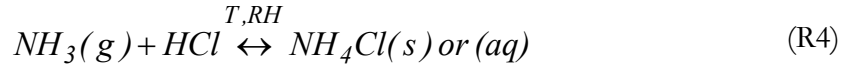
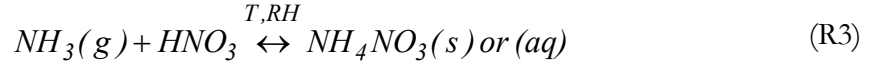


Another proposed formation mechanism of HONO is the heterogeneous conversion of NO₂ on aerosol surfaces [e.g., *Ammann et al.*, 1998; *Bröske et al.*, 2003]. HONO is rapidly photolyzed during daytime and therefore provides a direct source of OH radicals in the atmosphere. However, the most important sink of NO_x in the troposphere during daytime is the oxidation by OH radicals:



This process leads to the formation of nitric acid (HNO₃), which has the highest oxidation state of all reactive N compounds and, hence, terminates their conversion

chain in the atmosphere. SO_2 is oxidized in the atmosphere due to reaction with OH radicals (gas phase) and/or H_2O_2 and O_3 (aqueous phase), leading to the formation of sulfuric acid (H_2SO_4). The atmospheric acids HNO_3 , H_2SO_4 and also HCl are neutralized by NH_3 , which is the most abundant alkaline component in the atmosphere [Asman *et al.*, 1998]. As a consequence, secondary water-soluble inorganic aerosol compounds such as ammonium sulfate ($(\text{NH}_4)_2\text{SO}_4$), ammonium nitrate (NH_4NO_3) and ammonium chloride (NH_4Cl) are formed. Roughly half of the SO_2 emitted into the atmosphere is removed by conversion to particulate sulfate [Kerminen *et al.*, 2000 and references therein]. Whereas $(\text{NH}_4)_2\text{SO}_4$ is relatively stable and non-volatile, particulate NH_4NO_3 and NH_4Cl are thought to form via reversible thermodynamic phase equilibria with NH_3 , HNO_3 and HCl [Pio and Harrison, 1987b; Stelson *et al.*, 1979]. NH_4NO_3 and NH_4Cl are therefore considered to be semi-volatile and their stability strongly depends on ambient temperature (T) and relative humidity (RH).



NH_4Cl is considered to be more labile than NH_4NO_3 and usually represents only a minor fraction of atmospheric aerosols. NH_4NO_3 and NH_4Cl are, along with non-volatile $(\text{NH}_4)_2\text{SO}_4$, predominantly present in fine mode aerosols ($D_p \leq 2.5 \mu\text{m}$).

Aerosol climate forcing. Atmospheric aerosols influence the earth’s radiative balance *directly* by back-scattering and absorption of short- and long wave radiation [IPCC, 2001]. Aerosols with diameters between 0.1 and 2 μm are most relevant for back-scattering of short-wave radiation, which results in cooling of the earth’s surface [e.g., Slanina and Zhang, 2004]. Additionally, these fine mode aerosols may act as cloud condensation nuclei (CCN). Enhanced aerosol concentrations influence the earth’s radiative balance *indirectly* by increasing cloud reflectivity and cloud lifetime [Twomey, 1974; Albrecht, 1989]. *Direct* and *indirect* aerosol effects are largely influenced by ambient RH , aerosol water-solubility and chemical composition of the water-soluble material. Water-soluble aerosol compounds, such as ammonium (NH_4^+), nitrate (NO_3^-), chloride (Cl^-) and sulfate (SO_4^{2-}) play a major role in the nucleation and growth of cloud droplets [e.g., Roberts *et al.*, 2002]. Current estimates of direct and indirect aerosol forcing are still subject to large uncertainty [see IPCC, 2001] and solely account for carbonaceous aerosols, mineral dust and SO_4^{2-} aerosols [IPCC, 2001], whereas the contribution of NH_4NO_3 and NH_4Cl to aerosol climate forcing is not considered. The main reason for this is the lack of reliable information about the size-distribution and the

absolute concentration of these aerosol species. Most measurements of aerosol NO_3^- , but also of NH_4^+ and Cl^- , were performed using filter and/or impactor techniques that are – due to the semi-volatility of NH_4NO_3 and NH_4Cl (see R4 and R5) – prone to artifacts [e.g., *Appel et al.*, 1981; *Pio and Harrison*, 1987a]. It has been assumed in the past that NO_3^- predominantly occurs in coarse mode particles since most early measurements were made in coastal regions where NO_3^- is present as coarse mode NaNO_3 cf. [*Khlystov*, 1998]. However, aerosol NO_3^- was observed in fine mode aerosols during recent studies in Europe und North America using artifact-free measurement methods [e.g., *ten Brink et al.*, 1997; *Stolzenburg and Hering*, 2000; *Weber et al.*, 2003; *Slanina and Zhang*, 2004; *Schaap et al.*, 2004]. Hence, besides the relevance of $(\text{NH}_4)_2\text{SO}_4$ for aerosol climate forcing, a sizeable contribution of fine mode NH_4NO_3 is foreseeable. Up to date, however, no reliable information about aerosol NH_4^+ , NO_3^- and Cl^- concentrations is available from tropical environments.

Wet and dry deposition. Trace gases and aerosols are mainly removed from the troposphere by wet and dry deposition. Wet deposition refers to scavenging of atmospheric constituents by hydrometeors (cloud and fog droplets, rain, snow), which subsequently deliver the scavenged species to the earth’s surface [*Meixner*, 1994]. Dry deposition of species to the earth’s surface takes place by turbulent transport of gases and aerosol particles within the atmospheric surface layer [*Foken*, 2003]. The relative importance of dry deposition, as compared with wet deposition, for the removal of species depends on: (i.) the amount of precipitation in the region of interest, (ii.) the water-solubility of the substance (iii.) the terrain type and surface cover, (iv.) the concentration of the compound and (v.) the presence of the substance in gaseous or particulate form [*Seinfeld and Pandis*, 1998]. Considering the latter, particularly meteorological conditions (T and RH) determine whether nitrate, ammonium and chloride are present in the gas phase as NH_3 , HNO_3 and HCl or whether fine mode particulate NH_4NO_3 and NH_4Cl are formed (see R4 and R5). The dry deposition of gaseous species is generally considered to be more efficient than that of aerosol particles. Anthropogenic emissions of NO , NH_3 and SO_2 to the atmosphere have increased significantly, mainly caused by fossil fuel combustion and extensive fertilizer use in the Northern Hemisphere and by biomass burning and increasing fertilizer use in the Southern Hemisphere. This has led to enhanced wet and dry deposition rates of reactive nitrogen (N) compounds (e.g., NO_2 , NH_3 , HNO_3 and HONO), but moreover, to significant increases of the acidity of atmospheric deposition [*Galloway*, 2001]. As a result, reactive N has accumulated in environmental reservoirs, subsequently causing acidification and eutrophication of ecosystems.

Measurement methods. Reliable measurements of NH_3 , HNO_3 , HCl and SO_2 and their related aerosol species NH_4^+ , NO_3^- , Cl^- and SO_4^{2-} have been recognized as a non-trivial task in the last 30 years. The traditional collection of aerosol particles on

filter materials without pre or after-stages to trap gaseous compounds needs long sampling times (hours to days) to collect sufficient particulate material [Slanina *et al.*, 2001]. This may cause evaporation of semi-volatile species (NH_4NO_3 and NH_4Cl) from the filter material induced by a change of meteorological conditions (T and RH , see R4 and R5) during the long sampling period (negative artifact). Additionally, water-soluble gases (NH_3 , HNO_3 , HCl and SO_2) may be retained by filter substrates (positive artifact) and/or reaction between ambient species may occur during collection. In order to overcome these disadvantages and to quantitatively assess environmental problems and climatic impacts, such as acidification, eutrophication and aerosol climate forcing, new measurement techniques were developed in the last decades. Starting out with filter-pack methods and dry-coated diffusion denuders, several continuous sampling devices were developed. Recently, direct spectroscopic methods to measure water-soluble gases have been applied, which proved to be sensitive and reliable. However, their widespread application is restricted by their bulk and cost [Dasgupta, 1993]. The denuder technique to measure water-soluble gases was substantially improved in the last 10 years, nowadays allowing continuous measurements with high time resolution and high sampling efficiency [e.g., Simon and Dasgupta, 1993; Wyers *et al.*, 1993]. Moreover, continuous denuder devices may be combined with recently developed aqueous-phase aerosol collectors [e.g., Buhr *et al.*, 1995; Simon and Dasgupta, 1995b; Slanina *et al.*, 2001; Stolzenburg and Hering, 2000; Weber *et al.*, 2001; Zellweger *et al.*, 1999]. This is up to date the only approach to selectively and simultaneously collect gas and aerosol species with high time resolution.

1.2 Problem definition

Problem I: Artifact-free measurements under tropical conditions

In the past, inorganic aerosol constituents were sampled in the Amazon region by applying common filter methods [e.g., Talbot *et al.*, 1988; Allen and Miguel, 1995; Yamasoe *et al.*, 2000; Graham *et al.*, 2003a; Mace *et al.*, 2003]. However, high temperatures ($> 35^\circ\text{C}$ during daytime) and high RH s (close to 100 % at nighttime), accompanied by large day-night amplitudes, which are typical for this tropical region may lead to large positive or negative filter sampling artifacts. Moreover, high RH s may cause droplet formation on filter substrates, which favours SO_2 retention and subsequent aqueous phase oxidation, resulting in artifact particulate SO_4^{2-} formation [e.g., Appel *et al.*, 1984]. Additionally, tropical conditions promote the absorption of water-soluble gases (especially HNO_3) on inlet walls which are coated with water layers at $RH \sim 100$ %. In contrast to the dry season when biomass burning takes place, the Amazonian wet season is characterized by a

pristine background atmosphere. Thus, particularly under tropical conditions, the single most important prerequisite to measure NH_3 , HNO_3 , HCl and SO_2 and the related aerosol species NH_4^+ , NO_3^- , Cl^- and SO_4^{2-} is a method, which (i.) minimizes HNO_3 inlet losses, (ii.) allows separation of gas and aerosol phase before chemical speciation, (iii.) provides high time resolution and (iv.) provides low detection limits.

Problem II: Gas/aerosol partitioning

Environmental pollution in the temperate latitudes is largely driven by fossil fuel combustion and by agricultural practices, causing aerosol chemical composition usually to be dominated by inorganic compounds (mainly NH_4^+ , NO_3^- and SO_4^{2-}), that are mixed with sea-salt (NaCl) in coastal regions. By contrast, organic matter often accounts for 90 % of the total mass of Amazonian aerosols [Andreae and Crutzen, 1997], which is attributed to biomass burning emissions during the dry season and to biogenic emissions during the wet season. About 45 % to 75 % of the organic aerosol fraction is water-soluble [Mayol-Bracero *et al.*, 2002; Graham *et al.*, 2003a]. Additionally, fine mode biomass burning (pyrogenic) aerosols usually contain considerable amounts of potassium (K) - salts [Andreae, 1983]. The partitioning of semi-volatile ammonium, nitrate and chloride between gas and aerosol phase is strongly dependent on T and RH (R4 and R5), but also on the aerosol chemical composition. Aerosol chemical composition determines the water uptake as a function of ambient RH , which is most relevant for *direct* and *indirect* aerosol climate forcing. In turn, a change in RH affects gas/aerosol partitioning processes, hence increasing or decreasing the amount of semi-volatile species. Commonly, gas/aerosol partitioning is simulated using so-called thermodynamic equilibrium models (EQMs), which are, however usually limited to inorganic species. High temperatures, high RH s, the preponderance of aerosol organic matter, but also mineral cations (mainly K^+) present in fine mode Amazonian aerosols are likely to significantly affect gas/aerosol partitioning processes in this region.

Problem III: Nitrogen deposition

Total (dry + wet) N deposition have been experimentally quantified in the temperate latitudes (mainly Europe and North America) in the last decade, yet N inputs to tropical ecosystems, where biomass burning is the main source of reactive N, have remained uncertain. In particular, dry deposition rates of NH_3 , HNO_3 , HONO , aerosol NH_4^+ and NO_3^- are largely unknown in the tropics, since no data on the concentration of these species are available. The only estimates available are from global chemistry and transport models (CTMs) [e.g., Hauglustaine *et al.*, 2004; Holland *et al.*, 1999], which, however, cannot resolve local land use/surface

characteristics and transport/turbulence conditions. Burning of tropical rainforest causes a sizeable release of reactive N that is subsequently removed from the troposphere by wet and dry deposition. This redistribution of N in the biosphere may significantly disturb the local N cycle and may have sustainable consequences for ecosystem functioning. Assessing the impact of elevated N inputs on tropical ecosystems mandates the need for experimental determination of contemporary N deposition rates in tropical environments, such as the Amazon Basin.

1.3 Research objectives

The three main objectives of this study are:

1. Performance of reliable measurements of NH_3 , HNO_3 , HONO , HCl and SO_2 and aerosol NH_4^+ , NO_3^- , NO_2^- , Cl^- and SO_4^{2-} at a pasture site Amazon Basin under biomass burning and background conditions.
2. Investigation of the inorganic gas/aerosol system under tropical conditions, considering the presence of mineral cations and low-molecular weight (LMW) polar organic acids.
3. Estimation of local wet and dry N deposition rates, the relative contribution of the N species considered and the comparison to predictions by global CTMs.

1.4. Thesis outline

I. Evaluation and verification of the performed measurements

Chapter 2 of this thesis focuses on the detailed description and evaluation of the performed measurements of water-soluble inorganic trace gases (NH_3 , HNO_3 , HONO , HCl and SO_2) and related aerosol compounds (NH_4^+ , NO_3^- , NO_2^- , Cl^- and SO_4^{2-}). That includes (i.) a summary and short discussion of all measurement techniques available (ii.) the evaluation of the applied inlet system, (iii.) the estimation of measurement uncertainties and (iv.) the determination of the limit of detection (LOD), all under tropical conditions. Furthermore, the chapter will explain briefly the obtained seasonal and diel variations of ambient mixing ratios. The chapter builds the base for the forthcoming chapters, hence for assessing *Problem II and III*.

II Investigation of the inorganic gas/aerosol system in the Amazon Basin

Chapter 3 explicitly addresses gas/aerosol partitioning processes under tropical conditions in the Amazon Basin. The chapter makes use of simultaneously measured quantities, such as (i.) water-soluble inorganic trace gases and related aerosol species (ii.) meteorological parameters, (ii.) total fine particulate mass (PM 2.5) and (iii.) overall chemical aerosol composition (organic species and mineral cations). The ionic charge balance of the sampled aerosols and the thermodynamic phase equilibria (R4 and R5) are investigated. Four different thermodynamic equilibrium models (EQMs) are used to simulate the inorganic gas/aerosol system in this region, including mineral cations (mainly K^+). Low-molecular weight (LMW) polar organic acids are considered in one of the EQM frameworks as a first approach to assess their influence on inorganic gas/aerosol partitioning processes.

III Estimation of dry and wet N deposition

Chapter 4 presents results of estimated dry and wet deposition rates at the tropical pasture site based on experimentally derived data, that include results from measurements of (micro)-meteorological quantities and mixing ratios of NO , NO_2 and O_3 as well as water-soluble inorganic trace gases and related aerosol species. Surface-atmosphere exchanges of NO_2 , HNO_3 , NH_3 and $HONO$ are inferred using the “big leaf multiple resistance approach”, whereby fluxes of NH_3 and $HONO$ were considered to be bi-directional. Dry deposition fluxes of aerosol NH_4^+ and NO_3^- were estimated by applying an established empirical parameterization. The seasonal N deposition cycle and the estimated N budget at the Amazonian pasture site are discussed. Total (dry + wet) N deposition estimates are compared to predictions of global CTMs.

Finally, the thesis is concluded and summarized in chapter 5.

Real-time measurements of ammonia, acidic trace gases and water-soluble inorganic aerosol species at a rural site in the Amazon Basin

I. Trebs, F. X. Meixner, J. Slanina, R. Otjes, P. Jongejan, and M. O. Andreae
(*Atmospheric Chemistry and Physics* **4**, 967-987, 2004)

Abstract. We measured the mixing ratios of ammonia (NH_3), nitric acid (HNO_3), nitrous acid (HONO), hydrochloric acid (HCl), sulfur dioxide (SO_2) and the corresponding water-soluble inorganic aerosol species, ammonium (NH_4^+), nitrate (NO_3^-), nitrite (NO_2^-), chloride (Cl^-) and sulfate (SO_4^{2-}), and their diel and seasonal variations at a pasture site in the Amazon Basin (Rondônia, Brazil). This study was conducted within the framework of LBA-SMOCC (Large Scale Biosphere Atmosphere Experiment in Amazonia - Smoke Aerosols, Clouds, Rainfall and Climate: Aerosols from Biomass Burning Perturb Global and Regional Climate). Sampling was performed from 12 September to 14 November 2002, extending from the dry season (extensive biomass burning activity), through the transition period to the wet season (background conditions). Measurements were made continuously using a wet-annular denuder (WAD) in combination with a Steam-Jet Aerosol Collector (SJAC) followed by suitable on-line analysis. A detailed description and verification of the inlet system for simultaneous sampling of soluble gases and aerosol compounds is presented. Overall measurement uncertainties of the ambient mixing ratios usually remained below 15 %. The limit of detection (LOD) was determined for each single data point measured during the field experiment. Median LOD values (3σ – definition) were ≤ 0.015 ppb for acidic trace gases and aerosol anions and ≤ 0.118 ppb for NH_3 and aerosol NH_4^+ . Mixing ratios of acidic trace gases remained below 1 ppb throughout the measurement period, while NH_3 levels were an order of magnitude higher. Accordingly, mixing ratios of NH_4^+ exceeded those of other inorganic aerosol contributors by a factor of 4 to 10. During the wet season, mixing ratios decreased by nearly a factor of 3 for all compounds compared to those observed when intensive biomass burning took place. Additionally, N-containing gas and aerosol species featured pronounced diel variations. This is attributed to strong relative humidity and temperature variations between day and night as well as to changing photochemistry and stability conditions of the planetary boundary layer. HONO exhibited a characteristic diel cycle with high

mixing ratios at nighttime and was not completely depleted by photolysis during daylight hours.

2.1 Introduction

Every year, large emissions of aerosols and trace gases occur during the dry season (May through September) in the Amazon Basin from widespread biomass burning activity. Smoke from biomass burning leads to a significant increase in cloud condensation nuclei (CCN) concentration causing alteration of cloud properties. This is likely to have considerable impact on the large-scale dynamics of the atmosphere [Andreae *et al.*, 2002; Roberts *et al.*, 2001]. During the wet season, however, background conditions resemble CCN concentrations more typical of marine locations than most continental sites [Roberts *et al.*, 2001]. Both, water-soluble inorganic aerosol species and soluble gases are expected to play a major role in the nucleation and growth of cloud droplets under polluted as well as under clean conditions.

Ammonia (NH_3), in the tropics mostly emitted by combustion processes, volatilization from manure and fertilizer application, plays a key role in neutralizing acidic atmospheric compounds [Asman *et al.*, 1998]. Due to heterogeneous reactions involving gaseous NH_3 as well as sulfur dioxide (SO_2), non-volatile aerosol constituents like $(\text{NH}_4)_2\text{SO}_4$ and NH_4HSO_4 can be formed.

Moreover, the abundance of semi-volatile aerosol species such as NH_4NO_3 and NH_4Cl is strongly dependent on their gas-phase precursors, NH_3 , HNO_3 and HCl . NH_4NO_3 is believed to form via reversible phase equilibrium with gaseous NH_3 and HNO_3 [Stelson and Seinfeld, 1982a]. Comparably, gaseous NH_3 and HCl are precursors for the reversible formation of NH_4Cl [Pio and Harrison, 1987a]. These thermodynamic equilibria are strongly dependent on relative humidity and temperature, such that low temperature and high relative humidity will shift the equilibrium to the aerosol phase.

Nitrous acid (HONO) is of atmospheric importance due to its expected significant contribution to the production of OH radicals. Rapid HONO photolysis can lead to an integrated OH yield of up to 34 % at daytime [Kleffmann *et al.*, 2003 and references therein]. The observation of persistent daytime HONO (up to 150 ppt) was found by several investigators and it is expected to be mainly formed due to heterogeneous reaction of NO_2 with surface water [Harrison and Kitto, 1994; Zhou *et al.*, 2002; Alicke *et al.*, 2003; Aumont *et al.*, 2003; Genfa *et al.*, 2003; Kleffmann *et al.*, 2003].

Since the 1970's, adequate sampling of gaseous compounds and related semi-volatile aerosol species was recognized as a significant problem, especially with respect to the collection of HNO_3 , nitrate (NO_3^-), but also NH_3 , ammonium (NH_4^+), chloride (Cl^-) and sulfate (SO_4^{2-}) [Appel and Tokiwa, 1981; Appel *et al.*, 1984; Slanina *et al.*, 1992; Appel, 1993; Cheng and Tsai, 1997]. In particular, HNO_3 measurements without interferences are very difficult, since this molecule can

readily absorb on surfaces of inlets [Appel *et al.*, 1988; Neuman *et al.*, 1999] and sampling substrates (e.g., filter materials) [Appel *et al.*, 1984]. Furthermore, desorption and re-evaporation of HNO_3 from inlet surfaces or sampling substrates may considerably bias sampling results. The collection of aerosol species on filter materials without pre or after-stages to trap gaseous compounds leads to significant artifacts [Slanina *et al.*, 2001]. Long sampling times (hours to days) to collect sufficient aerosol on the filter material may result either in evaporation of semi-volatile aerosol species (negative artifact) or to collection of gaseous compounds (such as NH_3 , HNO_3 , HCl and SO_2) which may be retained by filter media (positive artifact).

To date there are no reliable measurements of NH_3 and acidic trace gases (HNO_3 , HONO , HCl , and SO_2) from the Amazon Basin, and in the past inorganic aerosol species were usually sampled by filter methods without accounting for possible artifacts. High temperatures and relative humidities (close to 100 % at nighttime) are typical for this tropical region, which may significantly influence gas/aerosol partitioning processes. During the wet season, conditions usually remain very clean (low aerosol and trace gas concentrations are present) in contrast to the dry season when biomass burning takes place. For these reasons a method which provides continuous measurements with (i.) high selectivity, (ii.) high time resolution (determination of diel variations for gas and aerosol compounds simultaneously), and (c) low detection limits is needed. Therefore, we applied the combination of a wet-annular denuder (WAD) and a Steam-Jet aerosol collector (SJAC) [Wyers *et al.*, 1993; Slanina *et al.*, 2001] followed by on-line analysis using ion chromatography (IC) and ammonium flow injection analysis (FIA). Here, we report the application of a sophisticated inlet system for simultaneous sampling of gas and aerosol species verified for potential sampling losses (particularly HNO_3). Furthermore, an evaluation of the measurement performance of the instrument (with particular emphasis on measurement uncertainty and limit of detection) and first results of seasonal and diel variations of the measured species are presented. For this purpose, we selected exemplary data from a period within the dry season (17 - 20 September), to show the reliability of the measurements compared to studies that have been carried out, e.g., in the Northern Hemisphere. The main scope of this paper is to report and validate first real-time measurements of inorganic aerosol species simultaneously with their gaseous precursors in a tropical environment.

2.2 Available measurement methods

Table 2.1 gives an overview of the most common sampling methods for the collection of inorganic gas and aerosol species with selected references. The filter-pack method, usually with Teflon, Nylon or impregnated filters in series, is the least accurate, but simplest and most commonly used sampling procedure [Appel, 1993]. This technique is laborious, and suffers from long sampling times as well as possible interference due to oxidation of nitrites collected on nylon filters, which may positively bias HNO_3 collection [Perrino *et al.*, 1988]. Also, evaporation of aerosol NO_3^- from Teflon filters has been reported [Appel *et al.*, 1981].

The most substantial approach for sampling a gas in the presence of corresponding aerosol particles is the denuder technique. Dry-coated diffusion denuders are reliable, but laborious and provide only long time-average concentration measurements [Dasgupta, 1993]. These drawbacks were overcome by various other developments. Simon *et al.* [1991] have proposed four different designs for wet effluent diffusion denuders coupled to ion chromatography systems with continuously renewed collection surfaces. Efficient retention of trace gases and a higher time resolution may be achieved by parallel-plate denuders coupled to on-line analysis. Keuken *et al.* [1989] developed an automated thermodenuder system for the determination of NH_3 in ambient air. A device that is becoming increasingly popular is the so called WAD which has the ability to maintain near-quantitative collection efficiencies at high sampling rates within a compact design [Dasgupta, 1993]. The first WAD operating in batch mode was reported by Keuken *et al.* [1988] and a continuously rotating annular denuder was first described by Wyers *et al.* [1993]. Diffusion scrubber and mist chamber techniques also provide measurements with higher time resolution and are less prone to artifacts.

The occurrence of artifacts during sampling of HNO_3 , but also NH_3 , has led to various intercomparison experiments [e.g., Hering *et al.*, 1988; Spicer *et al.*, 1982; Williams *et al.*, 1992]. In these studies, substantial discrepancies between different HNO_3 measurement techniques were observed emphasizing the need of artifact-free methods for accurate measurements of atmospheric HNO_3 . Although the replacement of filter-based methods by continuous denuder devices and optical measurement techniques (also listed in Table 2.1) was a positive development in the last decade, usually these methods are only capable of measuring either one single compound or species of the same physical state (i.e., either gas or aerosol). The combination of new aqueous-phase aerosol collectors with the denuder technique is up to date the only approach for the simultaneous collection of gas and aerosol species. Usually, these methods are continuous, followed by on-line analysis of the resulting aqueous solution. On-line IC has become the major analytical tool for these sampling systems, being able to measure ambient concentrations continuously in the low two-digit ppt range.

Table 2.1: Overview of sampling methods for NH_3 , acidic trace gases and inorganic aerosol species.

Method	Example	Measured species	References
Filter	Impregnated filters, Teflon and nylon filters in series	NH_3 , HNO_3 , aerosol NH_4^+ , NO_3^- , Cl^- and SO_4^{2-}	<i>Appel et al.</i> , 1980; <i>Appel et al.</i> , 1981; <i>Cadle et al.</i> , 1982; <i>Parrish et al.</i> , 1986; <i>Galasyn et al.</i> , 1987; <i>Solomon et al.</i> , 1988; <i>Appel et al.</i> , 1991
Denuder & filter	Denuder-filter pack (DFP)	NH_3 , HNO_3 , HONO , HCl , SO_2 , aerosol NH_4^+ , NO_3^- , Cl^- and SO_4^{2-}	<i>Kito and Harrison</i> , 1992; <i>Harrison et al.</i> , 1996; <i>Danalatos and Glavas</i> , 1999; <i>Possanzini et al.</i> , 1999
Diffusion denuder	Dry-coated diffusion denuder	NH_3 , HNO_3 , HONO , HCl and SO_2	<i>Eatough et al.</i> , 1985; <i>Durham et al.</i> , 1987; <i>Marshall and Dimmock</i> , 1992
	Wet-effluent diffusion denuder	NH_3 , HNO_3 , HONO , HCl and SO_2	<i>Simon et al.</i> , 1991; <i>Vecera and Dasgupta</i> , 1991; <i>Taira and Kanda</i> , 1993; <i>Buhr et al.</i> , 1995; <i>Zellweger et al.</i> , 1999
	Parallel-plate denuder	NH_3 , HNO_3 , HONO , HCl and SO_2	<i>Simon and Dasgupta</i> , 1993; <i>Boring et al.</i> , 1999; <i>Genfa et al.</i> , 2003
	Thermodenuder	NH_3 , HNO_3	<i>Keuken et al.</i> , 1989; <i>Klockow et al.</i> , 1989
	Wet-annular denuder	NH_3 , HNO_3 , HONO , HCl and SO_2	<i>Keuken et al.</i> , 1988; <i>Wyers et al.</i> , 1993; <i>Allegrini et al.</i> , 1994; <i>Slanina and Wyers</i> , 1994; <i>Oms et al.</i> , 1996; <i>Jongejan et al.</i> , 1997
	AiRRmonia	NH_3	<i>Erisman et al.</i> , 2001
Diffusion scrubber	Diffusion scrubber and mist chamber	NH_3 , HNO_3 , HONO , HCl and SO_2	<i>Matusca et al.</i> , 1984; <i>Cofer et al.</i> , 1985; <i>Philips and Dasgupta</i> , 1987; <i>Lindgren</i> , 1992; <i>Lefer et al.</i> , 1999; <i>Sanhueza and Garaboto</i> , 2002
Fluorescence	Laser-photolysis fragment-fluorescence (LPFF) and laser-Fluorescence derivatization	HONO , HNO_3	<i>Rodgers and Davis</i> , 1989; <i>Papenbrock and Stuhl</i> , 1990; <i>Papenbrock and Stuhl</i> , 1991
Spectroscopy	Differential optical absorption spectroscopy (DOAS)	NH_3 , aerosol NH_4^+	<i>Abbas and Tanner</i> , 1981; <i>Rapsomanikis et al.</i> , 1988
	Chemical ionization mass spectrometer (CIMS)	HNO_3 , HONO	<i>Perner and Platt</i> , 1979; <i>Plane and Nien</i> , 1992; <i>Winer and Biermann</i> , 1994; <i>Febo et al.</i> , 1996; <i>Stutz et al.</i> , 2002
	FT-IR spectrometer	HNO_3 , SO_2	<i>Huey et al.</i> , 1998; <i>Mauldin et al.</i> , 1998; <i>Furutani and Akinoto</i> , 2002; <i>Hauke et al.</i> , 2003
	Cavity ring-down spectroscopy	NH_3 , HNO_3	<i>Doyle et al.</i> , 1979
	Long path absorption photometer (LOPAP)	HONO	<i>Wang and Zhang</i> , 2000
	Particle mass spectrometer	aerosol NH_4^+ , NO_3^- , Cl^- and SO_4^{2-} and others	<i>Heland et al.</i> , 2001; <i>Kleffmann et al.</i> , 2003
Aqueous-phase aerosol collection	Particle-into-liquid sampler (PILS)	aerosol NH_4^+ , NO_3^- , NO_2^- , Cl^- and SO_4^{2-}	<i>Gard et al.</i> , 1997; <i>Jayne et al.</i> , 2000; <i>Mallina et al.</i> , 2000; <i>Lee et al.</i> , 2002; <i>Jimenez et al.</i> , 2003
	Particle collection system (PCS)	aerosol NO_3^- , NO_2^-	<i>Weber et al.</i> , 2001; <i>Orsini et al.</i> , 2003
	Vapor condensation aerosol collector system (VCACS)	aerosol NO_3^- , NO_2^-	<i>Simon and Dasgupta</i> , 1995a; <i>Simon and Dasgupta</i> , 1995b
	Wet effluent frit (WEF) and integrated collection and vaporization cell (ICVC)	aerosol NO_3^-	<i>Zellweger et al.</i> , 1999
	Steam jet aerosol collector (SJAC)	aerosol NH_4^+ , NO_3^- , NO_2^- , Cl^- and SO_4^{2-}	<i>Buhr et al.</i> , 1995; <i>Stolzenburg and Hering</i> , 2000
			<i>Khlystov et al.</i> , 1995; <i>Slanina et al.</i> , 2001

2.3 Experimental

2.3.1 Site description

Sampling was performed at a pasture site in the state of Rondônia, Brazil (Fazenda Nossa Senhora Aparecida, FNS, 10°45'44" S, 62°21'27" W, 315 m asl). Clearing of rain forest by fire in Rondônia has taken place since 1968, creating a typical “fishbone”-like pattern of plantations, pastures, degraded land and forest patches [see *Andreae et al.*, 2002]. The vegetation at FNS is dominated by grass (*Brachiaria brizantha*) with small patches of *Brachiaria humidicola* and very few isolated palms and bushes, and the site is used as a cattle ranch (~ 200 “Blanco” cattle, *Bos indicus hybrid*). Nearby the site, flat hills (300 to 440 m) are located at a distance of 3 to 4 km. The pasture is a rural, non-pristine site, with a highway (BR 364) at a distance of 10 km to the northeast. The towns Ouro Preto do Oeste (~ 40,800 inhabitants) and Ji-Paraná (~ 110,000 inhabitants) are situated approximately 8 km and 40 km to the WSW of the site, respectively.

The site is characterized by small seasonal temperature variations, ranging from 23 – 24 °C at the end of the wet season (June/July) to 25 – 26 °C during the dry season (September/October). Annual relative humidity values are high, with averages of about 70 % in the dry season and 80 % during the wet season. Prevailing wind speeds are relatively low (daily average ~ 1.5 m s⁻¹) with a minimum during nighttime. Precipitation in this region shows a seasonal cycle with lowest values in July and is highest from November to April (up to ~ 300 mm per month) [*Andreae et al.*, 2002]. A detailed description of the history of the site can be found in *Kirkman et al.* [2002].

Instrumentation for sampling and on-line analysis was arranged in a wooden house with several air conditioned laboratories. The house was surrounded by a fence (distance to the house ~ 10 m) to prevent cattle from approaching the sampling and measurement location.

2.3.2 Inlet system

2.3.2.1 Design

The sampling performance of the wet-annular denuder/steam-jet aerosol collector (WAD/SJAC) and the quality of the on-line analysis are strongly dependent on environmental parameters (i.e., air temperature and relative humidity). In order to provide controlled conditions for sampling and particularly for IC and FIA (i.e., minimal fluctuations of temperature and relative humidity), it was necessary to place the instrumentation in an air conditioned laboratory. An inlet system mounted to the wall outside of the air conditioned laboratory was used to bring sample air to the instruments (Fig. 2.1).

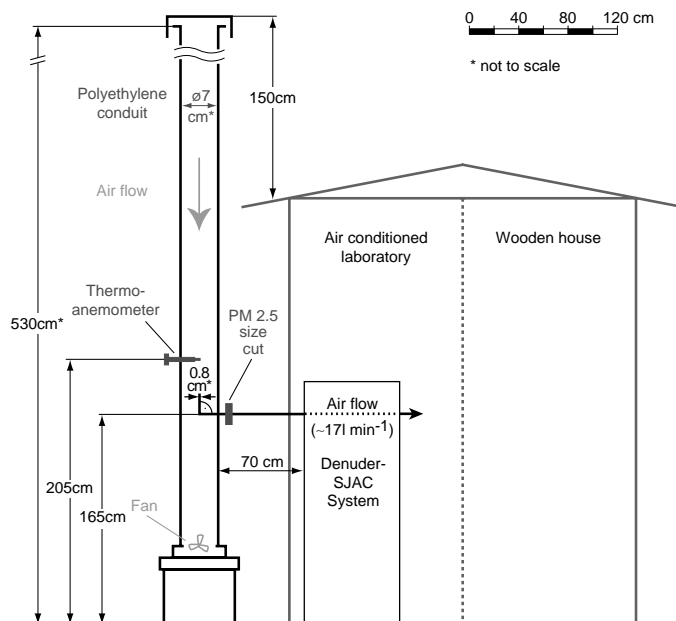


Figure 2.1: Design and setup of the inlet system for real-time measurements of water-soluble gases and inorganic aerosol species at FNS during SMOCC 2002.

For the design of this inlet system, three major requirements had to be considered: (i.) Minimizing gas-phase wall losses (particularly HNO_3), (ii.) Minimizing aerosol losses due to non-isokinetic sampling and (iii.) providing a reasonable sampling fetch. To meet these requirements, air was sampled from 530 cm above ground (150 cm above the roof of the house) through a vertical polyethylene conduit with an inner diameter of 7 cm. The conduit was wrapped on the outside with aluminum tape to reduce daytime heating of the material. The air flow in the conduit was generated by a suction fan assembled in the conduit bottom. A sub-sample of the air was aspirated from the center of the conduit's cross section area at a flow rate of $\sim 17 \text{ l min}^{-1}$ (STP: 298.15 K and 1000 hPa) through a steel elbow (90° angle of steel tubing, $d = 0.8 \text{ cm}$, inner surface PFA Teflon coated) mounted inside the conduit (Fig. 2.1). The sampled air was then drawn through a PFA Teflon tubing connection ($d = 0.8 \text{ cm}$, $l = 70 \text{ cm}$) to the sampling system in the air conditioned laboratory. The PFA Teflon tubing inside the laboratory had a length of only 5 cm before entering the instrument and was insulated thoroughly to prevent condensation. During the field experiment, the steel elbow was replaced periodically with a pre-impactor (PM 2.5 size cut; type 413, University Research Glassware, aluminum cyclone, PFA Teflon coated). Hence, aerosol samples of either PM 2.5 ($D_p \leq 2.5 \mu\text{m}$) or bulk aerosol fraction were collected in alternating cycles (1 – 3 days). Velocity, relative humidity and temperature of the air stream in the polyethylene conduit were continuously monitored (time resolution 1 min) using a thermo-anemometer sensor (Velocicalc Plus 8386, TSI Instruments).

Neuman et al. [1999] tested different inlet materials for sampling HNO_3 and found highest transmission efficiencies ($\geq 95\%$) for plastic materials at 22°C (e.g., PFA, TFE, FEP and PVDF), whereas HNO_3 loss on aluminum, steel or nylon materials was $\sim 85\%$. Plastic materials, such as polycarbonate [*Spicer and Schumacher*, 1979], polyethylene and PVC, are generally known to have a low affinity to adsorb HNO_3 vapor. During the EPA Atlanta Supersite Experiment (1999), PVC was used as inlet material for sampling HNO_3 and HONO and proved to be satisfactory [*Genfa et al.*, 2003]. On the basis of these results, the polyethylene inlet conduit was considered to be appropriate for sampling of HNO_3 and other soluble gases. Also, using Teflon coated aluminum cyclones as inlet under atmospheric conditions; *Appel et al.* [1988] observed transmission efficiencies for HNO_3 not significantly different from 100% . Nevertheless, to ensure the quality of our measurements, we present a theoretical verification of the applied inlet system in the following section.

2.3.2.2 Sampling efficiency of the inlet system

To minimize gas-phase losses (particularly HNO_3), laminar conditions in the conduit are necessary to avoid turbulence and to minimize the contact of the sampled air with the inlet walls. However, since simultaneous sampling of gases and aerosol species was intended, it was crucial to account for possible inlet losses of both, gases and aerosols. The required flow rate for the pre-impactor ($d = 0.8\text{ cm}$) was $\sim 17\text{ l min}^{-1}$ (STP). The mean air velocity in the polyethylene conduit generated by the suction fan was adjusted to $\sim 1\text{ m s}^{-1}$ (Reynolds number $Re_{mean} \sim 4500$) indicating the transition between laminar conditions and turbulence. This, in turn, led to slightly superisokinetic sampling at the entrance of the steel elbow and/or pre-impactor, since the mean air velocity at its entrance was around 8 m s^{-1} . Aerosol losses due to non-isokinetic sampling were calculated using the equation of Belyaev & Levin (1974) [*Hinds*, 1999]:

$$\frac{\Delta c}{c_0} = I - \left(I + \left(\frac{v_0}{v} - I \right) \times \left(I - \frac{I}{I + \left(2 + 0.62 \times \frac{v}{v_0} \right) \times Stk} \right) \right) \quad (2.1)$$

where $\Delta c/c_0$ is the relative aerosol loss between conduit and steel elbow and/or pre-impactor, v_0 is the air velocity in the conduit (m s^{-1}) (STP), v is the air velocity in the steel elbow and/or pre-impactor (m s^{-1}) (STP) and Stk is the corresponding Stokes number. Aerosol losses ($D_p \leq 2.5\text{ }\mu\text{m}$) were $\leq 3\%$ for during the entire experiment, and are subsequently neglected.

To verify the performance of the inlet regarding the transmission of gaseous compounds, “worst case” wall losses were calculated for HNO_3 . Therefore, a hypothetical complete coating of the inner conduit surface with water droplets and aerosols, and a HNO_3 uptake coefficient of $\alpha_{\text{HNO}_3} = 1$ (any molecule diffusing to the wall surface would be absorbed = “worst case scenario”) was assumed. The conduit was considered as a circular denuder tube with laminar flow conditions and hypothetical wall losses of HNO_3 were calculated by application of the following equation [Gormley and Kennedy, 1949; equation modified]:

$$\frac{\Delta c}{c_0} = 1 - \left(0.8191 \times e^{-3.6568 \times \Delta} + 0.0975 \times e^{-22.3 \times \Delta} + 0.0325 \times e^{-57 \times \Delta} + \dots \right) \quad (2.2)$$

$$\text{with} \quad \Delta = \frac{\pi \times D_G \times L_C}{Q_C} \quad (2.3)$$

where $\Delta c/c_0$ denotes the relative gas phase loss, D_G the HNO_3 diffusion coefficient ($\text{cm}^2 \text{s}^{-1}$), L_C the length of the conduit (cm) and Q_C the air flow in the conduit ($\text{cm}^3 \text{s}^{-1}$) (STP). The HNO_3 diffusion coefficient in air was experimentally determined by several investigators ranging from $0.04 \text{ cm}^2 \text{s}^{-1}$ to $0.121 \text{ cm}^2 \text{s}^{-1}$ (STP) [Braman *et al.*, 1982; Eatough *et al.*, 1985; Durham and Stockburger, 1986 and Deandrade *et al.*, 1992]. In this study, we used the highest value ($0.121 \text{ cm}^2 \text{s}^{-1}$). Mean hypothetical “worst case” gas-phase losses ($\alpha_{\text{HNO}_3} = 1$) of $\leq 30 \%$ were derived for the conditions observed during the entire measurement period. However, Kirchner *et al.* [1990], Van Doren *et al.* [1990] and Ponche *et al.* [1993] reported from laboratory studies $\alpha_{\text{HNO}_3} \ll 1$ for the heterogeneous uptake of HNO_3 by pure aqueous droplets (typically α_{HNO_3} was < 0.2 for $T > 260 \text{ K}$). Taking into account atmospheric conditions and possible coating of the inner conduit walls with strong electrolytic aerosol mixtures, we consider a HNO_3 uptake coefficient of $\alpha_{\text{HNO}_3} = 0.5$ as a conservative estimate, appropriate for our study. Therefore, theoretical mean gas phase HNO_3 losses for the entire experiment were estimated to $\leq 15 \%$. This estimate is, however, based on the assumption of laminar flow in the conduit, whereas actual flow conditions during the experiment were characterized by $Re_{\text{mean}} \sim 4500$ (see above), exceeding the laminar flow range ($Re \leq 2300$), but still at the lower end of the laminar-turbulent transition. Under (fully) turbulent conditions ($Re > 10000$), higher HNO_3 losses ($> 15 \%$) have to be expected. Therefore, we performed some empirical verification tests. Occasionally, the complete inlet system (conduit and steel elbow and/or pre-impactor) was removed, resulting in sampling straight through the 70 cm long PFA Teflon tubing. During this procedure, HNO_3 mixing ratios never significantly changed from “inlet system on” to “inlet system off”, which supports our estimates of HNO_3 wall losses $\leq 15 \%$.

2.3.3 Sampling and analysis

A detailed description of the WAD/SJAC and the analytical procedures is given elsewhere [Slanina *et al.*, 2001; Wyers *et al.*, 1993]. A simplified sketch of the sampling system is shown in Fig. 2.2. The air flow through the instrument ($\sim 17 \text{ l min}^{-1}$, STP) was generated by a scroll pump outside the wooden house and could be adjusted with a needle valve. The flow was measured continuously (1 min time resolution) with a mass flow meter (Bronkhorst, F-112AC-HA-55-V).

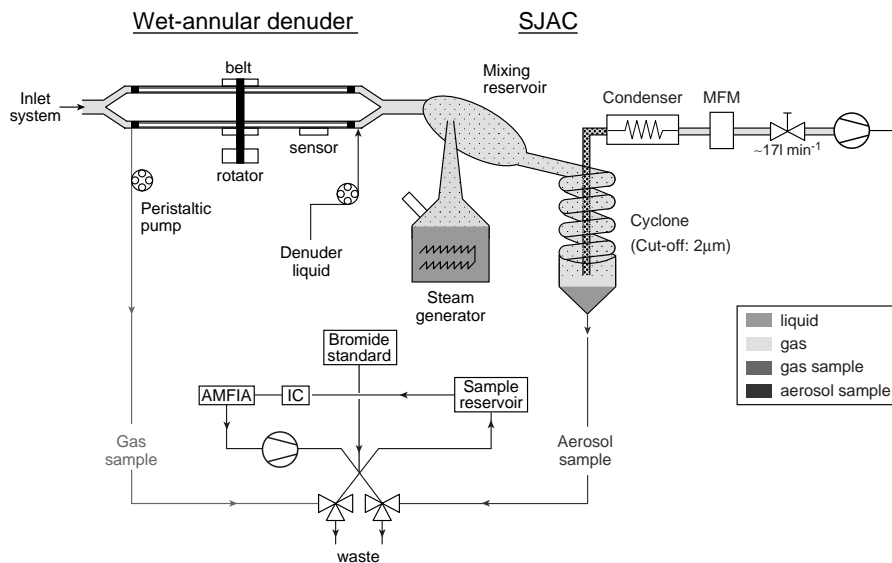


Figure 2.2: Simplified sketch of the WAD/SJAC system including analytical part.

After the sample air passed the steel elbow and/or pre-impactor and the PFA Teflon tubing, it entered a horizontally aligned WAD that scavenges soluble gaseous species. Trace gases (such as NH_3 , HNO_3 , HNO_2 , HCl and SO_2) were collected in a $10^{-4} \text{ M NaHCO}_3$ absorption solution. The liquid input was controlled automatically by an infrared sensor and a switching valve and the liquid was continuously pumped out of the denuder at a flow rate of $0.5 - 0.6 \text{ ml min}^{-1}$ by a peristaltic pump. The liquid effluent was collected in a sample reservoir (“gas sample”, see Fig. 2.2). Artifacts due to evaporation of aerosol phase species in the WAD can be excluded because the characteristic time for formation / evaporation of NH_4NO_3 is $> 10 \text{ s}$ [Dlugi, 1993], while the mean residence time of the sample air in the WAD is $\sim 0.002 \text{ s}$ (annulus volume: 0.0018 l , flow rate: $\sim 17 \text{ l min}^{-1}$).

After the WAD, the air entered a reservoir where it was mixed with steam of highly purified water. The supersaturation causes aerosol particles to grow rapidly (within 0.1 s) into droplets of at least $2 \mu\text{m}$ diameter. These droplets, containing the dissolved aerosol species were then collected in a cyclone [Khlystov *et al.*, 1995]. The

cyclone effluent (“aerosol sample”) was transferred into the sample reservoir by a peristaltic pump at a flow rate of $0.5 - 0.6 \text{ ml min}^{-1}$.

Collection of liquid samples in the sample reservoir and the following analytical cycles were performed successively for gas and aerosol sample. On-line analyses were carried out using a mobile IC with suppressed conductivity detection. The system was operated with an HPLC separation column (Dionex, IonPac AS12A, 4 mm) preceded by a guard column (Dionex, IonPac AG12A, 4x 50 mm). Samples were injected via a $199 \text{ } \mu\text{l}$ loop into $2.7 \text{ mM Na}_2\text{CO}_3 - 0.3 \text{ mM NaHCO}_3$ eluent. Internal Br^- standard addition using a peristaltic pump was performed continuously to calibrate the IC. The conductivity cell of the IC was temperature-stabilized at 30°C and therefore conductivity measurements were independent from room temperature.

Ammonium (NH_4^+) was determined by FIA [Wyers *et al.*, 1993]. The general principle is the addition of OH^- ions, converting NH_4^+ to NH_3 , which will then pass through a Teflon membrane and is taken up by highly purified water. Subsequent NH_4^+ -detection is based on conductometry. The conductivity cell of the FIA was not temperature controlled; therefore, conductivity measurements were dependent on temperature. Despite operating an air conditioner, diel temperature variations from 22°C at night to 30°C at daytime were observed in the laboratory. Fluctuations of the conductivity due to temperature changes in the air conditioned laboratory were corrected using:

$$\text{Condcorr} = \text{Cond} \times e^{(0.024 \times (20 - T))} \quad (2.4)$$

where *Condcorr* denotes the corrected conductivity value (mV), *Cond* is the original measured conductivity (mV) and *T* is the observed temperature ($^\circ\text{C}$) in the laboratory. The FIA was calibrated once every week using standard solutions of 50 ppb and 250 ppb NH_4^+ .

IC and FIA analyses were performed simultaneously for each sample. The analytical sample cycle was purged with ambient air after every run to avoid memory effects of the previous sample solution. The sampling system is fully automated and its software controls the sequence of sample injections and integrates detected peak areas. Cycle times for the successive analysis of aerosol and gas sample were set to 20 min (biomass burning season), 40 min (transition period) and 60 min (wet season).

Ambient mixing ratios for gas and aerosol species after IC analyses were determined using the following equation:

$$m = \frac{m_{liq} \times m_{Br(std)} \times Q_{Br} \times G \times M_{air}}{m_{Br} \times Q_{air} \times M_i} \quad (2.5)$$

where m is the ambient mixing ratio (ppb), m_{liq} is the mixing ratio of the compounds found in aerosol or gas sample (ppb), $m_{Br(std)}$ is the mixing ratio of the Br^- standard solution (ppb), Q_{Br} is the flow of the Br^- standard solution which is mixed into the liquid sample ($kg\ s^{-1}$), G is the factor to convert the molar weight of ionic compounds analyzed into the molecular weight of the corresponding trace gas (the factor is 1 for aerosol species). M_{air} is the molar mass of air at 298.15 K and 1000 hPa ($24.774\ kg\ kmol^{-1}$), m_{Br} is the analyzed Br^- mixing ratio (ppb), Q_{air} is the air mass flow through the system ($kg\ s^{-1}$) and M_i is the molar weight of compound i ($kg\ kmol^{-1}$). This equation is also valid for calculating ambient mixing ratios of NH_3 and aerosol NH_4^+ , except for parameters related to the Br^- standard addition and replacing Q_{Br} by Q_s , which is the liquid flow of “gas sample” (NH_3) or “aerosol sample” (NH_4^+) ($kg\ s^{-1}$).

2.4 Results and Discussion

The sampling period was chosen from 12 September to 14 November 2002, covering extensive biomass burning activity during the dry season (12 to 23 September), an intermediate phase (transition period, 07 to 31 October) and clean conditions during the wet season (01 to 14 November). Due to an instrument failure no samples were collected from 24 September to 7 October.

All results of our measurements of gas and aerosol species are presented as mixing ratios (ppb or $nmol\ mol^{-1}$). All quantities were calculated for standard conditions of 298.15 K, 1000 hPa and dry air, following the recommendations from *Schwartz and Warneck* [1995] and *Mills et al.* [1993].

2.4.1 Estimation of measurement uncertainty

The uncertainty of the measurements was estimated applying “Gaussian Error Propagation” to the relationship (2.5) which resulted in the following formula:

$$\sigma_m = m \times \sqrt{\left(\frac{\sigma_{m_{liq}}}{m_{liq}}\right)^2 + \left(\frac{\sigma_{m_{Br(std)}}}{m_{Br(std)}}\right)^2 + \left(\frac{\sigma_{Q_{Br}}}{Q_{Br}}\right)^2 + \left(\frac{\sigma_{m_{Br}}}{m_{Br}}\right)^2 + \left(\frac{\sigma_{Q_{air}}}{Q_{air}}\right)^2} \quad (2.6)$$

where σ_m is the estimated relative uncertainty of the ambient mixing ratio (ppb) and σ_x are the standard deviations of the corresponding parameters (see eq. 4.5). Equation (2.6) was also used to estimate uncertainties for ambient mixing ratios of

NH_3 and aerosol NH_4^+ , omitting the factors regarding Br^- standard addition and replacing Q_{Br} by Q_S and $\sigma_{Q_{Br}}$ by σ_{Q_S} .

Calculated total uncertainties σ_m for all measurements and compounds usually ranged from 10 – 15 %, indicating a reliable and stable performance of the instrument. The standard deviations σ_x contributing to the total measurement uncertainty σ_m including their sources are listed in Table 2.2.

Table 2.2: Standard deviations σ_x contributing to the total measurement uncertainty σ_m (index x is the mixing ratio of the compounds found in aerosol or gas sample (m_{liq}), the mixing ratio of the Br^- standard solution ($m_{Br(std)}$), the flow of the Br^- standard solution (Q_{Br}), the analyzed Br^- mixing ratio (m_{Br}) or the air mass flow through the system (Q_{air}), and index m is the ambient mixing ratio).

Standard deviations σ_x	Value/ Range	Source/ Determination	Mean contribution to σ_m
IC analyses			
$\sigma_{m_{liq}}$	0.002 - 6.8 ppb	5 % of m_{liq} , analysis of standard solutions	18 %
$\sigma_{m_{Br(std)}}$	20 ppb	2 % of $m_{Br(std)}$, estimated uncertainty of weighting procedures for creating Br^- standard solutions	2 %
$\sigma_{Q_{Br}}$	0.007 ml min ⁻¹	10 % of Q_{Br} , standard deviation of mean Q_{Br} for the entire experiment	57 %
$\sigma_{m_{Br}}$	2.9 - 12.0 ppb	5 % of m_{Br} , analysis of standard solutions	17 %
FIA			
$\sigma_{m_{liq}}(\text{gas})$	0.07–25.0 ppb	10 % of m_{liq} , analysis of standard solutions	84 %
$\sigma_{Q_S}(\text{gas})$	0.017 ml min ⁻¹	3 % of Q_S , standard deviation of mean Q_S for the entire experiment	10 %
$\sigma_{m_{liq}}(\text{aerosol})$	0.15–7.9 ppb	10 % of m_{liq} , analysis of standard solutions	57 %
$\sigma_{Q_S}(\text{aerosol})$	0.041 ml min ⁻¹	8 % of Q_S , standard deviation of mean Q_S for the entire experiment	37 %
$\sigma_{Q_{air}}$	0.02 - 10.6 l min ⁻¹	Standard deviation of mean Q_{air} for each sampling interval	6 %

For IC analyses, the contribution of $\sigma_{Q_{Br}}$ was highest (57 % of the total error, see Table 2.2) indicating that Br^- addition to the sample by the peristaltic pump is the largest source of measurement error. For FIA analyses, the value of $\sigma_{m_{liq}}$ had the highest contribution to σ_m (84 % and 57 % for NH_3 and NH_4^+ analyses, respectively). Reasons for that may be an incomplete removal of the temperature dependence by eq. (2.4), and also the temperature influence on the equilibrium constant of NH_4OH and the permeation of NH_3 through the membrane.

2.4.2 Limit of detection (LOD)

The accurate characterization and determination of the limit of detection is crucial for measurements in regions like the Amazon Basin since concentration levels can be extremely low during the wet season. The limit of detection ($LOD = 3\sigma$; σ = standard deviation of the background signal) was determined for actual field conditions for every individual data point and each compound. For anionic species analyzed with IC, the background noise (3σ) was calculated from the variation of the baseline at the beginning and the end of each chromatogram comprising 11 % ($n = 542$) of the total chromatogram data points. The limit of detection ($LOD = 3\sigma$) for the FIA analyses was determined analogously by background noise calculation before and after the NH_4^+ -peak, also comprising 11 % ($n = 111$) of the total measurements for each run. Frequency distributions of the LOD (given as atmospheric mixing ratios) for each compound during the entire field experiment are shown in histograms (Fig. 2.3). The determined median LOD values were 0.102 ppb for NH_3 , 0.011 ppb for HNO_3 , 0.012 ppb for HONO , 0.008 ppb for HCl , 0.004 ppb for SO_2 , 0.118 ppb for aerosol NH_4^+ , 0.015 ppb for NO_3^- , 0.009 ppb for NO_2^- , 0.008 ppb for Cl^- and 0.004 ppb for SO_4^{2-} . Higher LOD values (see Fig. 2.3), were a result of unstable and noisy baselines caused by insufficient purity of the water, which was used as matrix for the solutions applied during analyses. The LOD values obtained for FIA were about an order of magnitude higher than for IC, because of the influence of temperature on detection procedures.

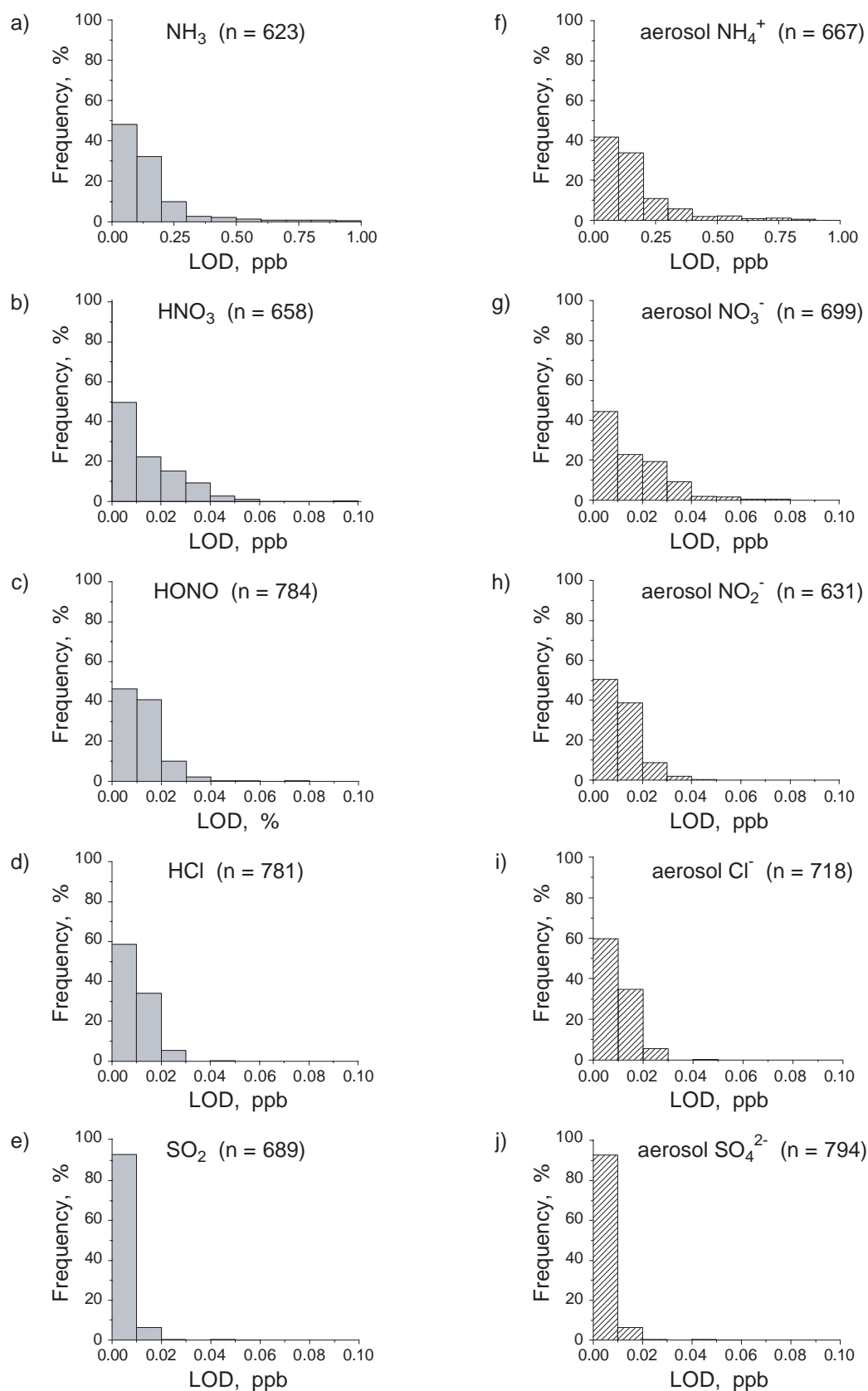


Figure 2.3 (a-j): Limit of detection (LOD) frequency distributions (given as atmospheric mixing ratios) of gaseous (a-e) and aerosol (f-j) species measured at FNS during SMOCC 2002 (n = total number of values).

2.4.3. Seasonal variation of mixing ratios

Measurements of 10 different compounds were performed during the field experiment which resulted in ~ 7000 data points of ambient mixing ratios. The proportion of rejected data points below the LOD was $\leq 20\%$ for all compounds, except for NH_3 and HNO_3 (25 %) and for aerosol NO_2^- (40 %).

Statistical illustrations of the seasonal pattern of mixing ratios are shown in Fig. 2.4 for gaseous compounds and in Fig. 2.5 for aerosol species.

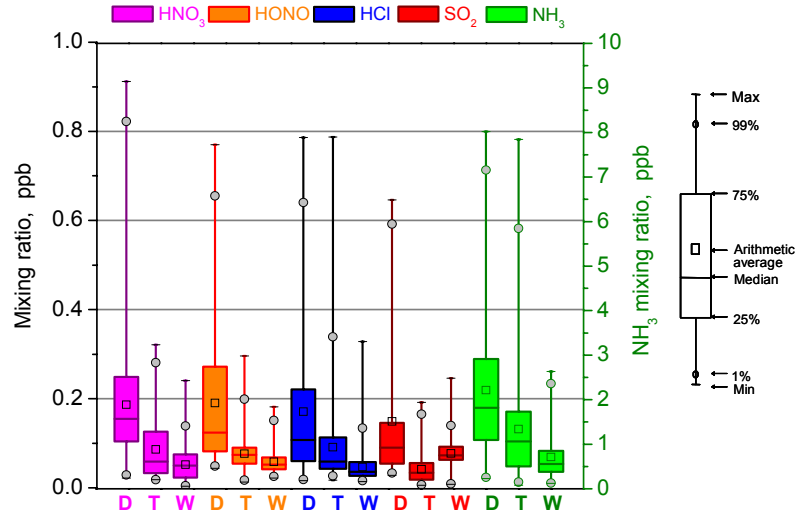


Figure 2.4: Box-and-whisker plots showing seasonal mixing ratio variations of gaseous compounds during dry season (D), transition period (T) and wet season (W) at FNS during SMOCC 2002.

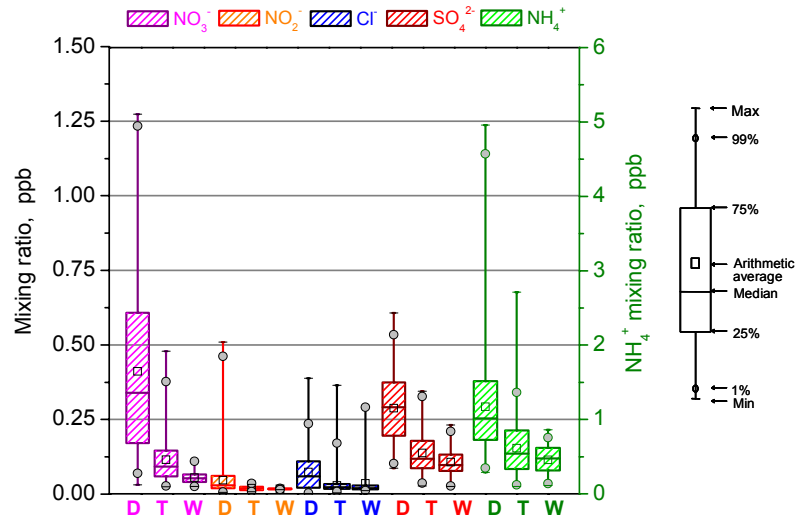


Figure 2.5: Box-and-whisker plots showing seasonal mixing ratio variations of aerosol species during dry season (D), transition period (T) and wet season (W) at FNS during SMOCC 2002. Aerosol measurements of bulk and fine fraction ($D_p \leq 2.5 \mu m$) were included.

A substantial decline of mixing ratio levels from dry season, through transition period to wet season was observed for all measured compounds. Gaseous NH_3 was abundant at mixing ratios an order of magnitude higher than acidic trace gases, and maxima reached 8 ppb under burning conditions. Correspondingly, aerosol NH_4^+ was also found to be at least 4 to 10 times higher than anionic aerosol species. Values of NH_3 and aerosol NH_4^+ declined by a factor of 2 - 3 from dry to wet season, suggesting that biomass burning is a strong source of these compounds. Also, NH_3 emissions from cattle waste contributed to the observed levels. The amount of NH_3 present during the wet season (~ 0.5 ppb, see Fig. 2.4), when biomass burning activity was nearly zero, is expected to be entirely attributed to biogenic emissions from vegetation (grass) or cattle manure.

All acidic trace gases showed mixing ratios within the same order of magnitude (0.01 – 0.9 ppb) and decreased by more than a factor of 2 to the wet season. SO_2 showed the lowest values (median < 0.1 ppb) and the least seasonal variation, suggesting that biomass burning is not a major source of this compound in this region. Mixing ratios of aerosol anions were highest during the biomass burning season. Unexpectedly, aerosol NO_3^- (max. ~ 1.25 ppb) was most abundant, followed by aerosol SO_4^{2-} (max. ~ 0.6 ppb). Aerosol NO_3^- dominated over SO_4^{2-} under biomass burning conditions and showed the strongest decrease to the wet season (factor ~ 4). Cl^- and NO_2^- contributed only very little to the aerosol inorganic composition and seasonal variations were smaller. Aerosol NH_4^+ in most cases exceeded the sum of NO_3^- , Cl^- and SO_4^{2-} equivalents. Consequently, other ions that were not measured by the WAD/SJAC system (e.g., dissociated organic acids, K^+ , Ca^{2+}) may play an important role for the aerosol ion balance at FNS. This matter will be addressed in full detail in chapter 3.

When widespread biomass burning occurred, NH_3 mixing ratios at this Brazilian rural pasture site were similar to values observed with the WAD/SJAC at an urban location [EPA Atlanta Supersite, 1999, *Zhang et al.*, 2002 and references therein]. Nevertheless, HNO_3 and HONO mixing ratios under burning conditions in the Amazon Basin were about five times lower than measured at the Atlanta Supersite [see *Genfa et al.*, 2003]. Aerosol NO_3^- measured with the SJAC system in Atlanta compared relatively well to the values observed in our study [see *Weber et al.*, 2003]. However, NH_4^+ was about five times and SO_4^{2-} an order of magnitude larger at the urban site [*Solomon et al.*, 2003; *Weber et al.*, 2003]. These results show that pollution in urban areas can be more severe than during biomass burning in the Amazon Basin.

2.4.4 Diel variations of trace gases

2.4.4.1 NH_3 and HNO_3

Fig. 2.6 shows diel cycles for NH_3 and HNO_3 from 17 to 20 Sep. 2002 (burning season), exhibiting a pronounced diel variation.

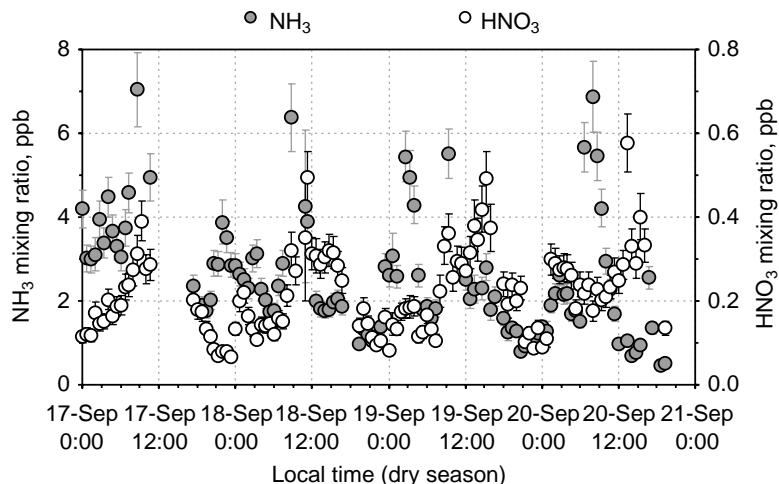


Figure 2.6: Diel variations of NH_3 and HNO_3 from 17 to 20 Sep. (biomass burning season) at FNS during SMOCC 2002. Error bars indicate measurement uncertainty for each data point.

NH_3 was relatively low from 1400 to 0500 LT (local time) (1 to 3 ppb), with one exception in the night from the 18 to 19 September. Usually, elevated NH_3 mixing ratios occurred from 0700 to 1000 LT with sharp peaks between 0800 and 0900 LT. However, these peaks did not correlate with wind speed or wind direction (not shown here). Presumably, this behavior is due to the increase of air temperature after sunrise causing re-evaporation of deposited NH_3 from wet surfaces (grass leaves). This is also discussed in more detail in chapter 3.

The diel variation observed for HNO_3 usually featured low values during the night from 1800 to 0600 LT (< 0.2 ppb) and high values at daytime reaching maxima around midday (0.4 to 0.6 ppb). Such diel cycles are typical for this compound and resemble those found in several other studies [e.g., *Tanner et al.*, 1989; *Meixner*, 1994; *Mehlmann and Warneck*, 1995; *Fehsenfeld et al.*, 1998; *Lefer et al.*, 1999; *Furutani and Akimoto*, 2002; *Huang et al.*, 2002; *Genfa et al.*, 2003]. The main reasons for this behavior are: (i.) intensive turbulent mixing from the free troposphere into the boundary layer during daytime, (ii.) deposition processes at night promoted by a stable thermal stratification of the nocturnal surface layer (limiting HNO_3 supply from residual layer), (iii.) higher temperature and lower relative humidity during daytime which enables evaporation of HNO_3 from the aerosol phase, and (iv.) daytime photochemistry (reaction of NO_2 with OH radical).

2.4.4.2 HONO

Spindler et al. [2003] have proposed a correction algorithm for artifact aqueous formation of HONO from dissolved NO_2 and SO_2 at wetted denuder walls. This has not been considered in our study for the following reasons: (i.) artifact HONO formation is only significant for alkaline aqueous solutions, whereas the pH of the absorption solution in our study was nearly neutral, (ii.) the observed SO_2 mixing ratios were at least 10 times lower (mostly < 0.3 ppb, see Fig. 2.4) than those relevant for artifact HONO formation according to *Spindler et al.* [2003], and (iii.) since the absorber liquid was continuously pumped through the denuder, the contact time of the gas with the liquid was limited to 2 or 3 minutes.

Fig. 2.7 shows diel patterns of HONO measured from 17 to 20 Sep. 2002 (biomass burning season) and from 17 to 20 Oct. 2002 (transition period). During the biomass burning season, HONO featured a pronounced diel cycle with higher values at night, reaching maxima just after 0000 LT (0.4 to 0.6 ppb). Heterogeneous reaction of NO_2 with surface water as reported recently by *Kleffmann et al.* [2003] may be regarded as a HONO source, especially for nighttime HONO accumulation at high relative humidities at the site. During the day, HONO levels were low, varying between 0.05 and 0.1 ppb. Similar HONO diel characteristics were observed in other studies [e.g., *Perner and Platt*, 1979; *Appel et al.*, 1990; *Harrison et al.*, 1996; *Huang et al.*, 2002; *Stutz et al.*, 2002; *Alicke et al.*, 2003]. Rapid photolysis during sunshine leads to a decline in HONO mixing ratios [*Harrison et al.*, 1996]. Moreover, our measurements in the Amazon Basin may be additional evidence for a continuous HONO source since a complete depletion at daytime did not occur.

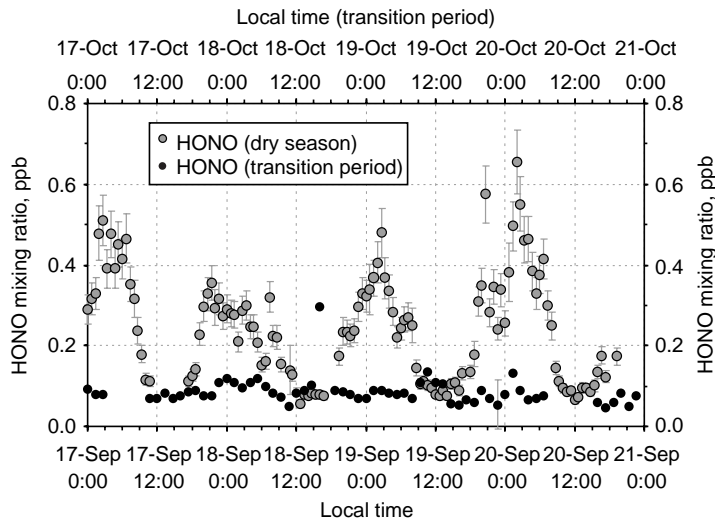


Figure 2.7: Diel variations of HONO from 17 to 20 Sep. (biomass burning season) and from 17 to 20-Oct. (transition period) at FNS during SMOCC 2002. Error bars indicate measurement uncertainty for each data point.

Diel patterns observed one month later (transition period, see Fig. 2.7) show distinctive differences to those observed during the biomass burning season. HONO levels were identical in daylight and during nighttime resembling those measured in daylight under biomass burning conditions. Since NO_2 is considered as the main reactant for heterogeneous HONO formation, obviously a declining NO_2 abundance under cleaner conditions will diminish HONO accumulation at night.

2.4.4.3 HCl and SO_2

Nighttime values of HCl and SO_2 (Fig. 2.8) were very low in the burning season (~ 0.05 to 0.1 ppb) while during daytime higher mixing ratios were found, with HCl exceeding SO_2 levels by a factor of two or three. The marked diel pattern of HCl has a maximum in the early to mid afternoon, which is generally coincident with the period of maximum concentration of HNO_3 , in agreement with several previous investigations [Graedel and Keene, 1995 and references therein]. While HCl is known to be emitted directly by biomass fires, accounting for a large fraction of the total emitted chlorine [Andreae et al., 1996], the observed SO_2 mixing ratios may have been largely caused by burning of charcoal and refuse nearby the site (Ouro Preto do Oeste). Apparently, turbulent mixing in an expanding boundary layer during daytime and a stable thermal stratification at night (deposition of acidic gases on wet surfaces) have caused diel fluctuations as shown in Fig. 2.8.

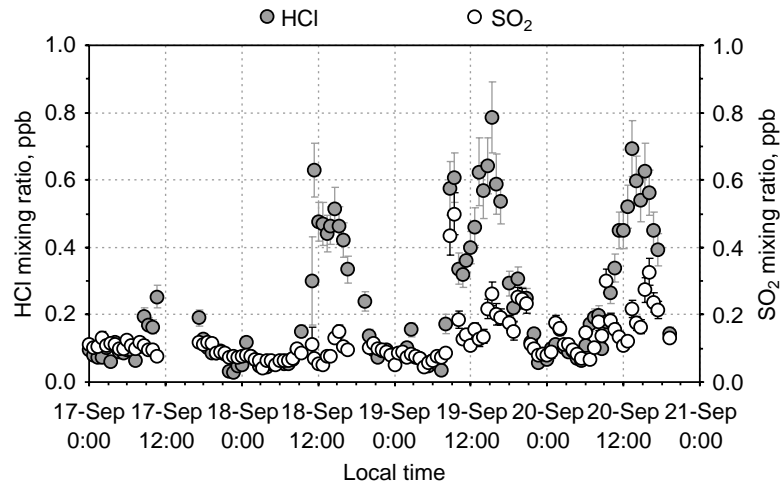


Figure 2.8: Diel variations of HCl and SO_2 from 17 to 20 Sep. (biomass burning season) at FNS during SMOCC 2002. Error bars indicate measurement uncertainty for each data point.

2.4.5. Diel variations of aerosol species

2.4.5.1 Aerosol NH_4^+ , NO_3^- and SO_4^{2-}

Observed diel variations for aerosol NH_4^+ , NO_3^- and SO_4^{2-} (fine fraction, $D_p \leq 2.5 \mu\text{m}$) from 17 to 20 Sep. 2002 are plotted in Fig. 2.9a. As for corresponding gaseous species, pronounced diel patterns were found for NH_4^+ and NO_3^- . Obviously, NH_4^+ was strongly influenced by its gas phase precursor NH_3 , peaking between 0800 and 0900 LT in the morning and revealing much higher mixing ratios than anionic aerosol species. Possible evaporation of NH_3 from wet surfaces at sunrise, when relative humidities were still high (see Fig. 2.9b and Section 2.4.4.1) might have caused a significant fraction of gaseous NH_3 to dissolve in still deliquescent aerosols, therefore enhancing aerosol NH_4^+ . Generally, NH_4^+ and NO_3^- began to increase at ~ 2200 LT and remained high during the night, while values found during daytime were usually two or three times lower (see Fig. 2.9a).

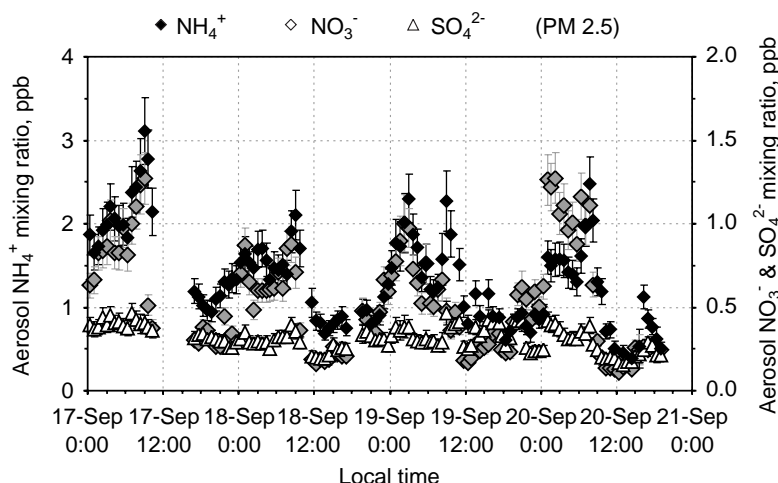


Figure 2.9a: Diel variations of aerosol NH_4^+ , NO_3^- and SO_4^{2-} (fine fraction, $D_p \leq 2.5 \mu\text{m}$) from 17 to 20 Sep. (biomass burning season) at FNS during SMOCC 2002. Error bars indicate measurement uncertainty for each data point.

Consequently, aerosol NO_3^- showed a strong anti-correlation to HNO_3 . The equilibrium assumption between NH_4NO_3 and its gas phase precursors, strongly affected by relative humidity and temperature, is expected to influence the measured gas and aerosol mixing ratios. High relative humidities and lower temperatures at night (Fig. 2.9b) should shift the equilibrium to the aerosol phase, causing the NH_4NO_3 content to increase and resulting in a simultaneous decrease of atmospheric gas phase constituents. At daytime, semi-volatile species can evaporate from the aerosol phase, induced by lower relative humidities and higher

temperatures (Fig. 2.9b), consequently raising the gas phase mixing ratios. The thermodynamic equilibrium assumption is discussed in chapter 3.

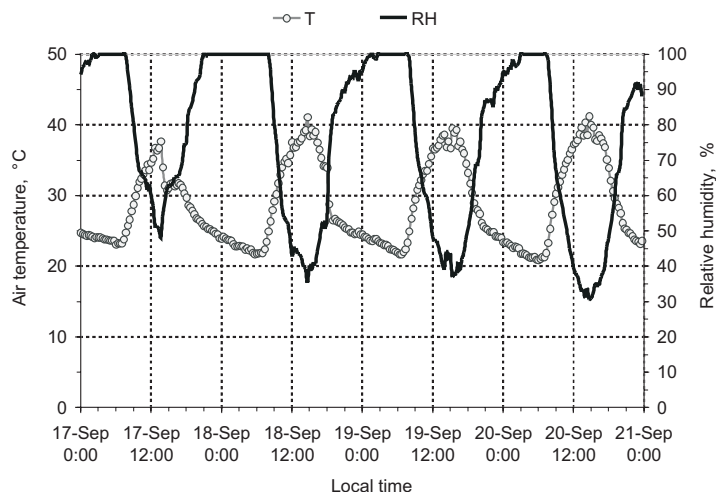


Figure 2.9b: Diel variations of air temperature and relative humidity measured in the polyethylene conduit from 17 to 20 Sep. (biomass burning season) at FNS during SMOCC 2002.

Time series of SO_4^{2-} did not show the same behavior. Mixing ratios were relatively stable throughout day and night, resembling those found for NO_3^- during daytime. Considering the non-volatility of SO_4^{2-} , relative humidity and temperature are not expected to influence the amount of SO_4^{2-} present in the sampled aerosol.

2.4.5.2. Aerosol Cl^- and NO_2^-

The diel cycles for aerosol Cl^- and NO_2^- (Fig. 2.10, fine fraction, $D_p \leq 2.5 \mu\text{m}$) during the burning season were less pronounced than for the other aerosol species. NO_2^- is higher at night, which may be an indication of heterogeneous HONO formation on aerosol surfaces. Cl^- mixing ratios featured less distinctive differences between day and night, suggesting that Cl^- may either be attached to NH_4^+ or also to involatile cations such as K^+ , Ca^{2+} and Na^+ , which are known to be present in fine and coarse mode biomass burning aerosols.

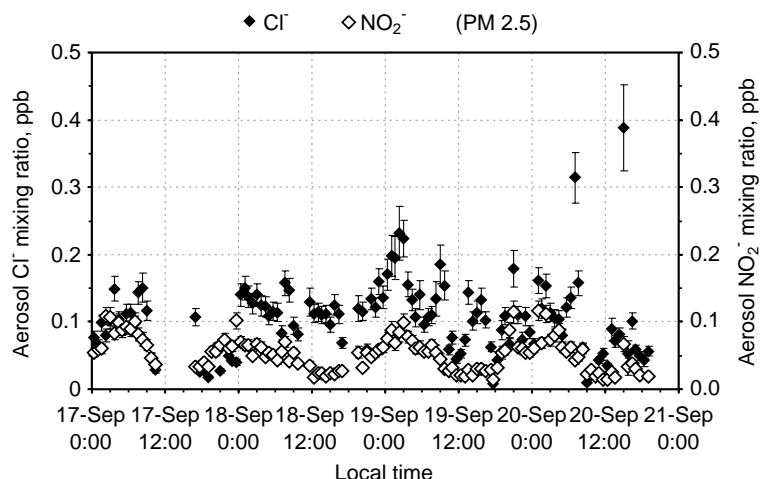


Figure 2.10: Diel variations of aerosol Cl^- and NO_2^- (fine fraction, $D_p \leq 2.5 \mu\text{m}$) from 17 to 20 Sep. (biomass burning season) at FNS during SMOCC 2002. Error bars indicate measurement uncertainty for each data point.

2.4.6. Diel characteristics of total ammonium, nitrate and chloride

The diel courses of aerosol species and their gaseous precursors presented in the previous sections are determined by (a) chemical production and loss, (b) horizontal and vertical transport within the planetary boundary layer, and (c) partitioning between gas and aerosol phase. Fig. 2.11(a-c) shows the temporal variation of total ammonium (aerosol $\text{NH}_4^+ + \text{NH}_3$), total nitrate (aerosol $\text{NO}_3^- + \text{HNO}_3$) and total chloride (aerosol $\text{Cl}^- + \text{HCl}$). For reasons of compactness and simplicity, diel variations are presented as medians with 0.25 and 0.75 percentiles of the individual data from 17 to 20 Sep. 2002 (dry season, biomass burning). In these figures, the influence of gas/aerosol partitioning is removed; thus they may give some insight to which extent gas phase chemistry and transport have caused the observed diel patterns.

Besides the sharp peaks occurring between 0800 and 0900 LT, total ammonium (Fig. 2.11a) did not exhibit a distinct diel pattern. Lower mixing ratios after midday may be attributed to turbulent mixing and dilution of air masses on a local scale. In contrast, total nitrate (Fig. 2.11b) was highest from midnight until 09:00. Apparently, this indicates accumulation of nitrate within the stable stratified nocturnal boundary layer, which was obviously dominated by the aerosol phase (see Fig. 2.9a). The decrease around noon may be attributed to the period of highest turbulent transport in the surface layer, which in turn might have caused a sizeable HNO_3 deposition to the grass surface. This period is followed by a slight increase of total nitrate in mid-afternoon indicating the influence of photochemical HNO_3 production. The diel cycle of total chloride (Fig. 2.11c) was clearly dominated by gaseous HCl (cf. Fig. 2.8 and 2.10). Since most of the chloride was present in the

gas phase, this diel variation was mainly determined by turbulent mixing at daytime and acid deposition to wet surfaces at night.

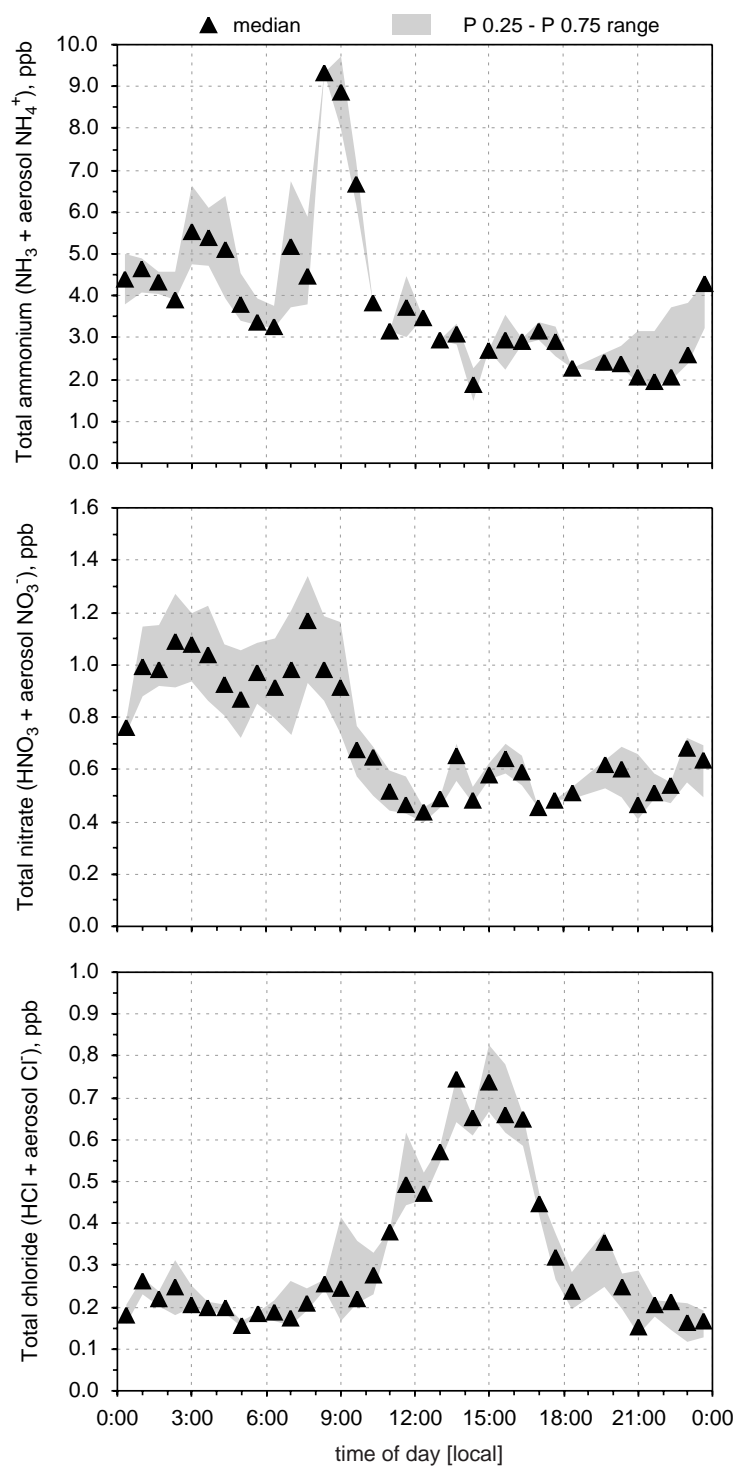


Figure 2.11a-c: Median diel variation of (a) total ammonium (aerosol $\text{NH}_4^+ + \text{NH}_3$), (b) total nitrate (aerosol $\text{NO}_3^- + \text{HNO}_3$) and (c) total chloride (aerosol $\text{Cl}^- + \text{HCl}$) covering a period during the biomass burning season (17-20 Sep.) at FNS during SMOCC 2002.

2.5 Conclusions

We employed a WAD/SJAC coupled with IC and ammonium FIA for the continuous measurement of NH_3 , acidic trace gases (HNO_3 , HONO , HCl and SO_2) and corresponding aerosol species (NH_4^+ , NO_3^- , NO_2^- , Cl^- and SO_4^{2-}) at a rural site in the Amazon Basin. A specially designed inlet system was applied for simultaneous sampling of gases and aerosols. Calculated inlet losses of aerosol species due to non-isokinetic sampling were below 3 % ($D_p \leq 2.5 \mu\text{m}$). HNO_3 is known as a problematic compound regarding absorption on inlet surfaces. Theoretical wall losses for HNO_3 were calculated to be ≤ 15 %, assuming an uptake coefficient of $\alpha_{\text{HNO}_3} = 0.5$ for the inlet surface.

Total measurement uncertainties of the mixing ratios in ambient air were usually below 15 %. The use of a peristaltic pump for the Br^- standard addition to calibrate the IC was found to have the greatest contribution (57 %) to the total measurement error. In order to reduce the influence of this factor, peristaltic pumps should be replaced by other devices (e.g., syringe pumps), which are capable to supply rather constant flows on a long-term scale.

The limit of detection ($LOD = 3\sigma$) was determined for each individual data point under actual field conditions. LOD median values remained below 0.015 ppb for all acidic trace gases and aerosol anions (IC analyses) but were higher (≤ 0.118 ppb) for NH_3 and aerosol NH_4^+ (FIA analyses). Higher background noises during NH_3 and aerosol NH_4^+ detection procedures were apparently caused by the temperature dependence of the FIA analyses, which should therefore be carried out under temperature controlled conditions in the future.

Widespread biomass burning in the Amazon Basin was found to be a strong source of NH_3 , present at mixing ratios about 3 times higher (max. ~ 8 ppb) than under clean conditions during the wet season. Also, levels of HNO_3 , HONO and HCl were considerably higher than during the wet season (at least two times) but were an order of magnitude lower (< 1 ppb) than NH_3 mixing ratios. The enhancement of gaseous compounds during the burning season significantly increased the amount of water-soluble inorganic aerosol constituents. Aerosol NH_4^+ was found to be at least 4 to 10 times higher than anionic aerosol species but declined substantially from dry to wet season. Generally, aerosol NO_3^- and SO_4^{2-} were the most abundant anions reaching maxima of 1.25 ppb and 0.6 ppb, respectively. During the biomass burning season, aerosol NO_3^- was the dominating anion and showed the strongest decrease to the wet season (~ 70 %). Aerosol NH_4^+ usually exceeded the sum of NO_3^- , Cl^- and SO_4^{2-} equivalents.

Additionally, N-containing gas and aerosol species exhibited pronounced diel variations, and both HCl and SO_2 varied distinctively with maxima at daytime and minima during the night. Turbulent mixing at daytime is considered to have a

major influence on the observed diel patterns, contributing to an increase of gaseous compounds at ground level. Deposition processes at night combined with high relative humidity and a stable thermal stratification of the nocturnal surface layer may cause a decline of trace gas mixing ratios (particularly HNO_3 , HCl and SO_2) at nighttime. Moreover, our measurements indicate that the partitioning between N-containing gas and corresponding aerosol constituents was dependent on relative humidity and air temperature, resulting in an enhancement of aerosol NO_3^- and NH_4^+ at nighttime. Non-volatile aerosol SO_4^{2-} did not show strong diel fluctuations and remained stable throughout day and night. Diel courses of total ammonium, nitrate and chloride (gas + aerosol) emphasize the role of photochemical HNO_3 production, vertical mixing as well as dry deposition of HNO_3 (daytime) and HCl (particularly nighttime) to the grass surface.

HONO showed a typical diel pattern when biomass burning occurred, exhibiting higher mixing ratios at night and lower values during daylight. Besides heterogeneous formation from NO_2 and surface water, our observations suggest a continuous HONO source since a complete depletion during sunlight hours did not occur.

Chapter 3 provides more detailed insights into aerosol ion balances and gas/aerosol partitioning processes at the FNS site. Additionally, the diel behavior of the measured species in combination with meteorological conditions is addressed.

The NH_4^+ - NO_3^- - Cl^- - SO_4^{2-} - H_2O aerosol system and its gas phase precursors at a pasture site in the Amazon Basin: How relevant are mineral cations and soluble organic acids?

I. Trebs, S. Metzger, F. X. Meixner, G. Helas, A. Hoffer, M.A.L. Moura, R. S. da Silva, Jr., Y. Rudich, A. H. Falkovich, P. Artaxo, J. Slanina and M. O. Andreae

(*Journal of Geophysical Research-Atmospheres* 110, D07303, doi:10.1029/2004JD005478, 2005)

Abstract. Real-time measurements of ammonia, nitric acid, hydrochloric acid, sulfur dioxide and the water-soluble inorganic aerosol species, ammonium, nitrate, chloride, and sulfate were performed at a pasture site in the Amazon Basin (Rondônia, Brazil). The measurements were made during the late dry season (biomass burning), the transition period, and the onset of the wet season (clean conditions) using a wet-annular denuder (WAD) in combination with a Steam-Jet Aerosol Collector (SJAC). Measurements were conducted from 12 Sep. to 14 Nov. 2002 within the framework of LBA-SMOCC (Large Scale Biosphere Atmosphere Experiment in Amazonia - Smoke Aerosols, Clouds, Rainfall and Climate: Aerosols from Biomass Burning Perturb Global and Regional Climate). Real-time data were combined with measurements of sodium, potassium, calcium, magnesium and low-molecular weight (LMW) polar organic acids determined on 12-, 24- and 48-hours integrated filter samples. The contribution of inorganic species to the fine particulate mass ($D_p \leq 2.5 \mu\text{m}$) was frequently below 20 % by mass, indicating the preponderance of organic matter. The measured concentration products of $\text{NH}_3 \times \text{HNO}_3$ and $\text{NH}_3 \times \text{HCl}$ persistently remained below the theoretical equilibrium dissociation constants of the $\text{NH}_3/\text{HNO}_3/\text{NH}_4\text{NO}_3$ and $\text{NH}_3/\text{HCl}/\text{NH}_4\text{Cl}$ systems during daytime ($\text{RH} < 90 \%$). The application of four thermodynamic equilibrium models (EQMs) indicates that the fine mode aerosol anions NO_3^- , Cl^- and SO_4^{2-} were balanced predominantly by mineral cations (particularly pyrogenic K^+) during daytime. At nighttime ($\text{RH} > 90 \%$) fine-mode NH_4NO_3 and NH_4Cl are predicted to be formed in the aqueous aerosol phase. Probably, Cl^- was driven out of the aerosol phase largely by reaction of pyrogenic KCl with HNO_3 and H_2SO_4 . As shown by an updated version of the equilibrium simplified aerosol model (EQSAM2), which incorporates mineral aerosol species

and lumped LMW polar organic acids, daytime aerosol NH_4^+ was mainly balanced by organic compounds.

3.1 Introduction

Widespread biomass burning emissions in the Amazon Basin significantly alter the chemical properties of the tropical pristine background atmosphere. This is reflected by elevated levels of carbon monoxide (CO), carbon dioxide (CO₂), nitric oxides (NO_x), ozone (O₃) and hydrocarbons (in particular methane (CH₄)) [Crutzen and Andreae, 1990]. When biomass burning takes place, particle number concentrations are enhanced by an order of magnitude compared to the clean conditions present during the wet season [Andreae et al., 2002; Artaxo et al., 2002; Guyon et al., 2003]. Amazonian aerosol particles consist, to a large extent of organic matter which often accounts for 90 % of the total aerosol mass, and 45 % to 75 % of the organic carbon (OC) is water-soluble [Andreae and Crutzen, 1997; Mayol-Bracero et al., 2002; Graham et al., 2003a]. Although inorganic aerosol compounds, mainly comprising ammonium (NH₄⁺), nitrate (NO₃⁻), chloride (Cl⁻), potassium (K⁺), and sulfate (SO₄²⁻), are minor components of Amazonian aerosols, they play a major role in the nucleation and growth of cloud droplets [Roberts et al., 2002]. Additionally, they may contribute efficiently to direct aerosol radiative forcing, which is strongly influenced by the water uptake of aerosols that accompanies an increase in RH [Pilinis et al., 1995]. In turn, aerosol chemical composition determines the water uptake as a function of ambient RH, and, concomitantly a change in RH affects gas/aerosol partitioning processes, hence increasing or decreasing the amount of semi-volatile aerosol species [Metzger, 2000].

Primary inorganic aerosol constituents such as sea-salt (NaCl) and mineral cations (K⁺, Ca²⁺, Mg²⁺) originate from sea-spray emissions and from soil dust or biomass burning emissions, respectively. These aerosol species are predominantly present in coarse mode aerosols ($D_p > 2.5 \mu\text{m}$). The fine mode of pyrogenic (biomass-burning derived) aerosols ($D_p \leq 2.5 \mu\text{m}$) usually contains a sizeable amount of K⁺ [Andreae, 1983]. All other inorganic aerosol components (NH₄⁺, NO₃⁻, SO₄²⁻ and to some extent Cl⁻) are formed by gas-to-particle conversion processes. Among these so-called secondary aerosol species, NH₄⁺ and SO₄²⁻ are mostly found in fine mode aerosols, whereas aerosol NO₃⁻ and Cl⁻ usually have bimodal size distributions. The presence of primary inorganic aerosol species sets up the initial aerosol inorganic composition by forming non-volatile salts (e.g., KCl, NaNO₃ and CaSO₄). Semi-volatile compounds, such as ammonium nitrate (NH₄NO₃) and ammonium chloride (NH₄Cl) are thought to form via reversible phase equilibria with gaseous ammonia (NH₃), nitric acid (HNO₃) and hydrochloric acid (HCl) [Pio and Harrison, 1987; Stelson et al., 1979]. These gas/aerosol equilibria are strongly dependent on ambient RH, temperature (T) and aerosol chemical composition. In chemical systems composed of NH₃, HNO₃, HCl, and H₂SO₄, the formation of non-volatile (NH₄)₂SO₄ is preferred [Seinfeld and

Pandis, 1998]. Only when NH_3 is available in excess of H_2SO_4 and when favorable meteorological conditions (low to moderate T and/or high RH) prevail, neutralization of HNO_3 and HCl vapor occurs. NH_3 and HCl are directly emitted by biomass fires [*Hegg et al.*, 1988; *Andreae et al.*, 1996], whereas the primary source of HNO_3 is the reaction of NO_2 with the OH radical in the troposphere during daytime. HNO_3 , HCl , H_2SO_4 and their salts are highly hygroscopic, therefore, aerosol-associated water plays a key role in gas/aerosol partitioning processes, particularly under very humid conditions in the tropics. An increase in RH causes the water activity of the aerosols to increase, leading to a decrease of solute molality which results in condensation of NH_3 , HNO_3 and HCl vapor [*Metzger et al.*, 2002].

Commonly, the simulation of gas/aerosol partitioning processes for inorganic compounds is performed by applying so-called thermodynamic equilibrium models (EQMs). Generally, EQMs are suitable to predict inorganic aerosol behavior for the $\text{NH}_4^+ - \text{NO}_3^- - \text{Cl}^- - \text{SO}_4^{2-} - \text{H}_2\text{O}$ system as shown by box model studies in temperate regions [e.g., *Ansari and Pandis*, 2000; *Ueda et al.*, 2000; *Zhang et al.*, 2002; *Kuhns et al.*, 2003]. As reported by *Fridlind and Jacobson* [2000] an EQM approach for inorganic species could explain observations over the Southern Ocean, where equilibrium was achieved between HNO_3 and fine mode aerosol NO_3^- . However, during that study, organic matter was not a dominant component of the measured aerosol. A possible effect of the presence of organic compounds on the inorganic gas/aerosol equilibrium was indicated by *Zhang et al.* [2002]. Although some attempts have been made to calculate the thermodynamic properties of soluble mixed inorganic/organic aerosols [e.g., *Clegg et al.*, 2001; *Pankow*, 2003], most of the widely used EQMs include inorganic aerosol species only.

To date, no information is available about inorganic gas/aerosol partitioning processes in the tropics. The first real-time measurements of NH_3 , HNO_3 , HCl , SO_2 and their chemically related aerosol species NH_4^+ , NO_3^- , Cl^- and SO_4^{2-} have been performed by us at a pasture site in southwest Amazonia (Rondônia, Brazil) (see chapter 2) during the LBA-SMOCC 2002 campaign (Large Scale Biosphere Atmosphere Experiment in Amazonia, Smoke Aerosols, Clouds, Rainfall and Climate: Aerosols from Biomass Burning Perturb Global and Regional Climate) [*Andreae et al.*, 2004]. In the present work we will use these results to study the characteristics of the inorganic gas/aerosol system in the Amazon Basin, which are expected to be mainly controlled by (i.) high RH and high temperatures, (ii.) the presence of mineral cations in the fine and coarse aerosol fraction, and (iii.) the dominance of organic matter. Diel variations of measured inorganic compounds in gas and aerosol phase and gas/aerosol partitioning coefficients (ratios aerosol / (gas + aerosol)) for ammonium, nitrate and chloride will be discussed in

detail. The fine mode aerosol ion balance in this region is studied by considering also mineral cations (K^+ , Ca^{2+} and Mg^{2+}) and low molecular weight (LMW) organic acids obtained from the analysis of aerosols collected on 12-, 24- and 48-hours integrated filter samples. Additionally, an evaluation of the thermodynamic equilibrium assumption under ambient conditions present at the measurement site is performed. We have applied four different EQMs, namely SCAPE2 [Kim *et al.*, 1993; Kim and Seinfeld, 1995; Meng *et al.*, 1995], ISORROPIA [Nenes *et al.*, 1998], GEFMN [Ansari and Pandis, 1999b], and EQSAM [Metzger *et al.*, 2002] to gain detailed insights into formation pathways of inorganic aerosol constituents under tropical conditions and to assess the influence of mineral cations on gas/aerosol partitioning processes. Information about the possible effect of LMW organic acids on the inorganic gas/aerosol system will be deduced from simulations using an updated version of EQSAM (henceforth referred to as EQSAM2), which includes lumped organic acids in addition to sea-salt and mineral cations [Metzger *et al.*, 2005].

3.2 Site description and methods

3.2.1 Measurement site

Field measurements were performed at a pasture site in the state of Rondônia, Brazil (Fazenda Nossa Senhora Aparecida (FNS), 10°45'44" S, 62°21'27" W, 315 m asl) located in the south-western part of the Amazon Basin. During the last 25 years, Rondônia has been progressively cleared of rain forest by slash and burn activities. The vegetation at FNS is dominated by grass (*Brachiaria brizantha*) with small patches of *Brachiaria humidicola* and very few isolated palms and bushes. The pasture is used as a cattle ranch. Near the site, flat hills (300 to 440 m) are located at a distance of 3 to 4 km. The towns Ouro Preto do Oeste (~ 40,800 inhabitants) and Ji-Paraná (~ 110,000 inhabitants) are situated approximately 8 km and 40 km to the ENE and ESE of the site, respectively. FNS is affected by widespread vegetation fires occurring every year in the state of Rondônia during the dry season (June through September). A more detailed description of the measurement site is given in Andreae *et al.* [2002] and Kirkman *et al.* [2002].

3.2.2 WAD/SJAC sampling and analysis

Air was sampled at a height of 530 cm above ground through a vertical polyethylene conduit with an inner diameter of 7 cm, protruding 150 cm above and 50 cm away from an air-conditioned wooden house where the sampling and analytical equipment was located. A sub-sample of the air was aspirated from the

center of the conduit's cross section area through a steel elbow (90° angle of steel tubing, inner surface PFA Teflon coated) or alternatively through a pre-impactor (PM 2.5 size cut; type 413, University Research Glassware, aluminum cyclone, PFA Teflon coated). Aerosol samples of either PM 2.5 ($D_p \leq 2.5 \mu\text{m}$) or total suspended particulate matter (TSP) were collected in alternating cycles (1-3 days). Soluble gases (NH_3 , HNO_3 , HCl and SO_2) were collected by a horizontally aligned, rotating wet-annular denuder (WAD) [Wyers *et al.*, 1993] which was continuously coated with a 10^{-4} M carbonate solution. Inorganic aerosol species (NH_4^+ , NO_3^- , Cl^- and SO_4^{2-}) were sampled continuously with a Steam-Jet Aerosol Collector (SJAC) [Khlystov *et al.*, 1995]. The resulting aqueous solutions of aerosol and gas were analyzed on-line using ion chromatography (IC) for anions and flow injection analysis (FIA) for ammonium (NH_4^+). Measurement intervals were set to 20 min (biomass burning season), 40 min (transition period) and 60 min (wet season). The measurement uncertainties of ambient mixing ratios as determined by Gaussian error propagation were below 15 % (cf. chapter 2). The median limit of detection ($\text{LOD} = 3\sigma$) was below 0.015 ppb for $\text{HNO}_3/\text{NO}_3^-$, HCl/Cl^- and $\text{SO}_2/\text{SO}_4^{2-}$ and was below 0.118 ppb for $\text{NH}_3/\text{NH}_4^+$ (cf. chapter 2). A detailed description and verification of the measurement method and of the inlet system can be found in Slanina *et al.* [2001] and in chapter 2.

3.2.3 Supporting measurements

In addition to the WAD/SJAC measurements, the following meteorological quantities were measured by an automatic weather station (AWS, 1 minute time resolution): wind speed and direction, air temperature, relative humidity, global radiation and surface wetness. The AWS was situated at a distance of ~ 20 m from the inlet of the WAD/SJAC system.

The total particulate mass (PM 2.5 and PM 10) was monitored on-line with an ambient particulate monitor (TEOM Series 1400a, Rupprecht & Patashnick Co., Inc). Furthermore, the overall inorganic and organic aerosol composition was determined using traditional filter sampling methods. Depending on the atmospheric aerosol concentration, the filter sampling periods were 12 hours daytime, 12 hours nighttime, 24 hours, and 48 hours. During the 24 and 48 hours sampling periods, sampling was performed during 2 or 3 consecutive days or nights, respectively. Aerosol samples (PM 2.0 and PM 10) were collected on Nuclepore filters using a Stacked Filter Unit (SFU) [Falkovich *et al.*, 2005]. The filter sampler was mounted at a height of 4 m above ground. Samples were stored at -25°C until analysis. Standard cation analyses were performed using a HPLC system (Varian ProStar; Detector: Dionex ED50 electrochemical detector) [cf. Falkovich *et al.*, 2005].

Fine mode aerosols ($\text{PM}_{2.5}$, $D_p \leq 2.5 \mu\text{m}$) were collected simultaneously on quartz filters (Pallflex Tissuquartz 2500 QAT-UP) using a high-volume dichotomous sampler (HVDS) [see *Mayol-Bracero et al.*, 2002 and references therein]. The sampling system was mounted on a tower 10 m above ground level. Loaded filters were placed in a prebaked glass jar and stored at -25°C until analysis. HVDS samples were analyzed by gas chromatography-mass spectrometry (GC/MS) for LMW polar organic acids [cf. *Graham et al.*, 2003b].

3.2.4 Thermodynamic equilibrium models (EQMs)

Four different EQMs, SCAPE2 [*Kim and Seinfeld*, 1995; *Kim et al.*, 1993; *Meng et al.*, 1995], ISORROPIA [*Nenes et al.*, 1998], GEFMN [*Ansari and Pandis*, 1999b], and EQSAM2 [*Metzger et al.*, 2002; *Metzger et al.*, 2005] were applied to simulate gas/aerosol partitioning at FNS. Table 3.1 shows the major features of these EQMs. All EQMs are based on the assumption that aerosol particles are internally mixed and that thermodynamic equilibrium exists between gas and aerosol phase. Based on these assumptions, EQMs explicitly calculate the equilibrium composition of the liquid or solid aerosol phase. The existence of an aqueous phase is determined by the lowest deliquescence RH of an inorganic salt compound (e.g., NH_4NO_3), or a hygroscopic salt mixture. It is generally agreed that ambient RH is not influenced by the deliquescence of aerosol particles, because of the large amount of water vapor present in the atmosphere compared to the aerosol water mass [*Metzger*, 2000]. This implies, neglecting the Kelvin effect, that the aerosol water activity is equal to ambient RH [*Bassett and Seinfeld*, 1983]. SCAPE2 is the most comprehensive EQM in terms of aerosol species considered, since it is the only model which explicitly incorporates mineral cations such as K^+ , Ca^{2+} and Mg^{2+} , while ISORROPIA is the most sophisticated EQM in terms of numerical accuracy. In ISORROPIA and SCAPE2 the equilibrium constant is derived for each single reaction [*Ansari and Pandis*, 1999a]. This results in a complex system of non-linear algebraic equations whose solution corresponds to a minimum of the Gibbs free energy. In contrast, the GEFMN model is based on an algorithm that directly minimizes the Gibbs free energy to meet the equilibrium condition of the system. Finally, the approach applied in EQSAM2 is the simplest one, since it uses a simplified, although rigorous, calculation of activity coefficients and solution molalities [*Metzger et al.*, 2002].

Table 3.1: Main characteristics of the thermodynamic equilibrium models applied for the simulation of inorganic gas/aerosol partitioning at FNS during LBA-SMOCC 2002 (parts of the table are taken from *Ansari and Pandis [1999a]*).

	EQSAM ¹	GEFMN ²	ISORROPIA ³	SCAPE2 ⁴
Species treated	Gas phase NH ₃ , HNO ₃ , HCl, H ₂ O			
Solid phase	Na ₂ SO ₄ NaHSO ₄ NaCl NH ₄ Cl NH ₄ NO ₃ (NH ₄) ₂ SO ₄ NH ₄ HSO ₄ (NH ₄) ₃ H(SO ₄) ₂ KCl, K ₂ SO ₄ KHSO ₄ , KNO ₃ CaCl ₂ , CaSO ₄ Ca(NO ₃) ₂ , MgCl ₂ MgSO ₄ , Mg(NO ₃) ₂	Na ₂ SO ₄ NaHSO ₄ NaCl NH ₄ Cl NH ₄ NO ₃ (NH ₄) ₂ SO ₄ NH ₄ HSO ₄ (NH ₄) ₃ H(SO ₄) ₂	Na ₂ SO ₄ NaHSO ₄ NaCl NH ₄ Cl NH ₄ NO ₃ (NH ₄) ₂ SO ₄ NH ₄ HSO ₄ (NH ₄) ₃ H(SO ₄) ₂	Na ₂ SO ₄ NaHSO ₄ NaCl NH ₄ Cl NH ₄ NO ₃ (NH ₄) ₂ SO ₄ NH ₄ HSO ₄ (NH ₄) ₃ H(SO ₄) ₂ KCl, K ₂ SO ₄ KHSO ₄ , KNO ₃ CaCl ₂ , CaSO ₄ Ca(NO ₃) ₂ , MgCl ₂ MgSO ₄ , Mg(NO ₃) ₂
Liquid phase	H ⁺ , NH ₄ ⁺ , Na ⁺ , NO ₃ ⁻ , Cl ⁻ , SO ₄ ²⁻ , HSO ₄ ⁻ , H ₂ SO ₄ , H ₂ O OH ⁻ , NH ₃ , Ca ²⁺ , Mg ²⁺ , K ⁺ , LMW organic acids	H ⁺ , NH ₄ ⁺ , Na ⁺ , NO ₃ ⁻ , Cl ⁻ , SO ₄ ²⁻ , HSO ₄ ⁻ , H ₂ SO ₄ , H ₂ O	H ⁺ , NH ₄ ⁺ , Na ⁺ , NO ₃ ⁻ , Cl ⁻ , SO ₄ ²⁻ , HSO ₄ ⁻ , H ₂ SO ₄ , H ₂ O, OH ⁻ , NH ₃	H ⁺ , NH ₄ ⁺ , Na ⁺ , NO ₃ ⁻ , Cl ⁻ , SO ₄ ²⁻ , HSO ₄ ⁻ , H ₂ SO ₄ , H ₂ O, OH ⁻ , NH ₃ , Ca ²⁺ , Mg ²⁺ , K ⁺
Multicomponent activity coefficient method	Theoretically derived [Metzger, 2000]	[Clegg <i>et al.</i> , 1997]	Bromley Pitzer	Kusik-Meissner Bromley Pitzer
Binary activity method	Theoretically derived [Metzger, 2000]	N/A	Kusik-Meissner	Kusik-Meissner
Temperature dependence of <i>DRH</i>	YES	YES	YES	YES
Composition dependence of <i>DRH</i>	YES	YES	YES	NO
Divided composition domain	YES	NO	YES	YES
Water activity	ZSR (Zdanovskii, Stokes and Robinson-relation)			

¹ EQSAM uses a simplified approach to calculate the equilibrium composition by which not all chemical reactions are explicitly solved for the liquid/solid partitioning and the aerosol water content (instead they are partly based on cation and anion ratios). However, the solute molalities and the aerosol activity (including activity coefficients) are theoretically derived and thus not empirically or semi-empirically in contrast to other approaches.

² GEFMN directly minimizes the Gibbs-free-energy based on thermodynamic data that are, however, not valid above *RH* > 94%.

³ ISORROPIA calculates the equilibrium composition based on high numerical accuracy and on either of the (semi-empirical) activity coefficient calculation methods depending on the aerosol composition.

⁴ SCAPE2 explicitly treats mineral cations and has an option to choose between the semi-empirical activity coefficient calculation methods. For this study, the Kusik-Meissner method was chosen.

The EQSAM2 approach implies that for atmospheric aerosols in equilibrium with ambient air, an increase in, e.g., NH_4NO_3 as a result of decreasing temperature and increasing RH is always associated with the condensation of a certain amount of water vapor [Metzger *et al.*, 2000]. Considering the change of aerosol water that is associated with an equilibrium reaction, the relationship between aerosol activity/solution molality and RH can be expressed using theoretically derived equations [Metzger *et al.*, 2002]. In this study we have applied an updated version of EQSAM (namely EQSAM2) that incorporates, besides sea-salt and mineral cations, lumped low molecular weight (LMW) polar organic acids, which, depending on their protonation constant, balance excess cations. The structure of EQSAM2 is the same as described in Metzger [2000], Metzger *et al.* [2002] and Metzger *et al.* [2005].

3.3 Results

Field measurements during SMOCC comprised three sampling periods. The first was a period of extensive biomass burning activity during the late dry season (12 - 30 September), the second an intermediate phase (transition period, 01 - 31 October) and the third represented fairly clean conditions during the onset of the wet season (01 - 14 November). Due to an instrument failure, no samples were collected with the WAD/SJAC system from 24 September to 7 October. In this study, we focus mainly on a period during the dry season (biomass burning, 12 - 23 September). Meteorological data were averaged and synchronized according to the time series obtained with the WAD/SJAC system.

3.3.1 Gas and aerosol phase mixing ratios

Table 3.2a-c presents an overview of average mixing ratios for the dry season, transition period and wet season for all measured species considered in this study. Individually identifiable LMW polar organic acids determined in aerosol particles (collected with the SFU or HVDS sampler (PM 2.5)) are grouped into three chemical classes: (i.) aliphatic mono-/di-/tricarboxylic acids (formic acid, acetic acid, oxalic acid, malonic acid, succinic acid, maleic acid, tricarballic acid), (ii.) aliphatic oxo-/hydroxyacids (glyoxylic acid, glycolic acid, lactic acid, glyceric acid, hydroxymalonic acid, malic acid, citric acid) and (iii.) aromatic carboxylic acids (3-hydroxy-benzoic acid, 4-hydroxy-benzoic acid, vanillic acid, syringic acid, phthalic acid) [cf. Falkovich *et al.*, 2005]. The least and the most abundant species in each class determine the ranges given in Table 3.2c.

Except for Na^+ , mixing ratios of all compounds showed at least a 2-fold decrease from the dry season (biomass burning) to the wet season (clean

conditions), indicating that biomass burning is a significant source of these species. Inorganic ionic aerosol composition at FNS was dominated by NH_4^+ , being present in mixing ratios at least 3 times higher than other ions (chapter 2). This was obviously caused by its gaseous precursor NH_3 , which was an order of magnitude more abundant than other water-soluble trace gases (see Table 3.2a). Other important inorganic ions contributing to the fine aerosol mass (PM 2.5) at FNS were K^+ , NO_3^- and SO_4^{2-} .

Table 3.2a-c: Average mixing ratios \pm standard deviation for (a) NH_3 , aerosol NH_4^+ , HNO_3 , aerosol NO_3^- , HCl , aerosol Cl^- , SO_2 and aerosol SO_4^{2-} (measured with the WAD/SJAC system), (b) aerosol Na^+ , K^+ , Ca^{2+} and Mg^{2+} (SFU sampler, PM 2.5), and (c) ranges of mono-/di-/tricarboxylic acids, aliphatic oxo-/hydroxyacids, and aromatic carboxylic acids (SFU or HVDS sampler, PM 2.5). Data represent the late dry (biomass burning) season (12-23 September) (**D**), the transition period (07-31 October) (**T**) and the onset of the wet season (01-14 November) (**W**) at FNS during LBA-SMOCC 2002.

(a)

	NH_3 (ppb)	NH_4^{+*} (ppb)	HNO_3 (ppb)	NO_3^{-*} (ppb)	HCl (ppb)	Cl^-* (ppb)	SO_2 (ppb)	SO_4^{2-*} (ppb)
D	2.22 \pm 1.57	1.17 \pm 0.69	0.19 \pm 0.13	0.41 \pm 0.30	0.17 \pm 0.16	0.07 \pm 0.06	0.15 \pm 0.13	0.29 \pm 0.11
T	1.34 \pm 1.19	0.61 \pm 0.35	0.09 \pm 0.07	0.12 \pm 0.08	0.09 \pm 0.08	0.03 \pm 0.02	0.04 \pm 0.03	0.14 \pm 0.07
W	0.72 \pm 0.56	0.46 \pm 0.19	0.07 \pm 0.04	0.06 \pm 0.02	0.05 \pm 0.04	0.04 \pm 0.05	0.08 \pm 0.03	0.11 \pm 0.04

* Data of TSP and PM 2.5 aerosol measurements were included in average values

(b)

	Na^+ (ppb)	K^+ (ppb)	Ca^{2+} (ppb)	Mg^{2+} (ppb)
D	0.016 \pm 0.022	0.527 \pm 0.180	0.152 \pm 0.102	0.039 \pm 0.029
T	0.021 \pm 0.017	0.106 \pm 0.038	0.021 \pm 0.015	0.011 \pm 0.007
W	0.028 \pm 0.013	0.032 \pm 0.007	0.017 \pm 0.011	0.006 \pm 0.003

(c)

	mono-/di-/tricarboxylic acids (ppb)	aliphatic oxo- /hydroxyacids (ppb)	aromatic carboxylic acids (ppb)
D	0.003 to 0.133	0.003 to 0.066	0.008 to 0.021
T	0.001 to 0.058	0.002 to 0.027	0.00 to 0.007
W	below detection limit	below detection limit	below detection limit

Total PM 2.5 decreased on average from $\sim 100 \mu\text{g m}^{-3}$ during the dry season, to $20 \mu\text{g m}^{-3}$ during the transition period to about $5 \mu\text{g m}^{-3}$ during the wet season (Fig. 3.1 (top)). The contribution of inorganic species to PM 2.5 showed a 4-fold increase from dry season to wet season. However, the contribution of inorganic species to total PM 2.5 always remained below 20 % (Fig. 3.1 (bottom)).

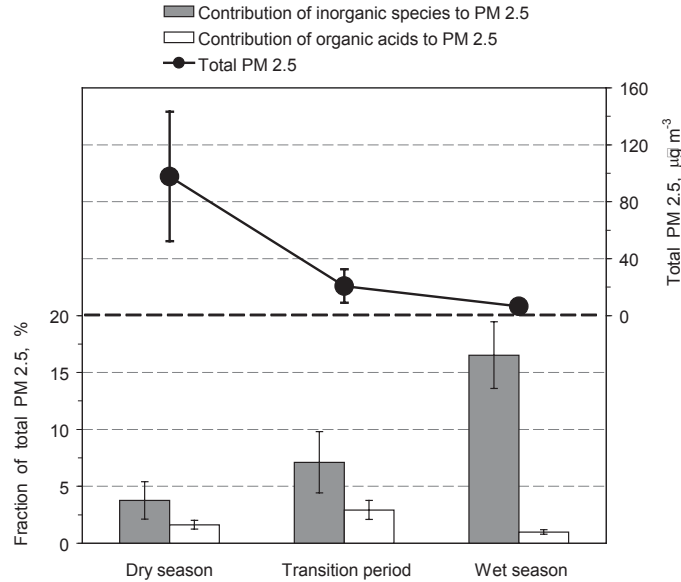


Figure 3.1: Average fine particulate mass (PM 2.5) (top), contribution of inorganic aerosol species to PM 2.5 (NH_4^+ , NO_3^- , Cl^- and SO_4^{2-} measured by the WAD/SJAC system and Na^+ , K^+ , Ca^{2+} , Mg^{2+} measured by the SFU sampler) and contribution of organic acids (the sum of species considered in this study measured by SFU and HVDS sampler) to PM 2.5 (bottom) for the late dry (biomass burning) season, transition period and the onset of the wet season at FNS during LBA-SMOCC 2002 (error bars indicate standard deviations of averages).

Neglecting a few other elements (e.g. Al, Zn, Si), which were not included in this study, 80 – 95 % of PM 2.5 can be attributed to organic matter. The contribution of organic acids to PM 2.5 was of minor importance and showed only marginal differences between the three different seasons (Table 3.2c, Fig. 3.1 (bottom)). The low seasonal variability of the organic acids may be related to the fact that they are associated with biogenic secondary organic aerosol (SOA) in addition to their pyrogenic sources. SOA are known to be a product of the photooxidation of volatile organic compounds (VOCs) that are emitted from the rain forest [see *Graham et al.*, 2003b, and references therein]. Organic acids are highly polar and may absorb water over the entire RH range [*Saxena and Hildemann*, 1997]. It should be noted that during LBA-EUSTACH-2 (1999) (biomass burning season), the overall sum of monocarboxylic, dicarboxylic, and

polycarboxylic acids accounted for about 51% of the water-soluble organic carbon (WSOC) at the FNS site [Mayol-Bracero *et al.*, 2002].

3.3.2 Meteorological conditions

The average meteorological conditions during 12 - 23 September (dry season, biomass burning) at FNS are presented in Fig. 3.2a-d. Daytime (0900 to 1700 LT) wind speeds (Fig. 3.2a) varied between 2 and 3 ms^{-1} . In contrast, nighttime wind speeds were very low, ranging from 0.5 to 1 m s^{-1} . This diel variation is a result of thermodynamic boundary layer characteristics observed frequently in the Amazon Basin [e.g., Nobre *et al.*, 1996; Fisch *et al.*, 2004]. Nighttime radiative cooling results in the formation of a shallow, nocturnal boundary layer of high thermodynamic stability and very low wind speeds. The growth of a convectively mixed layer starts with the heating of the surface in the morning. The daytime boundary layer is characterized by elevated wind speeds and strong turbulence. The wind direction (Fig. 3.2b) showed a diel variation with winds mostly originating from the S-SE sector during daytime and from the W-SW sector during nighttime hours. This wind system was most likely orographically induced by the channeling effect of small hills near the FNS pasture site. During mid-afternoon (1400-1500 LT) winds typically came from the E-NE sector coinciding with the direction of the town Ouro Preto do Oeste.

Ambient temperatures (Fig. 3.2c) exhibited a regular and pronounced diel cycle with high values (33-36°C) between 1200 and 1500 LT, while during nighttime (2300-0700 LT) temperatures were below 25°C, dropping to 22°C between 0600 and 0700 LT. The diel variation of relative humidity (RH) at FNS revealed the opposite pattern; between 0430 LT and 0730 LT RH was close to 100 %, and remained above 70 % until 0900 LT. The noontime maximum of the global radiation flux (Fig. 3.2d) reached 800 - 900 W m^{-2} . The variance of the radiation data was very low until 1030 LT and increased remarkably in the early afternoon: this indicates early morning clear sky conditions and the development of convective cloudiness and/or the presence of smoke plumes from 1100 LT onwards. According to the results of surface wetness measurements (Fig. 3.2d), the grass canopy at FNS was covered by dew every night (2100 to 0730 LT). As soon as global radiation exceeded 200 W m^{-2} (0730 LT), dew layers evaporated within 1 hour and formed again when global radiation dropped below 100 W m^{-2} (1730 LT).

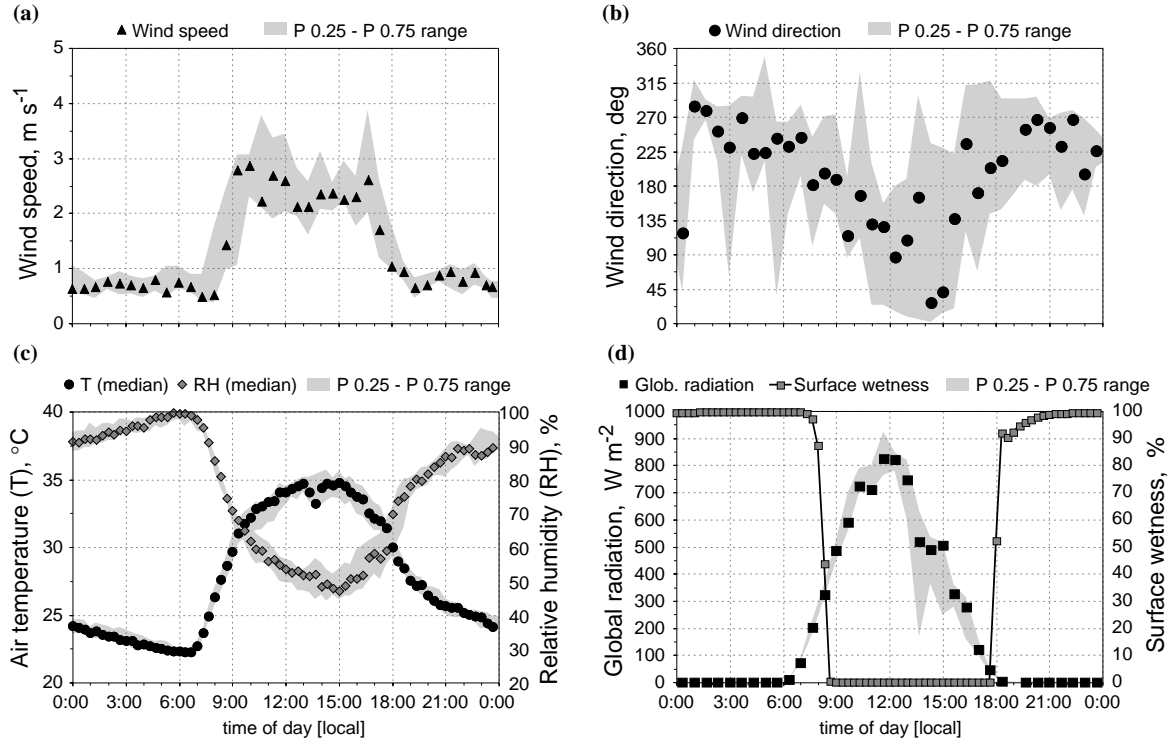


Figure 3.2a-d: Diel variations of (a) wind speed (b), wind direction, (c) air temperature (T) and relative humidity (RH), (d) global radiation flux and surface wetness during 12 - 23 September 2002 (dry season, biomass burning) at FNS during LBA-SMOCC 2002. Symbols and grey shading represent medians and interquartile ranges (0.25 to 0.75 percentiles), respectively.

The observed diel pattern of wind direction was diminished during the transition period (01 - 31 October) and the onset of the wet season (01 - 14 November). Through the transition period, characteristics of temperature and RH changed only marginally. However, minimum daytime RHs during the wet season were always above 55 %. Correspondingly, maximal temperatures were 2 to 5°C lower than during the dry season. Strong rain events ($\geq 30 \text{ mm h}^{-1}$) occurred in the afternoon hours (1300 to 1600 LT) during the transition period and the wet season.

3.3.3 Diel variations of species measured with the WAD/SJAC system

Fig. 3.3 a-h illustrates diel variations of the mixing ratios (median, 0.25 and 0.75 percentiles) of the trace gases NH_3 , HNO_3 , HCl , and SO_2 , as well as of inorganic aerosol species NH_4^+ , NO_3^- , Cl^- , and SO_4^{2-} (PM 2.5) during 12 - 23 September 2002 (dry season). Fig. 3.3a shows a sharp spike of NH_3 mixing ratios just before 0900 LT.

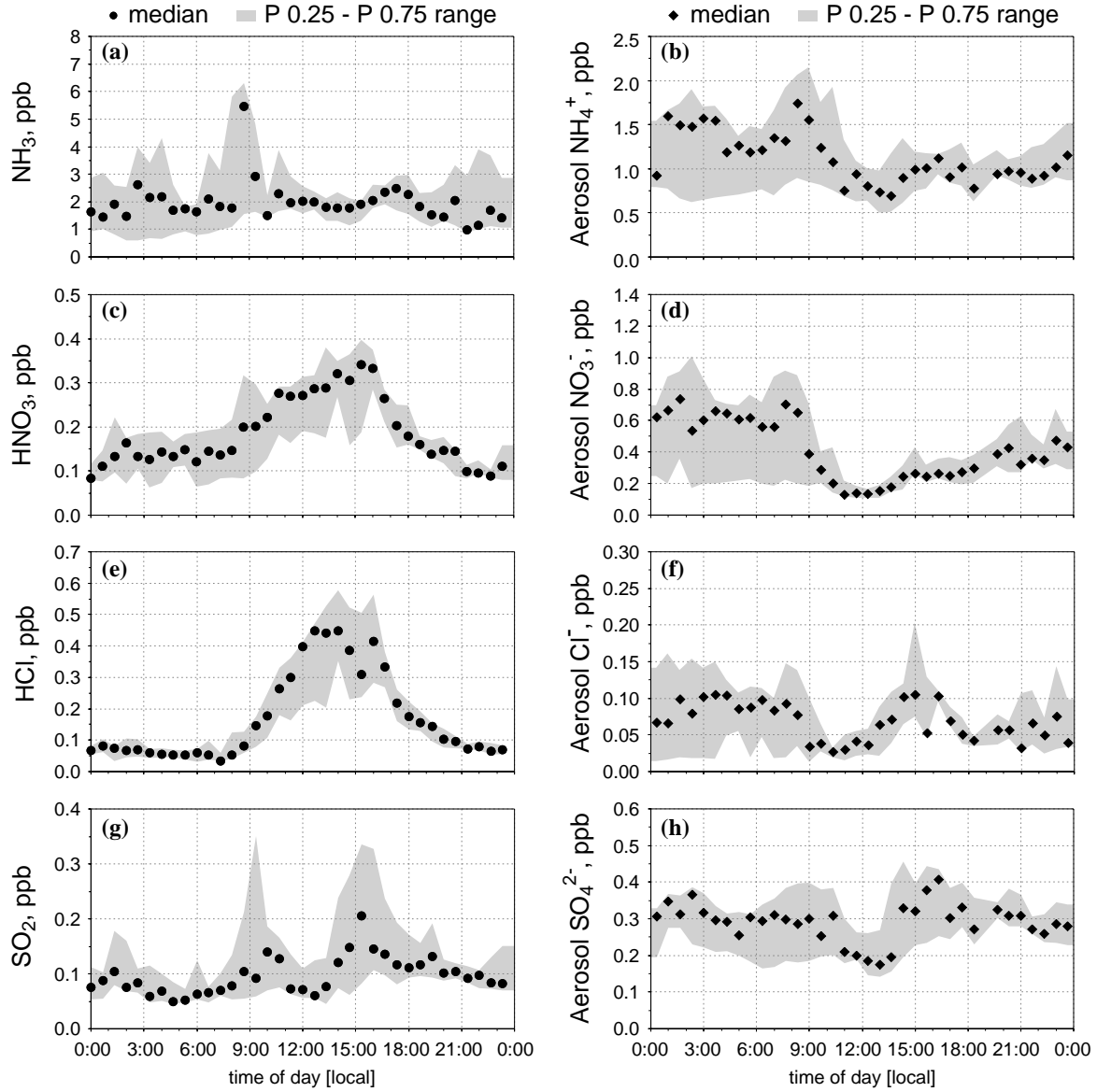


Figure 3.3a-h: Diel variations of (a) NH_3 (b) aerosol NH_4^+ (PM 2.5), (c) HNO_3 (d) aerosol NO_3^- (PM 2.5), (e) HCl , (f) aerosol Cl^- (PM 2.5), (g) SO_2 , and (h) aerosol SO_4^{2-} (PM 2.5) measured with the WAD/SJAC system during 12 - 23 September 2002 (dry season, biomass burning) at FNS during LBA-SMOCC 2002. Symbols and grey shading represent medians and interquartile ranges (0.25 to 0.75 percentiles), respectively.

This feature is considered to be attributed to the strong decrease of surface wetness (Fig. 3.2d), suggesting that NH_3 (most likely deposited and dissolved in epicuticular water films at nighttime) might evaporate in substantial amounts due to a temperature increase just after sunrise. This phenomenon was also observed in other studies [e.g., *Bussink et al.*, 1996; *Hesterberg et al.*, 1996]. During the same time period, an increase in aerosol NH_4^+ mixing ratio was observed (Fig.

3.3b). At still high RH (70 – 80 %, see Fig. 3.2c) it is likely that a significant fraction of NH_3 has dissolved in humid aerosols, thereby enhancing aerosol NH_4^+ . During the full expansion of the convective boundary layer after 0900 LT, surface air became more and more diluted by turbulent mixing with free tropospheric air, resulting in a decrease of NH_3 and aerosol NH_4^+ . Although NH_3 and aerosol NH_4^+ mixing ratios decreased significantly during the transition period and especially in the wet period, their diel courses were similar.

HNO_3 featured a typical diel cycle with high values at daytime and low values during the night (see Fig. 3.3c). Daytime maxima of ~ 0.4 ppb (median) occurred in the early afternoon hours. This diel variation was mainly caused by: (i.) turbulent mixing from the free troposphere into the boundary layer during daytime, (ii.) daytime photochemistry (reaction of NO_2 with OH radical), (iii.) evaporation of HNO_3 from the aerosol phase at daytime (high T and low RH) (see Fig. 3.2c), and (iv.) deposition of HNO_3 to wet vegetation elements at night (cf. chapter 2). It should be noted that HNO_3 mixing ratios remained unexpectedly high during nighttime. Within a thermodynamically stable stratified nocturnal boundary layer, it is expected that the very sticky and water-soluble HNO_3 molecule will rapidly deposit to wet surfaces, which should be reflected by very low mixing ratios. The relatively high nighttime HNO_3 mixing ratios might be due to heterogeneous HNO_3 formation initiated by the reaction of NO_2 with O_3 [Calvert *et al.*, 1985]. In contrast, the median diel pattern of aerosol NO_3^- is characterized by high mixing ratios at night and low values during daytime (Fig. 3.3d). Maximal mixing ratios occurred between 0000 and 0900 LT. Apparently, this was due to accumulation of NO_3^- in the aerosol phase under very humid conditions (Fig. 3.2c) within a thermally stable nocturnal boundary layer. Lower RH during daytime may enable evaporation of NO_3^- from the aerosol phase leading to a decrease of corresponding mixing ratios (see section 3.3.4).

The median diel pattern of HCl (Fig. 3.3e) is comparable to that of HNO_3 . However, nighttime mixing ratios of HCl were lower than corresponding HNO_3 mixing ratios. This suggests that, unlike HNO_3 , HCl did not have significant chemical sources at nighttime, but its mixing ratios were largely depleted through deposition to wet grass surfaces. While mixing ratios of aerosol Cl^- were low (Fig. 3.3f), they resembled the diel variations of aerosol NO_3^- , with the exception of a sharp peak of aerosol Cl^- around 1500 LT.

SO_2 generally showed higher mixing ratios at daytime (Fig. 3.3g) and the diel course of aerosol SO_4^{2-} was characterized by relatively constant mixing ratios, except for the period 1100 to 1300 LT (Fig. 3.3h). Aerosol SO_4^{2-} is known to be non-volatile, and time scales for its chemical formation (photo-chemical oxidation of SO_2) are large [Calvert *et al.*, 1985]. Therefore, the diel cycle of aerosol SO_4^{2-} broadly reflects advection of air masses.

The 1100 - 1300 LT minimum of aerosol SO_4^{2-} coincides with minima of gaseous SO_2 , aerosol Cl^- , NO_3^- , and NH_4^+ . Around noon, convective mixing, high T and low RH (cf. Fig. 3.2c) generally resulted in lower mixing ratios of aerosol species. Around 1500 LT distinctively higher mixing ratios of gaseous SO_2 and aerosol Cl^- , and also somewhat higher values of aerosol NH_4^+ and NO_3^- and SO_4^{2-} were observed. This is the only time of the day when winds arrived from E-NE; carrying pollutants from the town Ouro Preto do Oeste to the site.

Except for NH_3 and aerosol NH_4^+ , the diel courses of gas and aerosol phase mixing ratios were less pronounced during the transition period. Generally, diel fluctuations were diminished under cleaner conditions during the onset of the wet season.

3.3.4 Gas/aerosol relationships

The FNS site can be characterized as an NH_3 -rich environment (see Table 3.2a). The ratio of NH_3 to SO_2 mostly exceeded a value of 10, reaching values up to 100. The average ratio of aerosol $\text{NH}_4^+/\text{SO}_4^{2-}$ was 4.4. High levels of NH_3 are attributed to emissions from cattle manure and to biomass burning during the dry season (chapter 2). Human activities in this region do not appear to be strong sources of SO_2 . The transfer of HCl and HNO_3 from the gas to the aerosol phase is generally controlled by the neutralization of H_2SO_4 with NH_3 . Due to the large excess of NH_3 vapor pressure over that of HNO_3 , HCl and SO_2 at FNS, chemical limitations for the transfer of HCl and HNO_3 to the aerosol phase are very unlikely. Fig. 3.4 emphasizes that $(\text{NH}_4)_2\text{SO}_4$ formation is favored over that of NH_4NO_3 , which implies that NH_4NO_3 is assumed to be formed only when H_2SO_4 is already consumed and NH_3 mixing ratios are still high.

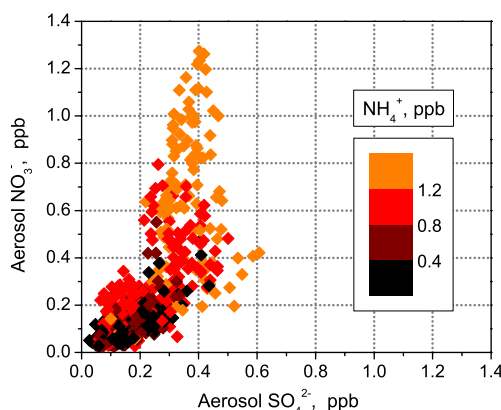


Figure 3.4: Aerosol NO_3^- versus SO_4^{2-} at different aerosol NH_4^+ mixing ratios (color coded) at FNS during LBA-SMOCC 2002. Results obtained with the WAD/SJAC system from all three seasons were combined ($n = 528$).

However, because of the limited H_2SO_4 and HNO_3 availability at the FNS site, excess NH_3 is expected to be largely neutralized by other acidic species. This will be investigated in detail below.

Gas/aerosol partitioning coefficients (ratios aerosol / (gas + aerosol)) for ammonium, nitrate and chloride are shown in Fig. 3.5a-f.

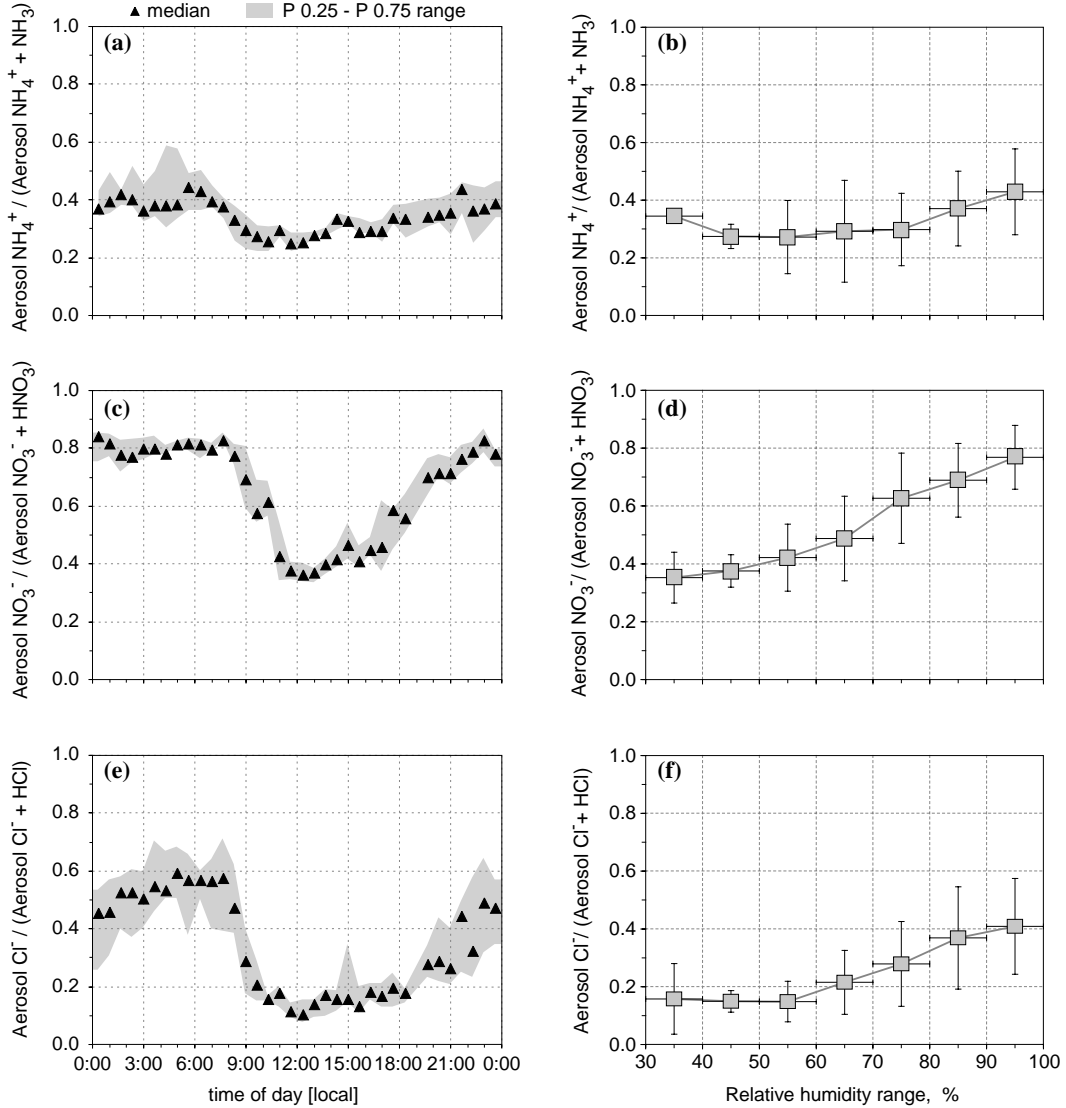


Figure 3.5a-f: (a) diel variation of aerosol NH_4^+ /total NH_4^+ ($n = 508$), (b) RH dependence of aerosol NH_4^+ /total NH_4^+ ($n = 508$), (c) diel variation of aerosol NO_3^- /total NO_3^- ($n = 483$), (d) RH dependence of aerosol NO_3^- /total NO_3^- ($n = 483$), (e) diel variation of aerosol Cl^- /total Cl^- ($n = 570$), and (f) RH dependence of aerosol Cl^- /total Cl^- ($n = 570$). For (a), (c) and (e) symbols and grey shading represent medians and interquartile ranges (0.25 to 0.75 percentiles), respectively. For (b), (d) and (f) y-error bars represent standard deviations of average ratios and x-error bars indicate RH range. Results obtained with the WAD/SJAC system from all three seasons at FNS during LBA-SMOCC 2002 were combined.

Although the diel course of the NH_4^+ partitioning coefficient (Fig. 3.5a) is not very pronounced, the fraction of aerosol NH_4^+ was slightly higher at night (0.4 – 0.5) and lower during daytime (0.2 – 0.3). The fraction of aerosol NH_4^+ started to increase at $\text{RH} > 80\%$ (Fig. 3.5b). In contrast, NO_3^- and Cl^- partitioning coefficients exhibited a remarkable dependence on RH (see Fig. 3.5d,f). The patterns of median diel cycles shown in Fig. 3.5c,e closely resemble that of RH (Fig. 3.2c). At nighttime, 80 % of the total NO_3^- was present in the aerosol phase. During daytime 60 % of the total NO_3^- was attributed to gaseous HNO_3 . A comparable behavior was found for Cl^- , although the fraction of aerosol Cl^- was lower than that observed for NO_3^- . At nighttime the maximum aerosol Cl^- fraction was only 0.4 – 0.5, decreasing to < 0.2 at daytime. Nevertheless, the difference of aerosol associated NO_3^- and Cl^- between day and night was identical (2- fold increase from day to nighttime). The higher NO_3^- aerosol fraction was most likely due to the strong tendency of HNO_3 to absorb on wet surfaces and subsequent uptake by the liquid phase. A similar finding was reported by *Mehlmann and Warneck* [1995] who showed that 95 % of the total NO_3^- was present in the aerosol phase at $\text{RH} = 85\%$.

It should be emphasized that the graphs in Fig. 3.5a-f were compiled including measurements from the late dry season, transition period and the onset of the wet season. Despite a strong decrease in the observed mixing ratios from the dry to the wet season, interquartile ranges and standard deviations in Fig. 3.5a-f are small. Obviously, partitioning of inorganic species between gas and aerosol phase at FNS is strongly controlled by ambient RH, regardless of season. Fig. 3.5a-f would reveal the opposite pattern for the temperature dependence of the partitioning coefficients, indicating that low temperatures favor condensation of gaseous compounds and high temperatures cause evaporation of semi-volatile species from aerosol particles.

3.4 Discussion

In order to explain the results presented above and to gain further insights into the complex gas/aerosol system at this tropical site, the aerosol ion balance and gas/aerosol partitioning processes will be discussed in the following sections. For the latter, thermodynamic theory is considered with the aid of four different EQMs.

3.4.1 Charge balance of ionic aerosol species

Electrical charge balances of the observed ionic aerosol components are a useful tool to test the accuracy of measurements and to judge on missing anions or cations. The ion balance presented in Fig. 3.6a considers only the ions measured with the WAD/SJAC system (NH_4^+ , NO_3^- , Cl^- and SO_4^{2-} , PM 2.5). The error bars represent measurement uncertainties determined by Gaussian error propagation based on results from chapter 2. The mean uncertainty is $\sim 8\%$ for the sum of anions (NO_3^- , Cl^- and SO_4^{2-}) and $\sim 14\%$ for NH_4^+ . NH_4^+ correlates well with the sum of NO_3^- , Cl^- and SO_4^{2-} equivalents ($r^2 = 0.67$, $n = 260$). The median cation/anion ratio for this case was 1.20 (P 0.25 = 0.99 and P 0.75 = 1.46) suggesting that there is abundant NH_3 to neutralize HNO_3 , HCl and H_2SO_4 . However, it can be argued that $\sim 20\%$ of the NH_4^+ present in the sampled fine mode aerosols must be balanced by additional counter ions that were not measured by the WAD/SJAC system.

In order to complete the ion balance, data obtained from the SFU and HVDS samplers (PM 2.5) are included (Fig. 3.6b,c). To allow for comparison of samples collected with different time resolutions, we assumed constant ambient mixing ratios determined on 12-, 24- and 48-hours integrated filter samples. Filter data were assigned to the corresponding data points obtained with the WAD/SJAC system every 20-, 40- and 60-min during the respective 12-, 24- and 48-hour interval. The inclusion of additional cations (Na^+ , K^+ , Ca^{2+} and Mg^{2+}) as shown in Fig. 3.6b, results in a significant shift of the charge balance away from the 1:1 relationship. For this case, the mean measurement uncertainty (error bars in Fig. 3.6b) is $\sim 8\%$ for the sum of anions and $\sim 10\%$ for the sum of cations. The median cation/anion ratio is now 2.18 (P 0.25 = 1.69 and P 0.75 = 2.96), strengthening the hypothesis that additional anions are necessary to balance aerosol cationic charges. This significant shift was primarily caused by the high abundance of K^+ in the fine mode aerosol (see Table 3.2b), which is directly emitted by biomass fires and vegetation in this region [Allen and Miguel, 1995; Yamasoe *et al.*, 2000 and references therein].

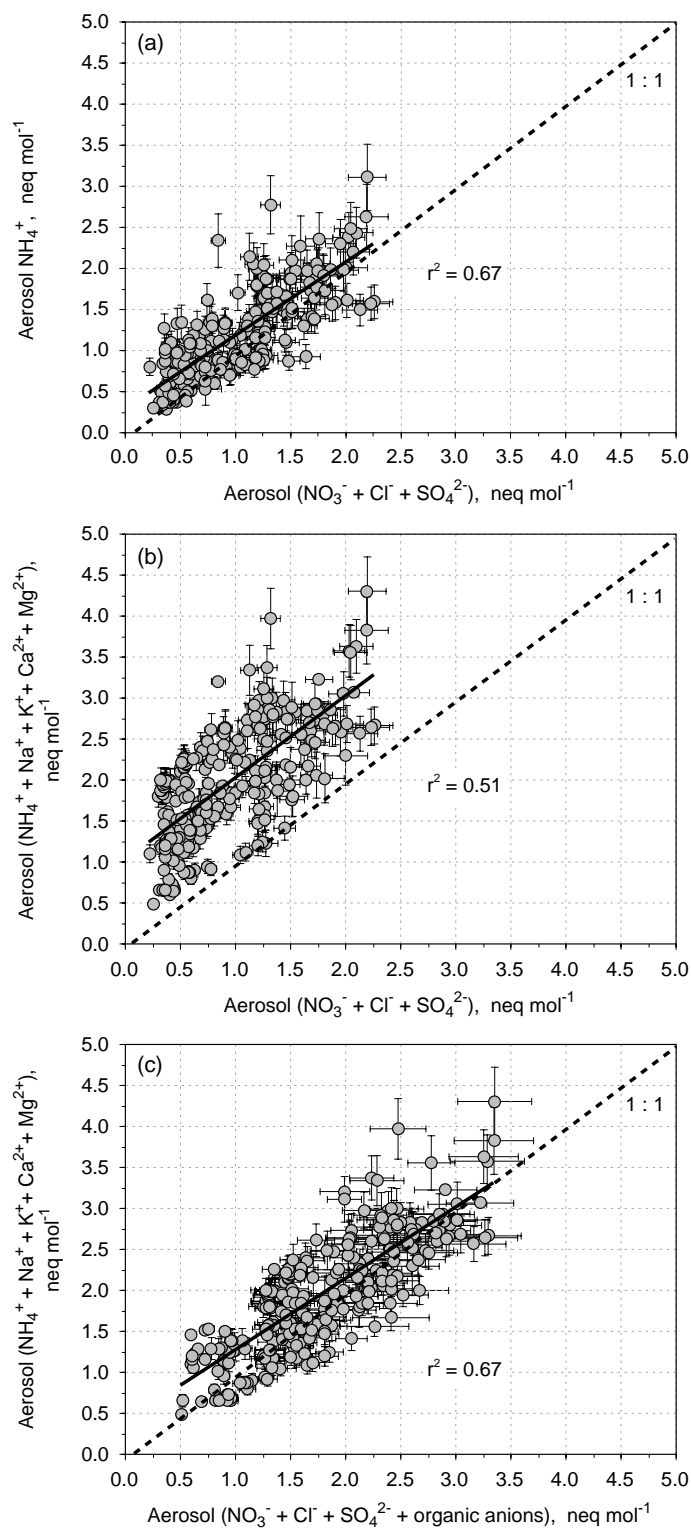
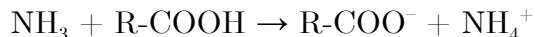


Figure 3.6a-c: Balances between anionic and cationic charges of the aerosol fine fraction (PM 2.5) sampled at FNS during SMOCC 2002 ($n = 260$): (a) balance for anions and cations measured with the WAD/SJAC system, (b) same as (a), but cation data (Na^+ , K^+ , Ca^{2+} and Mg^{2+}) from the SFU sampler are included, and (c) same as (b), but the sum of organic anions obtained from SFU and HVDS samplers are included.

Kerminen et al. [2001] and *Lee et al.* [2003] proposed that the presence of water-soluble organic anions may be of importance for the aerosol charge balance. Due to the high mixing ratios of gaseous NH_3 at our sampling site (see Table 3.2a) sufficient alkaline material to neutralize (deprotonate) organic acidic aerosol species (shown in Table 3.2c) may be provided:



The organic compounds included here belong to the group of the weak acids. As a first approximation, equivalent moles were calculated assuming that mono-, di-, and tricarboxylic acids form the respective mono-, di-, and tri-ammonium salts, which means they may donate all H^+ to neutralize NH_3 . Since the pH of the sampled aerosol is not known, it is difficult to estimate the degree of acid dissociation, but we may speculate that full acid dissociation occurred due to the excess of NH_3 available at the site. In Fig. 3.6c organic acids are added to the ionic charge balance accounting for the total of carboxylic groups. The mean measurement uncertainty (error bars in Fig. 3.6c) determined by Gaussian error propagation for anions including organic acids is $\sim 10\%$. The median cation/anion ratio for this case is 1.06 ($P\ 0.25 = 0.90$ and $P\ 0.75 = 1.31$), approaching a 1:1 ratio of cationic and anionic charges ($r^2 = 0.67$, $n = 260$). The remaining discrepancy between the measured anionic and cationic charges is only $\sim 6\%$. However, assuming that only mono-ammonium salts form from all carboxylic acids (except oxalic acid), this discrepancy increases to $\sim 27\%$. It has to be considered here that the sum of cationic and anionic charges is not complete. Species that are not detectable by the methods applied, such as H^+ , OH^- and CO_3^{2-} might influence the charge balances shown here. Also, most likely not all of the LMW polar organic acids present in the sampled aerosol could be detected by our techniques, and such undetected species may play a role in the charge balance.

Graham et al. [2003a] found a reasonably good ion balance for fine mode Amazonian aerosols measured with integrating filter samplers during the wet season when only inorganic ions and oxalate were included. However, for the coarse aerosol fraction they observed anion deficits that were probably attributed to additional organic anions. Likewise, previous studies using filter techniques suggested that the Amazonian dry season aerosol is acid-base neutral when inorganic ions and oxalic, acetic and formic acid are included in the charge balance [*Talbot et al.*, 1988].

Nevertheless, in our study we combined results of fine mode aerosol NH_4^+ , NO_3^- , Cl^- and SO_4^{2-} (measured with a real-time method, not prone to artifacts (cf. chapter 2) with results of Na^+ , K^+ , Ca^{2+} and Mg^{2+} and organic aerosol species (from integrating filter samplers) to determine the aerosol charge balance. The results suggest that, LMW organic acids besides oxalate, acetate and formate

contribute significantly to the charge balance of Amazonian fine mode aerosols. Due to the inclusion of organic acids into the inorganic aerosol ion balance the discrepancy of 100 % (factor 2) between anionic and cationic charges (see Fig. 3.6b) could be reduced by at least a factor of three to 6 – 27 % (Fig. 3.6c).

3.4.2 The thermodynamic equilibrium assumption at FNS

Following similar studies on equilibria of inorganic trace gases with related ionic aerosol compounds, we have tested if thermodynamic equilibrium was attained for the pure $\text{NH}_3/\text{HNO}_3/\text{NH}_4\text{NO}_3$ and $\text{NH}_3/\text{HCl}/\text{NH}_4\text{Cl}$ systems under the meteorological conditions prevailing at FNS. The theoretical equilibrium dissociation constant is computed and compared to the measured concentration products of NH_3 & HNO_3 and NH_3 & HCl . In Fig. 3.7a, the thermodynamically predicted equilibrium dissociation constant (K_e) for pure NH_4NO_3 and the measured concentration product ($K_m = \text{HNO}_3 \times \text{NH}_3$) are shown as a function of RH. Liquid phase equilibria of non-ideal solutions are based on the application of a theoretically derived formulation of solution molalities and activity coefficients according to *Metzger et al.* [2002]. For typical mean ambient temperatures of 25 – 28°C at the sampling site (see Fig. 3.2c) the measured concentration product ($K_m = \text{HNO}_3 \times \text{NH}_3$) is always 1 to 2 orders of magnitude below K_e for $\text{RH} < 90$ %. K_m approaches K_e at $\text{RH} > 90$ % and lower temperatures (nighttime).

The coincidence of high RH and high temperatures prevailing in the Amazon Basin is not very common in temperate latitudes, where previous studies have been conducted, which makes comparisons difficult. In contrast to our work, these studies showed that large differences between K_m and K_e for pure NH_4NO_3 at $\text{RH} < 90$ % are not common. *Tanner* [1980], *Erismann et al.* [1988] and *Harrison and Msibi* [1994] reported a good agreement of predicted K_e with K_m for temperatures of 0 – 20 °C and $\text{RH} < 80$ %. A study by *Harrison and Pio* [1983] showed that at $T < 10^\circ\text{C}$ and $\text{RH} > 60$ % equilibrium was achieved. In contrast, *Cadle et al.* [1982] and *Allen et al.* [1989] reported that at low temperatures or high RH the equilibrium condition is not met. It was confirmed by *Matsumoto and Tanaka* [1996], *Danalatos and Glavas* [1999], *Parmar et al.* [2001], and *Gupta et al.* [2003] that lower temperatures generally favor formation of NH_4NO_3 and that at higher temperatures gas/aerosol equilibrium is not achieved, which might explain the large deviations of K_m to K_e in our study.

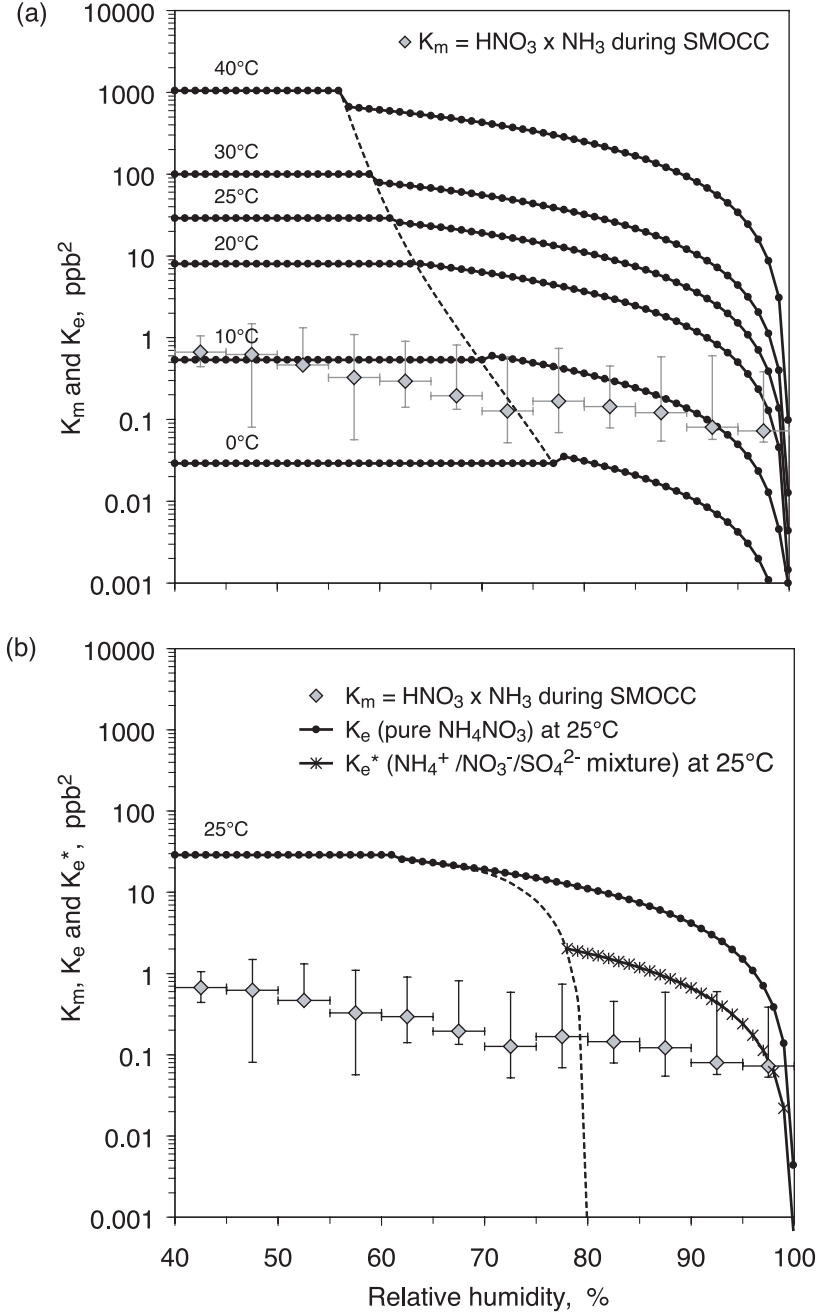


Figure 3.7a,b: Thermodynamically predicted equilibrium dissociation constant (K_e) for (a) pure NH_4NO_3 , and (b) $\text{NH}_4^+/\text{NO}_3^-/\text{SO}_4^{2-}$ mixtures at 25°C (K_e^*) in comparison to averages of the measured concentration product ($K_m = \text{HNO}_3 \times \text{NH}_3$) as a function of RH at FNS during LBA-SMOCC 2002 (including data from the late dry season, transition period and the onset of the wet season, $n = 474$); y-error bars indicate standard deviations of averages, x-error bars indicate the RH bin used for averaging; the dashed line indicates the transition from solid to non-ideal aqueous solution (adapted from *Stelson and Seinfeld* [1982a,c]).

Deviations from equilibrium may be due to: (i.) measurement artifacts, especially at long sampling times, (ii.) HNO_3 deposition faster than attainment of equilibrium, (iii.) mass transport limitations and kinetic constraints [Wexler and Seinfeld, 1992], particularly under highly polluted conditions or in case of freshly emitted NH_3 and HNO_3 , (iv.) long equilibration times due to the presence of large particles (equilibration times for coarse mode aerosols are usually longer than for fine mode particles [Meng and Seinfeld, 1996]), and (v.) formation of non-volatile NO_3^- salts by reaction of HNO_3 with sea salt or soil dust [Hildemann et al., 1984; Parmar et al., 2001].

For deliquescent aerosol particles, the coexistence of SO_4^{2-} considerably reduces K_e compared to pure NH_4NO_3 solutions [Stelson and Seinfeld, 1982c]. To determine K_e^* for the $\text{NH}_4^+/\text{NO}_3^-/\text{SO}_4^{2-}$ system, the NH_4NO_3 ionic strength fraction Y is calculated according to [Stelson and Seinfeld, 1982c]:

$$Y = \frac{[\text{NH}_4\text{NO}_3]}{[\text{NH}_4\text{NO}_3] + 3[(\text{NH}_4)_2\text{SO}_4]}$$

resulting in a median value of $Y = 0.16$. K_e^* was then derived by multiplying K_e with Y , which resulted in a K_e^* value that was significantly lower than K_e at 25°C (Fig. 7b). Although for $\text{RH} > 90\%$ K_m is nearly equal to K_e^* , K_m remains below K_e^* for $\text{RH} < 90\%$. These findings might suggest that at the high temperatures prevailing at the FNS site the vapor pressures of NH_3 and HNO_3 were too low to allow formation of NH_4NO_3 at $\text{RH} < 90\%$.

Since HCl is more volatile than HNO_3 [Matsumoto and Tanaka, 1996], K_e for the $\text{NH}_3/\text{HCl}/\text{NH}_4\text{Cl}$ system is somewhat higher than the theoretical value for the pure $\text{NH}_3/\text{HNO}_3/\text{NH}_4\text{NO}_3$ system [illustrated in Allen et al., 1989]. The HCl vapor pressures and diel variations measured at the site were comparable to those observed for HNO_3 (see Fig. 3.3c,e and Table 3.2a), thus K_m for the $\text{NH}_3/\text{HCl}/\text{NH}_4\text{Cl}$ system exhibits a similar behavior to K_m shown in Fig. 3.7a (i.e., $K_m < K_e$ for $\text{RH} < 90\%$). Nevertheless, aerosol NH_4^+ , NO_3^- and Cl^- were observed at FNS over the entire RH range (40 – 100 %), in disagreement with the thermodynamic equilibrium prediction for $\text{RH} < 90\%$.

3.4.3 Equilibrium model (EQM) simulations

The theoretical considerations above are restricted to the $\text{NH}_3/\text{HNO}_3/\text{NH}_4\text{NO}_3$ and $\text{NH}_3/\text{HCl}/\text{NH}_4\text{Cl}$ systems; thus, they may not entirely explain ionic balances, gas/aerosol partitioning and formation processes of inorganic aerosol constituents at FNS. Therefore, in this section, we will apply four EQMs that are capable of simulating a comprehensive multicomponent inorganic gas/liquid/solid aerosol system.

The input parameters for EQSAM2, ISORROPIA, GEFMN and SCAPE2 are ambient temperature, RH, total NH_4^+ , total NO_3^- , total Cl^- , aerosol SO_4^{2-} , aerosol Na^+ , and, if required, aerosol mineral cations (K^+ , Ca^{2+} , Mg^{2+}) and LMW polar organic acids (only for EQSAM2). Model simulations were based on gas/liquid/solid partitioning considering all physical states of the aerosol (solid/deliquescence/efflorescence). For the GEFMN model, thermodynamic data are not valid for $\text{RH} > 94\%$, thus RHs higher than 94 % were set equal to 94 % for all GEFMN runs. Our investigations focus on a period in the dry season (biomass burning, 17 - 20 Sep. 2002; PM 2.5). Model results will be discussed for the following three gas/liquid/solid aerosol systems:

- (I) $\text{Na}^+\text{-HCl/Cl}^-\text{-NH}_3/\text{NH}_4^+\text{-HNO}_3/\text{NO}_3^-\text{-H}_2\text{SO}_4/\text{SO}_4^{2-}\text{-H}_2\text{O}$
- (II) $\text{K}^+\text{-Ca}^{2+}\text{-Mg}^{2+}\text{-Na}^+\text{-HCl/Cl}^-\text{-NH}_3/\text{NH}_4^+\text{-HNO}_3/\text{NO}_3^-\text{-H}_2\text{SO}_4/\text{SO}_4^{2-}\text{-H}_2\text{O}$
- (III) $\text{K}^+\text{-Ca}^{2+}\text{-Mg}^{2+}\text{-Na}^+\text{-HCl/Cl}^-\text{-NH}_3/\text{NH}_4^+\text{-HNO}_3/\text{NO}_3^-\text{-H}_2\text{SO}_4/\text{SO}_4^{2-}\text{-H}_2\text{O}$ including lumped LMW polar organic acids (only EQSAM2).

Since SCAPE2 and EQSAM2 are the only EQMs that consider mineral cations in their modeling framework, these compounds are represented in ISORROPIA and GEFMN as equivalent mixing ratio of Na^+ . The implicit inclusion of mineral cations as Na^+ equivalent was applied before by *Moya et al.* [2001], who showed that ISORROPIA performs almost as well as SCAPE2 when using this approach. However, since the distinct behavior of mineral solid phase equilibria can not be resolved (MgCl_2 deliquesces already at $\text{RH} \sim 33\%$ (298.15 K) and NaCl at $\text{RH} \sim 75\%$ (298.15 K)), this approach is limited to gas/liquid equilibria and will lead to a considerable underestimation of the aerosol water content. Therefore, we will use SCAPE2 from now on as the reference model.

Plots of modeled aerosol SO_4^{2-} will not be presented here, since aerosol SO_4^{2-} is non-volatile and H_2SO_4 is fully neutralized in all cases. Therefore, mixing ratios of aerosol SO_4^{2-} remain the same as in the model input which corresponds to the measured values [shown for 17 - 20 September 2002 in chapter 2].

- (I) $\text{Na}^+\text{-HCl/Cl}^-\text{-NH}_3/\text{NH}_4^+\text{-HNO}_3/\text{NO}_3^-\text{-H}_2\text{SO}_4/\text{SO}_4^{2-}\text{-H}_2\text{O-system}$

Fig. 3.8a-f shows diel variations of inorganic compounds measured with the WAD/SJAC system along with the simulated values from the four EQMs for a system including only $\text{NH}_3/\text{NH}_4^+$, $\text{HNO}_3/\text{NO}_3^-$, HCl/Cl^- , $\text{H}_2\text{SO}_4/\text{SO}_4^{2-}$, and aerosol Na^+ (17 - 20 Sep. 2002).

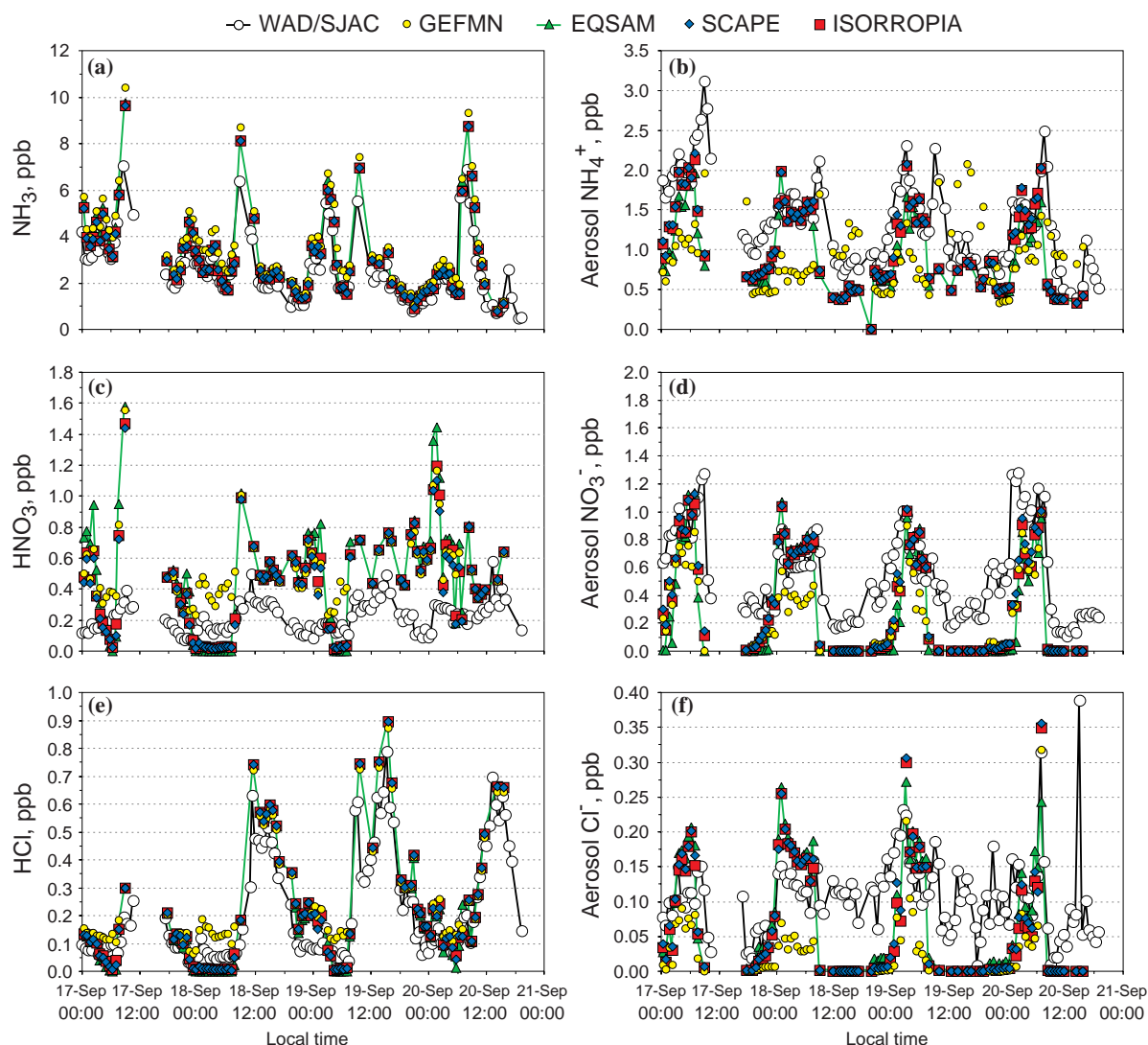


Figure 3.8a-f: Diel variations of (a) NH_3 , (b) aerosol NH_4^+ , (c) HNO_3 , (d) aerosol NO_3^- , (e) HCl , and (f) aerosol Cl^- measured with the WAD/SJAC system (PM 2.5) along with results of simulations with EQSAM, ISORROPIA, GEFMN and SCAPE2 for the $\text{Na}^+\text{-HCl/Cl}^-\text{-NH}_3/\text{NH}_4^+\text{-HNO}_3/\text{NO}_3^-\text{-H}_2\text{SO}_4/\text{SO}_4^{2-}\text{-H}_2\text{O}$ -system, 17 - 20 Sep. 2002, dry (biomass burning) season at FNS during LBA-SMOCC 2002.

Generally, the models overpredict gaseous compounds and underpredict inorganic aerosol species. Obviously, during daytime hours coinciding with lower RH (Fig. 3.2c), the EQMs fail to predict the existence of the observed aerosol NO_3^- and Cl^- , leading to a significant overprediction especially of HNO_3 , but also HCl (Fig. 3.8c,e). As a result, only the amount of NH_3 required for the neutralization of H_2SO_4 is simulated as NH_4^+ in the aerosol phase during daytime. In contrast, modeled inorganic aerosol species are much closer to the observations during nighttime. This finding is emphasized in Fig. 3.9; while the WAD/SJAC

measurements showed detectable fine mode aerosol NO_3^- that was increasing with increasing RH, SCAPE2 does not predict any aerosol NO_3^- at $\text{RH} < 90\%$. For $\text{RH} > 90\%$ SCAPE2 simulates aerosol NO_3^- in reasonable agreement with the measurements.

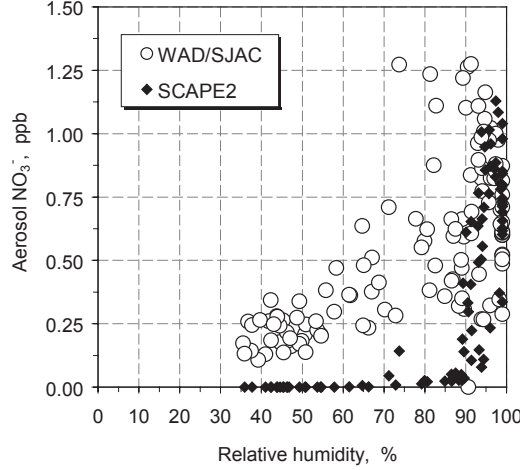


Figure 3.9: Relative humidity dependence of measured aerosol NO_3^- (PM 2.5) and SCAPE2 predicted aerosol NO_3^- for the $\text{Na}^+\text{-HCl/Cl}^-\text{-NH}_3/\text{NH}_4^+\text{-HNO}_3/\text{NO}_3^-$ - $\text{H}_2\text{SO}_4/\text{SO}_4^{2-}\text{-H}_2\text{O}$ -system, 17 - 20 Sep. 2002, dry (biomass burning) season at FNS during LBA-SMOCC 2002.

Model predictions of fine mode aerosol Cl^- are comparable to the findings for aerosol NO_3^- . Simulated values are lower than observations even at $\text{RH} > 90\%$ (not shown). In summary, the EQM simulations suggest that thermodynamic equilibrium between NH_3 , HNO_3 , HCl and aerosol NH_4NO_3 and NH_4Cl does not adequately represent the observed phase relationships for $\text{RH} < 90\%$, and that other components must be considered to explain the differences between observations and model results.

(II) $\text{K}^+\text{-Ca}^{2+}\text{-Mg}^{2+}\text{-Na}^+\text{-HCl/Cl}^-\text{-NH}_3/\text{NH}_4^+\text{-HNO}_3/\text{NO}_3^-\text{-H}_2\text{SO}_4/\text{SO}_4^{2-}\text{-H}_2\text{O}$ -system

In order to assess the role of the mineral cations (K^+ , Ca^{2+} , Mg^{2+}) we will now investigate a system consisting of $\text{NH}_3/\text{NH}_4^+$, $\text{HNO}_3/\text{NO}_3^-$, HCl/Cl^- , $\text{H}_2\text{SO}_4/\text{SO}_4^{2-}$, aerosol Na^+ , aerosol K^+ , aerosol Ca^{2+} , and aerosol Mg^{2+} . Fig. 3.10a shows that, when mineral cations are included, aerosol NO_3^- is predicted by SCAPE2 also at $\text{RH} < 90\%$. Apparently, besides the presence of NH_4NO_3 at $\text{RH} > 90\%$, a sizeable fraction of NO_3^- was balanced by mineral cations (predominantly K^+ , which was most abundant in the aerosol fine mode, see Table 3.2b).

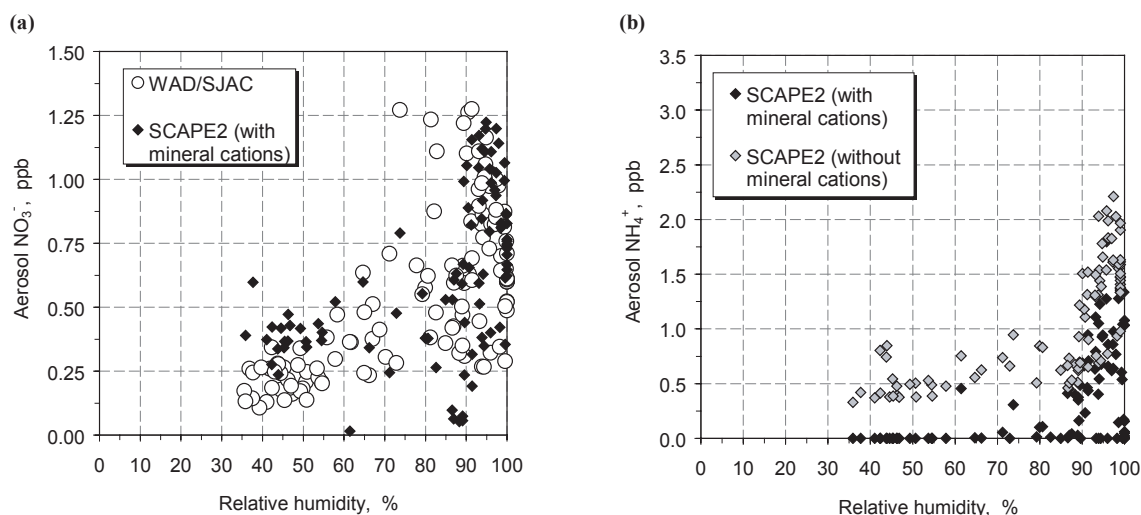


Figure 3.10a,b: Relative humidity dependence of (a) measured aerosol NO_3^- (PM 2.5) and SCAPE2 predicted aerosol NO_3^- for the $\text{K}^+ - \text{Ca}^{2+} - \text{Mg}^{2+} - \text{Na}^+ - \text{HCl}/\text{Cl}^- - \text{NH}_3/\text{NH}_4^+ - \text{HNO}_3/\text{NO}_3^- - \text{H}_2\text{SO}_4/\text{SO}_4^{2-} - \text{H}_2\text{O}$ -system and (b) SCAPE2 predicted aerosol NH_4^+ for the system in (a) and SCAPE2 predicted aerosol NH_4^+ for the $\text{Na}^+ - \text{HCl}/\text{Cl}^- - \text{NH}_3/\text{NH}_4^+ - \text{HNO}_3/\text{NO}_3^- - \text{H}_2\text{SO}_4/\text{SO}_4^{2-} - \text{H}_2\text{O}$ -system, 17 - 20 Sep. 2002, dry (biomass burning) season at FNS during LBA-SMOCC 2002.

According to the SCAPE2 simulations, daytime fine mode aerosol NO_3^- may solely be attributed to non-volatile nitrate salts, which were probably formed through heterogeneous uptake of HNO_3 by aerosol particles. Thus, once aqueous NH_4NO_3 has evaporated due to decreasing RH at sunrise (see Fig. 3.2c,d), only the amount of fine mode NO_3^- balanced by mineral cations remained in the aerosol phase at lower daytime RHs. However, SCAPE2 somewhat overpredicts aerosol NO_3^- at $\text{RH} < 60\%$ (see Fig. 3.10a). This may be caused by the fact that real-time measurements are combined with results from 12, 24 and 48 hours integrating filter samplers, which do not represent the diel variability of mineral cations. On the other hand, it is possible that aerosol NO_3^- did not achieve equilibrium with mineral cations because of transport limitations (mass transport of species between gas and aerosol phase is not considered in SCAPE2 and other EQM frameworks). Modeled fine mode aerosol Cl^- repeatedly shows a similar behavior to aerosol NO_3^- and is also predicted by SCAPE2 at $\text{RH} < 90\%$ when mineral cations are included (not shown). It may be assumed that aerosol Cl^- behaved similarly to aerosol NO_3^- , mainly because it was balanced by mineral cations at daytime while a considerable fraction was present as aqueous NH_4Cl at high nighttime RHs.

However, when the mineral cations are included, the underprediction of fine mode aerosol NH_4^+ by SCAPE2 becomes even larger than before. This is shown in Fig. 3.10b, where aerosol NH_4^+ predicted by SCAPE2 (with and without mineral cations) is plotted versus RH. When mineral cations are included, SCAPE2 does not predict any fine mode aerosol NH_4^+ for $\text{RH} < 90\%$, which is in strong contrast to our observations. Obviously, aerosol NH_4^+ is now replaced by other cations (mineral species, especially K^+) which preferentially balance NO_3^- , Cl^- and SO_4^{2-} . According to the model simulations, aerosol NH_4^+ would only be present at $\text{RH} > 90\%$, when thermodynamic equilibrium permits the formation of aqueous NH_4NO_3 and NH_4Cl . This implies that at lower RH during daytime, fine mode NO_3^- , Cl^- and SO_4^{2-} are solely balanced by mineral cations (especially K^+), revising the ion balance presented in Fig. 3.6a. These findings are supported by a study by *Li et al.* [2003], who found that smoke particles emitted by biomass fires in Southern Africa were dominated by potassium salts. Primary KCl-containing particles are emitted by biomass fires, and ageing of biomass smoke may lead to displacement of Cl from the aerosol phase [*Li et al.*, 2003 and references therein]. The analogous mechanism is known for sea-salt aerosols [e.g., *Ueda et al.*, 2000]. This might be an explanation for the low fraction of aerosol Cl^- observed at the FNS site (cf. section 3.3.4, Fig. 3.5e,f).

(III) K^+ - Ca^{2+} - Mg^{2+} - Na^+ -HCl/ Cl^- - NH_3 / NH_4^+ - HNO_3 / NO_3^- - H_2SO_4 / SO_4^{2-} - H_2O -system including lumped LMW polar organic acids

The ionic charge balance for the modeled aerosol systems (I) and (II) is not neutral, presumably due to the role of organic acids. Therefore, we investigated the effect of incorporating equivalent lumped LMW polar organic acids into the simplified modeling framework of EQSAM2. This is done by adding the sum of equivalent moles of organic acids (see Table 3.2c, Fig. 3.6c) to the gas/liquid/solid aerosol system (II), without explicitly modeling the thermodynamics of organic acids. Thus, semi-volatility of these species is not taken into account and their effect on aerosol water uptake is assumed to be the same as for other ammonium salts of the same charge. Fig. 3.11 illustrates measured aerosol NH_4^+ and EQSAM2-predicted aerosol NH_4^+ as a function of RH. Due to the inclusion of organic acids, EQSAM2 predicts fine mode aerosol NH_4^+ also for $\text{RH} < 90\%$. Compared to aerosol system (II), where solely mineral cations are included (Fig. 3.10b), the modeled aerosol NH_4^+ agrees much better with observations over the entire RH range. These findings indicate that during daytime ($\text{RH} < 90\%$) fine mode aerosol NH_4^+ was apparently balanced by organic anions. However, at $65\% < \text{RH} < 85\%$ EQSAM2 still predicts significantly lower aerosol NH_4^+ mixing ratios than observed with the WAD/SJAC system.

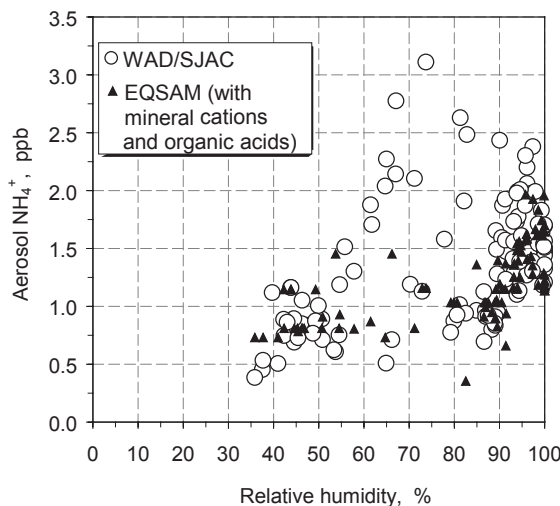


Figure 3.11: Relative humidity dependence of measured aerosol NH_4^+ (PM 2.5) and EQSAM predicted aerosol NH_4^+ for the $\text{K}^+ - \text{Ca}^{2+} - \text{Mg}^{2+} - \text{Na}^+ - \text{HCl}/\text{Cl}^- - \text{NH}_3/\text{NH}_4^+ - \text{HNO}_3/\text{NO}_3^- - \text{H}_2\text{SO}_4/\text{SO}_4^{2-} - \text{H}_2\text{O}$ -system extended by the sum of equivalent moles of organic acids, 17 - 20 Sep. 2002, dry (biomass burning) season at FNS during LBA-SMOCC 2002.

This RH range is coincident with the short-term NH_3 spike and aerosol NH_4^+ peak observed around 0900 LT at the FNS site (cf. Fig. 3.3a,b). Apparently, further organic acids in addition to the species included in our study could be present and neutralize excess NH_3 in the aqueous aerosol phase, forming additional NH_4^+ . These results provide strong evidence that the presence of polar organic aerosol compounds at our site played an important role in balancing the inorganic aerosol system.

3.4.4 Overall EQM performance

In order to underline our findings obtained with SCAPE2 and EQSAM2, model performances of all four EQMs (EQSAM2, ISORROPIA, GEFMN and SCAPE2) will be compared and discussed briefly for the gas/liquid/solid aerosol systems (I) – (III). For this purpose, normalized mean error (NME) and normalized mean bias (NMB) of the four EQMs are calculated based on the WAD/SJAC measurements, including data from the dry season, transition period and the wet season (Table 3.3a-c). When modeling the $\text{Na}^+ - \text{HCl}/\text{Cl}^- - \text{NH}_3/\text{NH}_4^+ - \text{HNO}_3/\text{NO}_3^- - \text{H}_2\text{SO}_4/\text{SO}_4^{2-} - \text{H}_2\text{O}$ -system the NME of EQSAM2, ISORROPIA, GEFMN and SCAPE2 is highest for HNO_3 and aerosol Cl^- (Table 3.3a).

Table 3.3a-c: Normalized mean error (NME*) and normalized mean bias (NMB*) of EQSAM, ISORROPIA, GEFMN and SCAPE2 for NH₃, HNO₃, HCl, aerosol NH₄⁺, NO₃⁻ and Cl⁻ for (a) the Na⁺-HCl/Cl⁻-NH₃/NH₄⁺-HNO₃/NO₃⁻-H₂SO₄/SO₄²⁻-H₂O-system, (b) the K⁺-Ca²⁺-Mg²⁺-Na⁺-HCl/Cl⁻-NH₃/NH₄⁺-HNO₃/NO₃⁻-H₂SO₄/SO₄²⁻-H₂O-system and (c) NME and NMB of EQSAM for NH₃ and aerosol NH₄⁺ (PM 2.5) for the systems in (a) and (b) compared to the system in (b) extended by LMW polar organic acids. NME and NMB of the four different models are based on WAD/SJAC measurements from the late dry (biomass burning) season, transition period, and the onset of the wet season at FNS during LBA-SMOCC 2002.

(a)

System I	EQSAM		ISORROPIA		GEFMN		SCAPE2	
	NME (%)	NMB (%)	NME (%)	NMB (%)	NME (%)	NMB (%)	NME (%)	NMB (%)
NH ₃	33	27	32	25	44	39	31	25
HNO ₃	148	129	132	118	146	145	128	113
HCl	37	15	37	19	38	29	36	18
Aerosol NH ₄ ⁺	42	-42	40	-37	55	-35	39	-37
Aerosol NO ₃ ⁻	65	-57	58	-52	67	-66	56	-50
Aerosol Cl ⁻	76	-45	74	-54	84	-84	73	-51

(b)

System II	EQSAM		ISORROPIA		GEFMN		SCAPE2	
	NME (%)	NMB (%)	NME (%)	NMB (%)	NME (%)	NMB (%)	NME (%)	NMB (%)
NH ₃	55	51	52	47	62	57	52	47
HNO ₃	100	5	85	-19	83	-6	82	-18
HCl	42	6	39	-2	34	3	39	-6
Aerosol NH ₄ ⁺	84	-84	83	-83	85	-84	82	-82
Aerosol NO ₃ ⁻	43	-2	37	8	38	2	35	8
Aerosol Cl ⁻	78	-24	69	-6	70	-24	72	-1

(c)

EQSAM (PM 2.5 only)	System I		System II		System III	
	NME (%)	NMB (%)	NME (%)	NMB (%)	NME (%)	NMB (%)
NH ₃	29	27	54	53	23	15
Aerosol NH ₄ ⁺	40	-38	86	-86	31	-15

(*)

$$NME = \frac{\sum_{i=1}^n |M_i - O_i|}{\sum_{i=1}^n O_i} \times 100\% \quad NMB = \frac{\sum_{i=1}^n (M_i - O_i)}{\sum_{i=1}^n O_i} \times 100\%$$

with M_i ...modeled value, O_i ...observed value

This is mainly caused by the frequent underprediction of aerosol NO_3^- and Cl^- for $\text{RH} < 90\%$ and the resulting overprediction of gaseous precursors. Consequently, the NMB is negative for all aerosol species and positive for gaseous species. Table 3.3 reveals that all EQM results for the simulation of the gas/liquid/solid aerosol system (I) are comparable, which emphasizes that exclusion of mineral cations and organic acids leads to significant deviations of EQM predictions from observations at FNS. Since inorganic aerosol species are underpredicted to a larger extent by GEFMN compared to the other EQMs in the high RH range (see nighttime periods in Fig. 3.8b,d,f), NME and NMB values are somewhat higher for GEFMN. This is due to an underestimation of aerosol water at RHs higher than 94 %.

Performances of all EQMs change markedly for the $\text{K}^+ \text{-Ca}^{2+} \text{-Mg}^{2+} \text{-Na}^+ \text{-HCl/Cl}^- \text{-NH}_3/\text{NH}_4^+ \text{-HNO}_3/\text{NO}_3^- \text{-H}_2\text{SO}_4/\text{SO}_4^{2-} \text{-H}_2\text{O}$ -system (system (II), Table 3.3b). NME and NMB for aerosol NO_3^- and HNO_3 decrease significantly. However, as discussed before, the inclusion of mineral cations even increases the charge imbalance, such that NME and NMB for gaseous NH_3 and aerosol NH_4^+ are doubled. The predictions of all four EQMs support our previous findings and it is shown that the approach used in EQSAM2 as well as the inclusion of mineral cations as Na^+ equivalent in ISORROPIA and GEFMN are applicable for our aerosol system. Note that, although values given in Table 3 a,b represent model runs for PM 2.5 and TSP samples, (which include the coarse aerosol fraction) the same overall findings are observed.

NME and NMB values for EQSAM2 simulations incorporating LMW polar organic acids are presented for PM 2.5 measurements only, since not all organic acids were analyzed for the coarse aerosol fraction (Table 3.3c). The inclusion of organic acids results in a substantial reduction of NME and NMB for aerosol NH_4^+ and NH_3 . When mineral cations and organic acids are incorporated, EQSAM2's model bias (NMB) is below $\pm 25\%$ for all inorganic aerosol species and gases (see Table 3.3a-c), confirming the ion balance presented in Fig. 3.6c.

3.5 Summary and conclusion

We have measured gaseous NH_3 , HNO_3 , HCl , SO_2 and their chemically related aerosol species NH_4^+ , NO_3^- , Cl^- , and SO_4^{2-} with high time resolution at a pasture site in the Amazon Basin during the late dry season (biomass burning, 12 - 30 September 2002), the transition period (01 - 31 October 2002), and the onset of the wet season (clean conditions, 01 - 14 November 2002). To our knowledge, these are the first real-time measurements of inorganic aerosol species simultaneously with their gaseous precursors in a tropical environment. To derive information about the relevance of mineral cations (K^+ , Ca^{2+} , Mg^{2+}) and low

molecular weight (LMW) polar organic acids, real-time data were combined with results obtained from the analysis of aerosols collected on 12-, 24- and 48-hours integrated filter samples. The sampled aerosol was dominated by organic matter. Mixing ratios of NH_3 were one order of magnitude higher than those of acidic gases. Consequently, aerosol NH_4^+ was the dominating inorganic aerosol constituent.

Our analyses, which included simulations using the four thermodynamic equilibrium models, EQSAM2, ISORROPIA, GEFMN and SCAPE2, suggest that:

- (i.) High ambient temperatures prevailing in the Amazon region and low vapor pressure products of $\text{NH}_3 \times \text{HNO}_3$ and $\text{NH}_3 \times \text{HCl}$ did not allow formation of aerosol fine mode ($D_p \leq 2.5 \mu\text{m}$) NH_4NO_3 and NH_4Cl at $RH < 90 \%$.
- (ii.) Thermodynamic equilibrium permitted the formation of aqueous NH_4NO_3 and NH_4Cl during nighttime only ($RH > 90 \%$).
- (iii.) Mineral cations (especially K^+) present in Amazonian fine mode aerosols significantly balanced aerosol NO_3^- and SO_4^{2-} , particularly during daytime.
- (iv.) Chloride was largely driven out of the aerosol phase by reaction of pyrogenic KCl with HNO_3 and H_2SO_4 .
- (v.) Due to high ratios of NH_3/SO_2 observed at the pasture site, $(\text{NH}_4)_2\text{SO}_4$ appeared to be only a minor component of the Amazonian fine mode inorganic aerosol.
- (vi.) Gaseous NH_3 was largely neutralized by LMW polar organic acids, forming aerosol NH_4^+ .

Finally, we like to state that in tropical regions, modeling multiphase equilibria considering only the $\text{Na}^+\text{-HCl/Cl}^-\text{-NH}_3/\text{NH}_4^+\text{-HNO}_3/\text{NO}_3^-\text{-H}_2\text{SO}_4/\text{SO}_4^{2-}\text{-H}_2\text{O}$ -system will lead to substantial discrepancies between simulations and observations. This is mainly caused by: (i.) high RH and high temperatures, (ii.) the presence of mineral cations in aerosol fine and coarse modes, (iii.) a significant amount of polar organic compounds, and (iv.) high NH_3/SO_2 and high $\text{NH}_4^+/\text{SO}_4^{2-}$ ratios, which are characteristic for tropical regions like the Amazon Basin. To derive valid information about gas/aerosol partitioning and aerosol ionic balances in these regions, it is necessary to include mineral cations into EQM frameworks. Furthermore, our study emphasizes that an explicit thermodynamic approach to simulate the organic/inorganic gas/liquid/solid aerosol system is required. It still needs to be investigated to what extent the water uptake by WSOC-rich aerosols might influence partitioning of inorganic species between gas and aerosol phase.

Dry and wet deposition of atmospheric inorganic nitrogen compounds in a tropical environment (Rondônia, Brazil)

I. Trebs, L. L. Lara, L. M. M. Zeri, L. V. Gatti, P. Artaxo, R. Dlugi, J. Slanina, M. O. Andreae and F. X. Meixner

(Submitted to Atmospheric Chemistry and Physics in March 2005)

Abstract. The input of nitrogen (N) to ecosystems has increased dramatically over the past decades. While total N deposition (wet + dry) has been extensively determined in temperate regions, only very few data sets exist about wet N deposition in tropical ecosystems, and moreover, experimental information about dry N deposition in tropical environments is lacking. In this study, we estimate dry and wet deposition of inorganic N for a remote pasture site in the Amazon Basin based on in-situ measurements. The measurements covered the late dry (biomass burning) season, a transition period and the onset of the wet season (clean conditions) (12 Sep. to 14 Nov. 2002, LBA-SMOCC). Ammonia (NH_3), nitric acid (HNO_3), nitrous acid (HONO), nitrogen dioxide (NO_2), nitric oxide (NO), ozone (O_3), aerosol ammonium (NH_4^+) and aerosol nitrate (NO_3^-) were measured in real-time, accompanied by simultaneous (micro-)meteorological measurements. Dry deposition fluxes of NO_2 and HNO_3 are inferred using the “big leaf multiple resistance approach” and particle deposition fluxes are derived using an established empirical parameterization. Bi-directional surface-atmosphere exchange fluxes of NH_3 and HONO are estimated by applying a “canopy compensation point model”. Dry and wet N deposition is dominated by NH_3 and NH_4^+ , which is largely the consequence of biomass burning during the dry season. The grass surface appeared to have a strong potential for daytime NH_3 (re-)emission, owing to high canopy compensation points, which are related to high surface temperatures and to direct NH_3 emissions from cattle excreta. NO_2 also significantly accounted for dry N deposition, whereas HNO_3 , HONO and N-containing aerosol species were only minor contributors. We estimated a total (dry + wet) N deposition of $7.3 - 9.8 \text{ kgN ha}^{-1} \text{ yr}^{-1}$ to the tropical pasture site, whereof $2 - 4.5 \text{ kgN ha}^{-1} \text{ yr}^{-1}$ are attributed to dry N deposition and $\sim 5.3 \text{ kgN ha}^{-1} \text{ yr}^{-1}$ to wet N deposition. Our estimate exceeds total (wet + dry) N deposition to tropical ecosystems predicted by global chemistry and transport models by at least factor of two.

4.1 Introduction

The supply of reactive nitrogen (N) to global terrestrial ecosystems has doubled as a consequence of human activities, such as fertilizer application, cultivation of N fixing legumes and production of nitrogen oxides by fossil-fuel burning [Galloway, 1998]. The deposition of atmospheric N species constitutes a major nutrient input to the biosphere. On a long-term scale, the increase of N inputs into terrestrial ecosystems may result in (i.) intensified trace gas exchange (ii.) enhanced leaching of nitrate and soil nutrients (e.g., K^+ , Mg^{2+} , Ca^{2+}), (iii.) ecosystem eutrophication and acidification, (iv.) reduction in biodiversity, and (v.) increased carbon storage [Vitousek *et al.*, 1997]. Enhanced carbon storage due to N deposition has been shown to increase the terrestrial carbon sink in N-limited temperate ecosystems, which may have substantial impacts on global CO_2 concentrations [e.g., Townsend *et al.*, 1996].

N deposition is considered to be relevant in the tropics due to widespread biomass burning activity and increasing fertilizer application. It was suggested by Matson *et al.* [1999] and Asner *et al.* [2001] that in contrast to temperate ecosystems, nitrogen-rich / phosphorus (P)-limited tropical rainforest soils may have a reduced productivity following excess N deposition, resulting in a decreased C-storage. Moreover, the humid tropical zone is a major source area for biogenic nitrous oxide (N_2O) and nitric oxide (NO) emissions from soils [Reiners *et al.*, 2002]. Enhanced N inputs to tropical forests are likely to increase nitrification/denitrification rates and, hence, the emission of NO and N_2O to the atmosphere [Hall and Matson, 1999]. The conversion of tropical rainforest into cultivated land and pasture may lead to a sustained disturbance of the natural N cycle. During clearing and burning of tropical rainforest, biomass-associated N is volatilized and a large fraction is emitted in form of gaseous NH_3 (cf. chapter 2), which may result in considerable N losses of tropical ecosystems [Kauffman *et al.*, 1998; Kauffman *et al.*, 1995]. This is affirmed by that fact that, in contrast to primary rain forests, plant growth in deforested areas is suggested to be limited by N rather than by P [Oliveira *et al.*, 2001; Davidson *et al.*, 2004].

The deposition of atmospheric N compounds occurs via dry and wet processes. Nitrogen dioxide (NO_2), ammonia (NH_3), nitric acid (HNO_3) and nitrous acid (HONO) are the most important contributors to dry N deposition. HNO_3 usually features a rapid downward (net deposition) flux to the surface [e.g., Huebert and Robert, 1985]. By contrast, the exchange of NO, NH_3 , HONO and also NO_2 between surface and atmosphere may be bi-directional. The rates of production and consumption in vegetation elements and/or soils mainly determine whether net emission or net deposition of these species takes place. Turbulent diffusion controls the transport of gases and particles from the surface layer to the earth's

surface. The uptake of trace gases by surfaces is considered to be dependent on physico-chemical and biological surface properties [Hicks *et al.*, 1987] and on the solubility and reactivity of the gaseous compound [e.g., Wesely, 1989]. Hence, soil characteristics, plant stomata activity and trace gas chemical properties largely determine the deposition velocity. The atmospheric dry removal of aerosol particles, which may contain N species such as ammonium (NH_4^+) and nitrate (NO_3^-), is a function of the particle size [e.g., Nicholson, 1988] but also depends on the particle density. Dry deposition is enhanced for large particles (especially those larger than a few micrometers) due to the additional influence of gravitational settling.

Wet N deposition is a result of in-cloud scavenging (“rainout”) and below-cloud scavenging (“washout”) of atmospheric N constituents [see Meixner, 1994]. The total (wet + dry) N deposition ranges from 1 – 2 kgN ha⁻¹ yr⁻¹ for rural locations (e.g., North Canada) up to 30 – 70 kgN ha⁻¹ yr⁻¹ for urban N receptor regions (e.g., North Sea, European NW coast and NE U.S.) [Howarth *et al.*, 1996]. In contrast to moderately fluctuating air pollution levels that prevail in Europe, the United States and Asia throughout the year, tropical environments such as the Amazon Basin experience every year a dramatic change from the “green ocean” clean background atmosphere to extremely polluted conditions during the biomass burning season. Only few studies exist where atmospheric wet N removal was determined experimentally in the tropics [e.g., Galloway *et al.*, 1982; Likens *et al.*, 1987; Srivastava and Ambast, 1994; Clark *et al.*, 1998]. The chemical composition of precipitation in the Amazon region was determined in previous studies by Stallard and Edmond [1981], Andreae *et al.* [1990], Lesack and Melack [1991] and Williams *et al.* [1997]. Global chemistry and transport models (CTMs) such as MOGUNTIA have been applied to estimate total N deposition on a global scale [e.g., Holland *et al.*, 1999]. Model results suggest that net N deposition in the northern temperate latitude exceeds contemporary tropical N deposition by almost a factor of two. However, quantitative experimental information about dry N deposition in tropical environments, required to validate these model predictions, is lacking.

Kirkman *et al.* [2002] determined the surface-atmosphere exchange of NO, NO₂ and ozone (O₃) at a pasture site in the Amazon Basin (Rondônia, Brazil). In this paper, we complement their study by additionally estimating the surface-atmosphere exchange fluxes of NH₃, HNO₃, HONO, aerosol NO₃⁻ and NH₄⁺ at the same pasture site. Our analysis is based on real-time measurements, supported by simultaneous measurements of (micro-)meteorological quantities covering the late dry (biomass burning) season, the transition period, and the onset of the wet season (clean conditions). Fluxes of NO₂, HNO₃, NH₃ and HONO are estimated by inferential methods. Wet N deposition was determined by collection of rainwater

and subsequent analyses. We estimate the total (dry + wet) annual N deposition at this pasture site and the relative contribution of the species considered.

4.2 Experimental

4.2.1 Field site

Measurements were performed during 12 - 23 Sep. 2002 (dry season, biomass burning), 07 - 31 Oct. 2002 (transition period) and 01 - 14 Nov. 2002 (wet season, clean conditions) at a pasture site in the state of Rondônia, Brazil (*Fazenda Nossa Senhora Aparecida*, FNS, 10°45'44" S, 62°21'27" W, 315 m asl). The site is located in the south-western part of the Amazon Basin. The location and a simplified sketch of the measurement site are shown in Fig. 4.1.

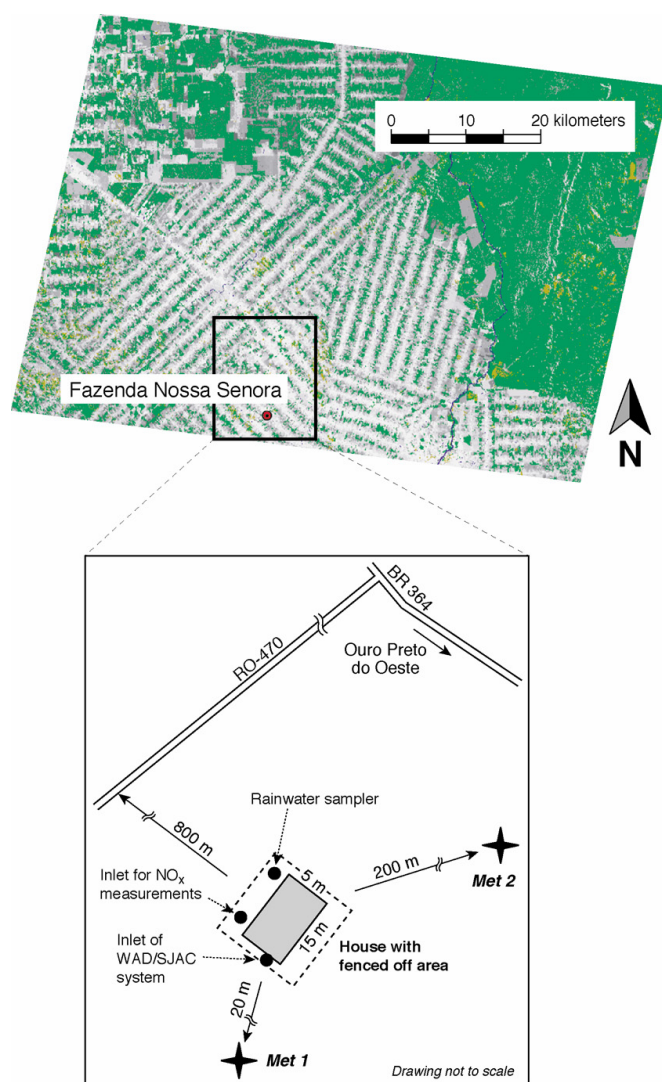


Figure 4.1: Location of the LBA-SMOCC measurement site *Fazenda Nossa Senhora Aparecida* (FNS) in Rondonia, Brazil.

The primary rain forest at FNS was cleared by slash & burn activities in 1977. The vegetation at FNS is dominated by grass (*Brachiaria brizantha*) with small patches of *Brachiaria humidicola* and very few isolated palms and bushes, and the site is used as a cattle ranch (~ 200 “Blanco” cattle, *Bos indicus hybrid*). FNS is located within a strip of cleared land about 4 km wide and several tens of kilometers long [Culf *et al.*, 1996]. The towns Ouro Preto do Oeste ($\sim 40,800$ inhabitants) and Ji-Paraná ($\sim 110,000$ inhabitants) are situated approximately 8 km and 40 km to the ENE and ESE of the site, respectively.

The instrumentation for trace gas/aerosol sampling and online analyses was arranged in an air conditioned wooden house. Rain samples were collected nearby the house (see Fig. 4.1). An automatic weather station (**Met 1**) was located in a distance of ~ 20 m to the S, and a meteorological tower (**Met 2**) was situated ~ 200 m to the NE of the inlets for trace gas and aerosol measurements. While the sampling site provides a sufficient uniform fetch expanding for 1 – 2 km from the sampling location in each direction [cf. *Andreae et al.*, 2002], local flow distortions may be caused by the wooden house and some instrument shelters. A more detailed description of the measurement site is given in *Andreae et al.* [2002] and *Kirkman et al.* [2002].

4.2.2 Sampling and analysis

Table 4.1 summarizes the specifications of the instruments for the measurement of trace gases, aerosol species and (micro)-meteorological quantities. Water-soluble N containing trace gases (NH_3 , HNO_3 and HONO) and related aerosol species (NH_4^+ and NO_3^-) were measured on-line. Air was taken from a height of 5.3 m above ground through a sophisticated inlet system, which was designed to reduce wall losses of soluble gases (especially HNO_3) and to minimize aerosol losses due to non-isokinetic sampling (cf. chapter 2). Soluble gases were scavenged with a wet-annular denuder (WAD) [Wyers *et al.*, 1993], which was combined with a Steam-Jet-Aerosol Collector (SJAC) [Khlystov *et al.*, 1995] to collect particulate N species. For both gaseous and aerosol compounds, sample collection was followed by subsequent online analysis (ion chromatography (IC)) for anions and flow-injection analyses (FIA) for NH_4^+ . Cycle times were set to 20 min (dry season), 40 min (transition period) and 60 min (wet season) (cf. chapter 2). Aerosol samples of either PM 2.5 ($D_p \leq 2.5 \mu\text{m}$) or total suspended particulate matter (TSP) were collected. A detailed description and verification of the measurement method and of the inlet system can be found in *Slanina et al.* [2001] and chapter 2.

Table 4.1: Specifications of the instrumentation for the measurement of trace gases, aerosol species and (micro)-meteorological quantities at FNS during LBA-SMOCC 2002 (all heights are above ground).

Parameter	Time resolution	Technique or sensor	Model, manufacturer	Detection limit/precision
NH ₃ , HNO ₃ , HONO (5.3 m)	20 - 60 min ⁽¹⁾	Wet-annular denuder (WAD), IC, FIA ⁽²⁾	ECN, Petten, Netherlands	≤ 0.015 ppb (3σ) for acids, ≤ 0.118 ppb (3σ) for NH ₃
Aerosol NH ₄ ⁺ , NO ₃ ⁻ (5.3 m)	20 - 60 min	Steam-Jet Aerosol Collector (SJAC), IC, FIA	ECN, Petten, Netherlands	≤ 0.015 ppb (3σ) for anions, ≤ 0.118 ppb (3σ) for aerosol NH ₄ ⁺
NO concentration (10 m)	5 min	Gas-phase chemiluminescence	Model 42C TL (trace level), Thermo Environment Instruments Inc., U.S.A	0.05 ± 0.025 ppb
NO ₂ concentration (10 m)	5 min	Catalytic conversion of NO ₂ to NO by molybdenum converter (at 325°C), gas phase chemiluminescence	Model 42C TL (trace level), Thermo Environment Instruments Inc., U.S.A	0.05 ± 0.025 ppb
O ₃ concentration (10 m)	5 min	UV absorption	Model 49C Thermo Environment Instruments Inc., U.S.A.	1 ± 0.5 ppb
Air temperature (<i>Met 1</i>) (0.5 m and 5 m)	1 min	Pt-100 Ω resistance sensor	MP-103A-CG030-W4W Rotronic, Switzerland	± 0.1 K
Relative humidity (<i>Met 1</i>) (0.5 m and 5 m)	1 min	Capacitive sensor	MP-103A-CG030-W4W Rotronic, Switzerland	± 1.5 %
Surface wetness (<i>Met 1</i>)	1 min	Surface wetness grids at soil surface	237 WSG, Campbell Scientific Ltd., U.K.	-
Global radiation flux (<i>Met 1</i>) (5 m)	1 min	Pyranometer sensor	LI200SZ (LI-COR, Lincoln, Nebraska, U.S.A.)	< ± 3 %
Eddy covariance; three dimensional wind and temperature fluctuations (<i>Met 2</i>) (4 m)	10 Hz	3-D ultrasonic anemometer	Solent 1012R2, Gill Instruments, U.K.	± 1.5 %
H ₂ O mixing ratio (<i>Met 2</i>) (4 m)	10 Hz	Infrared closed-path absorption	IRGA LI-COR 6262 (LI-COR, Lincoln, Nebraska, U.S.A.)	± 1 %
Shortwave radiation in and out (<i>Met 2</i>) (8.5 m)	1 min	Pyranometer sensor	Kipp & Zonen Pyranometer CM 21	± 2 %
Longwave radiation in and out (<i>Met 2</i>) (8.5 m)	1 min	Pyranometer sensor	Kipp & Zonen Pyrgeometer CG	± 3 %

⁽¹⁾ 20 min: dry season (12 - 13 Sept.), 40 min: transition period (07 - 31 Oct.), 60 min: wet season (01 - 14 Nov.)

⁽²⁾ IC: ion chromatography, FIA: flow injection analysis

The chemiluminescence NO/NO_x analyzer (Thermo Environment Instruments) was equipped with a molybdenum converter to transform ambient NO₂ to NO. However, the converter basically responds to the sum of NO₂ + HNO₃ + HONO + PAN + aerosol NO₃⁻ + organic nitrates. Therefore, it is likely that NO₂ measurements might be biased by a positive artifact [cf. *Fehsenfeld et al.*, 1990]. During our study, the inlet line for NO/NO_x measurements had a length of 25 m (inner diameter = 4.4 mm). Therefore, highly soluble and sticky species such as HNO₃ and HONO are assumed to be at least partly removed within the long inlet tubing. In addition, mixing ratios of HNO₃ and HONO were usually below 0.5 ppb (see chapter 2), indicating that interferences would be marginal in case any of these gases would reach the chemiluminescence analyzer. PAN is a thermally unstable compound at temperatures even well below those observed at FNS [*Kirkman et al.*, 2002] and aerosol NO₃⁻ was eliminated by the application of an inlet filter.

Also listed in Table 4.1 are those (micro)-meteorological sensors that were used to measure the quantities involved in this study, namely air temperature (T), relative humidity (RH), surface wetness, global radiation flux, momentum, latent and sensible heat flux and ingoing/outgoing short- and longwave radiation. Eddy covariance measurements were conducted using a Gill 3D-sonic anemometer. The H₂O mixing ratio was monitored by a fast LI-COR infrared gas analyzer, and its analog output was directly fed to the ultrasonic anemometer A/D converter. Post-processing of the eddy covariance data (EDDYWSC, software by Alterra, Wageningen University Research, Netherlands) resulted in 30 minutes averages of sensible heat flux, latent heat flux, friction velocity and Monin-Obukov length. More details on the eddy covariance measurements and corresponding data evaluation/calibration procedures are given in *Araujo et al.* [2002].

Precipitation was sampled from 12 September to 14 November 2002 using a wet-only rainwater collector (Aerochem Metrics). A total of 23 rainstorm events were collected representing 100 % of the precipitation in this period. Rain samples were stored in the dark at 4 °C using polyethylene bottles which were previously rinsed with deionized water and preserved with Thymol. In order to trace possible contaminations, the sample pH was measured directly after sampling and before analysis. Analyses of NH₄⁺, NO₃⁻ and NO₂⁻ were performed for all samples using a Dionex DX600 ion chromatograph at the Laboratório de Ecologia Isotópica, CENA/USP (São Paulo, Brazil). The detection limit was 0.05 µM for all species. More details about sampling and analysis procedures are provided by *Lara et al.* [2001].

Moreover, a twin Differential Mobility Particle Sizer (DMPS) was employed to measure the dry aerosol particle size distribution in the diameter range from 3 to 850 nm. The size distribution of particles with aerodynamic diameters from 1 to 4

μm was measured with an Aerodynamic Particle Sizer (APS) [see *Rissler et al.*, 2004; *Vestin et al.*, 2005].

4.3 Theory: Estimation of dry and wet N deposition

4.3.1 Trace gas fluxes

Dry deposition fluxes of trace gases have been estimated using the inferential method, which is based on the “big leaf multiple resistance approach” [Wesely and Hicks, 1977; Hicks et al., 1987]. The deposition flux (F) ($\mu\text{g m}^{-2} \text{ s}^{-1}$) of a nonreactive trace gas for which the surface is a sink under all ambient conditions is defined by:

$$F = -V_d \cdot X(z_{ref}) = -\frac{X(z_{ref})}{R_a + R_b + R_c} \quad (4.1)$$

where $X(z_{ref})$ is the trace gas concentration ($\mu\text{g m}^{-3}$) at the reference height z_{ref} (m) and V_d denotes the dry deposition velocity (m s^{-1}), which is the reciprocal of the sum of the turbulent resistance (R_a) (s m^{-1}), the quasi-laminar or viscous boundary layer resistance (R_b) (s m^{-1}), and the surface resistance (R_c) (s m^{-1}). According to Hicks et al. [1987] R_a between the reference height (z_{ref}) and the roughness length z_0 (m) is given by:

$$R_a = \frac{1}{\kappa \times u^*} \left[\ln \left(\frac{z_{ref}}{z_0} \right) - \Psi_H \left(\frac{z_{ref}}{L} \right) \right] \quad (4.2)$$

where κ denotes the von Karman constant (0.41) and L is the Monin-Obukov length (m), a measure of atmospheric stability that is derived from the sensible heat flux and the friction velocity u^* [Garratt, 1992]. $\Psi_H(z_{ref}/L)$ is the stability correction function for heat and inert tracers in its integral form [see Thom, 1975]. The roughness length z_0 of the grass surface at the FNS site was taken as 0.11 m [cf. Kirkman et al., 2002] and z_{ref} was 5.3 m and 10 m for the WAD/SJAC and for the NO_x measurements, respectively (Table 4.1). To account for conditions when the reliability of micrometeorological techniques was low, data were rejected for $u^* \leq 0.01 \text{ m s}^{-1}$ and $(z_{ref} - d)/L \leq 5$, i.e. when extremely low turbulence and/or very high thermal stability was prevailing. Also, data were rejected for $(z_{ref} - d)/L \geq -5$, which reflects cases of very high thermal turbulence production (when Monin-Obukov similarity is no longer valid [see Ammann, 1999]).

R_b determines the exchange of gaseous matter by molecular-turbulent diffusion across the viscous laminar sublayer immediately above the vegetation elements, and can be described by [Hicks et al., 1987]:

$$R_b = \frac{2}{\kappa \times u^*} \left(\frac{Sc}{Pr} \right)^{\frac{2}{3}} \quad (4.3)$$

where Sc and Pr are the Schmidt and Prandtl number, respectively. Pr is 0.72 and Sc is a strong function of the molecular diffusivity of the trace gas. Values for Sc were taken from *Hicks et al.* [1987] and *Erisman et al.* [1994] for the different trace gas species. The surface resistances R_c could not be directly determined from our field measurements; hence values were adopted from literature (see section 4.4.4).

The inferential method is valid for trace gases whose mixing ratio at the soil and/or vegetation elements is zero. The observation of a net NO_2 deposition flux to the FNS pasture [*Kirkman et al.*, 2002] justifies the application of the inferential model for NO_2 in our study. This is also valid for HNO_3 , since it is a sticky, highly water-soluble molecule which features a rapid downward flux with negligible R_c and corresponding high V_d [e.g., *Hanson and Lindberg*, 1991; *Dollard et al.*, 1987].

By contrast, NO , HONO and NH_3 may be both deposited to and emitted from surfaces. Formally, this can be accounted for by a so-called canopy compensation point concentration X_c ($\mu\text{g m}^{-3}$) [e.g., *Hesterberg et al.*, 1996], that generally refers to the concentration of the compound just above the soil and/or vegetation elements [cf. *Nemitz et al.*, 2004a]:

$$F = \frac{X_c - X(z_{ref})}{R_a + R_b + R_c} \quad (4.4)$$

When $X(z_{ref})$ drops below X_c net emission will occur, otherwise net deposition takes place. The net NO emission from the FNS pasture site determined by *Kirkman et al.* [2002] was very low ($0.65 \text{ ngN m}^{-2} \text{ s}^{-1}$ or $0.17 \text{ kgN ha}^{-1} \text{ yr}^{-1}$), thus we neglected any contribution of NO to the surface-atmosphere exchange of N species in our study. In case of HONO it is generally assumed that it is formed through heterogeneous reaction of NO_2 with surface water e.g., [*Harrison et al.*, 1996] and it may subsequently be emitted from plant foliar cuticles or soil surfaces. Since there is no indication for any direct HONO emissions by plants [*Schiemang et al.*, 2004], the HONO compensation point concentration $X_c(\text{HONO})$ is expected to be a function of the NO_2 mixing ratio (see section 4.4.4).

To predict the bi-directional surface-atmosphere exchange of NH_3 at the FNS site, we applied a simplified dynamic resistance model developed by *Sutton et al.* [1998]. Besides uptake and emission of NH_3 via plant stomata, the dynamic model accounts for absorption of NH_3 by epicuticular water films under very humid conditions, and subsequent re-evaporation. Contrary to straightforward resistance

models, the approach according to *Sutton et al.* [1998] treats leaf surface exchange as a capacitance, such that the flux is time dependent on the flux history. Since the FNS site is used as a cattle ranch and the NH_3 flux directly from the soil is assumed to be negligible compared to that originating from cattle excreta, we considered a direct NH_3 flux from cattle manure and urine $F(\text{NH}_3)_{\text{excreta}}$. The net NH_3 flux $F(\text{NH}_3)$ can be related directly to the NH_3 canopy compensation point concentration $X_c(\text{NH}_3)$. Hence, the model uses $X_c(\text{NH}_3)$ as a central parameter rather than $R_c(\text{NH}_3)$ [*Sutton et al.*, 1998] and $F(\text{NH}_3)$ is composed of its component fluxes through plant stomata, $F_s(\text{NH}_3)$, the flux in or out of the epicuticular water film (adsorption capacitor), $F_d(\text{NH}_3)$, and $F(\text{NH}_3)_{\text{excreta}}$:

$$\begin{aligned}
 F(\text{NH}_3)_t &= \underbrace{\frac{X_s(\text{NH}_3) - X_c(\text{NH}_3)}{R_s(\text{NH}_3)}}_{F_s(\text{NH}_3)} + \underbrace{\frac{X_d(\text{NH}_3)_t - X_c(\text{NH}_3)}{R_d(\text{NH}_3)}}_{F_d(\text{NH}_3)} + F(\text{NH}_3)_{\text{excreta}} \\
 &= \frac{X_c(\text{NH}_3) - X(\text{NH}_3, z_{\text{ref}})}{R_a + R_b}
 \end{aligned} \tag{4.5}$$

where $X_s(\text{NH}_3)$ denotes the NH_3 stomata compensation point concentration ($\mu\text{g m}^{-3}$) and $R_s(\text{NH}_3)$ denotes the NH_3 stomata resistance (s m^{-1}). $R_s(\text{NH}_3)$ and $X_s(\text{NH}_3)$ refer to the exchange of NH_3 between air and the leaf's intercellular fluid, containing dissolved NH_3 and NH_4^+ in thermodynamic equilibrium with the air within substomatal cavities [*Flechard et al.*, 1999]. $X_d(\text{NH}_3)_t$ is the NH_3 adsorption concentration ($\mu\text{g m}^{-3}$) associated with the “leaf surface capacitor” at time step t and $R_d(\text{NH}_3)$ is the charging resistance of the capacitor (s m^{-1}). $X_c(\text{NH}_3)$ is then determined by [*Sutton et al.*, 1998]:

$$X_c(\text{NH}_3)_t = \frac{X(\text{NH}_3, z_{\text{ref}})/(R_a + R_b) + X_s(\text{NH}_3)/R_s(\text{NH}_3) + X_d(\text{NH}_3)_t/R_d(\text{NH}_3) + F(\text{NH}_3)_{\text{excreta}}}{(R_a + R_b)^{-1} + R_s(\text{NH}_3)^{-1} + R_d(\text{NH}_3)^{-1}} \tag{4.6}$$

$X_s(\text{NH}_3)$ can be parameterized according to [*Farquhar et al.*, 1980; *Sutton et al.*, 1994]:

$$X_s(\text{NH}_3) = \frac{161512}{T_s} \cdot 10^{(-4507.11/T(z_0))} \cdot \Gamma \cdot 17000 \tag{4.7}$$

where T_s is the surface temperature (K) which was derived from the outgoing longwave radiation by applying the Stefan-Boltzmann law. Γ is the ratio of apoplastic $[\text{NH}_4^+]/[\text{H}^+]$ and was adopted from the literature (section 4.4.4). Particularly, under high temperature conditions, elevated NH_3 partial pressures within substomatal cavities above the dissolved NH_4^+ in the apoplastic fluid are common. During relatively dry daytime conditions and in the absence of precipitation, the algorithm of *Nemitz et al.* [2004a] to calculate $R_s(\text{NH}_3)$ from the measured latent heat flux LE (W m^{-2}) can be applied:

$$\begin{aligned} R_s(\text{NH}_3) &= \frac{D_{\text{H}_2\text{O}}}{D_{\text{NH}_3}} \cdot R_s(\text{H}_2\text{O}) \\ &= -\frac{D_{\text{H}_2\text{O}}}{D_{\text{NH}_3}} \cdot \frac{e_{\text{H}_2\text{O}}(z_0) - e_{\text{sat}}(T(z_0))}{LE} \end{aligned} \quad (4.8)$$

where $D_{\text{H}_2\text{O}}$ and D_{NH_3} denote the diffusion coefficients of H_2O ($0.26 \text{ cm}^2 \text{ s}^{-1}$) and NH_3 ($0.24 \text{ cm}^2 \text{ s}^{-1}$), respectively. The water vapor pressure $e_{\text{H}_2\text{O}}$ and the temperature T at z_0 were deduced from the sensible and latent heat flux using the flux-profile relationships for heat and water vapor [cf. *Ammann*, 1999]. However, during periods when evaporation of epicuticular water films contributed significantly to LE (0700–1000 LT) (cf. chapter 3) relationship (7) was not applied (see section 4.4.4).

Then $X_d(\text{NH}_3)$ at time step t was calculated as:

$$X_d(\text{NH}_3)_t = \frac{Q_{d,t}}{C_d} \quad (4.9)$$

where $Q_d(t)$ denotes the adsorption charge ($\mu\text{g m}^{-2}$) at time step t and C_d is the capacitance of the water film (m). Since leaf surface water layers are expected to have a certain capacitance C_d for a defined “water film thickness” and for a given pH according to Henry’s law, C_d was parameterized according to *Sutton et al.* [1998]:

$$C_d = M_{\text{H}_2\text{O}}^c \left[\frac{\{H^+\}}{(10^{1.6035 - 4207.6/T})} + 10^{1477.7/T_s - 1.6937} \right] \quad (4.10)$$

where $M_{H_2O}^c$ is the equivalent canopy area water film thickness (nm). *Sutton et al.* [1998] suggested a parameterization of $M_{H_2O}^c$ with the leaf area index (LAI) and the relative humidity (RH , %):

$$M_{H_2O}^c = LAI \cdot 20 \exp\left[\frac{(RH - 60)}{10}\right] \quad (4.11)$$

The LAI was taken as $1.5 \text{ m}^2 \text{ m}^{-2}$, based on the values of $1.2 \text{ m}^2 \text{ m}^{-2}$ and $2.1 \text{ m}^2 \text{ m}^{-2}$ reported by *Kirkman et al.* [2002]. The flux $F_d(NH_3)$ in and out of the adsorption capacitor (epicuticular water film) is derived by:

$$F_d(NH_3)_t = \frac{X_d(NH_3)_t - X_c(NH_3)_t}{R_d(NH_3)} \quad (4.12)$$

where $R_d(NH_3)$ denotes the charging resistance of the capacitor (s m^{-1}) and is a function of C_d (see section 4.4.4). The new capacitance charge after time step t is then:

$$Q_{d,(t+1)} = Q_{d,t} - F_d \cdot t + Q_{d,t} \cdot K_r \quad (4.13)$$

The term $Q_{d,t} \cdot K_r$ accounts for a so-called leaf uptake flux of the NH_4^+ stored in the epicuticular water film. Thereby, K_r is the rate constant which has a negative value for deposition (see section 4.4.4).

4.3.2 Aerosol fluxes

Whereas gases are mainly transported by molecular diffusion through the quasi-laminar boundary layer, particle transport and deposition basically take place through sedimentation, interception, and impaction and/or Brownian diffusion [e.g., *Seinfeld and Pandis*, 1998]. Up to date, no well established bulk resistance models exist for particle deposition and significant discrepancies have been observed between experimental results and model predictions [*Ruijgrok et al.*, 1995]. The theoretical framework proposed by *Slimm* [1982] is widely used in modeling studies to predict particle deposition velocities. However, *Wesely et al.* [1985] derived an empirical parameterization for the dry deposition velocity V_p (m s^{-1}) of submicron sulfate aerosols ($D_p = 0.1 - 1.0 \text{ } \mu\text{m}$) to grass surfaces:

$$V_p = u^* \cdot 0.002 \quad , \text{ for } L \geq 0 \quad (4.14a)$$

$$V_p = u^* \cdot 0.002 \cdot \left[1 + \left(\frac{-300}{L} \right)^{\frac{2}{3}} \right] \quad , \text{ for } L < 0 \quad (4.14b)$$

This approach generally results in much higher V_p values for submicron particles than predicted by the Slinn model. Several other studies [e.g., *Sievering et al.*, 1994; *Ratray and Sievering*, 2001, *Garland*, 2001; *Gallagher et al.*, 2002; *Nemitz et al.*, 2004b; *Vong et al.*, 2004] also showed that V_p to surfaces of low aerodynamic roughness may be much larger than predicted by the Slinn model, even for particles of different chemical composition than studied by *Wesely et al.* [1985]. In this study, however, either PM 2.5 or TSP was sampled. NH_4^+ it is known to be largely attributed to fine mode aerosols with $D_p \leq 1.0 \mu\text{m}$ [e.g., *Seinfeld and Pandis*, 1998], which was also observed during the SMOCC measurement campaign [*Decesari et al.*, 2005]. By contrast, aerosol NO_3^- exhibited a bimodal size distribution [*Falkovich et al.*, 2005]. Since we did not find an empirical relationship in the literature to estimate V_p for aerosols with $D_p \geq 1.0 \mu\text{m}$ and the contribution of coarse mode aerosol NO_3^- relative to that of fine mode aerosol NH_4^+ is presumably small (see below, Table 4.2), the parameterization by *Wesely et al.* [1985] is considered as a reasonable approximation for both PM 2.5 and TSP samples.

4.3.3 Determination of characteristic time scales

The resistance-based approaches presented above to calculate surface-atmosphere exchange fluxes rely on the “constant flux layer assumption”, which implies that the trace compounds considered are chemically-non-reactive tracers, such that their flux within the atmospheric surface layer is constant. When dealing with compounds that undergo rapid chemical transformation, divergence of the vertical fluxes should be taken into account [*Kramm et al.*, 1995]. However, sufficiently accurate fluxes of reactive species can be estimated without consideration of vertical flux divergence, as long as characteristic chemical time scales are much larger than turbulent transport times [*De Arellano and Duynkerke*, 1992]. The relation of turbulent timescales to chemical timescales is generally referred to as the Damköhler ratio (D_r). Fluxes of reactive species are considered not to be affected by chemical transformation processes if $D_r < 0.1$ [cf. *Nemitz et al.*, 2004a]. Following *De Arellano and Duynkerke*, [1992] the characteristic time of turbulent transport τ_{turb} (s) can be calculated as:

$$\tau_{turb} = K \cdot (z_{ref} + z_0) \cdot \left(\frac{\sigma_w^2}{u^*} \right)^{-1} \quad (4.15)$$

where σ_w denotes the standard deviation of the vertical wind component (m s^{-1}). Atmospheric stability strongly determines the time scale of turbulent transport, which typically ranges from a couple of seconds under unstable conditions up to 2.5 hours under stable conditions [e.g., *Dlugi*, 1993].

For the characteristic chemical time scale of the NO-NO₂-O₃ triad, its photo-stationary equilibrium has to be considered. NO₂ is rapidly photolyzed to NO in the troposphere and it is formed back by reaction of NO with O₃. The overall chemical time scale of the NO-NO₂-O₃ triad $\tau(\text{NO-NO}_2\text{-O}_3)$ is given by the combination of $\tau(\text{NO}) = (k_2 \times [\text{O}_3])^{-1}$, $\tau(\text{NO}_2) = k_1^{-1} = j(\text{NO}_2)^{-1}$ and $\tau(\text{O}_3) = (k_2 \times [\text{NO}])^{-1}$ [*Lenschow*, 1982] (where k is the reaction rate constant) and was calculated in accordance to *Kirkman et al.* [2002]. Thereby, $j(\text{NO}_2)$ was estimated from global radiation data using a relation derived from simultaneous measurements of global radiation and $j(\text{NO}_2)$ in Amazonia during LBA-EUSTACH [cf. *Kirkman et al.*, 2002]. The estimation of the chemical time scale for HONO is more complex. HONO is rapidly photolyzed during daylight hours. The chemical time scale for daytime HONO photolysis is given by $\tau(\text{HONO})_{\text{photol.}} = j(\text{HONO})^{-1}$, whereby the parameterization provided by *Kraus and Hofzumahaus* [1998] was used to relate $j(\text{HONO})$ to $j(\text{NO}_2)$. HONO formation largely occurs through heterogeneous reaction of NO₂ with surface water particularly under humid nighttime conditions, as suggested by e.g., *Harrison and Kitto* [1994] and *Kleffmann et al.* [2003]. To derive a realistic estimate for the chemical time scale of heterogeneous HONO formation at nighttime $\tau(\text{HONO})_{\text{het.}}$, we considered the HONO production rate P_{HONO} (ppb h⁻¹) determined directly from our measurements (see section 4.4.3.).

Homogeneous daytime HONO formation may proceed via reaction of NO with OH radicals; however, this process is very slow and can be neglected compared to daytime HONO photolysis [*Lammel and Cape*, 1996]. Photochemical reactions involving NH₃ and HNO₃ are not considered to contribute to any flux divergence since their chemical time scale is much larger than the time scale of turbulent transport. NH₃ reacts slowly with OH and has an atmospheric lifetime by this reaction of the order of 70 days [*Pandis et al.*, 1995]. The typical conversion rate of NO_x to HNO₃ is about 8 % per hour in the rural atmosphere during daytime [*Pandis et al.*, 1995] and the chemical lifetime of HNO₃ with respect to OH is about 83 days [*Finlayson-Pitts and Pitts*, 1986].

By contrast, time scales to achieve gas/aerosol equilibrium between gaseous NH₃, HNO₃ and particulate NH₄NO₃ may range from a couple of seconds for submicron particles up to some hours for larger ones [*Dlugi*, 1993; *Meng and*

Seinfeld, 1996]. They may therefore occur within the time frame of turbulent transport and have to be explicitly considered here. Particularly during periods of large temporal changes of temperature and relative humidity (e.g., around sunrise or sunset) rapid evaporation of semi-volatile aerosol species or condensation of the vapor phase can be expected. As reported in chapter 3, the measured concentration product of $\text{NH}_3 \times \text{HNO}_3$ was persistently below the theoretical equilibrium dissociation constant of the pure $\text{NH}_3/\text{HNO}_3/\text{NH}_4\text{NO}_3$ system during daytime ($RH < 90\%$). The desired equilibration time scale $\tau(\text{NH}_3\text{-HNO}_3\text{-NH}_4\text{NO}_3)$ can be estimated according to *Wexler and Seinfeld* [1992]:

$$\tau(\text{NH}_3 - \text{HNO}_3 - \text{NH}_4\text{NO}_3)^{-1} = 3\bar{D} \times \int_0^\infty \frac{m(R_p)dR_p}{\left(1 + \frac{\lambda}{\alpha + R_p}\right) \times R_p^2 \times \rho_p} \quad (4.16)$$

whereby the measured aerosol number size distribution was related to the aerosol mass size distribution $m(R_p)dR_p$. R_p is the particle radius (m), \bar{D} is the geometric mean of the diffusivity of semi-volatile gaseous species ($\text{m}^2 \text{s}^{-1}$), m is the water-soluble particle mass (kg m^{-3}), λ is the mean free path of air ($6.51 \times 10^{-8} \text{ m}$ at 293.15 K), α denotes the accommodation coefficient ($0.001 < \alpha < 1$) [*Wexler and Seinfeld*, 1990], and ρ_p is the particle density. A value of $\rho_p = 1.35 \pm 0.15 \text{ g cm}^{-3}$ was used as determined by *Reid and Hobbs* [1998] for Amazonian biomass burning aerosols. This value is in good agreement with the estimate derived from measurements during SMOCC [see *Vestin et al.*, 2005].

The comparison of τ_{turb} with $\tau(\text{NO-NO}_2\text{-O}_3)$, $\tau(\text{HONO})_{\text{photol.}}$, $\tau(\text{HONO})_{\text{het.}}$ and $\tau(\text{NH}_3\text{-HNO}_3\text{-NH}_4\text{NO}_3)$ allows to test whether reactive species can be treated as a passive tracer during their vertical transport within the surface layer ($D_r < 0.1$) and, consequently, if the application of the “big leaf multiple resistance approach” and the “canopy compensation point model” are justifiable.

4.3.4 Wet N deposition

Storm size influences the chemical composition of the rainwater, in the sense that larger storms tend to be more dilute. This dependence demands the use of volume weighted means (VWM) for the calculation of monthly and annual concentration averages. For each rainwater solute, the concentrations measured in the sample were combined to create a VWM concentration for each collection date:

$$\text{VWM}_a = \frac{\sum_{i=1}^n c_{ai} \times v_i}{\sum v_i} \quad (4.17)$$

where c_{ai} is the concentration of species a in sample i , n is the number of samples and v_i is the volume of precipitation solution for sample i . The corresponding wet deposition rates for September, October and November were derived by summation of the VWM concentration determined for each precipitation event throughout the month, and subsequent multiplication by the mean of rainfall in the respective month obtained from historical time series (see <http://www.aneel.gov.br>). The annual wet N deposition was derived in a similar way; for instance, the VWM concentration obtained during September was considered as representative of the entire dry season and then multiplied by the historical mean rainfall for the dry season. The same procedure was performed for October and November representing transition period and wet season, respectively.

4.4 Results and Discussion

In the following, the general patterns of our results will be shown as diel courses of the medians of measured and inferred quantities. Diel courses will be presented either for part of the dry season (biomass burning, 12 - 23 Sep.) or, where the investigated quantities are relatively independent of season, for the entire measurement campaign (12 Sep. - 14 Nov. 2002). To derive surface-atmosphere exchange fluxes of N-containing compounds, (micro)-meteorological data and NO_x/O_3 data were synchronized to the time resolution of the WAD/SJAC system. The convention of negative downward fluxes (net deposition) and positive upward fluxes (net emission) has been adopted.

4.4.1 Meteorological conditions

In the Amazon Basin, nighttime radiative cooling usually results in the formation of a shallow, decoupled nocturnal boundary layer of high thermodynamic stability characterized by very low wind speeds; while the development of a deepening, convectively mixed layer starts with the heating of the surface in the morning [e.g., *Nobre et al.*, 1996; *Fisch et al.*, 2004]. Median nighttime wind speeds at FNS were low ($\leq 1 \text{ m s}^{-1}$). By contrast, wind speeds were substantially higher during daytime, ranging from 2 to 3 m s^{-1} . The daytime boundary layer in the Amazon Basin is generally characterized by intensive turbulence (cf. chapter 3). The 24-h average friction velocity (u^*) was $\sim 0.16 \text{ m s}^{-1}$ and reached maxima of $\sim 0.4 \text{ m s}^{-1}$ around noon. Differences of u^* between the dry season, the transition period, and the wet season were marginal. As a consequence of high global radiation fluxes ($500 - 900 \text{ W m}^{-2}$, median) during daytime, ambient temperatures at the FNS site ranged between 30 and 36°C during sunlight hours, while nighttime temperatures were much lower (20 – 25°C). High relative

humidities (*RHs*) were observed during nighttime (90 – 100 %), while daytime *RH* values usually dropped to 40 – 50 % during afternoon hours. Local meteorology changed only marginally from the dry season to the wet season. Strong rain events ($\geq 30 \text{ mm h}^{-1}$) occurred in the afternoon hours during the transition period and the wet season. A more detailed description of diel meteorological conditions can be found in chapter 3.

4.4.2. Concentrations

Median diel variations of NO, NO₂, O₃, NH₃, HNO₃, HONO and the inorganic aerosol species NH₄⁺ and NO₃⁻ are shown in Fig. 4.2a-h for 12 to 23 September (dry season, biomass burning). Table 4.2a,b summarizes ambient mixing ratios measured during the dry season (12 - 23 Sep.), the transition period (07 - 31 Oct.) and the wet season (01 - 14 Nov.). A detailed discussion of seasonal and diel cycles observed for NH₃, HNO₃, HONO and aerosol NH₄⁺ and NO₃⁻ is given in chapter 2 and chapter 3.

Despite intensive biomass burning activity during the dry season, NO mixing ratios were very low (Fig. 4.2d). The sharp peak between 0600 and 0900 LT was most likely due to rapid photolysis of accumulated nighttime NO₂ shortly after sunrise, when O₃ mixing ratios were still too low to re-oxidize significant amounts of NO (see Fig. 4.2e,f). NO₂ was the most abundant N-containing trace gas during all three seasons and reached an average mixing ratio of ~ 5 ppb during the dry season. NO₂ featured a pronounced diel cycle with nighttime mixing ratios two times higher than during daytime (Fig. 4.2e). Apparently, NO₂ was accumulated in a shallow nocturnal boundary layer of high thermodynamic stability due to: (i.) the low water-solubility of NO₂ and consequently its low affinity to be taken up by epicuticular water films and (ii.) chemical production through reaction of NO with O₃ in the absence of NO₂ photolysis. During daytime, photolysis and convective mixing within the boundary layer led to a significant decrease of NO₂ mixing ratios. Through the transition period until the wet season, NO₂ mixing ratios declined by a factor of four. O₃ mixing ratios exhibited a typical diel variation, which mirrors that of NO₂ (high values during daytime and lower values during the night (Fig. 4.2f)). This was mainly caused by (i.) photochemical daytime production, (ii.) convective mixing within the boundary layer and from the free troposphere during daytime and (iii.) dry deposition and reaction with NO in a thermally stable stratified nocturnal boundary layer.

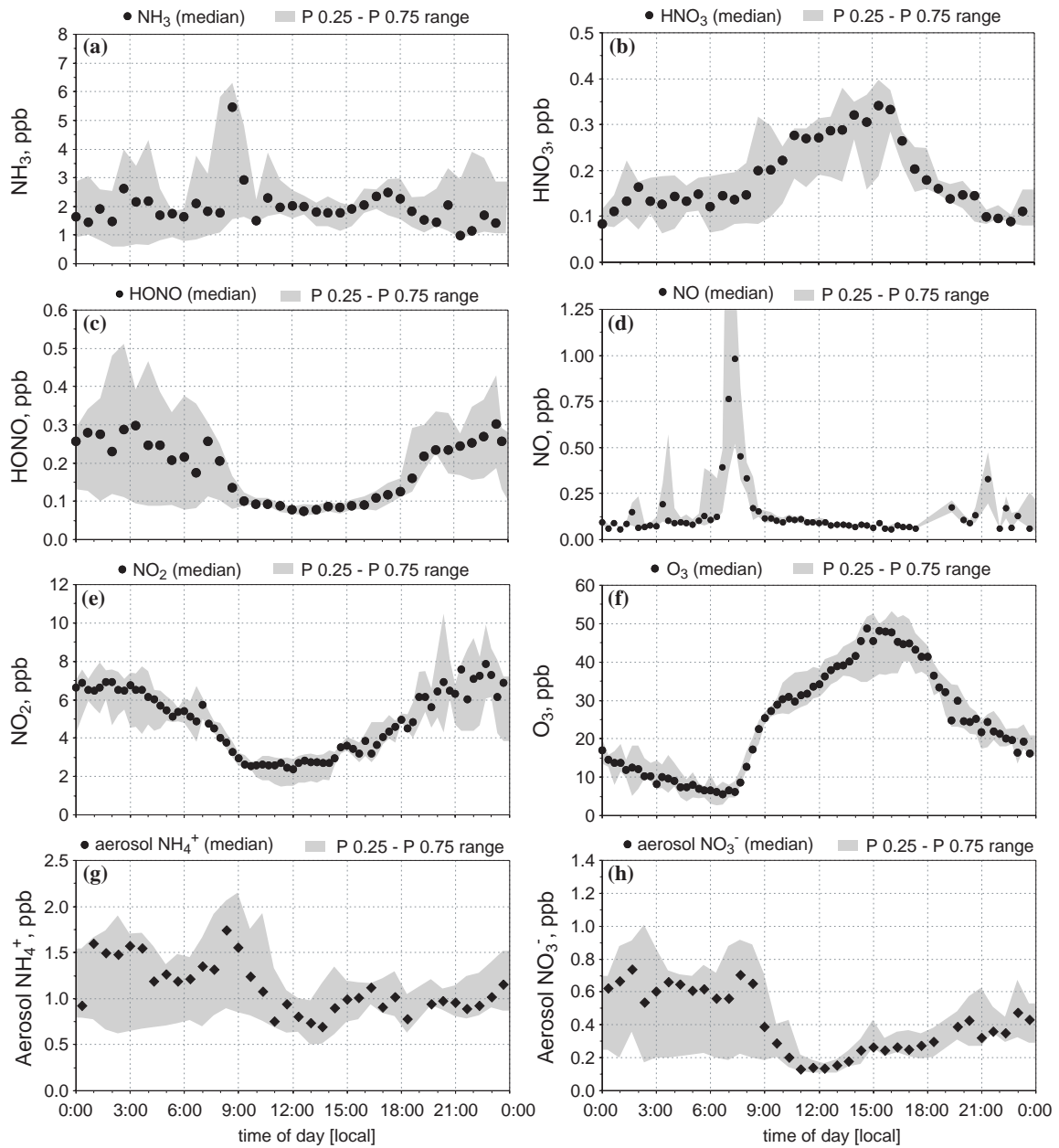


Figure 4.2a-h: Diel variations of (a) NH_3 , (b) HNO_3 , (c) HONO , (d) NO , (e) NO_2 , (f) O_3 , (g) aerosol NH_4^+ (PM 2.5) and (h) aerosol NO_3^- (PM 2.5) measured during 12 - 23 Sep. 2002 (dry season, biomass burning) at FNS during LBA-SMOCC 2002. Symbols and grey shading represent medians and interquartile ranges (0.25 to 0.75 percentiles), respectively.

Table 4.2: Summary of trace gas and aerosol mixing ratios^(*) during the dry season (12 - 13 Sept.), the transition period (07 - 31 Oct.) and the wet season (01 - 14 Nov.) at FNS during LBA-SMOCC 2002.

Species	Dry season				Transition period				Wet season			
	m (ppb)	P 0.25 (ppb)	P 0.75 (ppb)	n (1)	m (ppb)	P 0.25 (ppb)	P 0.75 (ppb)	n (1)	m (ppb)	P 0.25 (ppb)	P 0.75 (ppb)	n (1)
NO	0.09	0.07	0.15	372	0.09	0.07	0.17	295	0.12	0.07	0.13	229
NO ₂	4.54	2.85	6.46	630	1.78	1.23	2.56	697	1.07	0.82	1.76	268
O ₃	24.3	11.76	34.87	826	25.59	15.91	32.95	781	14.74	10.77	19.39	316
NH ₃	1.81	1.10	2.91	298	1.06	0.5	1.74	236	0.55	0.38	0.85	60
HNO ₃	0.16	0.10	0.25	317	0.06	0.03	0.13	210	0.06	0.04	0.08	52
HONO	0.12	0.08	0.27	323	0.07	0.05	0.09	315	0.06	0.04	0.07	139
Aerosol NH ₄ ⁺	1.01	0.73	1.51	291	0.54	0.33	0.85	267	0.47	0.32	0.62	66
Aerosol NO ₃ ⁻	0.34	0.17	0.61	297	0.09	0.06	0.15	282	0.06	0.04	0.07	33

^(*) m: median, P 0.25: 0.25 percentile, P 0.75: 0.75 percentile, n: number of determined data points above the limit of detection (for aerosol species PM 2.5 and bulk measurements were included). NO_x/O₃ data were synchronized to the WAD/SJAC data, i.e. one data point is available for each gas and each aerosol measurement of the WAD/SJAC).

4.4.3 Characteristic time scales

Characteristic turbulent time scales (τ_{turb}), shown in Fig. 4.3a-c, have been calculated according to eq. (4.15) for $z_{ref} = 10$ m (NO_x/O_3 measurements) and for $z_{ref} = 5.3$ m (WAD/SJAC measurements) (cf. Table 4.1).

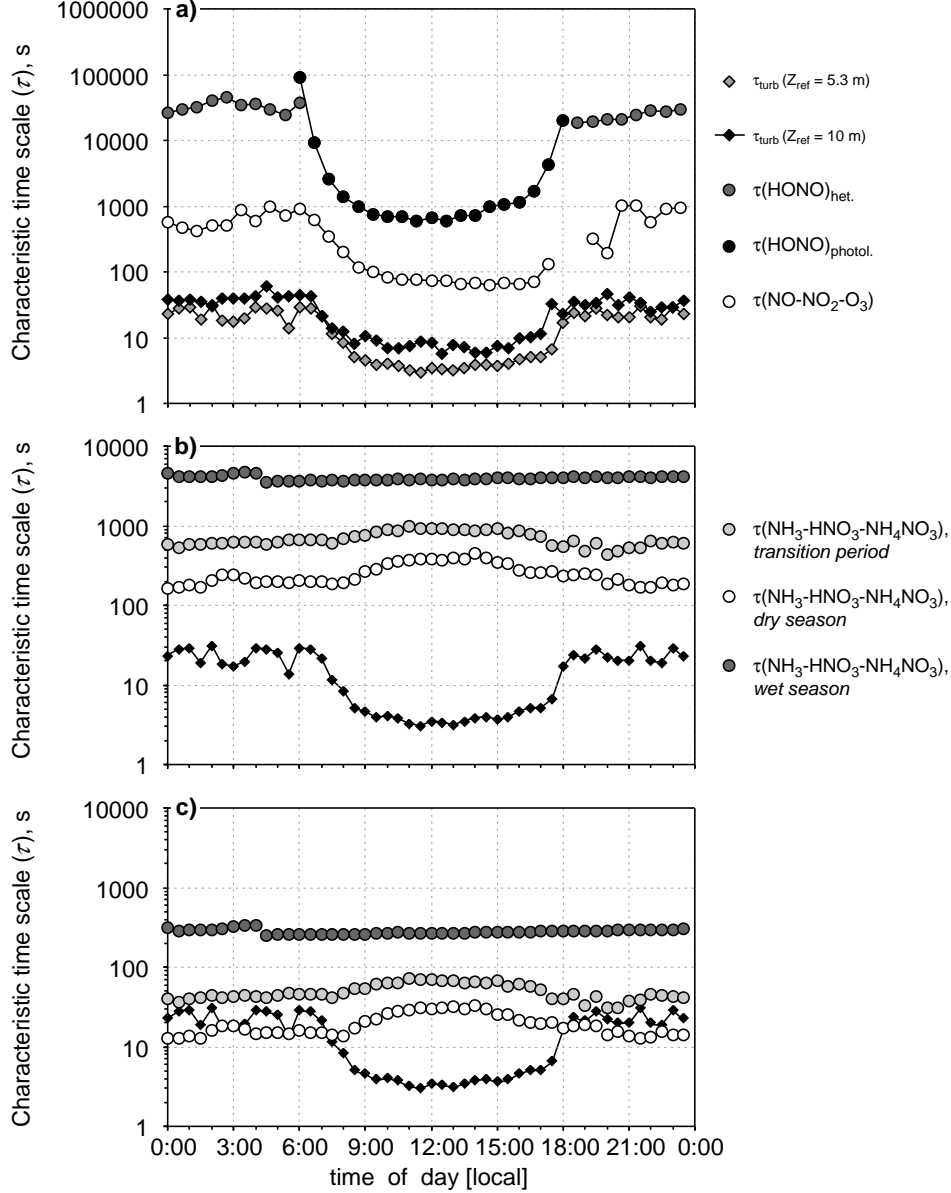


Figure 4.3a-c: Diel variation of characteristic turbulent time scale τ_{turb} for the reference heights $z_{ref} = 10$ m and $z_{ref} = 5.3$ m in comparison to (a) chemical time scale of the $\text{NO-NO}_2\text{-O}_3$ triad ($\tau(\text{NO-NO}_2\text{-O}_3)$), daytime HONO photolysis ($\tau(\text{HONO})_{photol.}$) and heterogeneous HONO formation at night ($\tau(\text{HONO})_{het.}$, dry season only), (b) upper estimate of equilibration time scales for the $\text{NH}_3/\text{HNO}_3/\text{NH}_4\text{NO}_3$ system ($\alpha = 0.1$, $\text{PM}_{inorg.} \leq 20\%$) and (c) lower estimate of $\tau(\text{NH}_3/\text{HNO}_3/\text{NH}_4\text{NO}_3)$ ($\alpha = 1$, $\text{PM}_{soluble} \leq 60\%$) at FNS during LBA-SMOCC 2002. Except for $\tau(\text{HONO})_{het.}$, data from all seasons were used.

To calculate the characteristic time scale for heterogeneous nighttime HONO buildup ($\tau(HONO)_{het.}$) (Fig. 4.3a), only dry season nighttime HONO production rates (P_{HONO}) were considered. For the transition period and the wet season P_{HONO} could not be determined since the HONO diel variation was substantially reduced (cf. chapter 2). Our measurements revealed a relatively small average value of $P_{HONO} = 0.04 \text{ ppb h}^{-1}$. By contrast, other studies reported values ranging from 0.12 to 0.47 ppb h^{-1} [Alicke *et al.*, 2003; Harrison and Kitto, 1994; Lammel and Cape, 1996]. Fig. 4.3a shows that τ_{turb} was at least two orders of magnitude smaller than $\tau(HONO)_{photol.}$ and $\tau(HONO)_{het.}$, resulting in $D_r \ll 0.1$. Considering the chemical time scale of the NO-NO₂-O₃ triad $\tau(NO-NO_2-O_3)$ (Fig. 4.3a), largest D_r values are found between 1700 LT and 2000 LT, exceeding a value of 0.2 ($z_{ref} = 10 \text{ m}$). However, during all other periods D_r for the NO-NO₂-O₃ triad ranged between 0.05 and 0.1. Therefore, we conclude that the application of eq. (4.1) and (4.4) to calculate surface-atmosphere exchange fluxes of NO₂ and HONO are justified, since chemical transformations are too slow to affect the vertical constancy of turbulent fluxes.

The estimation of the equilibration time scale $\tau(NH_3-NO_3-NH_4NO_3)$ was performed by integrating over the measured particle size distribution according to eq. (4.16), whereby two different cases were considered. Case 1 is an upper estimate (Fig. 4.3b), using an accommodation coefficient $\alpha = 0.1$ [Wexler and Seinfeld, 1992] and taking into account only the inorganic water-soluble aerosol fraction ($\leq 20 \%$ of PM_{tot}) (cf. chapter 3). Case 2, the lower estimate (Fig. 4.3c), was calculated using $\alpha = 1$ and considering also water-soluble organic carbon (WSOC). The total water-soluble fraction (organic and inorganic) accounted on average for $\sim 60 \%$ of the total aerosol mass [Decesari *et al.*, 2005]. As shown in Fig. 4.3b,c $\tau(NH_3-NO_3-NH_4NO_3)$ increased substantially from the dry season through the transition period to the wet season. This is obviously caused by much higher particle number concentrations measured during the dry season when biomass burning took place [see Vestin *et al.*, 2005]. For case 1 (upper estimate) (Fig. 4.3b), D_r for the $NH_3-NO_3-NH_4NO_3$ triad during the dry season ranges from 0.1 to 0.17 at nighttime and is smaller than 0.1 during the day. During the transition period and wet season, D_r for the $NH_3-NO_3-NH_4NO_3$ triad is always significantly smaller than 0.1 (Fig. 4.3b). However, for case 2 (lower estimate) (Fig. 4.3c) nighttime D_r substantially exceeds a critical value of 0.1 during the dry season and the transition period.

To verify the theoretically derived values, results from a laboratory study will be discussed briefly. Condensation and evaporation of NH₃ and HNO₃ to/from particles have been investigated under controlled laboratory conditions. Particles were collected during field campaigns in 1991 [e.g., Brunnemann *et al.*, 1996; Seidl *et al.*, 1996] and 1993/1994 in the eastern part of Germany (Melpitz). The

chemical aerosol composition was dominated by $(\text{NH}_4)_2\text{SO}_4$, NaCl and soot and is comparable to that described in *Brunnemann et al.* [1996] and *Seidl et al.* [1996]. More than 90 % of the NH_4NO_3 mass was found in the accumulation mode ($D_p \leq 1 \mu\text{m}$). Timescales $\tau(\text{NH}_3\text{-HNO}_3\text{-NH}_4\text{NO}_3)$ were calculated using the algorithm proposed by (i.) *Kramm and Dlugi* [1994] and (ii.) *Meng and Seinfeld* [1996], resulting in $\tau(\text{NH}_3\text{-HNO}_3\text{-NH}_4\text{NO}_3) = 100 - 500 \text{ s}$ for fine mode particles and $\geq 880 \text{ s}$ for coarse mode particles. These values are comparable to characteristic times reported by *Harrison et al.* [1990] and *Meng and Seinfeld* [1996] and are in strong favor of our case 1 (upper estimate, Fig. 4.3b), which implies that the equilibration time scale was always much larger than that of turbulent transport. Consequently, condensation/evaporation processes might not have influenced turbulent fluxes. Nevertheless, it should be noted that the influence of the large soluble organic aerosol fraction typical for the Amazon Basin (cf. chapter 3) on gas/aerosol partitioning processes is not exactly known. Taking into account the potential role of WSOC in enhancing aerosol water uptake and subsequently the uptake of gaseous species, equilibration time scales may be equal or even faster than turbulent transport (cf. Fig. 4.3c).

4.4.4 The inferential approach: Discussion of input parameters

Some surface parameters required for the inferential method to estimate of surface-atmosphere exchange fluxes for trace gases (eq. 4.1 – 4.13) could not be directly derived from the results of our field measurements. Thus, lower and upper scenarios were estimated, comprising a certain range of surface-atmosphere exchange fluxes. These scenarios were obtained by varying surface parameters over a selected range based on results obtained from studies in temperate latitudes. Note that for all parameters and quantities presented, values indicated as “low” and values indicated as “high” correspond to the resulting lower and upper flux estimates, respectively.

Surface resistances $R_c(\text{HNO}_3)$, $R_c(\text{HONO})$ and $R_c(\text{NO}_2)$: HNO_3 is commonly thought to be deposited with the maximal rate allowed by atmospheric turbulence, since $R_c(\text{HNO}_3)$ was found to be zero in many studies [e.g., *Dollard et al.*, 1987; *Huebert and Robert*, 1985]. Very recently, *Nemitz et al.* 2004a showed that non-zero, however, relatively small $R_c(\text{HNO}_3)$ may exist ($R_c = 15 - 95 \text{ s m}^{-1}$). $R_c(\text{HONO})$ is considered to be only slightly higher than that of HNO_3 [*Wesely and Hicks*, 2000]. The ranges of $R_c(\text{HNO}_3)$ and $R_c(\text{HONO})$ used to estimate lower and upper surface-atmosphere exchange fluxes are given in Table 4.3. The surface uptake of HNO_3 and HONO is considered to be enhanced by the presence of epicuticular water films under the humid conditions at the site. Thus, corresponding R_c values are set to lower values at nighttime (Table 4.3) when RHs

up to 100 % and a corresponding high surface wetness were prevailing (see below, Fig. 4.6). $R_c(\text{NO}_2)$ has already been determined previously at the FNS site by *Kirkman et al.* [2002], hence no flux scenario is calculated for NO_2 and median diel $R_c(\text{NO}_2)$ values are taken directly from *Kirkman et al.* [2002] ($R_c(\text{NO}_2) = 200 - 300 \text{ s m}^{-1}$).

Table 4.3: Ranges of surface resistances R_c for HNO_3 and HONO for daytime and nighttime used to estimate flux scenarios at FNS during LBA-SMOCC 2002.

Scenario		$R_c(\text{HNO}_3)$ [s m ⁻¹]	$R_c(\text{HONO})$ [s m ⁻¹]
Day	high	1	50
	low	50	200
Night	high	1	15
	low	15	100

Surface resistance $R_c(\text{NH}_3)$ and stomata resistance $R_s(\text{NH}_3)$: Since $R_s(\text{NH}_3)$ is not known for *Brachiaria brizantha* grass species, the range of $R_s(\text{NH}_3)$ is limited by considering the diffusion of water vapor and O_3 through plant stomata. For the upper NH_3 flux estimate, $R_s(\text{NH}_3)$ is derived from the measured latent heat flux (LE) during daytime (1000 – 1800 LT) according to eq. (4.8). This can be justified by the fact that the transfer of H_2O through plant stomata is considered as a very efficient process, representing an upper boundary for trace gas exchange through plant stomata. In contrast, the transfer of O_3 through plant stomata is considered to be limited by the low solubility of O_3 . Therefore, we have used the surface resistance of O_3 ($R_c(\text{O}_3)$) determined by *Kirkman et al.* [2002] to establish a lower flux estimate. $R_c(\text{O}_3)$ is assumed to be equal to the bulk surface resistance of NH_3 ($R_c(\text{NH}_3)$) during daytime, and $R_s(\text{NH}_3)$ is calculated as $R_s(\text{NH}_3)^{-1} = R_c(\text{O}_3)^{-1} - R_d(\text{NH}_3)^{-1}$, whereby the different diffusivities of O_3 and NH_3 are taken into account (for $R_d(\text{NH}_3)$ see below). From 0700 to 1000 LT, when evaporation of epicuticular water films contributed to LE , $R_s(\text{NH}_3)$ derived from $R_c(\text{O}_3)$ is used for both the lower and the upper flux estimate. Since stomata are thought to be closed during nighttime, $R_s(\text{NH}_3)$ is set to 1000 s m^{-1} for nighttime periods.

Compensation point concentration $X_c(\text{HONO})$: Up to date, only two studies provide an estimate for $X_c(\text{HONO})$ [*Harrison and Kitto*, 1994; *Stutz et al.*, 2002]. Here, the relationship $X_c(\text{HONO}) = 0.03 \cdot X(\text{NO}_2, z_{\text{ref}})$ was used, which was found for grassland in the recent study by *Stutz et al.* [2002]. This corresponds on average to $X_c(\text{HONO}) = 85 \text{ ppt}$ at the FNS site.

Apoplastic $[\text{NH}_4^+]/[\text{H}^+]$ ratio Γ , charging *resistance* $R_d(\text{NH}_3)$, epicuticular pH and rate constant K_r for direct NH_4^+ uptake from epicuticular water films: For Γ , we have chosen values of 100 and 200 (Table 4.4), which range at the lower end of data reported for grass in the literature [e.g., *Spindler et al.*, 2001; *Loubet et al.*, 2002; *van Hove et al.*, 2002]. This may be justified by the poor soil N status at FNS [*Kirkman et al.*, 2002], because N absorbed by the root medium strongly affects the leaf tissue NH_4^+ concentration [*Schjoerring et al.*, 1998a]. $R_d(\text{NH}_3)$ provides a time constant for charging and discharging of the epicuticular water film and is taken as $2500/C_d$ (equivalent to a 42 min time constant) and $5000/C_d$ (equivalent to an 83 min time constant, see *Sutton et al.* [1998]). The pH of epicuticular water films is predominantly acidic [*Flechard et al.*, 1999] and is taken as 4.0 and as 4.5 [cf. *Sutton et al.*, 1998]. Finally, the rate constant K_r for NH_4^+ uptake from epicuticular water films is set to -0.05 s^{-1} and to -0.01 s^{-1} [cf. *Sutton et al.*, 1998].

Table 4.4: Ranges of the apoplastic $[\text{NH}_4^+]/[\text{H}^+]$ ratio (Γ), the charging resistance (R_d), epicuticular pH and the rate constant for NH_4^+ uptake from epicuticular water films (K_r) used for the estimation of NH_3 flux scenarios at FNS during LBA-SMOCC 2002.

Scenario	Γ [1]	R_d [s m ⁻¹]	pH	K_r
high	200	$2500/C_d$	4.0	0.05
	$pH = 6$ $[\text{NH}_4^+] = 200 \mu\text{mol l}^{-1}$			
low	100	$5000/C_d$	4.5	0.01
	$pH = 6$ $[\text{NH}_4^+] = 100 \mu\text{mol l}^{-1}$			

NH_3 flux from cattle excreta $F(\text{NH}_3)_{\text{excreta}}$: In order to estimate the contribution of cattle excreta to the net NH_3 flux, we considered results of *Boddey et al.* [2004], who investigated the cycling of N in *Brachiaria* pastures in the south of the Brazilian province Bahia. According to their results, *Bos indicus* cattle excreted 37 kgN animal⁻¹ yr⁻¹ in manure and 49 kgN animal⁻¹ yr⁻¹ in urine when the pastures were stocked with two animals per hectare. The stocking rate at FNS was about one animal per hectare. About 8 % of the excreted N may be released as NH_3 [*Lex Bouwman*, personal communication, 2004]. Hence, the average $F(\text{NH}_3)_{\text{excreta}}$ is estimated to be $\sim 10 \text{ ngN m}^{-2} \text{ s}^{-1}$, which is applied for the entire LBA-SMOCC measurement period (eq. 4.5, 4.6).

4.4.5 Resistances, NH_3 canopy compensation point, transfer- and deposition velocities

The turbulent resistance R_a and the quasi-laminar boundary layer resistance R_b (Fig. 4.4a,b): These resistances feature a typical diel variation with lowest values during daytime ($R_a = 20 \text{ s m}^{-1}$, $R_b = 30 \text{ s m}^{-1}$), because of strong turbulent mixing within the surface layer, and higher values during nighttime ($R_a = 70 \text{ s m}^{-1}$ and $R_b = 50 \text{ s m}^{-1}$).

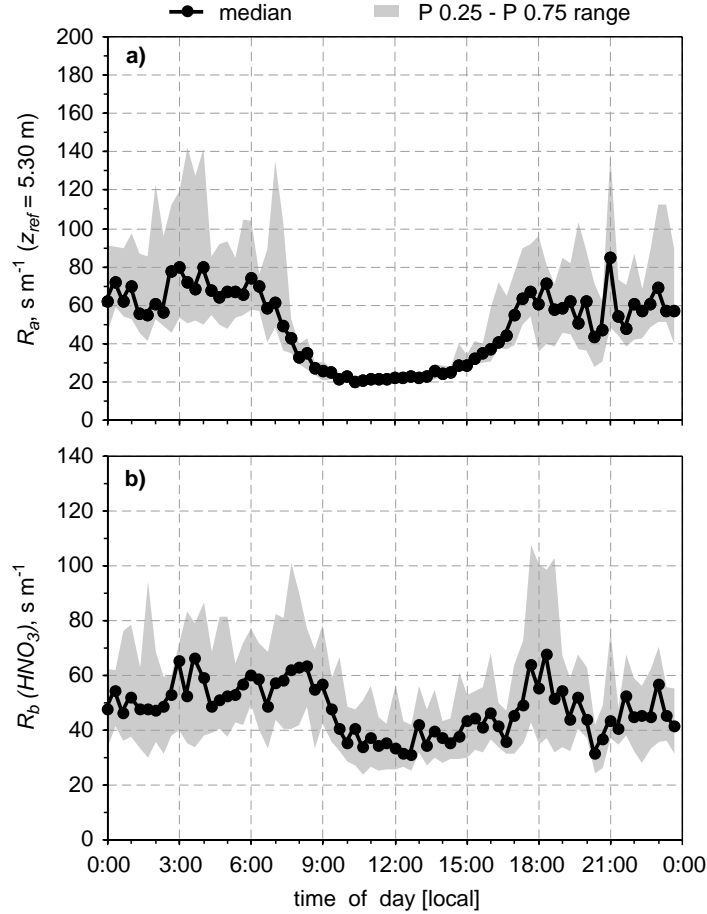


Figure 4.4a,b: Diel variations of (a) turbulent resistance (R_a) and (b) quasi-laminar boundary layer resistance (R_b) exemplary for HNO_3 at FNS during LBA-SMOCC 2002. Symbols and grey shading represent medians and interquartile ranges (0.25 to 0.75 percentiles), respectively. Data from all seasons were used.

The NH_3 stomata resistance $R_s(\text{NH}_3)$, the charging resistance $R_d(\text{NH}_3)$, and the bulk surface resistance $R_t(\text{NH}_3)$ (Fig. 4.5a-c): The median diel variation of $R_s(\text{NH}_3)$ estimated from LE during daytime (Fig. 4.5a, upper flux estimate) exhibits very low values, falling below 50 s m^{-1} between 1000 and 1400 LT. In the afternoon $R_s(\text{NH}_3)$ increases to 100 s m^{-1} after 1700 LT.

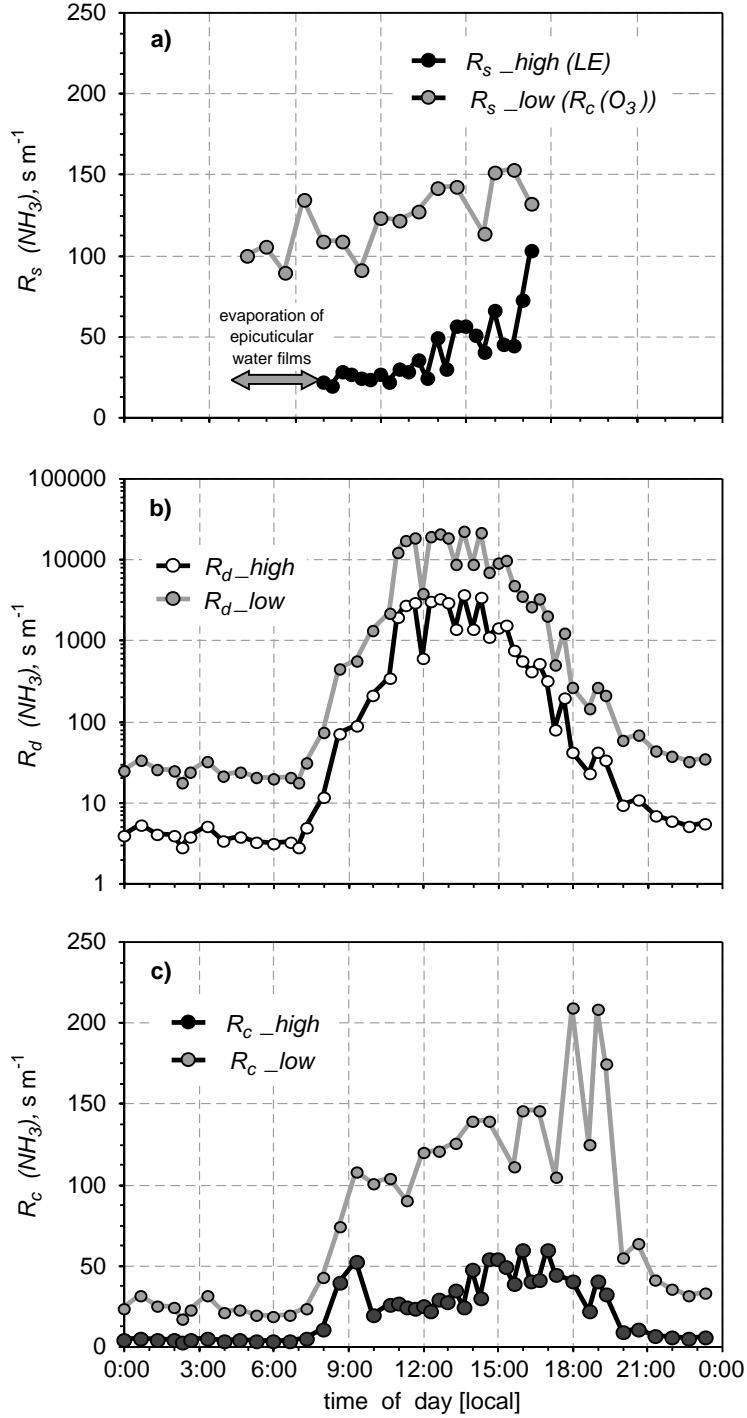


Figure 4.5a-c: Median diel variations of estimated lower (low) and upper (high) (a) NH_3 stomatal resistance $R_s(\text{NH}_3)$ during daytime, using the measured latent heat flux LE (high) and $R_c(O_3)$ from *Kirkman et al.* [2002] (low) ($R_s(\text{NH}_3)$ was set to 1000 m s^{-1} for nighttime periods), (b) NH_3 charging resistance of the surface water layer ($R_d(\text{NH}_3)$) and (c) total surface resistance $R_c(\text{NH}_3)$ (sum of the parallel resistances $R_s(\text{NH}_3)$ and $R_d(\text{NH}_3)$), used to predict the NH_3 canopy compensation point $X_c(\text{NH}_3)$ at FNS during LBA-SMOCC 2002.

The median diel variation of the stomatal resistance $R_s(NH_3)$ estimated from $R_c(O_3)$ (Fig. 4.5a, lower flux estimate) features higher values, varying between 100 and 150 s m⁻¹ throughout the day. Contrastingly, the simulated $R_d(NH_3)$ (Fig. 4.5b) is very high during daytime (> 1000 s m⁻¹) and remains below 100 s m⁻¹ at night. This is obviously due to the fact that grass leaves became dry during sunlight hours (see below, Fig. 4.6), resulting in a very low capacity of the foliar cuticle to adsorb NH₃. The median diel cycle of the total surface resistance $R_c(NH_3)$, that is the sum of the parallel resistances $R_s(NH_3)$ and $R_d(NH_3)$ (Fig. 4.5c) shows a pronounced diel fluctuation with higher values during sunlight hours and lower values at night. The upper estimate $R_c(NH_3)_{high}$ (estimated from $R_s(NH_3)_{LE}$ and $R_d(NH_3)_{high}$) varies between 20 and 60 s m⁻¹ during daytime and is estimated to be < 10 s m⁻¹ during the night. The lower estimate $R_c(NH_3)_{low}$ (estimated from $R_c(O_3)$ and $R_d(NH_3)_{low}$) ranges from 100 to 200 s m⁻¹ during the day and from 20 to 50 s m⁻¹ during nighttime.

The NH₃ canopy compensation point concentration $X_c(NH_3)$ (Fig. 4.6): The $X_c(NH_3)$ scenario for the dry season calculated according to eq. (4.6) and using the input shown in Table 4.4 lies well within the range of values determined for grassland in other studies [e.g., *Hesterberg et al.*, 1996; *Meixner et al.*, 1996; *Spindler et al.*, 2001; *Sutton et al.*, 2001] and is a strong function of surface temperature (cf. eq. 4.6, 4.7).

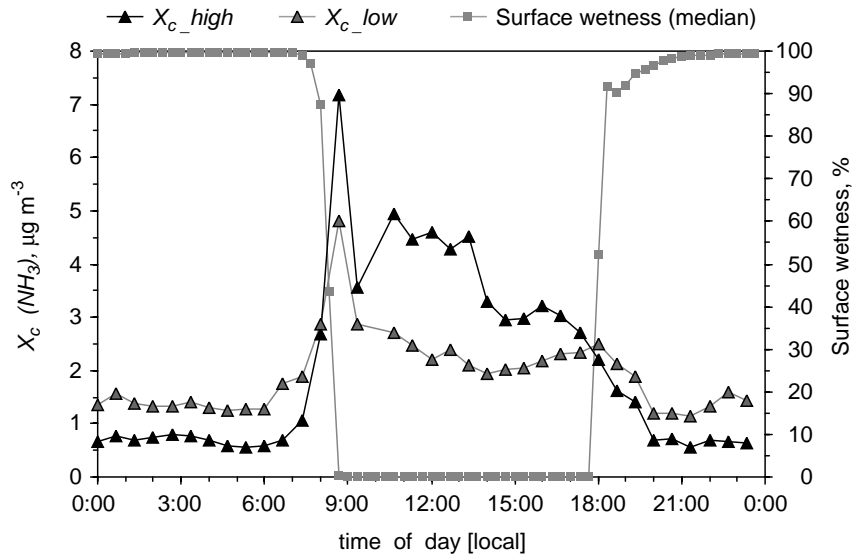


Figure 4.6: Median diel variation of the simulated lower (low) and upper (high) NH₃ canopy compensation point $X_c(NH_3)$, and the median diel variation of the measured surface wetness, shown exemplarily for a period during the dry season (12 - 23 Sep.) at FNS during LBA-SMOCC 2002. For details about low and high estimates, see text.

$X_c(NH_3)$ is predicted to be particularly high at daytime, although low values of I were used to run the model. This is caused by prevailing high surface temperatures at the FNS pasture site (35 – 40°C at daytime and 20 – 25 °C at night during the dry season). NH_3 deposits on epicuticular water films at high RHs during nighttime, a process followed by solvation and dissociation of the hydrated molecule into NH_4^+ and OH^- . The buffering capacity of the epicuticular aqueous solution decreases when the air temperature (and the surface temperature) will increase, which causes the epicuticular water layer to evaporate; potentially resulting in a NH_4^+ saturated water film [Cape, 1996]. Thus, the NH_3 partial pressure above the epicuticular solution increases in accordance to Henry's law, which is visible in Fig. 4.6 as a distinctive peak of $X_c(NH_3)$ after sunrise between 0800 and 0900 LT. Once most of the epicuticular NH_4^+ has evaporated, $X_c(NH_3)$ subsequently decreases (after 0900 LT). At higher surface temperatures during daytime, $X_c(NH_3)$ is simulated to be larger due to elevated NH_3 partial pressures within substomatal cavities above dissolved NH_4^+ in the apoplastic fluid. A decrease of the surface temperature during the transition period and the wet season led to lower estimates of $X_c(NH_3)$ (0.3 – 1 $\mu g\ m^{-3}$ during nighttime and 1 – 4 $\mu g\ m^{-3}$ during daytime).

Transfer- and deposition velocities $V_{tr}(NH_3)$, $V_{tr}(HONO)$, $V_d(HNO_3)$, $V_d(NO_2)$ (Fig. 4.7a-d) and $V_d(aerosol)$ (Fig. 4.8): For compounds featuring a bi-directional surface exchange, both deposition and emission occur simultaneously with rates depending on the relative concentrations of the gas in the atmosphere and within the canopy structure. This in turn means that the concept of a dry deposition velocity V_d is no longer useful [see e.g., Kramm and Dlugi, 1994]. Thus, for bi-directional NH_3 and HONO surface-atmosphere exchange the term transfer velocity (V_{tr}) will be used henceforth.

The estimated upper median diel variation of $V_{tr}(NH_3)$ (Fig. 4.7a) indicates net deposition (= downward flux) at nighttime ($V_{tr}(NH_3) > 0$) and net emission = upward flux ($V_{tr}(NH_3) < 0$) during the day, whereas the lower estimate of $V_{tr}(NH_3)$ shows only net emission. Typically, $V_{tr}(NH_3)$ is predicted to range between -1.5 $cm\ s^{-1}$ during the day and 1.0 $cm\ s^{-1}$ at night for the upper estimate, and $V_{tr}(NH_3)$ is estimated to vary between -0.25 $cm\ s^{-1}$ during the day and -1.0 $cm\ s^{-1}$ at night for the lower estimate. For cases of NH_3 net deposition, $V_{tr}(NH_3)$ is in good agreement with values of 0.1 – 2 $cm\ s^{-1}$ observed by e.g., Erisman and Wyers [1993], Hesterberg et al. [1996] and Phillips et al. [2004]. For cases of NH_3 net emission, $V_{tr}(NH_3)$ agrees well with values reported by e.g., Nemitz et al. [2004a].

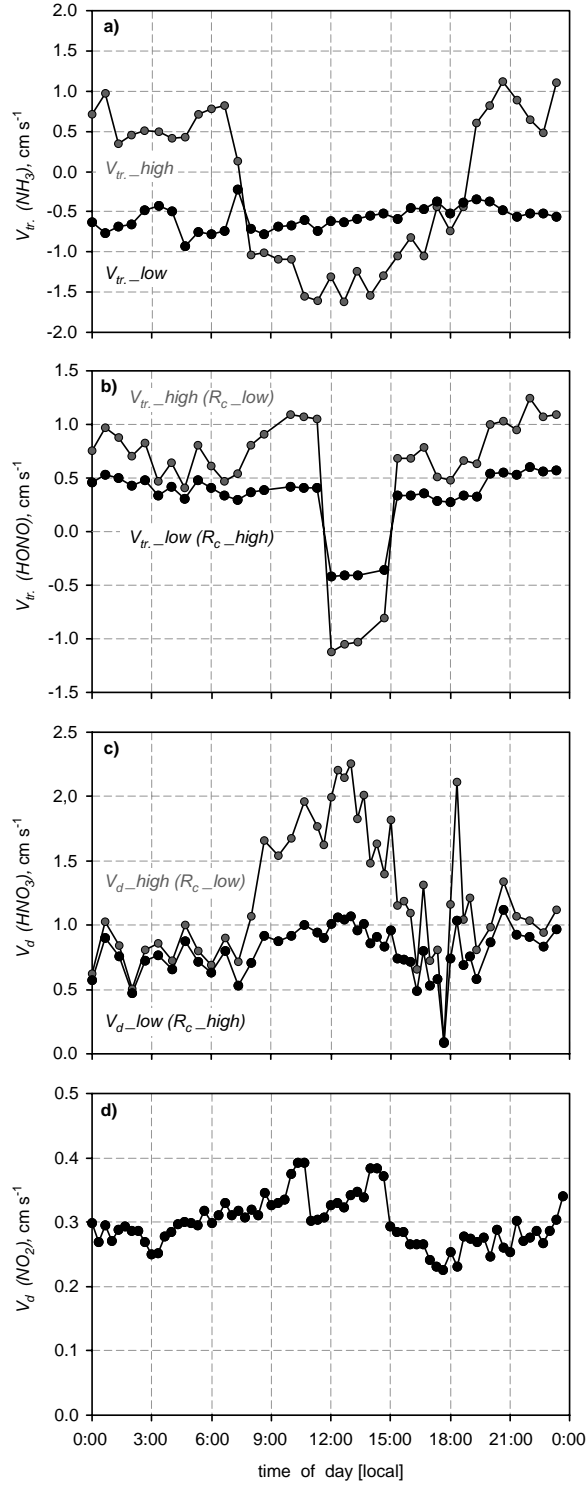


Figure 4.7a-d: Median diel variation of simulated lower (low) and upper (high) transfer velocity V_{tr} for bi-directional surface atmosphere exchange of (a) NH_3 , (b) HONO , and deposition velocity V_d for (c) HNO_3 and (d) NO_2 at FNS during LBA-SMOCC 2002. Data from all seasons were used, except for $V_{tr}(\text{HONO})$, which only represents results from the dry season, since negligible small upward HONO fluxes were predicted during transition period and wet season ($X(z_{ref}) < X_c(\text{HONO})$). For details about low and high NH_3 flux estimates, see text.

The estimated median diel variation of $V_{tr}(HONO)$ (Fig. 4.7b, dry season only) similarly shows net deposition at night and net emission during the day, with $V_{tr}(HONO)$ ranging from -1 cm s^{-1} to 1.3 cm s^{-1} (upper flux estimate) and between -0.5 cm s^{-1} and 0.5 cm s^{-1} (lower flux estimate). For cases of HONO deposition, these values are comparable to $V_{tr}(HONO)$ of $0 - 1.7 \text{ cm s}^{-1}$ reported by *Harrison and Kitto* [1994] and *Stutz et al.* [2002].

The estimates of $V_d(HNO_3)$ shown in Fig. 4.7c, reveal maximal median values of 2.3 cm s^{-1} at around 1300 LT when $R_c(HNO_3) = 1 \text{ s m}^{-1}$ is applied (see Table 4.3, upper flux estimate), coinciding with the period of highest turbulence. The lower estimate, when $R_c(HNO_3)$ is taken as 50 s m^{-1} during daytime and as 15 s m^{-1} during nighttime (see Table 4.3), results in median $V_d(HNO_3)$ values nearly equal during day and night ($\leq 1.1 \text{ cm s}^{-1}$), which is attributed to the compensating effect of lower surface uptake and low turbulent exchange during nighttime. Although $V_d(HNO_3)$ was found to be higher ($3 - 4 \text{ cm s}^{-1}$) in other studies [e.g., *Erisman et al.*, 1988], our values are still in reasonable agreement with deposition velocities determined by *Dollard et al.* [1987], *Müller et al.* [1993], *Ratray and Sievering* [2001] and *Nemitz et al.* [2004a] for vegetative canopies similar to that at FNS.

The median diel course of $V_d(NO_2)$ shown in Fig. 4.7d exhibits a less distinct pattern with maxima of $\sim 0.4 \text{ cm s}^{-1}$ during daytime (Fig. 4.7d). Values compare relatively well with $V_d(NO_2)$ reported by *Kirkman et al.* [2002]; however, the dry deposition of NO_2 is thought to be mainly featured by uptake through plant stomata, which would imply that much higher dry deposition velocities (and hence much lower R_c) occur during daytime. As stated in *Kirkman et al.* [2002], measured day- and nighttime R_c values for NO_2 at FNS were similar, which was assumed to be mainly a result of stomatal closure due to high water vapor pressure deficit at lower RH s during daytime.

Deposition velocities V_p predicted for particles (Fig. 4.8) are estimated to be highest during daytime ($\leq 0.8 \text{ cm s}^{-1}$) in accordance with higher values of u^* . During nighttime, V_p generally remains below 0.1 cm s^{-1} . As previously indicated, these values are much larger than V_p predicted by the Slinn model [*Slinn*, 1982] and are therefore considered as an upper estimate. It should be pointed out that aerosol water uptake at high RH s and particle growth during the deposition process may enhance deposition velocities [*Khlystov*, 1998; *Gallagher et al.*, 1997]. In our study, this would be particularly relevant for nighttime periods when RH usually exceeded 90 %. However, a quantification of this effect would go beyond the scope of this work.

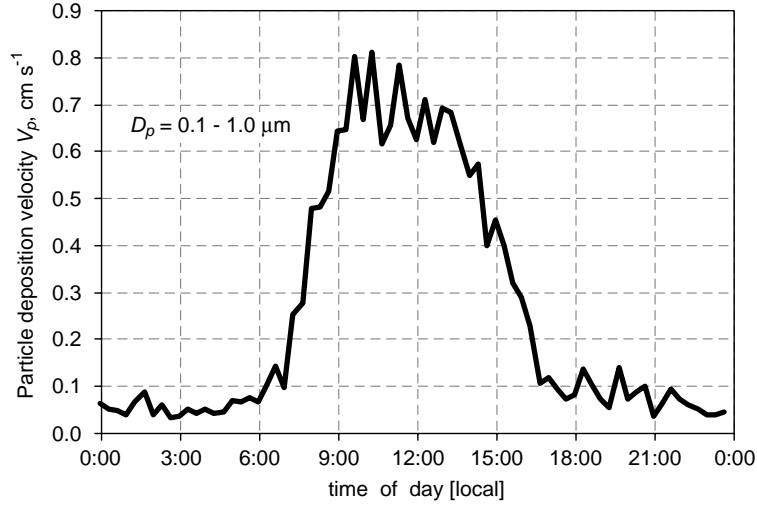


Figure 4.8: Median diel course of the particle deposition velocity V_p using the empirical parameterization derived by *Wesely et al.* [1985] for aerosol particles with $D_p = 0.1 - 1 \mu\text{m}$ at FNS during LBA-SMOCC 2002.

4.4.6 Surface-atmosphere exchange fluxes

In this section, the measured mixing ratios (section 4.4.2), the input parameters for the inferential approach (discussed in section 4.4.4) and the results presented in section 4.4.5 will be used to estimate and discuss surface-atmosphere exchange fluxes of N-containing trace gases and aerosol particles.

Bi-directional fluxes of gaseous NH_3 $F(\text{NH}_3)$ (Fig. 4.9a): The application of the dynamic resistance model from *Sutton et al.*, [1998], which uses non-zero $X_c(\text{NH}_3)$ values and takes into account that deposited NH_3 may (re-)evaporate from surfaces, represents a rather conservative N deposition estimate (lower boundary). Since $X_c(\text{NH}_3)$ was assumed to be zero in several studies [e.g., *Goulding et al.*, 1998; *Singh et al.*, 2001; *Tarnay et al.*, 2001; *Russell et al.*, 2003], which implies that NH_3 is persistently net deposited to the surface (see eq. 4.1), we have complemented the upper and lower bi-directional flux scenarios by additionally calculating a net deposition scenario for NH_3 (see Fig. 4.9a), assuming $X_c(\text{NH}_3) = 0$ (eq. 4.1) and using $R_c(\text{NH}_3)_{\text{high}}$ (Fig. 4.5c). The upper bi-directional estimate of $F(\text{NH}_3)$ for 12 - 23 Sep. 2002 (dry season, biomass burning) exhibits net emission (upward flux) during daytime and net deposition (downward flux) during nighttime. Comparable fluxes were found at locations in temperate regions with vegetative surfaces similar to the grass surface at FNS [e.g., *Erisman and Wyers*, 1993; *Meixner et al.*, 1996; *Plantaz et al.*, 1997; *Spindler et al.*, 2001]. The net emission peak between 0800 and 0930 LT in the upper estimate of the NH_3 flux (Fig. 4.9a), corresponds to the peak of the predicted NH_3 canopy compensation point (cf. Fig. 4.6) and the highest observed NH_3 mixing ratios (cf. Fig. 4.2a and chapter 2 and 3).

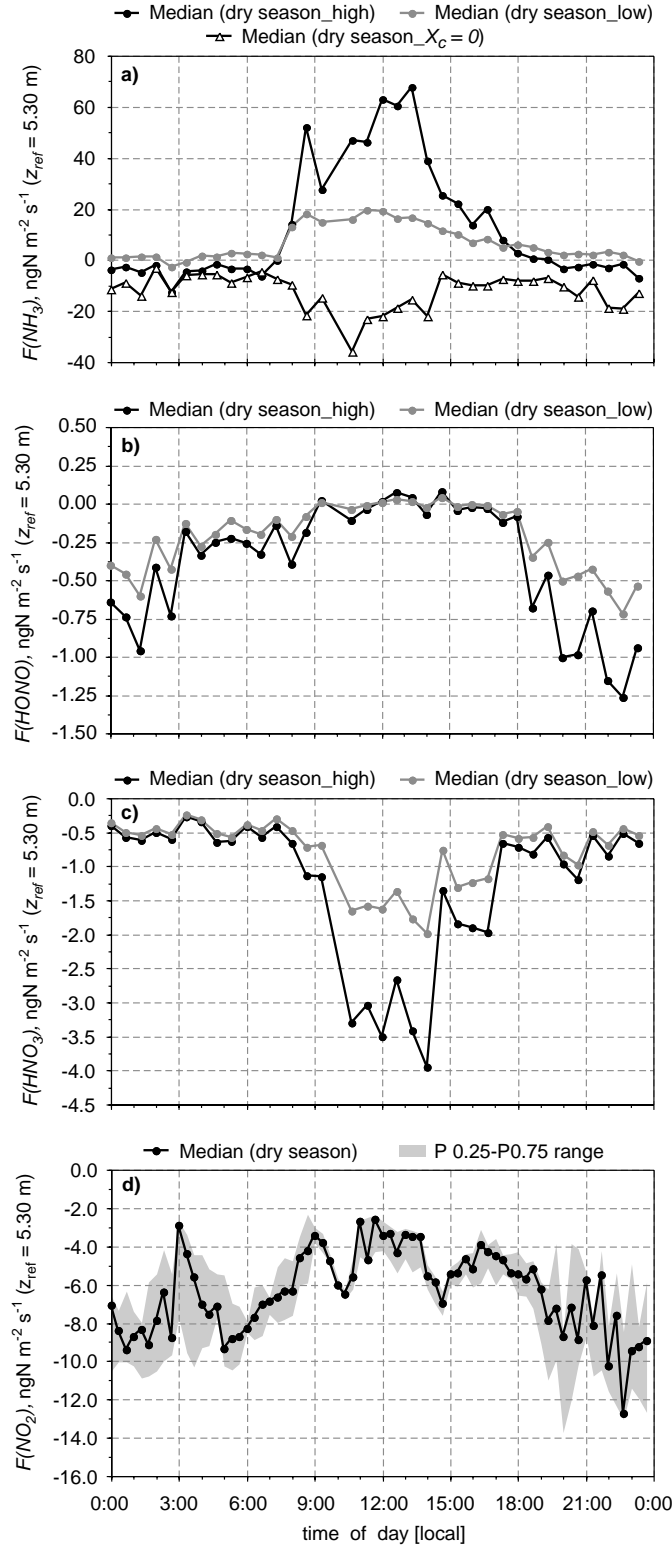


Figure 4.9a-d: Median diel courses of estimated lower (low) and upper (high) surface-atmosphere trace gas exchange fluxes for: (a) NH_3 , (b) HONO and (c) HNO_3 . Bi-directional NH_3 flux scenarios were complemented by a net deposition scenario ($X_c(\text{NH}_3) = 0$). The median flux of (d) NO_2 is estimated using R_c values from *Kirkman et al.* [2002] and is presented with interquartile ranges (0.25 to 0.75 percentiles). Medians have been calculated exemplarily for a period during the dry season (12 - 23 Sep.) at FNS during LBA- SMOCC 2002.

Relatively high median NH_3 net emission fluxes ($5 - 70 \text{ ngN m}^{-2} \text{ s}^{-1}$, upper estimate) during daytime (0800 – 1730 LT) are the result of (i.) relatively high NH_3 mixing ratios (Fig. 4.2a), (ii.) direct NH_3 emission from cattle excreta, (iii.) high surface temperatures and (iv.) corresponding high values of simulated $X_c(\text{NH}_3)$ (see Fig. 4.6). The simulated nighttime NH_3 net deposition (upper estimate) (1900 – 0630 LT) is on average $-2 - -13 \text{ ngN m}^{-2} \text{ s}^{-1}$. The lower NH_3 flux estimate shown in Fig. 4.9a suggests that surface-atmosphere exchange of NH_3 may be significantly smaller when a higher epicuticular pH (4.5), a lower uptake rate constant K_r , higher R_c values and also a lower apoplastic $[\text{NH}_4^+]/[\text{H}^+]$ ratio Γ are applied (see Table 4.4, Fig. 4.5c). The estimated NH_3 net deposition for this case during nighttime is negligible and the predicted daytime NH_3 net emission varies between 1 and $20 \text{ ngN m}^{-2} \text{ s}^{-1}$. During the transition period and the wet season, however, the lower NH_3 flux estimate (not shown) features emission during day and night, since $X_c(\text{NH}_3)$ is frequently higher than the measured mixing ratio. The NH_3 net deposition estimate (Fig. 4.9a) ($X_c(\text{NH}_3) = 0$) exhibits highest fluxes during daytime (0800 – 1500 LT), with values ranging between -20 and $-40 \text{ ngN m}^{-2} \text{ s}^{-1}$. At nighttime, net deposition fluxes between -5 and $-20 \text{ ngN m}^{-2} \text{ s}^{-1}$ were estimated. Median $V_{tr}(\text{NH}_3)$ values for this case range from 0.5 to 1.5 cm s^{-1} (not shown).

It should be noted, that e.g., in temperate regions under conditions when acidic trace gases, such as SO_2 , are abundant enough to be co-deposited [shown in *Erisman and Wyers*, 1993], NH_4^+ may be present to some extent as $(\text{NH}_4)_2\text{SO}_4$ and/or also NH_4NO_3 on the plant foliar cuticle. Conditions at the FNS site were dominated by molar ratios of $\text{NH}_3/\text{SO}_2 \geq 10$ (see chapter 3), such that a significant effect of co-deposited SO_2 on the NH_3 flux is not expected. The predicted bi-directional NH_3 flux scenarios are most sensitive to the pH of the epicuticular water film and the H^+ and NH_4^+ concentrations in the apoplastic fluid (Γ). If the pH of the epicuticular water film would be > 4.5 and Γ is constant ($100 - 200$), the upper NH_3 flux estimate would show net emission also during nighttime. On the other hand, increasing Γ beyond a value of 200 would result in daytime NH_3 net emissions significantly higher than observed in urban regions in Europe or North America.

Bi-directional fluxes of gaseous HONO $F(\text{HONO})$ (Fig. 4.9b): The estimated median diel HONO flux scenario during the dry season (12 to 23 Sep.), shows a small net emission during the afternoon but net deposition of up to $-1.3 \text{ ngN m}^{-2} \text{ s}^{-1}$ (upper estimate) from 1700 – 0840 LT. The net deposition for the lower flux estimate is smaller ($\geq -0.75 \text{ ngN m}^{-2} \text{ s}^{-1}$) in accordance to higher values of $R_c(\text{HONO})$ applied. We like to note, that the HONO flux scenario presented here probably reflects the largest uncertainty of all flux estimates since presently neither $R_c(\text{HONO})$ and $X_c(\text{HONO})$, nor the exact HONO formation mechanism is well known.

Fluxes of gaseous HNO_3 $F(\text{HNO}_3)$ (Fig. 4.9c): The estimated median diel HNO_3 flux scenario during the dry season is always directed downwards (net deposition) and is characterized by highest values from 0900 – 1630 LT ($\sim -0.5 - -4 \text{ ngN m}^{-2} \text{ s}^{-1}$, upper estimate), coinciding with highest estimated deposition velocities (cf. Fig. 4.7c) and the maximal observed HNO_3 mixing ratios (cf. Fig. 4.2b). Predicted nighttime HNO_3 deposition fluxes are lower in accordance with lower turbulence (lower V_d) and lower HNO_3 mixing ratios. The higher values of $R_c(\text{HNO}_3)$ applied for the lower flux estimate result in daytime net deposition fluxes that are a factor of two lower than for the upper flux estimate.

Fluxes of gaseous NO_2 $F(\text{NO}_2)$ (Fig. 4.9d): The diel course of the estimated NO_2 flux (dry season) is always characterized by downward fluxes (net deposition). Median nighttime fluxes (1800 – 0800 LT) are at least two times higher than during the day ($\geq -12 \text{ ngN m}^{-2} \text{ s}^{-1}$). This is mainly due to generally higher NO_2 mixing ratios measured during nighttime (Fig. 4.2e) and a small diel variation of $V_d(\text{NO}_2)$ (see Fig. 4.7d), caused by similar day- and nighttime $R_c(\text{NO}_2)$ determined by *Kirkman et al.* [2002].

Fluxes of aerosol NH_4^+ and NO_3^- $F(\text{aerosol})$ (Fig. 4.10): The estimated median diel flux of aerosol NH_4^+ for the dry season exhibits a net deposition pattern characterized by highest values just after 0900 LT ($\sim -7 \text{ ngN m}^{-2} \text{ s}^{-1}$), which is consistent with maximal aerosol NH_4^+ mixing ratios observed during this time (see Fig. 4.2g) and increased turbulent mixing (increasing u^*) after sunrise.

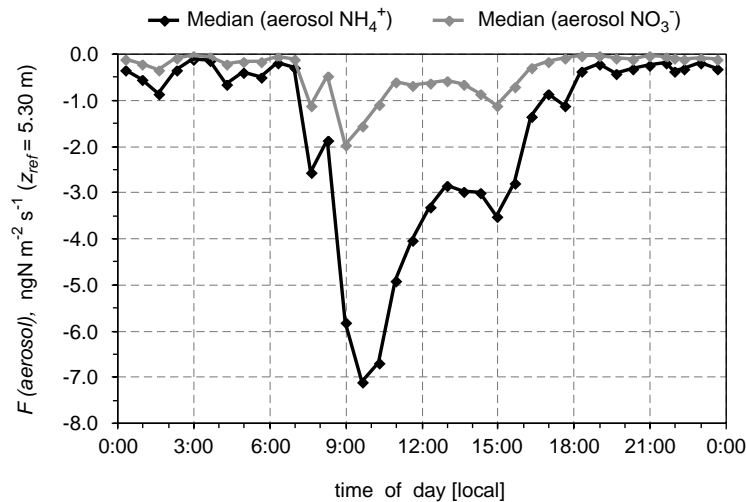


Figure 4.10: Median diel courses of inferred deposition fluxes of aerosol NH_4^+ and aerosol NO_3^- shown exemplarily for a period during the dry season (12 - 23 Sep.) at FNS during LBA-SMOCC 2002.

Although aerosol NH_4^+ mixing ratios were generally lower during daytime, the dry deposition of aerosol NH_4^+ is estimated to be highest because of high V_p predicted during sunlight hours (see Fig. 4.8). The maximum aerosol NH_4^+ net deposition between 0800 and 1000 LT coincides with a peak of the observed NH_3 mixing ratio (see Fig. 4.2a). At still high RH (70 - 80 %) during this time period, it is likely that a significant fraction of the emitted NH_3 will dissolve in humid aerosols and cause an increase of aerosol NH_4^+ , which subsequently deposits to the grass surface.

The median diel course of the aerosol NO_3^- flux shown in Fig. 4.10 for the dry season resembles that estimated for aerosol NH_4^+ , although the net deposition flux was at least three times lower than for aerosol NH_4^+ , which is a consequence of lower aerosol NO_3^- mixing ratios (see Fig. 4.2 g,h). The highest aerosol NO_3^- net deposition is predicted at around 0900 LT ($\sim -2 \text{ ngN m}^{-2} \text{ s}^{-1}$).

4.4.7 Seasonal cycles of dry and wet N deposition

Fig. 4.11a,b illustrates the absolute amounts of the estimated monthly N deposition, whereby for dry N deposition (Fig. 4.11a) only cases of net deposition were considered.

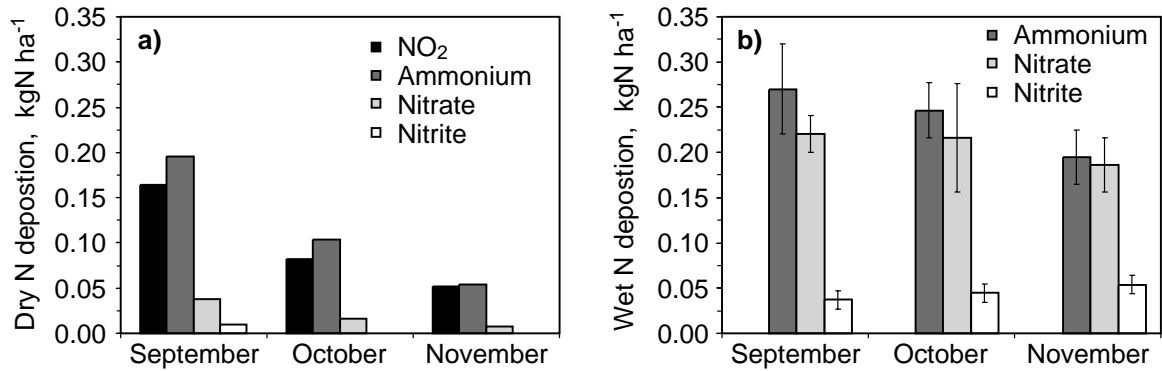


Figure 4.11a,b: Monthly estimates of (a) dry N deposition of NO_2 , total ammonium (aerosol $\text{NH}_4^+ + \text{NH}_3$), total nitrate (aerosol $\text{NO}_3^- + \text{HNO}_3$) and nitrite (HONO) (averages of lower and upper estimates are shown, except for NH_3 which represents an average of all three estimates (cf. Fig. 4.9a) and (b) wet N deposition of ammonium, nitrate and nitrite (error bars represent measurement uncertainties) for September (dry season, biomass burning), October (transition period) and November (wet season, clean conditions) at FNS during LBA-SMOCC 2002.

The dry deposition of NO_2 and total ammonium ($\text{NH}_3 + \text{aerosol } \text{NH}_4^+$) are estimated to be highest and decline by about 70 % from September (late dry season, biomass burning) to November (onset of the wet season, clean conditions) (Fig. 4.11a). This indicates the influence of biomass burning during the dry season, which significantly enhances the dry deposition of NO_2 and NH_3 . The dry deposition of total nitrate ($\text{HNO}_3 + \text{aerosol } \text{NO}_3^-$) also decreases by about 70 % from September to November (Fig. 4.11a), but was on average 4 times lower than that of NO_2 and total ammonium. This is in accordance with lower mixing ratios observed for nitrate in gas and aerosol phase (cf. Table 4.2 and chapter 2). The contribution of nitrite (HONO) to the dry deposition in September is smallest, and is negligible in October and November. This is due to the fact that in October and November the observed HONO mixing ratios were usually below the applied $X_c(\text{HONO})$ (see above).

Obviously, wet N deposition (Fig. 4.11b) is substantially higher than dry N deposition at the FNS site. Wet N removal is dominated by ammonium and nitrate, and wet deposition of nitrite is at least three times smaller. Interestingly, the decrease of wet deposition of ammonium and nitrate from September to November is only ~ 20 %, hence, much less pronounced than that for dry N deposition.

Fig. 4.12a-c shows the relative contribution of N species as well as of dry and wet deposition to the total N deposition estimated for the three different seasons. During the late dry season (biomass burning) in September, on average 44 % of the total N deposition can be attributed to dry deposition and ~ 56 % to wet deposition (Fig. 4.12a). With increasing rainfall amounts, the contribution of dry deposition drops to only 29 % and 21 % to the total N deposition during October (transition period) and November (onset of the wet season, clean conditions), respectively (Fig. 4.12b,c).

Dry N deposition at FNS was always dominated by NO_2 and NH_3 . During September (dry season, Fig. 4.12a) the contribution of NO_2 and NH_3 to the total N deposition is estimated to be 18 % and 16 %, respectively. By contrast, the dry N deposition of HNO_3 and HONO is estimated to be small, contributing only 2.8 % and 1.1 % to the total N deposition during the dry season, respectively (Fig. 4.12a). Aerosol NH_4^+ and aerosol NO_3^- show comparably small contributions to the total N deposition during the dry season (4.7 % and 1.2 %, respectively).

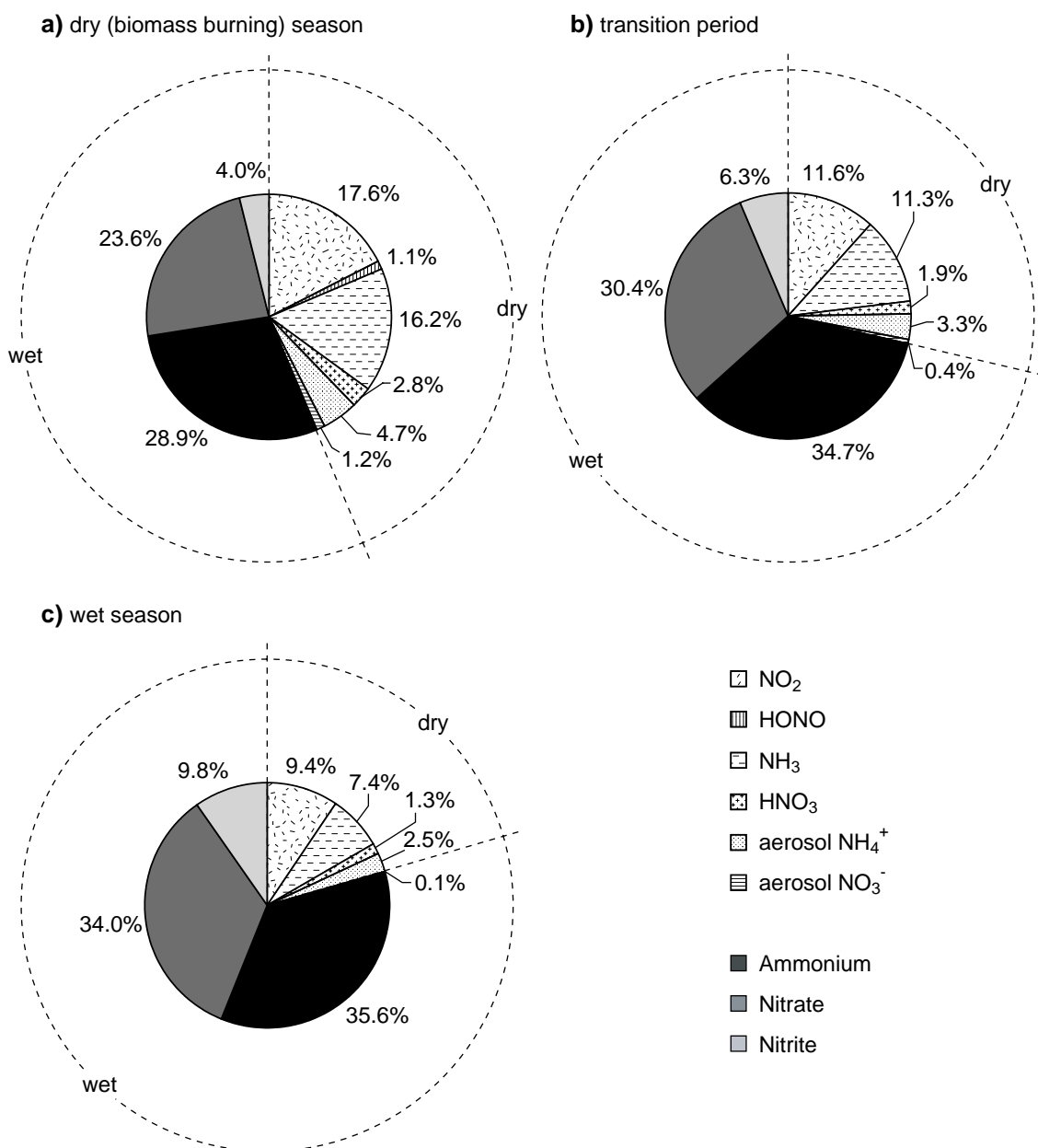


Figure 4.12a-c: Contribution of inorganic N compounds to the estimated total N deposition for (a) September (dry season, biomass burning), (b) October (transition period) and (c) November (wet season, clean conditions) at FNS during LBA-SMOCC 2002. Dry deposition of gaseous species is presented using averages of lower and upper estimates.

Through the transition period (October) until the wet season (November), the contribution of NO₂ dry deposition to the total deposition declines to about 10 % (Fig. 4.12b,c). The relative contribution of NH₃ to the total estimated N deposition decreases to 11 % during the transition period and to 7.4 % during the wet season. The dry N removal associated with HNO₃, HONO and aerosol NH₄⁺ and NO₃⁻ is estimated to be negligibly small during the transition period and the wet season (≤ 5 % in total).

4.4.8 Annual budget of surface-atmosphere exchange

The annual budget of surface-atmosphere exchange of inorganic N species at the FNS pasture site has been determined assuming that: (i.) September is representative for the entire dry season (May to September), (ii.) October is representative for the two transition periods (April and October), and (iii.) November is representative for the entire wet season (November to March). The annual deposition of inorganic N species at the FNS pasture site is estimated to $7.3 - 9.8 \text{ kgN ha}^{-1} \text{ yr}^{-1}$, whereof $2 - 4.5 \text{ kgN ha}^{-1} \text{ yr}^{-1}$ can be attributed to dry N deposition and $\sim 5.3 \text{ kgN ha}^{-1} \text{ yr}^{-1}$ to wet N deposition. Thus, dry deposition may contribute on average 30 % to the total annual N deposition. It is expected that $2.7 - 6.8 \text{ kgN ha}^{-1} \text{ yr}^{-1}$ are net (re-)emitted in form of gaseous NH_3 , HONO and NO from the pasture site (the annual estimate for net NO emission was taken from *Kirkman et al.* [2002]), whereof at least 90 % are expected to be in the form of NH_3 . Regarding soil emission of nitrous oxide (N_2O), not included in this study, *Garcia-Montiel et al.* [2003] reported that the emission of N_2O from Amazonian pastures is even smaller than that of NO. Our study suggests that NH_3 is net emitted on an annual time scale, owing to high surface temperatures (efficient NH_3 emission through plant stomata) and direct NH_3 emission from cattle excreta. The total N budget at FNS is most sensitive to the modeled NH_3 flux. The FNS site may constitute an effective net sink of total inorganic N, if a zero-canopy compensation point $X_c(\text{NH}_3)$ is assumed, or if $X_c(\text{NH}_3)$ is calculated using an epicuticular $\text{pH} \leq 4.5$ and a ratio of $\text{NH}_4^+ / \text{H}^+$ in the apoplastic fluid (I) ≤ 200 (Table 4.4, Fig. 4.9a).

Kirkman et al. [2002] reported that the FNS site constitutes a net NO_2 sink of $0.73 \text{ kgN ha}^{-1} \text{ yr}^{-1}$. However, based on our measurements and considering $R_c(\text{NO}_2)$ determined by *Kirkman et al.* [2002], we calculated an annual NO_2 deposition of $1.24 \text{ kgN ha}^{-1} \text{ yr}^{-1}$, which is nearly two times higher than the value derived by *Kirkman et al.* [2002]. This discrepancy is most likely due to higher NO_2 mixing ratios observed during the biomass burning season in our study.

Moreover, it should be noted that water-soluble organic nitrogen (WSO_N) constitutes a significant part of the total N fraction of Amazonian aerosols. It was found by *Mace et al.* [2003], that organic N may represent 45 % and 43 % of the total N in wet and dry season aerosol samples, respectively. Obviously, the total deposition of atmospheric N would be significantly higher if these organic species were also taken into account, which is, however, beyond the scope of this paper.

Wet deposition of nitrate and ammonium in Central Amazonia was previously estimated to $1.7 \text{ kgN ha}^{-1} \text{ yr}^{-1}$, $2.1 \text{ kgN ha}^{-1} \text{ yr}^{-1}$, and $2.8 \text{ kgN ha}^{-1} \text{ yr}^{-1}$ by e.g., *Stallard and Edmond* [1981], *Andreae et al.* [1990] and *Williams et al.* [1997], respectively. Since the measurement sites were situated in remote areas with less

fire density, these estimates are about a factor of two lower than the value of 4.7 kgN ha⁻¹ yr⁻¹ (only ammonium and nitrate) obtained in this study.

Finally, Fig. 4.13 shows a comparison of our estimated N deposition with predictions by global chemistry and transport models (CTMs) [*Holland et al.*, 1997; *Holland et al.*, 1999; *Dentener and Crutzen*, 1994; *Bouwman et al.*, 2002; *Hauglustaine et al.*, 2004].

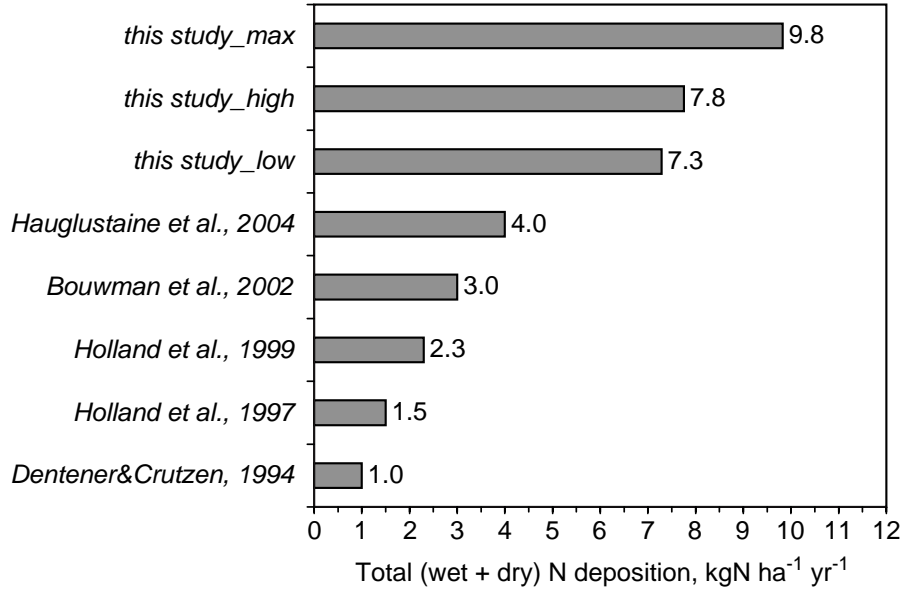


Figure 4.13: Comparison of the annual (dry + wet) N deposition predicted by global chemistry & transport models for the Amazon region with the annual (dry + wet) N deposition estimated in this study. “This study_low” and “this study_high” correspond to lower and upper flux estimates. “This study_max” corresponds to the upper flux estimate, but considering NH₃ to be net deposited ($X_c(\text{NH}_3) = 0$, cf. Fig. 4.9a).

The values from *Dentener and Crutzen* [1994] and *Holland et al.* [1997] are averages of N deposition predicted for the Amazon region (MOGUNTIA). The estimates from *Dentener and Crutzen* [1994] exclude dry deposition of NO_x. The value from *Holland et al.* [1999] (MOGUNTIA) represents predictions for tropical grasslands. *Bouwman et al.* [2002] (STOCHEM model) and *Hauglustaine et al.* [2004] (LMDz-INCA model) provide the total average N deposition for South America, which explains that their estimates are somewhat higher. *Hauglustaine et al.* [2004] do not take into account surface (re-)emission of NH₃ ($X_c(\text{NH}_3) = 0$). Not surprisingly, our N deposition estimate for the Amazonian pasture site is a factor of two to eight higher than model predictions for the Amazon region (Fig. 4.13).

4.5 Summary and conclusion

We have estimated dry and wet deposition of inorganic N at a tropical pasture site (Rondonia, Brazil) based on real-time measurements of inorganic N containing gases and aerosol species during the late dry season (biomass burning), the transition period and the onset of the wet season (clean conditions) (LBA-SMOCC 2002). HNO_3 , NO_2 , aerosol NH_4^+ and NO_3^- were considered to be net deposited to the pasture site under all ambient conditions, while surface-atmosphere exchanges of HONO and NH_3 were considered to be of bi-directional nature. All fluxes have been determined by inferential techniques, making use of aerodynamic and surface related resistances that have been deduced from measurements or were taken from recent literature. For the least-well defined quantities, lower and upper cases have been considered. Bi-directional NH_3 fluxes were predicted using a dynamic resistance model from *Sutton et al.* [1998]. NO_2 and NH_3 are the most important contributors to dry N deposition and fluxes of NO_2 and NH_3 largely control the total dry N deposition pattern at the pasture site. Mixing ratios of NO_2 and water-soluble N species in gas and aerosol phase are significantly enhanced when widespread biomass burning takes place during the dry season, resulting in high N deposition rates. The contribution of the dry N deposition to the total N deposition decreased substantially from the dry season (biomass burning) to the wet season. The estimated total (dry + wet) N deposition to this tropical pasture site is $7.3 - 9.8 \text{ kgN ha}^{-1} \text{ yr}^{-1}$, whereof $2 - 4.5 \text{ kgN ha}^{-1} \text{ yr}^{-1}$ are attributed to dry N deposition and $\sim 5.3 \text{ kgN ha}^{-1} \text{ yr}^{-1}$ to wet N deposition. Thus, dry deposition may contribute on average 30 % to the total N deposition. It is expected that $2.7 - 6.8 \text{ kgN ha}^{-1} \text{ yr}^{-1}$ are net (re-)emitted from the pasture site, mainly in the form of NH_3 . The largest uncertainties in our estimates are (i.) the epicuticular pH and (ii.) the ratio of NH_4^+ and H^+ concentration in the apoplastic fluid (Γ), that strongly control the NH_3 canopy compensation point concentration and, hence, the estimated bi-directional NH_3 flux. In this study, low values of (i.) the epicuticular pH (4 – 4.5) and (ii.) the ratio of NH_4^+ and H^+ concentration in the apoplastic fluid ($\Gamma = 100 - 200$) were assumed. The latter can be justified by the low soil N status of FNS, and, in combination with a low epicuticular pH, the daytime net emission and nighttime net deposition pattern of the NH_3 flux found in temperate latitudes could be reproduced. Our results suggest that – regardless of considering net deposition of NH_3 or bi-directional NH_3 exchange – the contemporary net N deposition to tropical ecosystems predicted by global CTMs may be underestimated at least by a factor of two. Up to now, approximately 15 % of the original Amazonian rainforest has been deforested and was mostly converted to cattle pastures. Our N deposition estimate is suggested to be representative for these areas, featuring comparable land use patterns and microclimates. N deposition in these regions may therefore be comparable to moderately polluted urban regions in, e.g., North America [*Munger et al.*, 1998;

Tarnay et al., 2001]. Our results emphasize the need for experimental studies that determine dry and wet N deposition in tropical regions, which provide key parameters that facilitate the improved mechanistic representation of surface-atmosphere exchange as a function of land use, which can be implemented in atmospheric CTMs.

Main findings, Conclusions and Outlook

5.1 Main findings and Conclusions

Motivated by the demand for reliable measurements of water-soluble inorganic trace gases (NH_3 , HNO_3 , HONO , HCl and SO_2) and their related aerosol compounds (NH_4^+ , NO_3^- , NO_2^- , Cl^- and SO_4^{2-}) in tropical environments, this dissertation is dedicated to the measurement of these atmospheric species and presents the results for the Amazon Basin. For the first time, these compounds were measured selectively and simultaneously with high time resolution under tropical conditions.

Measurements were conducted at a pasture site in the state of Rondônia, Brazil, which is used as a cattle ranch. Measurements extended from late dry (biomass burning) season (12 - 23 Sep. 2002), through the transition period (07 - 31 Oct. 2002) to the onset of the wet season (background conditions) (01 - 14 Nov. 2002) (LBA-SMOCC*). Air was sampled from 5.30 m above ground through a vertical polyethylene conduit that was specially designed to minimize gas-phase wall losses (particularly HNO_3) and aerosol losses due to non-isokinetic sampling. A continuously rotating wet-annular denuder (WAD) to scavenge water-soluble gases (NH_3 , HNO_3 , HONO , HCl and SO_2) was combined with a Steam-Jet Aerosol Collector (SJAC) to collect related aerosol species (NH_4^+ , NO_3^- , NO_2^- , Cl^- and SO_4^{2-}). Analyses were performed on-line using ion chromatography (IC) (for NO_3^- , NO_2^- , Cl^- and SO_4^{2-}) and flow injection analysis (FIA) (for NH_4^+). The time resolution was 20 min during the dry (biomass burning) season, 40 min during the transition period and 60 min during the wet season.

WAD/SJAC real-time measurements were supported by measurements of (i.) (micro)-meteorological conditions (ii.) total fine particulate mass (PM 2.5) (iii.) low-molecular weight (LMW) polar organic acids and mineral cations (K^+ , Ca^{2+} and Mg^{2+}) using integrating filter sampling techniques and (iv.) mixing ratios of NO , NO_2 and O_3 . These quantities are explicitly considered in this study. The results presented in this thesis particularly focus on the dry (biomass burning) season.

Meteorological situation. Ambient temperatures at the pasture site ranged from 20 – 25 °C during nighttime to 30 – 36 °C during afternoon hours. Nighttime *RHs* always exceeded 90 % and reached 100 % after 0500 LT, whereas daytime *RHs*

* LBA-SMOCC: Large Scale Biosphere Atmosphere Experiment in Amazonia - Smoke Aerosols, Clouds, Rainfall and Climate: Aerosols from Biomass Burning Perturb Global and Regional Climate)

typically ranged from 40 to 50 %. The global radiation flux reached maxima of 800 – 900 W m⁻² during noontime. The grass canopy at the site was covered by dew every night. As soon as global radiation exceeded 200 W m⁻² (0730 LT), dew layers evaporated within 1 hour and formed again when global radiation dropped below 100 W m⁻² (1730 LT). Daytime wind speeds ranged between 2 and 3 m s⁻¹. In contrast, nighttime wind speeds were very low, ranging from 0.5 to 1 m s⁻¹. Nighttime radiative cooling resulted in the formation of a shallow, nocturnal boundary layer of high thermodynamic stability and very low wind speeds. The daytime boundary layer was characterized by elevated wind speeds and strong turbulence. Strong rain events (≥ 30 mm h⁻¹) occurred in the afternoon hours (1300 to 1600 LT) during the transition period and the wet season.

WAD/SJAC: measurement verification and results. Theoretical inlet wall losses for HNO₃ were calculated to be ≤ 15 %, which was empirically validated by performing corresponding field tests. Calculated inlet losses of aerosol species due to non-isokinetic sampling were below 3 % ($D_p \leq 2.5$ μ m). Total measurement uncertainties of the mixing ratios in ambient air remained below 15 % during the entire measurement period. The limit of detection (LOD) was determined for each species under field conditions. LOD medians were below 0.015 ppb for all acidic trace gases and aerosol anions (IC analyses) but were higher (≤ 0.118 ppb) for NH₃ and aerosol NH₄⁺ (FIA analyses).

The determination of 10 different atmospheric compounds resulted in ~ 7000 data points of ambient mixing ratios. Widespread biomass burning activity in the Amazon Basin during the dry season (June through September) caused at least a 2-fold increase of all inorganic water-soluble gases and aerosol species. The pasture site was found to be an NH₃-rich environment. NH₃ was present in mixing ratios an order of magnitude higher ($\sim 0.5 - 8$ ppb) than those of acidic gases (HNO₃, HONO, HCl and SO₂), which was considered to be largely attributed to biomass burning, but also to NH₃ emission from cattle excreta. Mixing ratios of HNO₃, HONO, HCl and SO₂ always remained below 1 ppb. Consequently, inorganic ionic aerosol composition at FNS was dominated by NH₄⁺, being present in mixing ratios at least 4 to 10 times higher than aerosol NO₃⁻, NO₂⁻, Cl⁻ and SO₄²⁻. During the biomass burning season, aerosol NO₃⁻ was the dominating anion and showed the strongest decrease to the wet season (~ 70 %). Water-soluble trace gases exhibited pronounced diel variations. The diel course of NH₃ generally featured a sharp spike of mixing ratios just before 0900 LT. This was assumed to be a result of NH₃ deposition to wet surfaces during nighttime and subsequent (re-)evaporation due to a temperature increase after sunrise. Dry season diel cycles of HNO₃, HCl and SO₂ were characterized by daytime mixing ratios at least a factor of three higher than during nighttime. This was attributed to: (i.) convective mixing within the boundary layer and from the free troposphere during daytime that contributes to an increase of trace gases at ground level, (ii.) deposition to wet surfaces at night and a

stable thermal stratification of the nocturnal surface layer, (iii.) in case of HNO_3 , photochemical daytime production (see R3), (iv.) lower relative humidities (RH s) (40 – 50 %) and higher temperatures (32 – 36 °C) during daytime, that allow evaporation of semi-volatile species (NH_4^+ , NO_3^- , Cl^-) from the aerosol phase. Correspondingly, the diel patterns of semi-volatile aerosol species mirrored those of their gaseous precursors. Nighttime mixing ratios of aerosol NH_4^+ , NO_3^- and Cl^- during the dry season usually exceeded daytime values by a factor of two or three. By contrast, non-volatile aerosol SO_4^{2-} showed a marginal diel fluctuation, indicating the independence of its formation from ambient RH and temperature.

During the dry season, a typical HONO diel course was observed. Nighttime HONO mixing ratios were at least a factor of three higher than during the day, but HONO was not completely depleted by rapid photolysis during sunlight hours. This suggests – besides heterogeneous conversion of NO_2 on surfaces – an additional HONO production mechanism that is more efficient than photolytic HONO destruction during daytime.

The inorganic gas/aerosol system. On the basis of the performed real-time measurements of NH_3 , HNO_3 , HONO, HCl , SO_2 and the related aerosol species NH_4^+ , NO_3^- , NO_2^- , Cl^- and SO_4^{2-} , the aerosol ion balance and the partitioning of semi-volatile species between gas and aerosol phase were investigated.

The contribution of inorganic species to the fine particulate mass was frequently below 20 % by mass, indicating the preponderance of organic matter. Gas/aerosol partitioning coefficients (ratios aerosol / {gas + aerosol}) for ammonium, nitrate and chloride substantially increased with increasing RH . Nitrate was found to be predominantly present in the aerosol phase (80 % at $RH > 90$ % during nighttime). By contrast, the fraction of aerosol Cl^- was much lower (40 – 50 % at $RH > 90$ % during nighttime). The aerosol ion balance of inorganic charges revealed that cations (NH_4^+ , Na^+ , K^+ , Ca^{2+} and Mg^{2+}) exceeded the sum of anions (NO_3^- , Cl^- and SO_4^{2-}) by about a factor of two. Furthermore, it was tested if thermodynamic phase equilibrium (R4 and R5) was attained for the pure $\text{NH}_3/\text{HNO}_3/\text{NH}_4\text{NO}_3$ and $\text{NH}_3/\text{HCl}/\text{NH}_4\text{Cl}$ systems under prevailing meteorological conditions at the field site. In contrast to experiments conducted in temperate latitudes, such as North America, Europe and Asia, the theoretical equilibrium dissociation constants of the pure $\text{NH}_3/\text{HNO}_3/\text{NH}_4\text{NO}_3$ and $\text{NH}_3/\text{HCl}/\text{NH}_4\text{Cl}$ systems persistently exceeded the measured concentration products of $\text{NH}_3 \times \text{HNO}_3$ and $\text{NH}_3 \times \text{HCl}$ by a factor of 10 to 100 during daytime ($RH < 90$ %) at this tropical site. Even by taking into account the coexistence of SO_4^{2-} , which lowers the vapor pressures products of $\text{NH}_3 \times \text{HNO}_3$ and $\text{NH}_3 \times \text{HCl}$ over aqueous solutions, this discrepancy could not be removed.

In order to comprehensively investigate ionic balances, gas/aerosol partitioning and formation processes of inorganic aerosol constituents, four thermodynamic

equilibrium models (EQMs) (EQSAM, ISORROPIA, GEFMN and SCAPE2) were applied. These models commonly assume that thermodynamic equilibrium exists between gas and aerosol phase and they solely consider inorganic aerosol species in their modeling framework. Due to the simplified structure of EQSAM which, in contrary to ISORROPIA, GEFMN and SCAPE2, calculates the aerosol activity and equilibrium composition of the aqueous aerosol phase noniteratively, lumped LMW polar organic acids were incorporated as a first approach.

In case mineral cations and LMW polar organic acids were excluded in simulating the inorganic gas/aerosol system, EQMs failed to predict aerosol NO_3^- and Cl^- during daytime ($RH < 90\%$), such that mixing ratios of HNO_3 and HCl were significantly overpredicted. Due to an extension of the modeled aerosol system by mineral cations (K^+ , Ca^{2+} and Mg^{2+}), aerosol NO_3^- and Cl^- were predicted also during daytime. For this case, however, the observed daytime mixing ratios of aerosol NH_4^+ could not be simulated by the EQMs. Obviously, aerosol NH_4^+ was now replaced by other cations (mineral species, especially pyrogenic K^+) which preferentially balance aerosol NO_3^- and SO_4^{2-} . Due to an inclusion of lumped LMW polar organic acids in to the framework of EQSAM, daytime aerosol NH_4^+ mixing ratios were predicted in reasonable agreement with the observations.

Thus, it can be concluded that:

- (vii.) High ambient temperatures prevailing in the Amazon region and low vapor pressure products of $\text{NH}_3 \times \text{HNO}_3$ and $\text{NH}_3 \times \text{HCl}$ did not allow formation of NH_4NO_3 and NH_4Cl at $RH < 90\%$.
- (viii.) Thermodynamic equilibrium permitted the formation of aqueous NH_4NO_3 and NH_4Cl only during nighttime ($RH > 90\%$).
- (ix.) Mineral cations (especially K^+) present in Amazonian fine mode aerosols significantly balanced aerosol NO_3^- and SO_4^{2-} , particularly during daytime.
- (x.) Chloride was largely driven out of the aerosol phase by reaction of pyrogenic KCl with HNO_3 and H_2SO_4 .
- (xi.) Due to high ratios of NH_3/SO_2 observed at the pasture site, $(\text{NH}_4)_2\text{SO}_4$ appeared to be only a minor component of the Amazonian inorganic aerosol fraction.
- (xii.) Gaseous NH_3 was largely neutralized by LMW polar organic acids, forming aerosol NH_4^+ .

The performance of the four applied EQMs showed a reasonable agreement, which strengthens these findings. Contrary to the application of EQMs in temperate latitudes, modeling the inorganic gas/aerosol system in the Amazon Basin requires the inclusion of mineral cations into EQM frameworks. Moreover, this study emphasizes that for regions where aerosols are dominated by organic matter, an

explicit thermodynamic approach to simulate the organic/inorganic gas/liquid/solid aerosol system is needed.

Dry and wet N deposition. A further scope of this thesis is the estimation of dry and wet nitrogen (N) deposition rates to the tropical pasture site. Wet deposition was determined by collection of rainwater and subsequent analyses for NH_4^+ , NO_3^- and NO_2^- . To estimate dry N deposition rates, results from simultaneously performed measurements of mixing ratios of NO, NO_2 , O_3 as well as results from eddy covariance measurements (e.g., momentum, latent and sensible heat flux, friction velocity and Monin-Obukov length) were used, in addition to results obtained by the WAD/SJAC real-time technique.

The characteristic chemical conversion time scales of HONO, the NO- NO_2 - O_3 triad and the NH_3 - HNO_3 - NH_4NO_3 triad were estimated to be much larger than turbulent transport times. Hence, these compounds were treated as chemically-non-reactive tracers, implying that their vertical flux within the atmospheric surface layer is constant. Thus, surface-atmosphere exchange fluxes of these species could be estimated with sufficient accuracy by the “big leaf multiple resistance approach” and the “canopy compensation point model”. Whereas NO_2 , HNO_3 , aerosol NH_4^+ and NO_3^- were considered to be net deposited to the pasture site, the fluxes of NH_3 and HONO were considered to be of bi-directional nature. A dynamic resistance model [Sutton et al., 1998] was applied to estimate bi-directional surface-atmosphere exchange of NH_3 , whereby the contribution of direct NH_3 emission from cattle excreta was taken into account.

The turbulent resistance (R_a) and the quasi-laminar boundary layer resistances (R_b) were determined from micrometeorological quantities obtained from the eddy covariance measurements. However, some physico-chemical surface parameters required for the estimation of surface-atmosphere exchange fluxes could not be directly derived from our field measurements. These were (i.) uptake of trace gases by plant stomata and epicuticular water layers (expressed as surface resistances R_c) and (ii.) the concentration of the compound (in this case NH_3 and HONO) just above the soil and/or vegetation elements (expressed as compensation point concentration X_c). Hence, these surface parameters were varied over a selected range based on results obtained from studies in the temperate latitudes, resulting in the estimation of lower and upper flux scenarios.

The estimated NH_3 compensation point concentration and subsequently the diel pattern of the bi-directional NH_3 flux showed a pronounced maximum after sunrise, coinciding with the period of highest NH_3 mixing ratios. NH_3 deposited to epicuticular water films at high *RHs* during nighttime was predicted to (re-) evaporate just after sunrise due to a temperature increase. Bi-directional flux scenarios for NH_3 were complemented by additionally calculating a net deposition

scenario ($X_c(NH_3) = 0$). Estimated NH_3 flux scenarios during the dry season ranged from $-40 \text{ ngN m}^{-2} \text{ s}^{-1}$ (net deposition) to $70 \text{ ngN m}^{-2} \text{ s}^{-1}$ (net emission). The estimated NH_3 flux was found to be particularly sensitive to the plant apoplastic $[NH_4^+]/[H^+]$ ratio (I) and the epicuticular pH. Low values of I (100 – 200) were used, which was justified by the low soil N status of the pasture site, and in combination with an epicuticular pH of 4, the daytime net emission and nighttime net deposition pattern of the NH_3 fluxes observed in temperate latitudes could be reproduced. The application of higher I values would result in daytime NH_3 emissions significantly higher than observed in urban regions of Europe or North America.

Since HONO formation is considered to occur largely via heterogeneous conversion of NO_2 on surfaces, bi-directional HONO fluxes were calculated by assuming $X_c(HONO)$ to be a function of the NO_2 mixing ratio. Estimated median diel HONO fluxes during the dry season showed a small net emission during the afternoon but net deposition of up to $-1.3 \text{ ngN m}^{-2} \text{ s}^{-1}$ during the rest of the day. The estimated median diel HNO_3 net deposition flux during the dry season was characterized by highest values during daytime ($\sim 0.5 - 4 \text{ ngN m}^{-2} \text{ s}^{-1}$), coinciding with the period of highest HNO_3 mixing ratios and highest turbulence. During this period, maximal deposition velocities were 2.3 cm s^{-1} when $R_c(HNO_3) = 1 \text{ s m}^{-1}$ was applied. Contrastingly, the diel course of the NO_2 net deposition flux during the dry season exhibited nighttime values exceeding those during daytime by at least a factor of two ($\leq 12 \text{ ngN m}^{-2} \text{ s}^{-1}$).

Dry N deposition at FNS was dominated by NO_2 and NH_3 , which was attributed to widespread biomass burning activities during the dry season. However, the estimated dry N deposition rates are most sensitive to the predicted bi-directional NH_3 flux. The estimated total (dry + wet) N deposition to this tropical grassland site is $7.3 - 9.8 \text{ kgN ha}^{-1} \text{ yr}^{-1}$, whereof $2 - 4.5 \text{ kgN ha}^{-1} \text{ yr}^{-1}$ are attributed to dry N deposition and $\sim 5.3 \text{ kgN ha}^{-1} \text{ yr}^{-1}$ to wet N deposition. Dry deposition may contribute on average 30 % to the total annual N deposition. The grass surface appeared to have a strong potential for daytime NH_3 (re-)emission, owing to high canopy compensation points, which are related to high surface temperatures and to direct NH_3 emissions from cattle excreta. It is expected that $2.7 - 6.8 \text{ kgN ha}^{-1} \text{ yr}^{-1}$ are net (re-)emitted from the pasture site, mainly in form of NH_3 , but also as HONO and NO. Up to now, approximately 15 % of the original Amazonian rainforest has been deforested and was commonly converted to cattle pastures. Our N deposition estimate is suggested to be representative for these areas of the Amazon Basin. This suggests that the total (dry + wet) N deposition predicted by global chemistry and transport models for the Amazon region may be underestimated at least by a factor of two.

5.2 Outlook

Traditional filter sampling methods still find widespread application to sample inorganic aerosol species (NH_4^+ , NO_3^- , Cl^- and SO_4^{2-}) in the presence of their gaseous precursors. During the LBA-SMOCC measurement campaign in the Amazon Basin, overall chemical aerosol composition, including inorganic ions, such as NH_4^+ , NO_3^- , Cl^- and SO_4^{2-} were measured with stacked filter units (SFUs) and high volume filter samplers. Future work aims at a comprehensive qualitative and quantitative intercomparison of the WAD/SJAC real-time data with results obtained from these integrating filter samplers. This will contribute to gain a better understanding of possible filter sampling artifacts, which may be caused by high ambient temperatures and high *RHs* as well as by an aerosol chemical composition that differs significantly from that found in temperate latitudes.

Future work will focus on the determination of surface-atmosphere exchange fluxes of NH_3 , HNO_3 , HONO , HCl , SO_2 and their related aerosol compounds. Therefore, gradient measurements will be performed using the *Gradient Analyzer for Aerosols and Gases* (GRAEGOR) that was developed by the Energy Research Center of the Netherlands (ECN). Gradient measurements, along with measured micrometeorological quantities, will allow deducing surface-atmosphere exchange fluxes. GRAEGOR is a state of the art instrument based on techniques used in other instruments developed by ECN, like the ammonia monitors AMANDA, AMOR and AiRRmonia. The measurement principle of GRAEGOR is based on the method used also for the measurements described in this study. However, it consists of two WAD/SJAC systems that will selectively and simultaneously sample trace gases and aerosols at two different aerodynamic reference heights. The instrument currently reaches a precision of about 1 % at ambient mixing ratios and has a detection limit of 1 to 10 ppt. GREAGOR constitutes the prerequisite to accurately determine dry N deposition rates in regions where N deposition has not been experimentally determined yet (e.g., China, Africa).

Bibliography

- Abbas, R., and R.L. Tanner (1981), Continuous Determination of Gaseous Ammonia in the Ambient Atmosphere Using Fluorescence Derivatization, *Atmospheric Environment*, **15** (3), 277-281.
- Albrecht, B.A. (1989), Aerosols, Cloud Microphysics, and Fractional Cloudiness, *Science*, **245** (4923), 1227-1230.
- Alicke, B., A. Geyer, A. Hofzumahaus, F. Holland, S. Konrad, H.W. Patz, J. Schafer, J. Stutz, A. Volz-Thomas, and U. Platt (2003), OH formation by HONO photolysis during the BERLIOZ experiment, *Journal of Geophysical Research-Atmospheres*, **108** (D4), 8247, doi:10.1029/2001JD000579.
- Allegrini, I., A. Febo, C. Perrino, and P. Masia (1994), Measurement of Atmospheric Nitric-Acid in Gas-Phase and Nitrate in Particulate Matter by Means of Annular Denuders, *International Journal of Environmental Analytical Chemistry*, **54** (3), 183-201.
- Allen, A.G., R.M. Harrison, and J.W. Erisman (1989), Field-Measurements of the Dissociation of Ammonium-Nitrate and Ammonium-Chloride Aerosols, *Atmospheric Environment*, **23** (7), 1591-1599.
- Allen, A.G., and A.H. Miguel (1995), Biomass Burning in the Amazon - Characterization of the Ionic Component of Aerosols Generated from Flaming and Smoldering Rain-Forest and Savanna, *Environmental Science & Technology*, **29** (2), 486-493.
- Ammann, C. (1999), On the applicability of relaxed eddy accumulation and common methods for measuring trace gas fluxes, in *Zürcher Geographische Schriften*, pp. 1-50, ETH, Zürich.
- Ammann, M., M. Kalberer, D.T. Jost, L. Tobler, E. Rossler, D. Piguet, H.W. Gaggeler, and U. Baltensperger (1998), Heterogeneous production of nitrous acid on soot in polluted air masses, *Nature*, **395** (6698), 157-160.
- Andreae, M.O., D. Rosenfeld, P. Artaxo, A.A. Costa, G.P. Frank, K.M. Longo, and M.A.F. Silva-Dias (2004), Smoking rain clouds over the Amazon, *Science*, **303** (5662), 1337-1342.
- Andreae, M.O., P. Artaxo, C. Brandao, F.E. Carswell, P. Ciccioli, A.L. da Costa, A.D. Culf, J.L. Esteves, J.H.C. Gash, J. Grace, P. Kabat, J. Lelieveld, Y. Malhi, A.O. Manzi, F.X. Meixner, A.D. Nobre, C. Nobre, M. Ruivo, M.A. Silva-Dias, P. Stefani, R. Valentini, J. von Jouanne, and M.J. Waterloo (2002), Biogeochemical cycling of carbon, water, energy, trace gases, and aerosols in Amazonia: The LBA-EUSTACH experiments, *Journal of Geophysical Research-Atmospheres*, **107** (D20), 8066, doi:10.1029/2001JD000524.
- Andreae, M.O., P. Artaxo, H. Fischer, S.R. Freitas, J.M. Gregoire, A. Hansel, P. Hoor, R. Kormann, R. Krejci, L. Lange, J. Lelieveld, W. Lindinger, K. Longo, W. Peters, M. de Reus, B. Scheeren, M. Dias, J. Strom, P.F.J. van Velthoven, and J. Williams (2001), Transport of biomass burning smoke to the upper troposphere by deep convection in the equatorial region, *Geophysical Research Letters*, **28** (6), 951-954.
- Andreae, M.O., E. Atlas, G.W. Harris, G. Helas, A. deKock, R. Koppmann, W. Maenhaut, S. Mano, W.H. Pollock, J. Rudolph, D. Scharffe, G. Schebeske,

- and M. Welling (1996), Methyl halide emissions from savanna fires in southern Africa, *Journal of Geophysical Research-Atmospheres*, *101* (D19), 23603-23613.
- Andreae, M.O., and P.J. Crutzen (1997), Atmospheric aerosols: Biogeochemical sources and role in atmospheric chemistry, *Science*, *276* (5315), 1052-1058.
- Andreae, M.O., R.W. Talbot, H. Berresheim, and K.M. Beecher (1990), Precipitation Chemistry in Central Amazonia, *Journal of Geophysical Research-Atmospheres*, *95* (D10), 16987-16999.
- Andreae, M.O. (1983), Soot Carbon and Excess Fine Potassium - Long-Range Transport of Combustion-Derived Aerosols, *Science*, *220* (4602), 1148-1151.
- Ansari, A.S., and S.N. Pandis (1998), Response of inorganic PM to precursor concentrations, *Environmental Science & Technology*, *32* (18), 2706-2714.
- Ansari, A.S., and S.N. Pandis (1999a), An analysis of four models predicting the partitioning of semivolatile inorganic aerosol components, *Aerosol Science and Technology*, *31* (2-3), 129-153.
- Ansari, A.S., and S.N. Pandis (1999b), Prediction of multicomponent inorganic atmospheric aerosol behavior, *Atmospheric Environment*, *33* (5), 745-757.
- Ansari, A.S., and S.N. Pandis (2000), The effect of metastable equilibrium states on the partitioning of nitrate between the gas and aerosol phases, *Atmospheric Environment*, *34* (1), 157-168.
- Appel, B.R. (1993), Sampling of Selected Labile Atmospheric Pollutants, *Advances in Chemistry Series* (232), 1-40.
- Appel, B.R., V. Povard, and E.L. Kothny (1988), Loss of Nitric-Acid within Inlet Devices Intended to Exclude Coarse Particles During Atmospheric Sampling, *Atmospheric Environment*, *22* (11), 2535-2540.
- Appel, B.R., and Y. Tokiwa (1981), Atmospheric Particulate Nitrate Sampling Errors Due to Reactions with Particulate and Gaseous Strong Acids, *Atmospheric Environment*, *15* (6), 1087-1089.
- Appel, B.R., Y. Tokiwa, and M. Haik (1981), Sampling of Nitrates in Ambient Air, *Atmospheric Environment*, *15* (3), 283-289.
- Appel, B.R., Y. Tokiwa, M. Haik, and E.L. Kothny (1984), Artifact Particulate Sulfate and Nitrate Formation on Filter Media, *Atmospheric Environment*, *18* (2), 409-416.
- Appel, B.R., Y. Tokiwa, V. Povard, and E.L. Kothny (1991), The Measurement of Atmospheric Hydrochloric-Acid in Southern California, *Atmospheric Environment Part a-General Topics*, *25* (2), 525-527.
- Appel, B.R., S.M. Wall, Y. Tokiwa, and M. Haik (1980), Simultaneous Nitric-Acid, Particulate Nitrate and Acidity Measurements in Ambient Air, *Atmospheric Environment*, *14* (5), 549-554.
- Appel, B.R., A.M. Winer, Y. Tokiwa, and H.W. Biermann (1990), Comparison of Atmospheric Nitrous-Acid Measurements by Annular Denuder and Differential Optical-Absorption Systems, *Atmospheric Environment Part a-General Topics*, *24* (3), 611-616.
- Araujo, A.C., A.D. Nobre, B. Kruijt, J.A. Elbers, R. Dallarosa, P. Stefani, C. von Randow, A.O. Manzi, A.D. Culf, J.H.C. Gash, R. Valentini, and P. Kabat (2002), Comparative measurements of carbon dioxide fluxes from two nearby towers in a central Amazonian rainforest: The Manaus LBA site, *Journal of Geophysical Research-Atmospheres*, *107* (D20).

- Artaxo, P., J.V. Martins, M.A. Yamasoe, A.S. Procopio, T.M. Pauliquevis, M.O. Andreae, P. Guyon, L.V. Gatti, and A.M.C. Leal (2002), Physical and chemical properties of aerosols in the wet and dry seasons in Rondonia, Amazonia, *Journal of Geophysical Research-Atmospheres*, *107* (D20).
- Asman, W.A.H., M.A. Sutton, and J.K. Schjorring (1998), Ammonia: emission, atmospheric transport and deposition, *New Phytologist*, *139* (1), 27-48.
- Asner, G.P., A.R. Townsend, W.J. Riley, P.A. Matson, J.C. Neff, and C.C. Cleveland (2001), Physical and biogeochemical controls over terrestrial ecosystem responses to nitrogen deposition, *Biogeochemistry*, *54* (1), 1-39.
- Aumont, B., F. Chervier, and S. Laval (2003), Contribution of HONO sources to the NO_x/HO_x/O₃ chemistry in the polluted boundary layer, *Atmospheric Environment*, *37* (4), 487-498.
- Bassett, M., and J.H. Seinfeld (1983), Atmospheric Equilibrium-Model of Sulfate and Nitrate Aerosols, *Atmospheric Environment*, *17* (11), 2237-2252.
- Boddey, R.M., R. Macedo, R.M. Tarre, E. Ferreira, O.C. de Oliveira, C.D. Rezende, R.B. Cantarutti, J.M. Pereira, B.J.R. Alves, and S. Urquiaga (2004), Nitrogen cycling in Brachiaria pastures: the key to understanding the process of pasture decline, *Agriculture Ecosystems & Environment*, *103* (2), 389-403.
- Boring, C.B., S.K. Poruthoor, and P.K. Dasgupta (1999), Wet effluent parallel plate diffusion denuder coupled capillary ion chromatograph for the determination of atmospheric trace gases, *Talanta*, *48* (3), 675-684.
- Bouwman, A.F., D.P. Van Vuuren, R.G. Derwent, and M. Posch (2002), A global analysis of acidification and eutrophication of terrestrial ecosystems, *Water Air and Soil Pollution*, *141* (1-4), 349-382.
- Braman, R.S., T.J. Shelley, and W.A. McClenny (1982), Tungstic Acid for Pre-Concentration and Determination of Gaseous and Particulate Ammonia and Nitric-Acid in Ambient Air, *Analytical Chemistry*, *54* (3), 358-364.
- Bröske, R., J. Kleffmann, and P. Wiesen (2003), Heterogeneous conversion of NO₂ on secondary organic aerosol surfaces: A possible source of nitrous acid (HONO) in the atmosphere?, *Atmospheric Chemistry and Physics*, *3*, 469-474.
- Brunnemann, G., L. Kins, and R. Dlugi (1996), Physical and chemical characterisation of the atmospheric aerosol: An overview of the measurements during the SANA 2 campaign at Melpitz, *Meteorologische Zeitschrift, N.F.* *5*, 245-256.
- Buhr, S.M., M.P. Buhr, F.C. Fehsenfeld, J.S. Holloway, U. Karst, R.B. Norton, D.D. Parrish, and R.E. Sievers (1995), Development of a Semicontinuous Method for the Measurement of Nitric-Acid Vapor and Particulate Nitrate and Sulfate, *Atmospheric Environment*, *29* (19), 2609-2624.
- Bussink, D.W., L.A. Harper, and W.J. Corre (1996), Ammonia transport in a temperate grassland: 2. Diurnal fluctuations in response to weather and management conditions, *Agronomy Journal*, *88* (4), 621-626.
- Cadle, S.H., R.J. Countess, and N.A. Kelly (1982), Nitric-Acid and Ammonia in Urban and Rural Locations, *Atmospheric Environment*, *16* (10), 2501-2506.
- Calvert, J.G., A. Lazrus, G.L. Kok, B.G. Heikes, J.G. Walega, J. Lind, and C.A. Cantrell (1985), Chemical Mechanisms of Acid Generation in the Troposphere, *Nature*, *317* (6032), 27-35.

- Cape, J.N. (1996), Surface wetness and pollutant deposition, in *Plant cuticles*, edited by G. Kerstiens, BIOS Scientific Publishers, Oxford.
- Charron, A., R.M. Harrison, S. Moorcroft, and J. Booker (2004), Quantitative interpretation of divergence between PM₁₀ and PM_{2.5} mass measurement by TEOM and gravimetric (Partisol) instruments, *Atmospheric Environment*, *38*, 415–423.
- Cheng, Y.H., and C.J. Tsai (1997), Evaporation loss of ammonium nitrate particles during filter sampling, *Journal of Aerosol Science*, *28* (8), 1553–1567.
- Clark, K.L., N.M. Nadkarni, D. Schaefer, and H.L. Gholz (1998), Atmospheric deposition and net retention of ions by the canopy in a tropical montane forest, Monteverde, Costa Rica, *Journal of Tropical Ecology*, *14*, 27–45.
- Clegg, S.L., P. Brimblecombe, Z. Liang, and C.K. Chan (1997), Thermodynamic properties of aqueous aerosols to high supersaturation 2. A model of the system $\text{Na}^+ - \text{Cl}^- - \text{NO}_3^- - \text{SO}_4^{2-} - \text{H}_2\text{O}$ at 298.15 K, *Aerosol Science and Technology*, *27* (3), 345–366.
- Clegg, S.L., J.H. Seinfeld, and P. Brimblecombe (2001), Thermodynamic modelling of aqueous aerosols containing electrolytes and dissolved organic compounds, *Journal of Aerosol Science*, *32* (6), 713–738.
- Cofer, W.R., V.G. Collins, and R.W. Talbot (1985), Improved Aqueous Scrubber for Collection of Soluble Atmospheric Trace Gases, *Environmental Science & Technology*, *19* (6), 557–560.
- Crutzen, P.J., and M.O. Andreae (1990), Biomass Burning in the Tropics - Impact on Atmospheric Chemistry and Biogeochemical Cycles, *Science*, *250* (4988), 1669–1678.
- Culf, A.D., J.L. Esteves, A. de O. Marques Filho, and H.R. Da Rocha (1996), Radiation, temperature and humidity over forest and pasture in Amazonia, in *Amazonian Deforestation and Climate*, edited by J.H.C. Gash, Nobre, C. A., Roberts, J. M. e Victoria, R. L., pp. 413–424, John Wiley, New York.
- Danalatos, D., and S. Glavas (1999), Gas phase nitric acid, ammonia and related particulate matter at a Mediterranean coastal site, Patras, Greece, *Atmospheric Environment*, *33* (20), 3417–3425.
- Dasgupta, P.K. (1993), Automated Measurement of Atmospheric Trace Gases - Diffusion- Based Collection and Analysis, *Advances in Chemistry Series* (232), 41–90.
- Davidson, E.A., C.J.R. Carvalho, I.C.G. Vieira, R.O. Figueiredo, P. Moutinho, F.Y. Ishida, M.T.P. dos Santos, J.B. Guerrero, K. Kalif, and R.T. Sabá (2004), Nutrient limitation of biomass growth in a tropical secondary forest: Early results of a nitrogen and phosphorus amendment experiment, *Ecological Applications*, *in press*.
- De Arellano, J.V.-G., and P.G. Duynkerke (1992), Influence of Chemistry on the Flux-Gradient Relationships for the NO-O₃-NO₂ System, *Boundary-Layer Meteorology*, *61* (4), 375–387.
- Deandrade, J.B., N.M. Dearagao, and F.R.J. Araujo (1992), Nitric-Acid Air-Diffusion Coefficient - Experimental-Determination Using a Diffusion Cell, *International Journal of Environmental Analytical Chemistry*, *49* (1–2), 103–109.
- Decesari, S., S. Fuzzi, M.C. Facchini, W. Maenhaut, M. Claeys, Y. Rudich, P. Artaxo, P. Guyon, M.O. Andreae, O.L. Mayol-Bracero, and G. Fisch

- (2005), Overview of the inorganic and organic composition of size-segregated aerosol in Rondonia, Brazil, from the biomass burning period to the onset of the wet season, *in preparation*.
- Dentener, F.J., and P.J. Crutzen (1994), A 3-Dimensional Model of the Global Ammonia Cycle, *Journal of Atmospheric Chemistry*, *19* (4), 331-369.
- Dlugi, R. (1993), Interaction of NO_x and VOCs within vegetation, in *Photo-oxidants: Precursors and Products, Proceedings of EUROTRAC Symposium '92*, edited by P.B. P. M. Borrell, T. Cvitas and W. Seiler, pp. 682-688, Academic Publishing, The Hague.
- Dollard, G.J., D.H.F. Atkins, T.J. Davies, and C. Healy (1987), Concentrations and Dry Deposition Velocities of Nitric-Acid, *Nature*, *326* (6112), 481-483.
- Doyle, G.J., E.C. Tuazon, R.A. Graham, T.M. Mischke, A.M. Winer, and J.N. Pitts (1979), Simultaneous Concentrations of Ammonia and Nitric-Acid in a Polluted Atmosphere and Their Equilibrium Relationship to Particulate Ammonium-Nitrate, *Environmental Science & Technology*, *13* (11), 1416-1419.
- Durham, J.L., L.L. Spiller, and T.G. Ellestad (1987), Nitric-Acid Nitrate Aerosol Measurements by a Diffusion Denuder - a Performance Evaluation, *Atmospheric Environment*, *21* (3), 589-598.
- Durham, J.L., and L. Stockburger (1986), Nitric-Acid Air Diffusion-Coefficient - Experimental- Determination, *Atmospheric Environment*, *20* (3), 559-563.
- Eatough, D.J., V.F. White, L.D. Hansen, N.L. Eatough, and E.C. Ellis (1985), Hydration of Nitric-Acid and Its Collection in the Atmosphere by Diffusion Denuders, *Analytical Chemistry*, *57* (3), 743-748.
- Erisman, J.W., R. Otjes, A. Hensen, P. Jongejan, P. van den Bulk, A. Khlystov, H. Mols, and J. Slanina (2001), Instrument development and application in studies and monitoring of ambient ammonia, *Atmospheric Environment*, *35* (11), 1913-1922.
- Erisman, J.W., A. Vanpul, and P. Wyers (1994), Parametrization of Surface-Resistance for the Quantification of Atmospheric Deposition of Acidifying Pollutants and Ozone, *Atmospheric Environment*, *28* (16), 2595-2607.
- Erisman, J.W., A.W.M. Vermetten, W.A.H. Asman, A. Waijers-Ijpelaan, and J. Slanina (1988), Vertical-Distribution of Gases and Aerosols - the Behavior of Ammonia and Related Components in the Lower Atmosphere, *Atmospheric Environment*, *22* (6), 1153-1160.
- Erisman, J.W., and G.P. Wyers (1993), Continuous Measurements of Surface Exchange of SO₂ and NH₃ - Implications for Their Possible Interaction in the Deposition Process, *Atmospheric Environment Part a-General Topics*, *27* (13), 1937-1949.
- Falkovich, A.H., E.R. Graber, G. Schkolnik, Y. Rudich, W. Maenhaut, and P. Artaxo (2005), Low molecular weight organic acids in aerosol particles from Rondonia, Brazil, during the biomass-burning, transition and wet periods, *Atmospheric Chemistry and Physics*, *5*, 781-797.
- Farquhar, G.D., P.M. Firth, R. Wetselaar, and B. Weir (1980), On the Gaseous Exchange of Ammonia between Leaves and the Environment - Determination of the Ammonia Compensation Point, *Plant Physiology*, *66* (4), 710-714.

- Febo, A., C. Perrino, and I. Allegrini (1996), Measurement of nitrous acid in Milan, Italy, by DOAS and diffusion denuders, *Atmospheric Environment*, *30* (21), 3599-3609.
- Fehsenfeld, F.C., J.W. Drummond, U.K. Roychowdhury, P.J. Galvin, E.J. Williams, M.P. Buhr, D.D. Parrish, G. Hubler, A.O. Langford, J.G. Calvert, B.A. Ridley, F. Grahek, B.G. Heikes, G.L. Kok, J.D. Shetter, J.G. Walega, C.M. Elsworth, R.B. Norton, D.W. Fahey, P.C. Murphy, C. Hovermale, V.A. Mohnen, K.L. Demerjian, G.I. Mackay, and H.I. Schiff (1990), Intercomparison of No₂ Measurement Techniques, *Journal of Geophysical Research-Atmospheres*, *95* (D4), 3579-3597.
- Fehsenfeld, F.C., L.G. Huey, D.T. Sueper, R.B. Norton, E.J. Williams, F.L. Eisele, R.L. Mauldin, and D.J. Tanner (1998), Ground-based intercomparison of nitric acid measurement techniques, *Journal of Geophysical Research-Atmospheres*, *103* (D3), 3343-3353.
- Finlayson-Pitts, B.J., and J.N. Finlayson-Pitts (1986), *Atmospheric Chemistry: Fundamentals and Experimental Techniques*, John Wiley & Sons, New York.
- Fisch, G., J. Tota, L.A.T. Machado, M. Dias, R.F.D. Lyra, C.A. Nobre, A.J. Dolman, and J.H.C. Gash (2004), The convective boundary layer over pasture and forest in Amazonia, *Theoretical and Applied Climatology*, *78* (1-3), 47-59.
- Flechar, C.R., D. Fowler, M.A. Sutton, and J.N. Cape (1999), A dynamic chemical model of bi-directional ammonia exchange between semi-natural vegetation and the atmosphere, *Quarterly Journal of the Royal Meteorological Society*, *125* (559), 2611-2641.
- Foken, T. (2003), *Angewandte Meteorologie, Micrometeorologische Methoden*, Springer Verlag, Berlin, Heidelberg, New York (in German).
- Foken, T., R. Dlugi, and G. Kramm (1995), On the determination of dry deposition and emission of gaseous compounds at the biosphere-atmosphere-interface, *Meteorologische Zeitschrift*, *4*, 91-118.
- Fridlind, A.M., and M.Z. Jacobson (2000), A study of gas-aerosol equilibrium and aerosol pH in the remote marine boundary layer during the First Aerosol Characterization Experiment (ACE 1), *Journal of Geophysical Research-Atmospheres*, *105* (D13), 17325-17340.
- Furutani, H., and H. Akimoto (2002), Development and characterization of a fast measurement system for gas-phase nitric acid with a chemical ionization mass spectrometer in the marine boundary layer, *Journal of Geophysical Research-Atmospheres*, *107* (D1-D2), ACH, doi:10.1029/2000JD000269.
- Galasyn, J.F., K.L. Tschudy, and B.J. Huebert (1987), Seasonal and Diurnal Variability of Nitric-Acid Vapor and Ionic Aerosol Species in the Remote Free Troposphere at Mauna-Loa, Hawaii, *Journal of Geophysical Research-Atmospheres*, *92* (D3), 3105-3113.
- Gallagher, M.W., J. Fontan, G.P. Wyers, W. Ruijgrok, J. Duyzer, P. Hummelshoj, K. Pilegaard, and D. Fowler (1997), Atmospheric particles and their interactions with natural surfaces, in *Biosphere-Atmosphere Exchange of Pollutants and Trace substances EUROTRAC-BIATEX*, edited by J. Slanina, pp. 45-92, Springer.

- Galloway, J.N., G.E. Likens, W.C. Keene, and J.M. Miller (1982), The Composition of Precipitation in Remote Areas of the World, *Journal of Geophysical Research-Oceans and Atmospheres*, *87* (NC11), 8771-8786.
- Galloway, J.N. (1998), The global nitrogen cycle: changes and consequences, *Environmental Pollution*, *102*, 15-24.
- Galloway, J.N. (2001), Acidification of the world - Natural and anthropogenic, *Water Air and Soil Pollution*, *130* (1-4), 17-24.
- Galloway, J.N., J.D. Aber, J.W. Erisman, S.P. Seitzinger, R.W. Howarth, E.B. Cowling, and B.J. Cosby (2003), The nitrogen cascade, *Bioscience*, *53* (4), 341-356.
- Garcia-Montiel, D.C., P.A. Steudler, M. Piccolo, C. Neill, J. Melillo, and C.C. Cerri (2003), Nitrogen oxide emissions following wetting of dry soils in forest and pastures in Rondonia, Brazil, *Biogeochemistry*, *64* (3), 319-336.
- Gard, E., J.E. Mayer, B.D. Morrical, T. Dienes, D.P. Fergenson, and K.A. Prather (1997), Real-time analysis of individual atmospheric aerosol particles: Design and performance of a portable ATOFMS, *Analytical Chemistry*, *69* (20), 4083-4091.
- Garland, J.A. (2001), On the size dependence of particle deposition, *Water, Air and Soil Pollution: Focus*, *1* (5-6), 323-332.
- Garratt, J.R. (1992), *The atmospheric boundary layer*, Cambridge University Press, Cambridge, 315.
- Gash, J.H.C., C. Huntingford, J.A. Marengo, R.A. Betts, P.M. Cox, G. Fisch, R. Fu, A.W. Gandu, P.P. Harris, L.A.T. Machado, C. von Randow, and M.A.S. Dias (2004), Amazonian climate: results and future research, *Theoretical and Applied Climatology*, *78* (1-3), 187-193.
- Genfa, Z.F., S. Slanina, C.B. Boring, P.A.C. Jongejan, and P.K. Dasgupta (2003), Continuous wet denuder measurements of atmospheric nitric and nitrous acids during the 1999 Atlanta Supersite, *Atmospheric Environment*, *37* (9-10), 1351-1364.
- Gormley, P.G., and M. Kennedy (1949), Diffusion from a stream flowing through a cylindrical tube, *Proceedings of the Royal Irish Academy*, *52A*, 163-169.
- Goulding, K.W.T., N.J. Bailey, N.J. Bradbury, P. Hargreaves, M. Howe, D.V. Murphy, P.R. Poulton, and T.W. Willison (1998), Nitrogen deposition and its contribution to nitrogen cycling and associated soil processes, *New Phytologist*, *139* (1), 49-58.
- Graedel, T.E., and W.C. Keene (1995), Tropospheric Budget of Reactive Chlorine, *Global Biogeochemical Cycles*, *9* (1), 47-77.
- Graham, B., P. Guyon, W. Maenhaut, P.E. Taylor, M. Ebert, S. Matthias-Maser, O.L. Mayol-Bracero, R.H.M. Godoi, P. Artaxo, F.X. Meixner, M.A.L. Moura, C. Rocha, R. Van Grieken, M.M. Glovsky, R.C. Flagan, and M.O. Andreae (2003a), Composition and diurnal variability of the natural Amazonian aerosol, *Journal of Geophysical Research-Atmospheres*, *108* (D24), 4765, doi:10.1029/2003JD004049.
- Graham, B., P. Guyon, P.E. Taylor, P. Artaxo, W. Maenhaut, M.M. Glovsky, R.C. Flagan, and M.O. Andreae (2003b), Organic compounds present in the natural Amazonian aerosol: Characterization by gas chromatography-mass spectrometry, *Journal of Geophysical Research-Atmospheres*, *108* (D24), 4766, doi:10.1029/2003JD003990.

- Gupta, A., R. Kumar, K.M. Kumari, and S.S. Srivastava (2003), Measurement of NO₂, HNO₃, NH₃ and SO₂ and related particulate matter at a rural site in Rampur, India, *Atmospheric Environment*, *37* (34), 4837- 4846.
- Guyon, P., B. Graham, J. Beck, O. Boucher, E. Gerasopoulos, O.L. Mayol-Bracero, G.C. Roberts, P. Artaxo, and M.O. Andreae (2003), Physical properties and concentration of aerosol particles over the Amazon tropical forest during background and biomass burning conditions, *Atmospheric Chemistry and Physics*, *3*, 951-967.
- Hall, S.J., and P.A. Matson (1999), Nitrogen oxide emissions after nitrogen additions in tropical forests, *Nature*, *400* (6740), 152-155.
- Hanke, M., B. Umann, J. Uecker, F. Arnold, and H. Bunz (2003), Atmospheric measurements of gas-phase HNO₃ and SO₂ using chemical ionization mass spectrometry during the MINATROC field campaign 2000 on Monte Cimone, *Atmospheric Chemistry and Physics*, *3*, 417-436.
- Hanson, P.J., and S.E. Lindberg (1991), Dry Deposition of Reactive Nitrogen-Compounds - a Review of Leaf, Canopy and Non-Foliar Measurements, *Atmospheric Environment Part a-General Topics*, *25* (8), 1615-1634.
- Hao, W.M., and M.H. Liu (1994), Spatial and Temporal Distribution of Tropical Biomass Burning, *Global Biogeochemical Cycles*, *8* (4), 495-503.
- Harrison, R.M., and A.M.N. Kitto (1994), Evidence for a Surface Source of Atmospheric Nitrous-Acid, *Atmospheric Environment*, *28* (6), 1089-1094.
- Harrison, R.M., and I.M. Msibi (1994), Validation of Techniques for Fast-Response Measurement of HNO₃ and NH₃ and Determination of the [NH₃] [HNO₃] Concentration Product, *Atmospheric Environment*, *28* (2), 247-255.
- Harrison, R.M., J.D. Peak, and G.M. Collins (1996), Tropospheric cycle of nitrous acid, *Journal of Geophysical Research-Atmospheres*, *101* (D9), 14429-14439.
- Harrison, R.M., and C.A. Pio (1983), An Investigation of the Atmospheric HNO₃-NH₃-NH₄NO₃ Equilibrium Relationship in a Cool, Humid Climate, *Tellus Series B-Chemical and Physical Meteorology*, *35* (2), 155-159.
- Harrison, R.M., W.T. Sturges, A.M.N. Kitto, and Y.Q. Li (1990), Kinetics of Evaporation of Ammonium-Chloride and Ammonium-Nitrate Aerosols, *Atmospheric Environment Part a-General Topics*, *24* (7), 1883-1888.
- Hauglustaine, D.A., F. Hourdin, L. Jourdain, M.A. Filiberti, S. Walters, J.F. Lamarque, and E.A. Holland (2004), Interactive chemistry in the Laboratoire de Meteorologie Dynamique general circulation model: Description and background tropospheric chemistry evaluation, *Journal of Geophysical Research-Atmospheres*, *109* (D4).
- Hegg, D.A., L.F. Radke, P.V. Hobbs, and P.J. Riggan (1988), Ammonia Emissions from Biomass Burning, *Geophysical Research Letters*, *15* (4), 335-337.
- Heland, J., J. Kleffmann, R. Kurtenbach, and P. Wiesen (2001), A new instrument to measure gaseous nitrous acid (HONO) in the atmosphere, *Environmental Science & Technology*, *35* (15), 3207-3212.
- Hering, S.V., D.R. Lawson, I. Allegrini, A. Febo, C. Perrino, M. Possanzini, J.E. Sickles, K.G. Anlauf, A. Wiebe, B.R. Appel, W. John, J. Ondo, S. Wall, R.S. Braman, R. Sutton, G.R. Cass, P.A. Solomon, D.J. Eatough, N.L. Eatough, E.C. Ellis, D. Grosjean, B.B. Hicks, J.D. Womack, J. Horrocks, K.T. Knapp, T.G. Ellestad, R.J. Paur, W.J. Mitchell, M. Pleasant, E. Peake, A. Maclean, W.R. Pierson, W. Brachaczek, H.I. Schiff, G.I. Mackay, C.W. Spicer, D.H.

- Stedman, A.M. Winer, H.W. Biermann, and E.C. Tuazon (1988), The Nitric-Acid Shootout - Field Comparison of Measurement Methods, *Atmospheric Environment*, *22* (8), 1519-1539.
- Hesterberg, R., A. Blatter, M. Fahrni, M. Rosset, A. Neftel, W. Eugster, and H. Wanner (1996), Deposition of nitrogen-containing compounds to an extensively managed grassland in central Switzerland, *Environmental Pollution*, *91* (1), 21-34.
- Hicks, B.B., D.D. Baldocchi, T.P. Meyers, R.P. Hosker, and D.R. Matt (1987), A Preliminary Multiple Resistance Routine for Deriving Dry Deposition Velocities from Measured Quantities, *Water Air and Soil Pollution*, *36* (3-4), 311-330.
- Hildemann, L.M., A.G. Russell, and G.R. Cass (1984), Ammonia and Nitric-Acid Concentrations in Equilibrium with Atmospheric Aerosols - Experiment Vs Theory, *Atmospheric Environment*, *18* (9), 1737-1750.
- Hinds, W.C. (1999), *Aerosol Technology, Properties, Behavior and Measurement of Airborne Particles*, John Wiley & Sons, New York.
- Holland, E.A., B.H. Braswell, J.F. Lamarque, A. Townsend, J. Sulzman, J.F. Muller, F. Dentener, G. Brasseur, H. Levy, J.E. Penner, and G.J. Roelofs (1997), Variations in the predicted spatial distribution of atmospheric nitrogen deposition and their impact on carbon uptake by terrestrial ecosystems, *Journal of Geophysical Research-Atmospheres*, *102* (D13), 15849-15866.
- Holland, E.A., F.J. Dentener, B.H. Braswell, and J.M. Sulzman (1999), Contemporary and pre-industrial global reactive nitrogen budgets, *Biogeochemistry*, *46* (1-3), 7-43.
- Howarth, R.W., G. Billen, D. Swaney, A. Townsend, N. Jaworski, K. Lajtha, J.A. Downing, R. Elmgren, N. Caraco, T. Jordan, F. Berendse, J. Freney, V. Kudeyarov, P. Murdoch, and Z.L. Zhu (1996), Regional nitrogen budgets and riverine N&P fluxes for the drainages to the North Atlantic Ocean: Natural and human influences, *Biogeochemistry*, *35* (1), 75-139.
- Huang, G., X.L. Zhou, G.H. Deng, H.C. Qiao, and K. Civerolo (2002), Measurements of atmospheric nitrous acid and nitric acid, *Atmospheric Environment*, *36* (13), 2225-2235.
- Huebert, B.J., and C.H. Robert (1985), The Dry Deposition of Nitric-Acid to Grass, *Journal of Geophysical Research-Atmospheres*, *90* (ND1), 2085-2090.
- Huey, L.G., E.J. Dunlea, E.R. Lovejoy, D.R. Hanson, R.B. Norton, F.C. Fehsenfeld, and C.J. Howard (1998), Fast time response measurements of HNO₃ in air with a chemical ionization mass spectrometer, *Journal of Geophysical Research-Atmospheres*, *103* (D3), 3355-3360.
- IPCC (2001), *Climate Change 2001, Working Group I: The Scientific Basis*, Cambridge University Press.
- Jacob, D.J. (1999), *Introduction to Atmospheric Chemistry*, Princeton University Press.
- Jayne, J.T., D.C. Leard, X.F. Zhang, P. Davidovits, K.A. Smith, C.E. Kolb, and D.R. Worsnop (2000), Development of an aerosol mass spectrometer for size and composition analysis of submicron particles, *Aerosol Science and Technology*, *33* (1-2), 49-70.

- Jimenez, J.L., J.T. Jayne, Q. Shi, C.E. Kolb, D.R. Worsnop, I. Yourshaw, J.H. Seinfeld, R.C. Flagan, X.F. Zhang, K.A. Smith, J.W. Morris, and P. Davidovits (2003), Ambient aerosol sampling using the Aerodyne Aerosol Mass Spectrometer, *Journal of Geophysical Research-Atmospheres*, *108* (D7), 8425, doi:10.1029/2001JD001213.
- Jongejan, P.A.C., Y. Bai, A.C. Veltkamp, G.P. Wyers, and J. Slanina (1997), An automated field instrument for the determination of acidic gases in air, *International Journal of Environmental Analytical Chemistry*, *66* (4), 241-251.
- Kauffman, J.B., D.L. Cummings, and D.E. Ward (1998), Fire in the Brazilian Amazon 2. Biomass, nutrient pools and losses in cattle pastures, *Oecologia*, *113* (3), 415-427.
- Kauffman, J.B., D.L. Cummings, D.E. Ward, and R. Babbitt (1995), Fire in the Brazilian Amazon 1. Biomass, Nutrient Pools, and Losses in Slashed Primary Forests, *Oecologia*, *104* (4), 397-408.
- Keene, W.C., M.A.K. Khalil, D.J. Erickson, A. McCulloch, T.E. Graedel, J.M. Lobert, M.L. Aucott, S.L. Gong, D.B. Harper, G. Kleiman, P. Midgley, R.M. Moore, C. Seuzaret, W.T. Sturges, C.M. Benkovitz, V. Koropalov, L.A. Barrie, and Y.F. Li (1999), Composite global emissions of reactive chlorine from anthropogenic and natural sources: Reactive Chlorine Emissions Inventory, *Journal of Geophysical Research-Atmospheres*, *104* (D7), 8429-8440.
- Kerminen, V.M., R. Hillamo, K. Teinila, T. Pakkanen, I. Allegrini, and R. Sparapani (2001), Ion balances of size-resolved tropospheric aerosol samples: implications for the acidity and atmospheric processing of aerosols, *Atmospheric Environment*, *35* (31), 5255-5265.
- Kerminen, V.M., L. Pirjola, M. Boy, A. Eskola, K. Teinila, L. Laakso, A. Asmi, J. Hienola, A. Lauri, V. Vainio, K. Lehtinen, and M. Kulmala (2000), Interaction between SO₂ and submicron atmospheric particles, *Atmospheric Research*, *54* (1), 41-57.
- Keuken, M.P., C.A.M. Schoonebeek, A. Wensveen-Louter, and J. Slanina (1988), Simultaneous Sampling of NH₃, HNO₃, HCl, SO₂ and H₂O₂ in Ambient Air by a Wet Annular Denuder System, *Atmospheric Environment*, *22* (11), 2541-2548.
- Keuken, M.P., A. Waijers-Ijpelaan, J.J. Mols, R.P. Otjes, and J. Slanina (1989), The Determination of Ammonia in Ambient Air by an Automated Thermodenuder System, *Atmospheric Environment*, *23* (10), 2177-2185.
- Khlystov, A. (1998), Cloud forming properties of ambient aerosol in the Netherlands and resultant shortwave radiative forcing of climate, PhD thesis, University of Wageningen, Wageningen.
- Khlystov, A., G.P. Wyers, and J. Slanina (1995), The Steam-Jet Aerosol Collector, *Atmospheric Environment*, *29* (17), 2229-2234.
- Kim, Y.P., and J.H. Seinfeld (1995), Atmospheric Gas-Aerosol Equilibrium 3. Thermodynamics of Crustal Elements Ca²⁺, K⁺, and Mg²⁺, *Aerosol Science and Technology*, *22* (1), 93-110.
- Kim, Y.P., J.H. Seinfeld, and P. Saxena (1993), Atmospheric Gas Aerosol Equilibrium 1. Thermodynamic Model, *Aerosol Science and Technology*, *19* (2), 157-181.

- Kirchner, W., F. Welter, A. Bongartz, J. Kames, S. Schweighoefer, and U. Schurath (1990), Trace Gas-Exchange at the Air-Water-Interface - Measurements of Mass Accommodation Coefficients, *Journal of Atmospheric Chemistry*, *10* (4), 427-449.
- Kirkman, G.A., A. Gut, C. Ammann, L.V. Gatti, A.M. Cordova, M.A.L. Moura, M.O. Andreae, and F.X. Meixner (2002), Surface exchange of nitric oxide, nitrogen dioxide, and ozone at a cattle pasture in Rondonia, Brazil, *Journal of Geophysical Research-Atmospheres*, *107* (D20), 8083, doi:10.1029/2001JD000523.
- Kitto, A.M.N., and R.M. Harrison (1992), Nitrous and Nitric-Acid Measurements at Sites in South-East England, *Atmospheric Environment Part a-General Topics*, *26* (2), 235-241.
- Kleffmann, J., R. Kurtenbach, J. Lörzer, P. Wiesen, N. Kalthoff, B. Vogel, and H. Vogel (2003), Measured and simulated vertical profiles of nitrous acid—Part I: Field measurements, *Atmospheric Environment*, *37* (21), 2949-2955.
- Klockow, D., R. Niessner, M. Malejczyk, H. Kiendl, B. Vomberg, M.P. Keuken, A. Waijers-Ijpelaan, and J. Slanina (1989), Determination of Nitric-Acid and Ammonium-Nitrate by Means of a Computer-Controlled Thermodenuder System, *Atmospheric Environment*, *23* (5), 1131-1138.
- Kramm, G., and R. Dlugi (1994), Modeling of the Vertical Fluxes of Nitric-Acid, Ammonia, and Ammonium-Nitrate, *Journal of Atmospheric Chemistry*, *18* (4), 319-357.
- Kramm, G., R. Dlugi, G.J. Dollard, T. Foken, N. Molders, H. Muller, W. Seiler, and H. Sievering (1995), On the Dry Deposition of Ozone and Reactive Nitrogen Species, *Atmospheric Environment*, *29* (21), 3209-3231.
- Kraus, A., and A. Hofzumahaus (1998), Field measurements of atmospheric photolysis frequencies for O-3, NO₂, HCHO, CH₃CHO, H₂O₂, and HONO by UV spectroradiometry, *Journal of Atmospheric Chemistry*, *31* (1-2), 161-180.
- Kuhns, H., V. Bohdan, J.C. Chow, V. Etyemezian, M.C. Green, D. Herlocker, S. Kohl, M. McGown, J. Ramsdell, W.R. Stockwell, M. Toole, and J. Watson (2003), The Treasure Valley secondary aerosol study I: measurements and equilibrium modeling of inorganic secondary aerosols and precursors for southwestern Idaho, *Atmospheric Environment*, *37* (4), 511-524.
- Lammel, G., and J.N. Cape (1996), Nitrous acid and nitrite in the atmosphere, *Chemical Society Reviews*, *25* (5), 361-&.
- Lara, L., P. Artaxo, L.A. Martinelli, R.L. Victoria, P.B. Camargo, A. Krusche, G.P. Ayers, E.S.B. Ferraz, and M.V. Ballester (2001), Chemical composition of rainwater and anthropogenic influences in the Piracicaba River Basin, Southeast Brazil, *Atmospheric Environment*, *35* (29), 4937-4945.
- Laurance, W.F., A.K.M. Albernaz, P.M. Fearnside, H.L. Vasconcelos, and L.V. Ferreira (2004), Deforestation in Amazonia, *Science*, *304* (5674), 1109-1109.
- Lee, S.H., D.M. Murphy, D.S. Thomson, and A.M. Middlebrook (2002), Chemical components of single particles measured with Particle Analysis by Laser Mass Spectrometry (PALMS) during the Atlanta SuperSite Project: Focus on organic/sulfate, lead, soot, and mineral particles, *Journal of Geophysical Research-Atmospheres*, *107* (D1-D2), doi:10.1029/2000JD000011.

- Lee, Y.N., R. Weber, Y.L. Ma, D. Orsini, K. Maxwell-Meier, D. Blake, S. Meinardi, G. Sachse, C. Harward, T.Y. Chen, D. Thornton, F.H. Tu, and A. Bandy (2003), Airborne measurement of inorganic ionic components of fine aerosol particles using the particle-into-liquid sampler coupled to ion chromatography technique during ACE-Asia and TRACE-P, *Journal of Geophysical Research-Atmospheres*, *108* (D23), 8646, doi:10.1029/2002JD003265.
- Lefer, B.L., R.W. Talbot, and J.W. Munger (1999), Nitric acid and ammonia at a rural northeastern US site, *Journal of Geophysical Research-Atmospheres*, *104* (D1), 1645-1661.
- Lenschow, D.H. (1982), Reactive trace species in the boundary layer from a micrometeorological perspective, *J. Meteorol. Soc. Jpn.*, *60*, 161–172.
- Lesack, L.F.W., and J.M. Melack (1991), The Deposition, Composition, and Potential Sources of Major Ionic Solutes in Rain of the Central Amazon Basin, *Water Resources Research*, *27* (11), 2953-2977.
- Li, J., M. Posfai, P.V. Hobbs, and P.R. Buseck (2003), Individual aerosol particles from biomass burning in southern Africa: 2, Compositions and aging of inorganic particles, *Journal of Geophysical Research-Atmospheres*, *108* (D13), 8484, doi:10.1029/2002JD002310.
- Likens, G.E., W.C. Keene, J.M. Miller, and J.N. Galloway (1987), Chemistry of Precipitation from a Remote, Terrestrial Site in Australia, *Journal of Geophysical Research-Atmospheres*, *92* (D11), 13299-13314.
- Lindgren, P.F. (1992), Diffusion Scrubber-Ion Chromatography for the Measurement of Trace Levels of Atmospheric HCl, *Atmospheric Environment Part a-General Topics*, *26* (1), 43-49.
- Loubet, B., C. Milford, P.W. Hill, Y.S. Tang, P. Cellier, and M.A. Sutton (2002), Seasonal variability of apoplastic NH₄⁺ and pH in an intensively managed grassland, *Plant and Soil*, *238* (1), 97-110.
- Mace, K.A., P. Artaxo, and R.A. Duce (2003), Water-soluble organic nitrogen in Amazon Basin aerosols during the dry (biomass burning) and wet seasons, *Journal of Geophysical Research-Atmospheres*, *108* (D16), 4512, doi:10.1029/2003JD003557.
- Mallina, R.V., A.S. Wexler, K.P. Rhoads, and M.V. Johnston (2000), High speed particle beam generation: A dynamic focusing mechanism for selecting ultrafine particles, *Aerosol Science and Technology*, *33* (1-2), 87-104.
- Marshall, G.B., and N.A. Dimmock (1992), Determination of Nitric-Acid in Ambient Air Using Diffusion Denuder Tubes, *Talanta*, *39* (11), 1463-1469.
- Matson, P.A., W.H. McDowell, A.R. Townsend, and P.M. Vitousek (1999), The globalization of N deposition: ecosystem consequences in tropical environments, *Biogeochemistry*, *46* (1-3), 67-83.
- Matsumoto, K., and H. Tanaka (1996), Formation and dissociation of atmospheric particulate nitrate and chloride: An approach based on phase equilibrium, *Atmospheric Environment*, *30* (4), 639-648.
- Matusca, P., B. Schwarz, and K. Bächmann (1984), Measurements of Diurnal Concentration Variations of Gaseous HCl in Air in the Subnanogram Range, *Atmospheric Environment*, *18* (8), 1667-1675.
- Mauldin, R.L., D.J. Tanner, and F.L. Eisele (1998), A new chemical ionization mass spectrometer technique for the fast measurement of gas phase nitric acid in

- the atmosphere, *Journal of Geophysical Research-Atmospheres*, *103* (D3), 3361-3367.
- Mayol-Bracero, O.L., P. Guyon, B. Graham, G. Roberts, M.O. Andreae, S. Decesari, M.C. Facchini, S. Fuzzi, and P. Artaxo (2002), Water-soluble organic compounds in biomass burning aerosols over Amazonia - 2. Apportionment of the chemical composition and importance of the polyacidic fraction, *Journal of Geophysical Research-Atmospheres*, *107* (D20), 8091, doi:10.1029/2001JD000522.
- Mehlmann, A., and P. Warneck (1995), Atmospheric Gaseous HNO₃ Particulate Nitrate, and Aerosol-Size Distributions of Major Ionic Species at a Rural Site in Western Germany, *Atmospheric Environment*, *29* (17), 2359-2373.
- Meixner, F.X. (1994), Surface exchange of odd nitrogen oxides, *Nova Acta Leopoldina*, *70* (288), 299-348.
- Meixner, F.X., G.P. Wyers, and A. Neftel (1996), Bi-directional exchange of ammonia over cereals, in *Proceedings of EUROTRAC Symposium '96*, edited by P.B. P.M. Borrell, T. Cvitas, K. Kelly, W. Seiler, Computational Mechanics Publications, Southampton.
- Meng, Z.Y., and J.H. Seinfeld (1996), Time scales to achieve atmospheric gas-aerosol equilibrium for volatile species, *Atmospheric Environment*, *30* (16), 2889-2900.
- Meng, Z.Y., J.H. Seinfeld, P. Saxena, and Y.P. Kim (1995), Atmospheric Gas-Aerosol Equilibrium 4. Thermodynamics of Carbonates, *Aerosol Science and Technology*, *23* (2), 131-154.
- Metzger, S. (2000), Gas /aerosol partitioning: A simplified method for global modeling, PhD thesis, University of Utrecht, The Netherlands, ISBN: 90-393-2510-3, <http://www.library.uu.nl/digiarchief/dip/diss/1930853/inhoud.htm>, Utrecht.
- Metzger, S., F. Dentener, S. Pandis, and J. Lelieveld (2002), Gas/aerosol partitioning: 1. A computationally efficient model, *Journal of Geophysical Research-Atmospheres*, *107* (D16), 4312, doi:10.1029/2001JD001102.
- Metzger, S., and J. Lelieveld (2005), Technical note: New version of the equilibrium simplified aerosol model (EQSAM2), to be submitted to *Atmospheric Chemistry and Physics*.
- Middlebrook, A.M., D.M. Murphy, S.H. Lee, D.S. Thomson, K.A. Prather, R.J. Wenzel, D.Y. Liu, D.J. Phares, K.P. Rhoads, A.S. Wexler, M.V. Johnston, J.L. Jimenez, J.T. Jayne, D.R. Worsnop, I. Yourshaw, J.H. Seinfeld, and R.C. Flagan (2003), A comparison of particle mass spectrometers during the 1999 Atlanta Supersite Project, *Journal of Geophysical Research-Atmospheres*, *108* (D7), 8424, doi:10.1029/2001JD000660.
- Mills, I., T. Cvitas, K. Homann, and K. Kuchitsu (1993), *Quantities, Units and Symbols in Physical Chemistry*, p. 48 pp., Blackwell Scientific Publications, Oxford.
- Moya, M., A.S. Ansari, and S.N. Pandis (2001), Partitioning of nitrate and ammonium between the gas and particulate phases during the 1997 IMADA-AVER study in Mexico City, *Atmospheric Environment*, *35* (10), 1791-1804.
- Müller, H., G. Kramm, F. Meixner, G.J. Dollard, D. Fowler, and M. Possanzini (1993), Determination of HNO₃ Dry Deposition by Modified Bowen-Ratio

- and Aerodynamic Profile Techniques, *Tellus Series B-Chemical and Physical Meteorology*, 45 (4), 346-367.
- Munger, J.W., S.M. Fan, P.S. Bakwin, M.L. Goulden, A.H. Goldstein, A.S. Colman, and S.C. Wofsy (1998), Regional budgets for nitrogen oxides from continental sources: Variations of rates for oxidation and deposition with season and distance from source regions, *Journal of Geophysical Research-Atmospheres*, 103 (D7), 8355-8368.
- Nemitz, E., M.A. Sutton, G.P. Wyers, and P.A.C. Jongejan (2004a), Gas-particle interactions above a Dutch heathland: I. Surface exchange fluxes of NH₃, SO₂, HNO₃ and HCl, *Atmospheric Chemistry and Physics*, 4, 989-1005.
- Nemitz, E., M.A. Sutton, G.P. Wyers, R.P. Otjes, M.G. Mennen, E.M. van Putten, and M.W. Gallagher (2004b), Gas-particle interactions above a Dutch heathland: II. Concentrations and surface exchange fluxes of atmospheric particles, *Atmospheric Chemistry and Physics*, 4, 1007-1024.
- Nenes, A., S.N. Pandis, and C. Pilinis (1998), ISORROPIA: A new thermodynamic equilibrium model for multiphase multicomponent inorganic aerosols, *Aquatic Geochemistry*, 4 (1), 123-152.
- Neuman, J.A., L.G. Huey, T.B. Ryerson, and D.W. Fahey (1999), Study of Inlet Materials for Sampling Atmospheric Nitric Acid, *Environmental Science & Technology*, 33 (7), 1133 -1136.
- Nicholson, K.W. (1988), The Dry Deposition of Small Particles - a Review of Experimental Measurements, *Atmospheric Environment*, 22 (12), 2653-2666.
- Nobre, C.A., G. Fisch, H.R. da Rocha, R.F.D. Lyra, E.P. da Rocha, A.C.L. da Costa, and V.N. Ubarana (1996), Observations of the atmospheric boundary layer in Rondônia, in *Amazonian Deforestation and Climate*, edited by J.H.C. Gash, Nobre, C. A., Roberts, J. M. e Victoria, R. L., pp. 413-424, John Wiley, New York.
- Oliveira, O.C., I.P.d. Oliveira, E. Ferreira, B.J.R. Alves, C.H.B. Miranda, L. Vilela, S. Urquiaga, and R.M. Boddey (2001), Response of degraded pastures in the Brazilian Cerrado to chemical fertilisation, *Pasturas Tropicales*, 23, 14-18.
- Oms, M.T., P.A.C. Jongejan, A.C. Veltkamp, G.P. Wyers, and J. Slanina (1996), Continuous monitoring of atmospheric HCl, HNO₂, HNO₃, and SO₂, by wet-annular denuder air sampling with on-line chromatographic analysis, *International Journal of Environmental Analytical Chemistry*, 62 (3), 207-218.
- Orsini, D.A., Y.L. Ma, A. Sullivan, B. Sierau, K. Baumann, and R.J. Weber (2003), Refinements to the particle-into-liquid sampler (PILS) for ground and airborne measurements of water soluble aerosol composition, *Atmospheric Environment*, 37 (9-10), 1243-1259.
- Pandis, S.N., A.S. Wexler, and J.H. Seinfeld (1995), Dynamics of Tropospheric Aerosols, *Journal of Physical Chemistry*, 99 (24), 9646-9659.
- Pankow, J.F. (2003), Gas/particle partitioning of neutral and ionizing compounds to single and multi-phase aerosol particles. 1. Unified modeling framework, *Atmospheric Environment*, 37 (24), 3323-3333.
- Papenbrock, T., and F. Stuhl (1990), A Laser-Photolysis Fragment-Fluorescence (LPFF) Method for the Detection of Gaseous Nitric-Acid in Ambient Air, *Journal of Atmospheric Chemistry*, 10 (4), 451-469.

- Papenbrock, T., and F. Stuhl (1991), Measurement of Gaseous Nitric-Acid by a Laser-Photolysis Fragment-Fluorescence (LPFF) Method in the Black-Forest and at the North-Sea Coast, *Atmospheric Environment Part a-General Topics*, *25* (10), 2223-2228.
- Parmar, R.S., G.S. Satsangi, A. Lakhani, S.S. Srivastava, and S. Prakash (2001), Simultaneous measurements of ammonia and nitric acid in ambient air at Agra (27 degrees 10 ' N and 78 degrees 05 ' E) (India), *Atmospheric Environment*, *35* (34), 5979-5988.
- Parrish, D.D., R.B. Norton, M.J. Bollinger, S.C. Liu, P.C. Murphy, D.L. Albritton, F.C. Fehsenfeld, and B.J. Huebert (1986), Measurements of HNO₃ and NH₃-Particulates at a Rural Site in the Colorado Mountains, *Journal of Geophysical Research-Atmospheres*, *91* (D5), 5379-5393.
- Perner, D., and U. Platt (1979), Detection of Nitrous-Acid in the Atmosphere by Differential Optical-Absorption, *Geophysical Research Letters*, *6* (12), 917-920.
- Perrino, C., F. Desantis, and A. Febo (1988), Uptake of Nitrous-Acid and Nitrogen-Oxides by Nylon Surfaces - Implications for Nitric-Acid Measurement, *Atmospheric Environment*, *22* (9), 1925-1930.
- Philips, D.A., and P.K. Dasgupta (1987), A Diffusion Scrubber for the Collection of Gaseous Nitric-Acid, *Separation Science and Technology*, *22* (4), 1255-1267.
- Phillips, S.B., S.P. Arya, and V.P. Aneja (2004), Ammonia Flux and dry deposition velocity from near-surface concentration gradient measurements over a grass surface in North Carolina, *Atmos. Environ.*, *38*, 3469-3480.
- Pickering, K.E., A.M. Thompson, Y.S. Wang, W.K. Tao, D.P. McNamara, V. Kirchhoff, B.G. Heikes, G.W. Sachse, J.D. Bradshaw, G.L. Gregory, and D.R. Blake (1996), Convective transport of biomass burning emissions over Brazil during TRACE A, *Journal of Geophysical Research-Atmospheres*, *101* (D19), 23993-24012.
- Pilinis, C., S.N. Pandis, and J.H. Seinfeld (1995), Sensitivity of Direct Climate Forcing by Atmospheric Aerosols to Aerosol-Size and Composition, *Journal of Geophysical Research-Atmospheres*, *100* (D9), 18739-18754.
- Pio, C.A., and R.M. Harrison (1987a), The Equilibrium of Ammonium-Chloride Aerosol with Gaseous Hydrochloric-Acid and Ammonia under Tropospheric Conditions, *Atmospheric Environment*, *21* (5), 1243-1246.
- Pio, C.A., and R.M. Harrison (1987b), Vapor-Pressure of Ammonium-Chloride Aerosol - Effect of Temperature and Humidity, *Atmospheric Environment*, *21* (12), 2711-2715.
- Plane, J.M.C., and C.F. Nien (1992), Differential Optical-Absorption Spectrometer for Measuring Atmospheric Trace Gases, *Review of Scientific Instruments*, *63* (3), 1867-1876.
- Ponche, J.L., C. George, and P. Mirabel (1993), Mass-Transfer at the Air-Water-Interface - Mass Accommodation Coefficients of SO₂, HNO₃, NO₂ and NH₃, *Journal of Atmospheric Chemistry*, *16* (1), 1-21.
- Possanzini, M., F. De Santis, and V. Di Palo (1999), Measurements of nitric acid and ammonium salts in lower Bavaria, *Atmospheric Environment*, *33* (22), 3597-3602.

- Rapsomanikis, S., M. Wake, A.M.N. Kitto, and R.M. Harrison (1988), Analysis of Atmospheric Ammonia and Particulate Ammonium by a Sensitive Fluorescence Method, *Environmental Science & Technology*, *22* (8), 948-952.
- Ratray, G., and H. Sievering (2001), Dry deposition of ammonia, nitric acid, ammonium, and nitrate to alpine tundra at Niwot Ridge, Colorado, *Atmospheric Environment*, *35* (6), 1105-1109.
- Reid, J.S., and P.V. Hobbs (1998), Physical and optical properties of young smoke from individual biomass fires in Brazil, *Journal of Geophysical Research-Atmospheres*, *103* (D24), 32013-32030.
- Reiners, W.A., S. Liu, K.G. Gerow, M. Keller, and D.S. Schimel (2002), Historical and future land use effects on N₂O and NO emissions using an ensemble modeling approach: Costa Rica's Caribbean lowlands as an example, *Global Biogeochemical Cycles*, *16* (4).
- Rissler, J., E. Swietlicki, J. Zhou, G. Roberts, M.O. Andreae, L.V. Gatti, and P. Artaxo (2004), Physical properties of the sub-micrometer aerosol over the Amazon rain forest during the wet-to-dry season transition - comparison of modeled and measured CCN concentrations, *Atmospheric Chemistry and Physics*, *4*, 2119-2143.
- Roberts, G.C., P. Artaxo, J.C. Zhou, E. Swietlicki, and M.O. Andreae (2002), Sensitivity of CCN spectra on chemical and physical properties of aerosol: A case study from the Amazon Basin, *Journal of Geophysical Research-Atmospheres*, *107* (D20).
- Roberts, M.C., M.O. Andreae, J.C. Zhou, and P. Artaxo (2001), Cloud condensation nuclei in the Amazon Basin: "Marine" conditions over a continent?, *Geophysical Research Letters*, *28* (14), 2807-2810.
- Rodgers, M.O., and D.D. Davis (1989), A UV-Photofragmentation Laser-Induced Fluorescence Sensor for the Atmospheric Detection of HONO, *Environmental Science & Technology*, *23* (9), 1106-1112.
- Ruijgrok, W., C.I. Davidson, and K.W. Nicholson (1995), Dry Deposition of Particles - Implications and Recommendations for Mapping of Deposition over Europe, *Tellus Series B-Chemical and Physical Meteorology*, *47* (5), 587-601.
- Russell, K.M., W.C. Keene, J.R. Maben, J.N. Galloway, and J.L. Moody (2003), Phase partitioning and dry deposition of atmospheric nitrogen at the mid-Atlantic US coast, *Journal of Geophysical Research-Atmospheres*, *108* (D21).
- Sanhueza, E., and A. Garaboto (2002), Gaseous HCl at a remote tropical continental site, *Tellus Series B-Chemical and Physical Meteorology*, *54* (4), 412-415.
- Saxena, P., and L.M. Hildemann (1997), Water absorption by organics: Survey of laboratory evidence and evaluation of UNIFAC for estimating water activity, *Environmental Science & Technology*, *31* (11), 3318-3324.
- Schiemang, R., E. Kleist, J. Kleffman, and J. Wildt (2004), Uptake of nitrous acid (HONO) by plants, *Geophysical Research Abstracts*, *6* (02812), SRef-ID: 1607-7962/gra/EGU04-A-02812.
- Schjoerring, J.K., S. Husted, and M. Mattsson (1998a), Physiological parameters controlling plant-atmosphere ammonia exchange, *Atmospheric Environment*, *32* (3), 491-498.

- Schwartz, S.E., and P. Warneck (1995), Units for Use in Atmospheric Chemistry, *Pure and Applied Chemistry*, *67* (8-9), 1377-1406.
- Seidl, W., G. Brunnemann, L. Kins, E. Köhler, K. Reuswig, and R. Dlugi (1996), On the ionic composition of aerosol particles and related gas phase species at two sites during the SANA 2 campaign, *Meteorologische Zeitschrift, N.F.* *5*, 257-268.
- Seinfeld, J.H., and S.N. Pandis (1998), *Atmospheric Chemistry and Physics*, 491-541 pp., John Wiley & Sons, Inc., New York.
- Simon, P.K., and P.K. Dasgupta (1993), Wet Effluent Denuder Coupled Liquid Ion Chromatography Systems - Annular and Parallel-Plate Denuders, *Analytical Chemistry*, *65* (9), 1134-1139.
- Simon, P.K., and P.K. Dasgupta (1995a), Continuous Automated Measurement of Gaseous Nitrous and Nitric- Acids and Particulate Nitrite and Nitrate, *Environmental Science & Technology*, *29* (6), 1534-1541.
- Simon, P.K., and P.K. Dasgupta (1995b), Continuous Automated Measurement of the Soluble Fraction of Atmospheric Particulate Matter, *Analytical Chemistry*, *67* (1), 71-78.
- Simon, P.K., P.K. Dasgupta, and Z. Vecera (1991), Wet Effluent Denuder Coupled Liquid Ion Chromatography Systems, *Analytical Chemistry*, *63* (13), 1237-1242.
- Singh, S.P., G.S. Satsangi, P. Khare, A. Lakhani, K. Maharaj Kumari, and S.S. Srivastava (2001), Multiphase measurement of atmospheric ammonia, *Atmos. Environ.*, *3* (1), 107-116.
- Slanina, J., P.J. de Wild, and G.P. Wyers (1992), *The application of denuder systems to the analysis of atmospheric components*, 129-154 pp., John Wiley & Sons, New York.
- Slanina, J., H.M. ten Brink, R.P. Otjes, A. Even, P. Jongejan, A. Khlystov, A. Waijers-Ijpelaan, and M. Hu (2001), The continuous analysis of nitrate and ammonium in aerosols by the steam jet aerosol collector (SJAC): extension and validation of the methodology, *Atmospheric Environment*, *35* (13), 2319-2330.
- Slanina, J., and G.P. Wyers (1994), Monitoring of Atmospheric Components by Automatic Denuder Systems, *Fresenius Journal of Analytical Chemistry*, *350* (7-9), 467-473.
- Slanina, J., and Y. Zhang (2004), Aerosols: connections between regional climatic change and air quality, *Pure and Applied Chemistry*, *76* (6), 1241-1253.
- Slinn, W.G.N. (1982), Predictions for Particle Deposition to Vegetative Canopies, *Atmospheric Environment*, *16* (7), 1785-1794.
- Smith, G.D., E. Woods, T. Baer, and R.E. Miller (2003), Aerosol uptake described by numerical solution of the diffusion - Reaction equations in the particle, *Journal of Physical Chemistry A*, *107* (45), 9582-9587.
- Solomon, P., K. Baumann, E. Edgerton, R. Tanner, D. Eatough, W. Modey, H. Marin, D. Savoie, S. Natarajan, M.B. Meyer, and G. Norris (2003), Comparison of integrated samplers for mass and composition during the 1999 Atlanta Supersites project, *Journal of Geophysical Research-Atmospheres*, *108* (D7), 8423, doi:10.1029/2001JD001218.
- Solomon, P.A., S.M. Larson, T. Fall, and G.R. Cass (1988), Basinwide Nitric-Acid and Related Species Concentrations Observed During the Claremont

- Nitrogen Species Comparison Study, *Atmospheric Environment*, 22 (8), 1587-1594.
- Spicer, C.W., J.E. Howes, T.A. Bishop, L.H. Arnold, and R.K. Stevens (1982), Nitric-Acid Measurement Methods - an Intercomparison, *Atmospheric Environment*, 16 (6), 1487-1500.
- Spindler, G., J. Hesper, E. Brüggemann, R. Dubois, T. Müller, and H. Herrmann (2003), Wet annular denuder measurements of nitrous acid: laboratory study of the artefact reaction of NO₂ with S(IV) in aqueous solution and comparison with field measurements, *Atmospheric Environment*, 37 (19), 2643-2662.
- Spindler, G., U. Teichmann, and M.A. Sutton (2001), Ammonia dry deposition over grassland - micrometeorological flux-gradient measurements and bidirectional flux calculations using an inferential model, *Quarterly Journal of the Royal Meteorological Society*, 127 (573), 795-814.
- Srivastava, A.K., and R.S. Ambasht (1994), Nitrogen Deposition in Casuarina-Equisetifolia (Forst) Plantation Stands in the Dry Tropics of Sonbhadra, India, *Forest Ecology and Management*, 70 (1-3), 341-348.
- Stallard, R.F., and J.M. Edmond (1981), Geochemistry of the Amazon 1. Precipitation Chemistry and the Marine Contribution to the Dissolved-Load at the Time of Peak Discharge, *Journal of Geophysical Research-Oceans and Atmospheres*, 86 (NC10), 9844-9858.
- Stelson, A.W., S.K. Friedlander, and J.H. Seinfeld (1979), Note on the Equilibrium Relationship between Ammonia and Nitric-Acid and Particulate Ammonium-Nitrate, *Atmospheric Environment*, 13 (3), 369-371.
- Stelson, A.W., and J.H. Seinfeld (1982a), Relative-Humidity and Temperature-Dependence of the Ammonium-Nitrate Dissociation-Constant, *Atmospheric Environment*, 16 (5), 983-992.
- Stelson, A.W., and J.H. Seinfeld (1982c), Thermodynamic Prediction of the Water Activity, NH₄NO₃ Dissociation-Constant, Density and Refractive-Index for the NH₄NO₃-(NH₄)₂SO₄-H₂O System at 25-Degrees-C, *Atmospheric Environment*, 16 (10), 2507-2514.
- Stolzenburg, M.R., and S.V. Hering (2000), Method for the automated measurement of fine particle nitrate in the atmosphere, *Environmental Science & Technology*, 34 (5), 907-914.
- Stutz, J., B. Alicke, and A. Neftel (2002), Nitrous acid formation in the urban atmosphere: Gradient measurements of NO₂ and HONO over grass in Milan, Italy, *Journal of Geophysical Research-Atmospheres*, 107 (D22), 8192, doi:10.1029/2001JD000390.
- Sutton, M.A., W.A.H. Asman, and J.K. Schjorring (1994), Dry Deposition of Reduced Nitrogen, *Tellus Series B-Chemical and Physical Meteorology*, 46 (4), 255-273.
- Sutton, M.A., J.K. Burkhardt, D. Guerin, E. Nemitz, and D. Fowler (1998), Development of resistance models to describe measurements of bi-directional ammonia surface-atmosphere exchange, *Atmospheric Environment*, 32 (3), 473-480.
- Sutton, M.A., C. Milford, E. Nemitz, M.R. Theobald, P.W. Hill, D. Fowler, J.K. Schjoerring, M.E. Mattsson, K.H. Nielsen, S. Husted, J.W. Erisman, R. Otjes, A. Hensen, J. Mosquera, P. Cellier, B. Loubet, M. David, S.

- Genermont, A. Neftel, A. Blatter, B. Herrmann, S.K. Jones, L. Horvath, E.C. Fuhrer, K. Mantzanas, Z. Koukoura, M. Gallagher, P. Williams, M. Flynn, and M. Riedo (2001), Biosphere-atmosphere interactions of ammonia with grasslands: Experimental strategy and results from a new European initiative, *Plant and Soil*, *228* (1), 131-145.
- Taira, M., and Y. Kanda (1993), Wet Effluent Diffusion Denuder for Sampling of Atmospheric Gaseous Nitric-Acid, *Analytical Chemistry*, *65* (21), 3171-3173.
- Talbot, R.W., M.O. Andreae, T.W. Andreae, and R.C. Harriss (1988), Regional Aerosol Chemistry of the Amazon Basin During the Dry Season, *Journal of Geophysical Research-Atmospheres*, *93* (D2), 1499-1508.
- Tanner, R.L. (1980), An Ambient Experimental-Study of Phase-Equilibrium in the Atmospheric System - H^+ , NH_4^+ , SO_4^{2-} , NO_3^- -- $NH_3(G)$, $HNO_3(G)$, *Abstracts of Papers of the American Chemical Society*, *180* (AUG), 187-ENVR.
- Tanner, R.L., T.J. Kelly, D.A. Dezaró, and J. Forrest (1989), A Comparison of Filter, Denuder, and Real-Time Chemi- Luminescence Techniques for Nitric-Acid Determination in Ambient Air, *Atmospheric Environment*, *23* (10), 2213-2222.
- Tarnay, L., A.W. Gertler, R.R. Blank, and G.E. Taylor (2001), Preliminary measurements of summer nitric acid and ammonia concentrations in the Lake Tahoe Basin air-shed: implications for dry deposition of atmospheric nitrogen, *Environmental Pollution*, *113* (2), 145-153.
- ten Brink, H.M., C. Kruisz, G.P.A. Kos, and A. Berner (1997), Composition/size of the light-scattering aerosol in The Netherlands, *Atmospheric Environment*, *31* (23), 3955-3962.
- Thom, A.S. (1975), Vegetation and the atmosphere, in *Momentum, mass and heat exchange*, edited by J.L. Moneith, pp. 57-109, Academic Press, Chichester, UK.
- Townsend, A.R., B.H. Braswell, E.A. Holland, and J.E. Penner (1996), Spatial and temporal patterns in terrestrial carbon storage due to deposition of fossil fuel nitrogen, *Ecological Applications*, *6* (3), 806-814.
- Twomey, S. (1974), Pollution and Planetary Albedo, *Atmospheric Environment*, *8* (12), 1251-1256.
- Ueda, H., T. Takemoto, Y.P. Kim, and W.M. Sha (2000), Behaviors of volatile inorganic components in urban aerosols, *Atmospheric Environment*, *34* (3), 353-361.
- Van Doren, J.M., L.R. Watson, P. Davidovits, D.R. Worsnop, M.S. Zahniser, and C.E. Kolb (1990), Temperature-Dependence of the Uptake Coefficients of HNO_3 , HCl , and N_2O_5 by Water Droplets, *Journal of Physical Chemistry*, *94* (8), 3265-3269.
- van Hove, L.W.A., P. Heeres, and M.E. Bossen (2002), The annual variation in stomatal ammonia compensation point of rye grass (*Lolium perenne* L.) leaves in an intensively managed grassland, *Atmospheric Environment*, *36* (18), 2965-2977.
- Vecera, Z., and P.K. Dasgupta (1991), Measurement of Atmospheric Nitric and Nitrous Acids with a Wet Effluent Diffusion Denuder and Low-Pressure Ion Chromatography Postcolumn Reaction Detection, *Analytical Chemistry*, *63* (20), 2210-2216.

- Vestin, A., J. Rissler, E. Swietlicki, and G. Frank (2005), Cloud nucleating properties of the Amazonian dry season biomass burning aerosol - measurements and modeling, *in preparation*.
- Vitousek, P.M., J.D. Aber, R.W. Howarth, G.E. Likens, P.A. Matson, D.W. Schindler, W.H. Schlesinger, and D.G. Tilman (1997), Human alteration of the global nitrogen cycle: Sources and consequences, *Ecological Applications*, 7 (3), 737-750.
- Vong, R.J., D. Vickers, and D.S. Covert (2004), Eddy correlation measurements of aerosol deposition to grass, *Tellus Series B-Chemical and Physical Meteorology*, 56 (2), 105-117.
- Wang, L.M., and J.S. Zhang (2000), Detection of nitrous acid by cavity ring down spectroscopy, *Environmental Science & Technology*, 34 (19), 4221-4227.
- Weber, R., D. Orsini, Y. Duan, K. Baumann, C.S. Kiang, W. Chameides, Y.N. Lee, F. Brechtel, P. Klotz, P. Jongejan, H. ten Brink, J. Slanina, C.B. Boring, Z. Genfa, P. Dasgupta, S. Hering, M. Stolzenburg, D.D. Dutcher, E. Edgerton, B. Hartsell, P. Solomon, and R. Tanner (2003), Intercomparison of near real time monitors of PM_{2.5} nitrate and sulfate at the U.S. Environmental Protection Agency Atlanta Supersite, *J. Geophys. Res.-Atmos.*, 108 (D7), 8421, doi:10.1029/2001JD001220.
- Weber, R.J., D. Orsini, Y. Daun, Y.N. Lee, P.J. Klotz, and F. Brechtel (2001), A particle-into-liquid collector for rapid measurement of aerosol bulk chemical composition, *Aerosol Science and Technology*, 35 (3), 718-727.
- Wesely, M.L. (1989), Parameterization of Surface Resistances to Gaseous Dry Deposition in Regional-Scale Numerical-Models, *Atmospheric Environment*, 23 (6), 1293-1304.
- Wesely, M.L., D.R. Cook, R.L. Hart, and R.E. Speer (1985), Measurements and Parameterization of Particulate Sulfur Dry Deposition over Grass, *Journal of Geophysical Research-Atmospheres*, 90 (ND1), 2131-2143.
- Wesely, M.L., and B.B. Hicks (1977), Some Factors That Affect Deposition Rates of Sulfur-Dioxide and Similar Gases on Vegetation, *Journal of the Air Pollution Control Association*, 27 (11), 1110-1116.
- Wesely, M.L., and B.B. Hicks (2000), A review of the current status of knowledge on dry deposition, *Atmospheric Environment*, 34 (12-14), 2261-2282.
- Wexler, A.S., and J.H. Seinfeld (1990), The Distribution of Ammonium-Salts among a Size and Composition Dispersed Aerosol, *Atmospheric Environment Part A-General Topics*, 24 (5), 1231-1246.
- Wexler, A.S., and J.H. Seinfeld (1992), Analysis of Aerosol Ammonium-Nitrate - Departures from Equilibrium During SCAQS, *Atmospheric Environment Part a-General Topics*, 26 (4), 579-591.
- Williams, M.R., T.R. Fisher, and J.M. Melack (1997), Chemical composition and deposition of rain in the central Amazon, Brazil, *Atmospheric Environment*, 31 (2), 207-217.
- Williams, E.J., S.T. Sandholm, J.D. Bradshaw, J.S. Schendel, A.O. Langford, P.K. Quinn, P.J. Lebel, S.A. Vay, P.D. Roberts, R.B. Norton, B.A. Watkins, M.P. Buhr, D.D. Parrish, J.G. Calvert, and F.C. Fehsenfeld (1992), An Intercomparison of 5 Ammonia Measurement Techniques, *Journal of Geophysical Research-Atmospheres*, 97 (D11), 11591-11611.

- Winer, A.M., and H.W. Biermann (1994), Long Pathlength Differential Optical-Absorption Spectroscopy (DOAS) Measurements of Gaseous HONO, NO₂ and HCHO in the California South Coast Air Basin, *Research on Chemical Intermediates*, *20* (3-5), 423-445.
- Wyers, G.P., R.P. Otjes, and J. Slanina (1993), A Continuous-Flow Denuder for the Measurement of Ambient Concentrations and Surface-Exchange Fluxes of Ammonia, *Atmospheric Environment Part a-General Topics*, *27* (13), 2085-2090.
- Yamasoe, M.A., P. Artaxo, A.H. Miguel, and A.G. Allen (2000), Chemical composition of aerosol particles from direct emissions of vegetation fires in the Amazon Basin: water-soluble species and trace elements, *Atmospheric Environment*, *34* (10), 1641-1653.
- Zellweger, C., M. Ammann, P. Hofer, and U. Baltensperger (1999), NO_y speciation with a combined wet effluent diffusion denuder- aerosol collector coupled to ion chromatography, *Atmospheric Environment*, *33* (7), 1131-1140.
- Zhang, J., W.L. Chameides, R. Weber, G. Cass, D. Orsini, E. Edgerton, P. Jongejan, and J. Slanina (2002), An evaluation of the thermodynamic equilibrium assumption for fine particulate composition: Nitrate and ammonium during the 1999 Atlanta Supersite Experiment, *Journal of Geophysical Research-Atmospheres*, *108* (D7), 8414, doi:10.1029/2001JD001592.
- Zhou, X.L., K. Civerolo, H.P. Dai, G. Huang, J. Schwab, and K. Demerjian (2002), Summertime nitrous acid chemistry in the atmospheric boundary layer at a rural site in New York State, *Journal of Geophysical Research-Atmospheres*, *107* (D21), 4590, doi:10.1029/2001JD001539.

Curriculum Vitae

Ivonne Trebs was born on the 17th of February 1978 in Borna (Germany). From 1992 to 1996 she visited the secondary school in Geithain (Germany). From 1996 until 2001 she studied environmental engineering at the Leipzig University of Applied Sciences (HTWK Leipzig). During her studies, she worked for six month as an intern in the Department of Environmental Science, Policy and Management of the DaimlerChrysler AG, Stuttgart. She complemented her studies by working as a part-time research assistant at the HTWK Leipzig. She worked for 6 month as a visiting researcher in the Department of Chemistry & Chemical Engineering at the University of Paisley (Scotland, Great Britain). Since October 2000, she is employed at the Max Planck Institute for Chemistry (MPIC) (Mainz, Germany), where she did her diploma work from 2000 to 2001. In 2001 she took part in the LBA-CLAIRE measurement campaign (Manaus, Brazil). From 2002 until 2005 she did her PhD work at the MPIC, which included instrument training at the Energy Research Center of the Netherlands and an extensive field campaign in Rondônia, Brazil (LBA-SMOCC).